NATIONAL TECHNICAL UNIVERSITY OF ATHENS

SCHOOL OF MECHANICAL ENGINEERING

VIABILITY CONTROL FOR NONHOLONOMIC SYSTEMS. APPLICATION TO THE COMPENSATION OF DISTURBANCES FOR UNDERWATER ROBOTIC VEHICLES

DOCTORAL DISSERTATION

by

DIMITRA PANAGOU

(Diploma in Mechanical Engineering, N.T.U.A.)

Supervisor:
K. Kyriakopoulos, Professor

Athens, April 2012

NATIONAL TECHNICAL UNIVERSITY OF ATHENS

SCHOOL OF MECHANICAL ENGINEERING

SECTION OF MECHANICAL DESIGN AND AUTOMATIC CONTROL

Viability Control for Nonholonomic Systems. Application to the Compensation of Disturbances for Underwater Robotic Vehicles

DOCTORAL DISSERTATION

by

DIMITRA PANAGOU

(Diploma in Mechanical Engineering, N.T.U.A. (2006))

PhD Advisory Committee

1. Prof. K. Kyriakopoulos (N.T.U.A.) (Advisor)
2. Prof. E. Papadopoulos (N.T.U.A.)
3. Prof. (Emeritus) N. Krikelis (N.T.U.A.)

PhD Defense Committee

1. Prof. K. Kyriakopoulos (N.T.U.A.) (Advisor)
2. Prof. E. Papadopoulos (N.T.U.A.)
3. Prof. (Emeritus) N. Krikelis (N.T.U.A.)
4. Prof. G. Papavassilopoulos (N.T.U.A.)
5. Assist. Prof. K. Tzafestas (N.T.U.A.)
6. Assist. Prof. D. Dimarogonas (K.T.H.)
7. Lecturer G. Papalambrou (N.T.U.A.)

Athens, April 2012

Η έγκριση της διδακτορικής διατριβής από την Ανώτατη Σχολή Μηχανολόγων Μηχανικών του Ε.Μ.Π. δεν υποδηλώνει αποδοχή των γνωμών του συγγραφέα (Ν. 5343/1932, Άρθρο 202)

Σα βγεις στον πηγαιμό για την Ιθάκη,
να εύχεσαι νάναι μακρύς ο δρόμος,
γεμάτος περιπέτειες, γεμάτος γνώσεις.
Τους Λαιστρυγόνας και τους Κύκλωπας,
τον θυμωμένο Ποσειδώνα μη φοβάσαι,
τέτοια στον δρόμο σου ποτέ σου δεν θα βρεις,
αν μέν᾽ η σκέψις σου υψηλή, αν εκλεκτή
συγκίνησις το πνεύμα και το σώμα σου αγγίζει.

Η Ιθάκη σ᾽ έδωσε τ᾽ ωραίο ταξείδι.
Χωρίς αυτήν δεν θάβγαινες στον δρόμο.
Άλλα δεν έχει να σε δώσει πια.
Κι αν πτωχική την βρεις, η Ιθάκη δεν σε γέλασε.
Ετσι σοφός που έγινες, με τόση πείρα,
ήδη θα το κατάλαβες οι Ιθάκες τι σημαίνουν.

Κ. Π. Καβάφης

Acknowledgements

Η παρούσα διατριβή εκπονήθηκε στο Εργαστήριο Αυτομάτου Ελέγχου του Τομέα Μηχανολογικών Κατασκευών και Αυτομάτου Ελέγχου της Σχολής Μηχανολόγων Μηχανικών του Εθνικού Μετσοβίου Πολυτεχνείου, από το Νοέμβριο 2006 έως τον Απρίλιο 2012.

Θα ήθελα να εκφράσω τις θερμές και ειλικρινείς μου ευχαριστίες στον Επιβλέποντα Καθηγητή Κωνσταντίνο Ι. Κυριακόπουλο, για την ουσιαστική και πολύτιμη καθοδήγηση και συμπαράσταση που μου προσέφερε καθόλη τη διάρκεια των προπτυχιακών και μεταπτυχιακών σπουδών μου στο Εργαστήριο Αυτομάτου Ελέγχου. Οι ιδέες του κατά τις συνεχείς μας συζητήσεις και ο ενθουσιασμός που πάντοτε μου εμφυσούσε για την επίτευξη όσο πιο υψηλών στόχων υπήρξαν διδακτικά, εποικοδομητικά και καταλυτικά στοιχεία για την ολοκλήρωση αυτής της προσπάθειας. Εξίσου ευχαριστώ τα άλλα δύο μέλη της τριμελούς επιτροπής, τους Καθηγητές Ε. Παπαδόπουλο και Ν. Κρικέλη.

Επίσης, θα ήθελα να απευθύνω τις θερμές ευχαριστίες μου στον Καθηγητή Herbert G. Tanner, για την πρόσκλησή του να επισκεφθώ το University of Delaware και να εργαστώ μαζί του για τις ανάγκες ενός ερευνητικού προγράμματος κατά το Εαρινό Εξάμηνο 2009, αλλά και για τη μέχρι σήμερα συνεργασία μας. Η συμβολή του στη διαμόρφωση των τεχνικών κατευθύνσεων και των γνώσεών μου υπήρξε καθοριστική για την εξέλιξη και την ολοκλήρωση αυτής της προσπάθειας. Ομοίως, ευχαριστώ τον καθηγητή Vijay Kumar, για την πρόσκλησή του να επισκεφθώ το University of Pennsylvania και να συνεργαστώ με την ομάδα του στο πλαίσιο ενός ερευνητικού προγράμματος κατά το Χειμερινό Εξάμηνο 2010.

Θα ήταν παράλειψη να μην αναφερθώ στη συμβολή των μελών του Εργαστηρίου Αυτομάτου Ελέγχου στη δημιουργία ενός εποικοδομητικού και ευχάριστου κλίματος εργασίας και συνεργασίας όλα αυτά τα χρόνια. Κυρίως θα ήθελα να ευχαριστήσω όσους με στήριξαν ενόσω βρισκόμουν στο δύσκολο στάδιο του ξεκινήματος αυτής της περιπέτειας.

Τέλος, επιθυμώ να αφιερώσω την προσπάθεια αυτή στην οικογένειά μου' τον πατέρα μου, Γιάννη, τη μητέρα μου, Έλσα και τον αδελφό μου, Κώστα. Χωρίς την αγάπη, την κατανόηση και την αμέριστη συμπαράστασή τους όλα αυτά τα χρόνια, τόσο την υλική αλλά κυρίως την ηθική, είναι βέβαιο ότι δε θα είχα φτάσει στο σημείο που βρίσκομαι σήμερα. Τους ευχαριστώ ειλικρινά που με έμαθαν να μην εγκαταλείπω ποτέ τον αγώνα, παρά τις όποιες δυσκολίες, που στηρίζουν έμπρακτα και ουσιαστικά κάθε μου εγχείρημα, και που πάντοτε είμαστε ενωμένοι σαν γροθιά, ακόμα κι όταν βρισκόμαστε μακριά, στα τέσσερα σημεία του ορίζοντα.

Αθήνα, Απρίλιος 2012

Viability Control For Nonholonomic Systems. Application to the Compensation of Disturbances for Underwater Robotic Vehicles.

ABSTRACT

This thesis presents a framework on the state feedback control design for a class of underactuated systems that are subject to nonholonomic constraints, state constraints and additive bounded disturbances. The framework is based on concepts from viability theory, as well as on a novel method on the state feedback control design for nonholonomic systems. The overall idea is that the control design for such problems is recast into designing feedback control laws so that system trajectories always remain viable in the set K defined by state (viability) constraints and furthermore converge to a goal set G in K.

In particular, the main components and developments are:

■ A novel method on the state feedback control design for a class of n-dimensional nonholonomic systems, which is based on the novel concept of a family of N-dimensional reference vector fields, where $\mathrm{N} \leq n$, and their connection with Pfaffian nonholonomic constraints.

The proposed method comprises a control strategy which brings a uniform logic into the control design for a wide class of n-dimensional nonholonomic systems. The main idea is that, given an n-dimensional (kinematic) nonholonomic system, subject to κ Pfaffian constraints $\boldsymbol{A}(\boldsymbol{q})\dot{\boldsymbol{q}} = \boldsymbol{b}(\boldsymbol{q})$, one can define a smooth N-dimensional reference vector field $\mathbf{F}(\cdot)$ on a subspace $\mathcal{L}$ of the configuration space $\mathcal{C}$, which is non-vanishing everywhere except for the origin of the local coordinate system on $\mathcal{L}$. The origin is by construction the unique critical point of $\mathbf{F}(\cdot)$ of dipole type, which implies that all integral curves begin and end at the origin.

The dimension N of the vector field $\mathbf{F}$ is specified by the explicit form of the Pfaffian constraints in the following sense: depending on the column structure of $\boldsymbol{A}(\boldsymbol{q})$, the configuration space $\mathcal{C}$ is trivially decomposed into $\mathcal{L} \times \mathcal{T}$, where $\mathcal{L}$ is the "leaf" space, $\mathcal{T}$ is the "fiber" space, $n = \dim \mathcal{L} + \dim \mathcal{T}$, $N = \dim \mathcal{L}$. The local coordinates $\boldsymbol{x} \in \mathbb{R}^{\mathrm{N}}$ on $\mathcal{L}$ are called leafwise states and the local coordinates $\boldsymbol{t} \in \mathbb{R}^{n-\mathrm{N}}$ on the fiber are called transverse states. The vector field $\mathbf{F}$ is defined in terms of the leafwise states $\boldsymbol{x}$, tangent to the leaf space $\mathcal{L}$, and is non-vanishing everywhere on $\mathcal{L}$ except for the origin $\boldsymbol{x} = \mathbf{0}$. The characteristic property of the vector field $\mathbf{F}(\cdot)$ is that the origin $\boldsymbol{x} = \mathbf{0}$ is a dipole, which implies that all integral curves begin and end at the critical point.

The vector field $\mathbf{F}$ serves as a velocity reference for the system; this means that at each configuration $\boldsymbol{q} \in \mathcal{C}$ the system vector field $\dot{\boldsymbol{q}} \in T_{\boldsymbol{q}}\mathcal{C}$ is steered to be made parallel to $\mathbf{F}$. This is codified by defining the output $h(\boldsymbol{q}) \triangleq \boldsymbol{A}(\boldsymbol{q})\mathbf{F}(\cdot)$, which expresses the "misalignment" of the system vector field with the vector field $\mathbf{F}(\cdot)$, and choosing the control inputs such that $h(\boldsymbol{q}) \to 0$. In this sense, instead of trying to stabilize the system to the origin, one can use the available control authority to steer the system vector field onto the tangent bundle of the integral curves of $\mathbf{F}$ and "flow" along the reference vector field on its way to the origin. These two objectives suggest the choice of particular Lyapunov-like functions in terms of the leafwise states and the transverse states, and enable one to establish convergence to the origin based on standard techniques.

The method has been applied to the control design of kinematic nonholonomic systems in chained form, and extended to a class of dynamic nonholonomic systems with drift, describing underactuated marine vehicles. Robustness with respect to unknown, bounded disturbances has been also addressed.

■ A viability-based switching feedback control approach for a class of nonlinear systems that are subject to inequality state constraints. The approach is based on concepts from viability theory. State constraints are realized as viability constraints defining a closed subset K of the state space, called the viability set K. Using tools from viability theory, in particular the concept of tangency to a set K of inequality constraints, which is realized via the contingent cone to the set K, the necessary and sufficient conditions for selecting viable controls are given.

Furthermore, the state feedback nonholonomic control solutions resulting from the vector field approach described above are redesigned by means of switching control, so that nonholonomic system trajectories starting in a set K are always viable in K and converge to a goal set G in K. A switching signal orchestrates the switching among viable in K controls and convergent to G controls, based on the value of the constraint functions. The approach can be applied, but is not limited to, the class of problems whose objective can be recast as to control a nonholonomic system so that resulting trajectories remain forever in a subset K of the state space, until they converge into a goal set G.

The method has been applied to the design of viable feedback control laws for an underactuated marine vehicle in a constrained configuration set K; the set K essentially describes the limited sensing area (in terms of position and orientation) resulting from a vision-based sensor system with limited range and limited field-of-view. Moreover, its robustness has been considered for bounded external perturbations.

The method has been also used for the cooperative motion planning and control design for a leader-follower formation of two nonholonomic mobile robots in obstacle environments, under visibility constraints. Visibility constraints arise due to the limited sensing of the follower (limited sensing range and limited field-of-view) and are realized as nonlinear inequality state constraints which determine a visibility set K. Maintaining visibility is thus translated into controlling the robots so that system trajectories starting in K always remain in K. The necessary conditions under which visibility is maintained are given, as well as a control scheme that forces the follower to converge and remain into a set of desired configurations with respect to the leader, while maintaining visibility. A cooperative control scheme for the motion of the formation in a known obstacle environment has been also developed, so that both collision avoidance and maintaining visibility are ensured. The control schemes are decentralized, in the sense that there is no direct communication between the robots, nor global state feedback is available to them.

Contents

List of Figures

Chapter 1

Extended Abstract / Overview

1.1 Control of nonholonomic systems

From a theoretical viewpoint, nonholonomic control has been and still remains a highly challenging and attractive problem. Related research during the past two decades has attributed various control design methodologies addressing stabilization, path, and trajectory tracking problems for nonholonomic systems of different types, which nowadays feature a solid framework within control theory.

It is well known that nonholonomic systems do not satisfy Brockett's condition [Bro83], and therefore can not be asymptotically stabilized by continuously differentiable, time-invariant state feedback control laws. In fact, nonholonomic mechanical systems can not be asymptotically stabilized to a single equilibrium using any control method that employs smooth, or even continuous, time-invariant feedback [BRM92]. Indicative of the peculiarity of the case of stabilization to the origin using time-invariant feedback is the careful way in which asymptotic stability is defined in [LS93], which involves *neighborhoods* of the equilibrium rather than balls as in the classical asymptotic stability definition in the Lyapunov sense, since arbitrarily small perturbations in initial conditions around the equilibrium might require some extensive maneuvering to bring the system back to rest.

To overcome the limitation pertaining to the nonexistence of a continuous time-invariant feedback stabilizing controller, research has focused on solutions that can be broadly classified into two groups: those that employ *time-varying* feedback, either smooth [Pom92, TMW95, Sam95, Jia99, TL02, MS03, MS09] or non-smooth w.r.t. the state [SE95, MS96, GE97, MM97, MS00, OV05], and those that use *time-invariant*, *non-smooth* state feedback. The latter approach includes piecewise continuous [BRM92, tdWS92], discontinuous [Ast96, BD96, TTR97b, TTR97a, BDK98, LT98, WHX99, XM01, MA03], and hybrid/switching control solutions [LO96, KRM96, KM96, HM99, SGHL01, CAP05]. Among the variety of nonholonomic systems encountered in real world applications, the class of n-dimensional chained systems [MS93] has received special attention.

Among the existing control solutions, those which employ non-smooth feedback can yield exponential convergence in the chained system states, and may therefore be preferable from an application standpoint. In this case, the control design often employs nonlinear state transformations [Ast96, TTR97a, WHX99, Jia99, SGHL00, XM01, MA03], and the control laws are extracted in the new coordinate system using either linear [Ast96], nonlinear [TTR97b], or invariant manifold based techniques [TTR97a]. However, the coordinate transformations are not always straightforward and thus the derivation of the control law remains non-trivial.

Contribution

In Chapter 4, we present one of the main contributions of this thesis, which is the introduction of a uniform logic into the control design of n-dimensional nonholonomic systems. The proposed control strategy comprises formal guidelines for the construction of state feedback (discontinuous) control laws for n-dimensional nonholonomic systems, subject to either kinematic, or dynamic Pfaffian constraints. The approach is based on a geometric view and generalization of one of our earlier control designs for the steering of the unicycle to the origin, described in Chapter 2, which has been inspired by the Dipolar Navigation Function, originally introduced in [TK00].

Compared to existing methods, the novelty of the proposed approach is that it recasts the initial problem of steering the state to the origin into an output regulation problem. The regulated output expresses the misalignment of the system vector field w.r.t. a reference vector field, which by construction has a unique, isolated critical point of *rose* type.[1] Thus, the geometric generalization relies on the consideration of higher dimensional systems and the regulation of an output vector to zero, which along with a suitably selected Lyapunov-like function is used to establish formal convergence of the system trajectories to the origin. The proposed formulation and design methodology offers justification for the choice of control law, which carries over to a variety of nonholonomic systems subject to kinematic (first-order), or dynamic (second-order) nonholonomic constraints.

In some of the case studies analyzed, the controllers obtained are similar to existing ones; for instance, in the case of chained systems (Section 4.3), the obtained controllers are similar to those proposed in [Ast96]. However, the main difference between our approach and the one in [Ast96] is that the control design takes place in the initial system coordinates, without the need to apply the σ-process of [Ast96], by using a vector field as a reference and by completing the convergence analysis using a singular-perturbation argument. The rather broad applicability of the proposed design strategy leads us to believe that the structure of nonholonomic systems subject to Pfaffian constraints can afford a common approach.

Furthermore, although preserving the nonholonomic nature and the structural complexity of the original formulation, the new one offers a more intuitive treatment of the inputs w.r.t. the controlled states, and allows a uniform stability analysis with standard tools. The new geometric perspective also exposes the interdependence of the state variables and highlights a time-scale decomposition, which permits the use of additional analysis techniques, such as those related to singular perturbations and slowly varying systems. ■

1.2 Nonholonomic control design for robotic applications

From a practical viewpoint, nonholonomic systems have been of particular interest within the fields of robotics, mechatronics and multi-agent control systems, in part since they model a wide class of mechanical systems, including mobile robots with trailers, snake robots, underactuated robotic manipulators, unmanned vehicles (aerial, underwater, ground), surface vessels and spacecraft, as well as the manipulation of objects with multi-fingered robotic hands.

[1] An isolated critical point is called a *rose* if it has elliptic type of sectors only, i.e. if in a neighborhood around it, all integral curves begin and end at the critical point; an example is the dipole [Hen94].

The literature is abundant in control solutions for nonholonomic systems with catastatic Pfaffian constraints[2]. In this case, control laws are usually designed under the assumptions that no model uncertainty and/or no additive disturbances apply to the system.

However, these assumptions are usually unrealistic for real world applications, since the control design in this case pertains to realistic, complex systems, which should perform efficiently and reliably. Therefore, robustness of control solutions w.r.t. uncertainty and additive disturbances is an important parameter which highly affects the performance, or even safety, of the considered systems.

In part for this reason, the development of robust nonholonomic controls has received special attention. Robust controllers with regard to model parametric uncertainty, either adaptive or switching, have been proposed in [BR95, CBG98, HLM99b, DXH00, DDZB01, MTX02].

The regulation of nonholonomic systems with additive (external) disturbances, which may be either *vanishing* [tdWK95, Jia00, DDZB01, LAN03, GWL03, PA03, Guo05, WZ08] or *non-vanishing* [CLO99, GWLZ01, LO01, MS03, FBP03, VA03, ZDCH07] at the origin, has also received special attention. Non-vanishing perturbations are typically more challenging, in the sense that a single desired configuration might no longer be an equilibrium for the system [Kha02]. In this case, one should rather pursuit the ultimate boundedness of state trajectories; this problem is often addressed as *practical stabilization*. In the case of non-vanishing perturbations, it is usually assumed that the disturbances are small and bounded, or that the perturbation vector field satisfies certain conditions; for instance, in [FBP03] the perturbation vector field belongs into the subspace spanned by the control vector fields. In a similar context, the development of ISS as a fundamental concept of modern nonlinear feedback analysis and design, has allowed the formulation of robustness considerations for nonholonomic systems into the ISS framework [LSW02, Tan04, LA05, AHP07b].

1.2.1 Dynamic positioning of underactuated marine vehicles

An interesting problem where additive disturbances serve as non-vanishing perturbations at a desired configuration is the *dynamic positioning* of underactuated marine vehicles (ships, surface vessels, underwater vehicles) in the presence of environmental disturbances. Dynamic positioning typically refers to a computer controlled system, in order to automatically maintain a vessel's position and heading by using its own propellers and thrusters. The dynamic positioning control problem thus reduces into finding a feedback control law that asymptotically stabilizes both position and orientation of the vessel to desired constant values.

In general, the control design for underactuated underwater vehicles and surface vessels has received great interest over the past fifteen years, motivated by their extensive use in oil industry, scientific explorations, search and rescue missions, etc. The design of stabilizing controllers for this class of vehicles is challenging, since they usually exhibit second-order nonholonomic constraints and therefore can not be stabilized by continuous, time invariant state feedback control laws [Bro83]. Furthermore, their dynamics include nonlinear, complex hydrodynamic terms which should not be neglected during the control design. Finally, environmental dis-

[2]Pfaffian constraints are of the form $\boldsymbol{A}(\boldsymbol{q})\dot{\boldsymbol{q}} = \boldsymbol{b}(\boldsymbol{q})$, where $\boldsymbol{q} \in \mathbb{R}^n$ is the system state vector, $\boldsymbol{A}(\boldsymbol{q}) \in \mathbb{R}^{\kappa \times n}$ and $\boldsymbol{b}(\boldsymbol{q}) \in \mathbb{R}^{\kappa}$. If $\boldsymbol{b}(\boldsymbol{q}) = \boldsymbol{0}$ the constraints are called catastatic, whereas if $\boldsymbol{b}(\boldsymbol{q}) \neq \boldsymbol{0}$ the constraints are called acatastatic

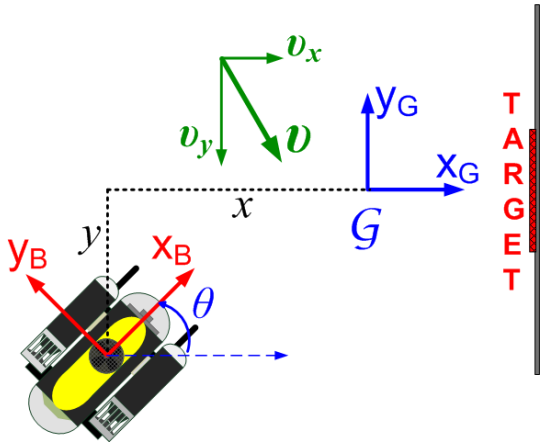

Figure 1.1: The considered scenario: The unicycle-like marine vehicle should be driven and remain into a neighborhood of the origin $\boldsymbol{q_G} = [0 \quad 0 \quad 0]^\top$, despite the effect of the current disturbance $\boldsymbol{v}$

turbances should be also considered so that the closed-loop system performs efficiently in real environmental conditions.

Various control strategies have been proposed for the stabilization of underactuated marine vehicles. Pioneer work has been done in [WSE95a], where a smooth state-feedback law stabilizes an underactuated ship to an equilibrium manifold. Smooth, time-varying controllers yielding asymptotic stability to the origin are proposed in [PE99, PF00, DJPN02, DG05] whereas discontinuous controllers in [Rey96, FLMP00, AP01, GMBD06, CYZ02]. Hybrid control schemes have been also presented in [KBH02, AP02b, GH08].

None of the aforementioned studies takes into account the influence of environmental disturbances. To the best of our knowledge, pioneer work in this direction was presented in [PN00], which considers the dynamic positioning of a ship. The proposed time-varying control law provides semi-global practical asymptotic stability. In [AP07] the dynamic positioning of an underactuated AUV in the presence of a constant, unknown current is considered. An adaptive controller yields convergence to a desired target point, whereas the final orientation is aligned with the direction of the current. The same philosophy regarding the final orientation is adopted in [PDS08], which addresses the station-keeping for a surface vessel in the presence of wind disturbances. In [AHP07a] a switching feedback control law stabilizes an underactuated AUV around a small neighborhood of the origin, yielding input-to-state practical stability in the presence of disturbances and measurement noise.

Despite these contributions, it is generally accepted that the stabilization of underactuated underwater vehicles in the presence of disturbances has only been partially addressed and is still open in many respects.

In principle, allowing the desired orientation of the marine vehicle to be ruled by external disturbances, as done, for instance, in [PF00, PN01, PDS08] is not acceptable in many marine applications, either for safety or for performance reasons. One such example is the case of a unicycle-like underwater vehicle or surface vessel, under the presence of a current disturbance $\boldsymbol{v}$, which is used to inspect a stationary target through its onboard camera, see Fig. 1.1. For the inspection task to be effective, the vehicle is required to converge to the origin $\boldsymbol{q_G} = \begin{bmatrix} 0 & 0 & 0 \end{bmatrix}^\top$

of the global frame $\mathcal{G}$. However, the perturbation induced by the current is non-vanishing at $\boldsymbol{q_G}$, and thus the origin is not an equilibrium point. Consequently, it is meaningless to search for control laws that yield the system asymptotically stable at $\boldsymbol{q_G}$. Instead, one can aim at rendering the system uniformly ultimately bounded within a set that contains the origin, addressing thus the practical stabilization problem.

Contribution

In Chapter 3, we propose a hysteresis-based switching control strategy which yields global, practical stability for a unicycle-like marine vehicle, under current-induced, non-vanishing perturbations. Under the proposed control scheme, the vehicle converges and remains into a set G around the origin. The resulting performance is achieved via state-based switching among three controllers. The first controller is active outside the set G, and drives the system trajectories into G using a dipole-like vector field [PTK10]. The other two controllers are active inside G, and alternately regulate the position and the orientation of the vehicle. The switched system is shown to be robust, in the sense that the system trajectories enter and remain into G even when only a maximum bound $\|\boldsymbol{v}\|_{\max}$ on the current disturbance is given.

Compared to earlier relevant work on dynamic positioning which drop the specification on the desired orientation, the proposed control strategy allows also for the regulation of the vehicle's orientation to zero, during the time intervals when the corresponding controller is active. This feature, along with the robustness property, renders the proposed solution suitable for applications where both the position and orientation of a robot are critical, e.g. for inspection tasks. ■

1.2.2 Underactuated systems under configuration constraints

From a practical viewpoint, one furthermore should not overlook that control systems are subject to (hard) state constraints, encoding safety or performance criteria. An illustrative paradigm is the classical motion planning problem, involving one (or more) agent(s) moving in obstacle environments while avoiding collisions; the obstacle space represents a subset of the configuration space where the agent(s) should never enter, and can thus be codified via inequality configuration constraints, which should never be violated. This problem has been widely addressed and various methodologies have appeared [CLH$^+$05].

Another example of hard state constraints is encountered in the case of agents that have limited sensing capabilities while accomplishing a task. For instance, consider an underactuated robotic vehicle equipped with sensors (e.g. cameras) with limited range and angle-of-view, which has to surveil a target of interest; the requirement of always having the target in the camera field-of-view (f.o.v.) imposes a set of inequality state constraints, which should never be violated so that the target is always visible. This problem, often termed as *maintaining visibility*, applies in leader-follower formations where the leader is required to always be visible to the follower [DFK$^+$02,CSVS03,MBP11], in landmark-based navigation [KR05,BMCH07,LK07], in autonomous inspections where an underwater robotic vehicle is used to inspect a (stationary) target in the presence of environmental disturbances [PMS$^+$09], or in visibility-based pursuit-evade problems, see [DFB10] and the references therein. Similar specifications in terms of state

constraints apply in *maintaining connectivity* problems, involving n nonholonomic agents with limited sensing and/or communication capabilities that have to accomplish a common task while always staying connected [BCM09].

It is noteworthy that all the above mentioned control problems of various formulations and objectives have in common that the control design pertains to nonlinear systems which are subject to both nonholonomic and state constraints.

Contribution

In Chapter 5 we propose a control design methodology for a class of nonholonomic systems which are subject to hard state constraints. The state constraints are realized as nonlinear inequalities w.r.t. the state variables, which constitute a closed subset K of the state space $\mathcal{Q}$. The set K is thus the subset of state space in which the system trajectories should evolve $\forall t \geq 0$. System trajectories which either start out of K, or escape K for some $t > 0$ immediately violate the state constraints and thus are not acceptable. Therefore, the control objective reduces into finding a (possibly switching) state feedback control law, so that system trajectories starting in K converge to a goal set G in K without ever leaving K.

The proposed approach combines concepts from viability theory[3] and results from our work on the state feedback control of n-dimensional nonholonomic systems with Pfaffian constraints (Chapter 4). In the sequel, following [Aub91], state constraints are called *viability* constraints, the set K is called the *viability set* of the system, and system trajectories that remain in K $\forall t \geq 0$ are called *viable*.

In particular, we adopt the concept of tangency to a set K defined by inequality constraints [Aub91], and provide the necessary conditions under which the admissible velocities of a kinematic nonholonomic system are viable in K, as well as the necessary conditions for selecting viable controls. In addition, given the control solutions in Chapter 4, we propose a way of redesigning them by means of switching control, so that the resulting trajectories are viable in K and furthermore converge to a goal set $G \subset K$.

As a case study, we consider the motion planning for an underactuated marine vehicle which is subject to configuration constraints because of limited sensing; the onboard sensor system consists of a camera with limited angle-of-view and two laser pointers of limited range. The task is defined as to control the vehicle so that it converges to a desired configuration w.r.t. a target of interest, while the target is always visible in the camera f.o.v.; in that sense, this is also a problem of maintaining visibility. The visibility maintenance requirement, along with limited sensing, impose a set of configuration constraints that define a viability set K. The robustness of the proposed control approach under a class of bounded perturbations is also studied.

Compared to similar existing approaches, let us mention that the problem formulation is similar to the characterization of viable capture basins of a target set C in a constrained set K [Aub01], which is based on the Frankowska method that characterizes the backward invariance and (local) forward viability of subsets by means of the value function of an optimal control problem.

[3]Viability theory describes the evolution of systems under the consideration that for different reasons, not all system evolutions are acceptable or possible. The system must obey state (viability) constraints, and system solutions should be viable in the sense that they must satisfy, at each time instant, these constraints [Aub91].

However, we rather address the problem in terms of set invariance [Bla99, BM08], where the objective is to render the viability set K a positively invariant (or controlled invariant) set, and the goal set G the largest invariant set of the system by means of state feedback control.[4]

The notion of controlled invariance for linear systems has been utilized for the control design of systems with first-order (kinematic) nonholonomic constraints, after linearizing the nonlinear system equations around the equilibrium [MBP11]; compared to this work, here we present a method which addresses a wider class of constrained underactuated systems, including the class of nonholonomic systems with second-order (dynamic) nonholonomic constraints, without the need for linearizing the system equations, but rather working in the initial coordinates.

Finally, the motion control of underactuated marine (underwater, surface) vehicles and ships has been treated in the past using various control design techniques, see for instance [Leo95, PE99, PF00, AP02a, DJPN04]; however, to the best of our knowledge, none of the relevant work considers any additional state (configuration) constraints on the system. ■

1.2.3 Control of Leader-Follower formation in environment with obstacles

The control design proposed in Chapters 4, 5 can be applied to other applications as well. To illustrate this, in Chapter 6 we consider the case of two mobile robots with unicycle kinematics that have to operate in a leader-follower fashion in a known environment with obstacles, while communication between them is not available. We assume that one of the robots (the leader L) is given a high-level motion plan for moving from an initial to a goal state in the free space, while the task for the second robot (the follower F) is to move while keeping a fixed distance and orientation w.r.t. L, using the information from an onboard camera only, while also avoiding collisions. Since explicit communication is absent, the robots can stay connected if and only if L is always visible in the f.o.v. of F. The latter specification imposes a set of visibility constraints, which should never be violated so that F always maintains visibility with L. Furthermore, avoiding collisions with obstacles, as well as between robots should be guaranteed.

Contribution

In Chapter 6 we propose a cooperative control scheme for the motion of the formation in a known obstacle environment, so that both collision avoidance and maintaining visibility are ensured. Following the approach described in Chapters 4, 5, visibility constraints are realized as nonlinear inequalities in terms of the system states, that determine a closed subset K of the state space, called the visibility set K. Maintaining visibility is thus translated into controlling the robots so that system trajectories starting in K always remain in K. Thus, inspired by ideas from viability theory and using the notion of dipolar vector fields, we provide the conditions for visibility maintenance, as well as a control scheme that forces F to converge and remain into a set of desired configurations w.r.t. L while maintaining visibility. Furthermore, based on a tractor-trailer consideration, we propose a cooperative control scheme for the $\mathrm{L}-\mathrm{F}$ motion in a known obstacle environment, so that both collision avoidance and maintaining visibility

[4]The viability property has been introduced as “controlled invariance" for linear and smooth nonlinear systems [Aub91].

are ensured. The proposed control schemes are decentralized, in the sense that there is no direct communication between the robots, nor global state feedback is available to them. The follower is localized w.r.t. L, however is aware neither of the leader's navigation plan, nor of its velocities at each time instant. The leader is not aware of the follower's state, but rather moves in a way that indirectly ensures collision avoidance for both of them. The efficacy of our algorithms is evaluated through simulations. ■

Finally, in Chapter 7 we present a viability formulation which is based on optimal control, for the control of an underactuated underwater vehicle under the influence of a known, constant current and state constraints. The overall control problem is described by three problems in terms of viability theory. We present a solution to the first problem which addresses the safety of the system, i.e. guarantees that there exists a control law such that the vehicle always remains into the safe set of state constraints. In particular, we have adopted the theoretical results of [Lyg04], which connect viability with optimal control. Then, considering a safe set of state constraints, resulting from the task specifications and the limited sensing capability of the vehicle, we investigate whether there exists a control law that keeps the vehicle in this safe set, despite the influence of the current. The resulting "bang-bang" control law guarantees that the vehicle will remain in the safe set. In order to overcome the computational limitations due to the high dimension of the system we develop a two-stage approach, based on forward reachability and game theory. The control law is thus the safety controller when the system viability is at stake, i.e. close to the boundary of the safe set. The viability kernel and the control law are numerically computed.

Chapter 2

Control Design using Dipole-like Vector Fields: Motivation and Preliminary Results

Abstract

This chapter introduces a **preliminary** form of dipolar vector fields, which we call the *dipole-like* vector fields, originally appeared in [PTK10]. We present the analytical construction of the dipole-like vector fields, which is inspired by the form of the flow lines of the electric point dipole. This preliminary form served as the basis for later introducing the family of dipolar vector fields, presented in detail in Chapter 4. Moreover, a preliminary connection between a dipole-like vector field and a single Pfaffian constraint is presented, which motivates the introduction of a framework of formal guidelines, that guide the design of discontinuous state feedback control laws for nonholonomic systems; this framework is described in detail in Chapter 4. In this chapter, these preliminary guidelines are applied to the state feedback control design for the unicycle and for the NDI. The efficacy of the derived control laws is demonstrated through simulation results.

The chapter is organized as follows: Section 2.1 provides a brief introduction on Pfaffian constraints. Section 2.2 describes the electric point dipole and the proposed dipole-like vector field. In Section 2.3 the connection between a single nonholonomic Pfaffian constraint and the dipole-like vector field is presented, and state feedback controllers for the unicycle and of the nonholonomic double integrator are proposed. Preliminary conclusions and thoughts on possible extensions are summarized in Section 2.4.

2.1 Pfaffian Constraints

Let us consider the class of nonlinear systems described by

$$\dot{\boldsymbol{q}} = \boldsymbol{f}(\boldsymbol{q}, \boldsymbol{u}), \tag{2.1}$$

where $\boldsymbol{q} \in \mathcal{C}$ is the configuration vector, $\mathcal{C} \subseteq \mathbb{R}^n$ is the configuration space, $\boldsymbol{u} \in \mathcal{U}$ is the vector of $m < n$ control inputs, $\mathcal{U} \subset \mathbb{R}^m$ is the control space, $\boldsymbol{f} : \mathbb{R}^n \times \mathbb{R}^m \to \mathbb{R}^n$ is a vector-valued map describing the system dynamics. The configuration vector $\boldsymbol{q} = \begin{bmatrix} q_1 & \cdots & q_n \end{bmatrix}^\top$ is the vector of generalized coordinates [Blo03].

Let us assume that (2.1) is subject to $\kappa < n$ constraint equations. Each constraint i is of the form

$$\textstyle\sum_{j=1}^{n} a_{ij}(q_1, \ldots, q_n, t)\dot{q}_j + b_i(q_1, \ldots, q_n, t) = 0. \tag{2.2}$$

The differential or Pfaffian form of (2.2) is

$$\textstyle\sum_{j=1}^{n} a_{ij}(q_1, \ldots, q_n, t)\mathrm{d}q_j + b_i(q_1, \ldots, q_n, t)\mathrm{d}t = 0, \tag{2.3}$$

and represents a restriction on the amount by which the generalized coordinates may change in a time interval dt.

If a constraint equation (2.2) is integrable, i.e. if it can be expressed in terms of the generalized coordinates *only*, i.e. as

$$h_i(q_1, \ldots, q_n, t) = 0,$$

it is called a *holonomic* constraint. Otherwise, the constraint is *nonholonomic*. Holonomic constraints may explicitly depend on t (rheonomic), or may be time-independent (scleronomic). A constraint equation (2.2) can be also classified according to the coefficient $b_i(\boldsymbol{q}, t)$. If $b_i(\boldsymbol{q}, t) = 0$ then the constraint is catastatic, whereas $b_i(\boldsymbol{q}, t) \neq 0$ implies that the constraint is acatastatic [Gin95].

In general, a constraint equation represents a restriction on the values that the configuration vector $\boldsymbol{q} \in \mathbb{R}^n$ may have. A **holonomic** constraint implies that the configuration vector $\boldsymbol{q}$ must lie on the $(n-1)$ dimensional surface defined by the constraint equation. The constraint also requires that any new point that results from a displacement in the configuration space should also be on the constraint surface. The corresponding Pfaffian form (2.3) of the constraint equation implies that the infinitesimal displacement of the system must be along the plane in the configuration space that is tangent to the constraint surface. Any other type of displacement would move the point in the configuration space off the constraint surface.

However, when the constraint is **nonholonomic**, it is not possible to identify a constraint surface of the form $h_i(q_1, \ldots, q_n, t) = 0$. Nevertheless, the effect of the Pfaffian constraint equation is to restrict the infinitesimal displacements of the system to lie on a common tangent plane that is dictated by the *current* state of motion. Such a plane may be considered to be a local manifestation of a constraint surface [Gin95].

Nonholonomic constraints in mechanical systems typically arise due to the condition of rolling without sliding, which results in first-order (also called kinematic or velocity) constraints, i.e. constraints on the generalized velocities $\dot{\boldsymbol{q}}$, or due to underactuation, which results in second-order (also called dynamic or acceleration) constraints, i.e. constraints on the generalized accelerations $\ddot{\boldsymbol{q}}$, see for instance the case of underactuated robotic manipulators [ON91] and underactuated underwater vehicles [WSE95b].

In this chapter, we consider a class of nonlinear systems described by (2.1), which are subject to $\kappa = 1$ kinematic nonholonomic, time-independent constraint of the form (2.2). We describe the inspiration for and the construction of the family of 2-dimensional and 3-dimensional dipole-like vector fields and their connection to systems with catastatic Pfaffian constraints, where $b(\boldsymbol{q}) = 0$.

2.2 The Dipole-like Vector Field

The analytical construction of the proposed 2-dimensional and 3-dimensional *dipole-like* vector fields is inspired by the vector field of the *point electric dipole* in a Euclidean workspace $\mathcal{W}$. The characteristic property of the vector field of the point electric dipole, which serves as the motivation for the construction of the dipole-like vector fields and the proposed control strategy, is that *all* flow lines converge to a specific position in $\mathcal{W}$, tangent to a specific direction.

2.2.1 The Electric Dipole

The **physical** electric dipole (Fig. 2.1) is a pair of point charges of equal magnitude but opposite sign, $Q_1 = +Q$, $Q_2 = -Q$, separated by a distance $2a$, where $a > 0$. Let us consider an electric dipole in a workspace $\mathcal{W} \subseteq \mathbb{R}^2$, with the charges located at $\boldsymbol{r}_{Q_1} = \begin{bmatrix} a & 0 \end{bmatrix}^\top$ and $\boldsymbol{r}_{Q_2} = \begin{bmatrix} -a & 0 \end{bmatrix}^\top$ respectively, where $\boldsymbol{r}_{Q_i} \in \mathbb{R}^2$ is the position vector of the charge i with respect to the origin. The dipole moment $\boldsymbol{p}$ of the physical dipole is defined as $\boldsymbol{p} = Q_1 \boldsymbol{r}_{Q_1} + Q_2 \boldsymbol{r}_{Q_2} =$

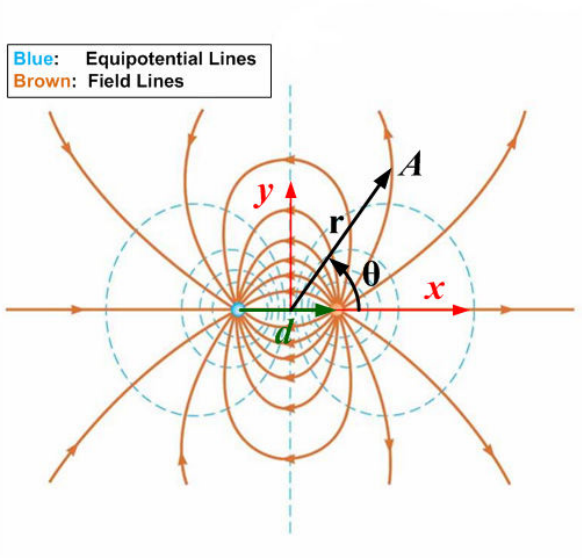

Figure 2.1: Field lines and Equipotential lines of the Electric Dipole

$Q(\boldsymbol{r}_{Q_1} - \boldsymbol{r}_{Q_2}) = Q\boldsymbol{d}$, where $\boldsymbol{d}$ is the vector from the negative to the positive charge.

The **point** dipole is an idealization of the physical dipole, obtained as the distance between the charges tends to zero, $\boldsymbol{d} \to \boldsymbol{0}$, while the dipole moment $\boldsymbol{p}$ is kept constant.

Using polar coordinates, the (electrostatic) potential $V_{\text{dip}}(\boldsymbol{r})$ at a point A in the workspace $\mathcal{W}$, due to a point electric dipole at the origin, is given as [Gri99]

$$V_{\text{dip}}(\boldsymbol{r}) = \frac{1}{4\pi\varepsilon_0} \frac{\boldsymbol{p} \cdot \hat{\boldsymbol{r}}}{r^2} = \frac{1}{4\pi\varepsilon_0} \frac{p \cos\theta}{r^2}, \tag{2.4}$$

where (r, θ) are the polar coordinates of the position vector $\boldsymbol{r}$ of the point A, $\hat{\boldsymbol{r}}$ is the unit vector along the direction of $\boldsymbol{r}$, and ε_0 is a constant.

The electric vector field $\boldsymbol{E}_{\text{dip}}(\boldsymbol{r})$ of the point dipole is defined as the negative gradient of the electric potential $V_{\text{dip}}(\boldsymbol{r})$, $\boldsymbol{E}_{\text{dip}} = -\nabla V_{\text{dip}}$. The intensity of this electric field at the point A is written in polar coordinates as [Gri99]

$$\boldsymbol{E}_{\text{dip}}(r, \theta) = E_r \hat{\boldsymbol{r}} + E_\theta \hat{\boldsymbol{\theta}} = \left(\frac{2p \cos\theta}{4\pi\varepsilon_0 r^3} \right) \hat{\boldsymbol{r}} + \left(\frac{p \sin\theta}{4\pi\varepsilon_0 r^3} \right) \hat{\boldsymbol{\theta}}, \tag{2.5}$$

where $\hat{\boldsymbol{r}}, \hat{\boldsymbol{\theta}}$ are the unit vectors along the directions of the polar coordinates (r, θ), respectively. The **flow (or field) lines** are curves that are tangent to the vector field $\boldsymbol{E}_{\text{dip}}$ at each point of

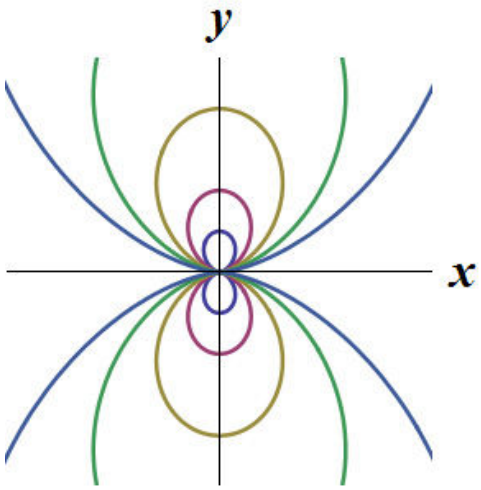

Figure 2.2: Flow lines of the Electric Point Dipole.

the workspace; in other words, the tangent unit vector $\mathrm{d}\boldsymbol{l} = \begin{bmatrix}\mathrm{d}r & r\mathrm{d}\theta\end{bmatrix}^T$ of a flow line at each point of the workspace satisfies: $\mathrm{d}\boldsymbol{l} \times \boldsymbol{E} = \boldsymbol{0}$, where the symbol $\times$ stands for the cross product. From the definition of a flow line one has

$$\frac{\mathrm{d}r}{r\mathrm{d}\theta} = \frac{E_r}{E_\theta} \Rightarrow \frac{\mathrm{d}r}{r\mathrm{d}\theta} = \frac{2\cos\theta}{\sin\theta} \Rightarrow \frac{1}{r}\mathrm{d}r = \frac{2\cos\theta}{\sin\theta}\mathrm{d}\theta \Rightarrow \ln r = 2\ln(\sin\theta) + \text{constant} \Rightarrow$$
$$\ln r = \ln(\sin^2\theta) + \ln R \Rightarrow$$
$$\ln r = \ln(R\sin^2\theta) \Rightarrow r = R\sin^2\theta,$$

where $R > 0$ is a constant associated with the particular flow line [dW01]. Thus, as the distance to the origin tends to zero, $r \to 0$, then $\sin\theta \to 0 \Rightarrow \theta \to 0$ if $x \geq 0$, or $\theta \to \pi$ if $x < 0$, i.e. the flow lines of the point dipole converge to the origin with direction parallel to x-axis, see Fig. 2.2. Similarly one can show that the flow lines of a point dipole having a moment $\boldsymbol{p}$ of polar coordinates (p, θ_1) always converge to the origin with direction parallel to $\boldsymbol{p}$, since they are described by $r = R\sin^2(\theta - \theta_1)$.

In general, the field of the electric point dipole, defined by a dipole moment $\boldsymbol{p} \in \mathbb{R}^3$ in a workspace $\mathcal{W} \subset \mathbb{R}^3$ is [Gri99]

$$\boldsymbol{E}_{\text{dip}}(\boldsymbol{r}) = \frac{1}{4\pi\varepsilon_0 r^3}\big(3(\boldsymbol{p}\cdot\hat{\boldsymbol{r}})\hat{\boldsymbol{r}} - \boldsymbol{p}\big) - \frac{1}{3\varepsilon_0}\boldsymbol{p}\delta^3(\boldsymbol{r}), \tag{2.6}$$

where $\delta^3(\cdot)$ is a 3-dimensional Dirac function. Using spherical coordinates, one can show that if the field is axial-symmetric, then the flow lines converge to the origin, parallel with the dipole moment $\boldsymbol{p}$.

Motivated by and following (2.6), we propose the class of *dipole-like vector fields*

$$\mathbf{F}(\boldsymbol{q}) = \overbrace{\lambda(\boldsymbol{p}\cdot\boldsymbol{q})\boldsymbol{q} - \boldsymbol{p}}^{\mathbf{F_1}(\boldsymbol{q})} + \overbrace{\boldsymbol{p}\exp^{-\|\boldsymbol{q}\|^2}}^{\mathbf{F_2}(\boldsymbol{q})}, \tag{2.7}$$

where $\boldsymbol{q} \in \mathbb{R}^n$ is a vector of generalized coordinates, $\boldsymbol{p} \in \mathbb{R}^n$ is the dipole moment vector, $\|\boldsymbol{q}\|$ is the Euclidean norm of $\boldsymbol{q}$ and $\lambda \geq 2$ is a constant.

To illustrate the properties of the dipole-like vector fields (2.7), let us take $\boldsymbol{q} = \begin{bmatrix} x & y \end{bmatrix}^\top \in \mathbb{R}^2$, where x, y are the position coordinates w.r.t. a cartesian frame $\mathcal{G}$ in a workspace $\mathcal{W} \subset \mathbb{R}^2$, $\lambda = 3$ and $\boldsymbol{p} = \begin{bmatrix} 1 & 0 \end{bmatrix}^\top$. The analytical expression of (2.7) then reads $\mathbf{F}(x, y) = \mathrm{F}_x \, \hat{\boldsymbol{x}} + \mathrm{F}_y \, \hat{\boldsymbol{y}}$, where

$$\mathrm{F}_x = 3x^2 - 1 + e^{-(x^2+y^2)}, \tag{2.8a}$$

$$\mathrm{F}_y = 3xy. \tag{2.8b}$$

The vector field (2.8) is illustrated in Fig. 2.3(b). Note that the dipole-like vector field (2.8) vanishes only at the origin, i.e. $\mathbf{F}(\boldsymbol{q}) = \mathbf{0}$ if and only if $\boldsymbol{q} = \mathbf{0}$. One can verify this by setting $\mathrm{F}_x = \mathrm{F}_y = 0$, which holds if and only if $x = y = 0$. The origin is thus the unique critical (or singular) point of the vector field.

Note also that it is the vector field $\mathbf{F_2}(\boldsymbol{q})$ that actually establishes the desired convergence properties near the origin $(0, 0)$; to verify this, consider the Fig. 2.3(a), which depicts the 2-dimensional vector field $\mathbf{F_1}(x, y)$. The flow lines of $\mathbf{F_1}(x, y)$ are similar with those of the physical electric dipole (Fig. 2.1). Thus, the influence of $\mathbf{F_2}(x, y)$, when added to $\mathbf{F_1}(x, y)$, is what produces the flow lines of the desired convergence properties near the origin $(0, 0)$, as shown in Fig. 2.3(b). A more detailed analysis regarding on the type of the critical point and the local behavior of the flow lines in a neighborhood around it is given in Chapter 4.

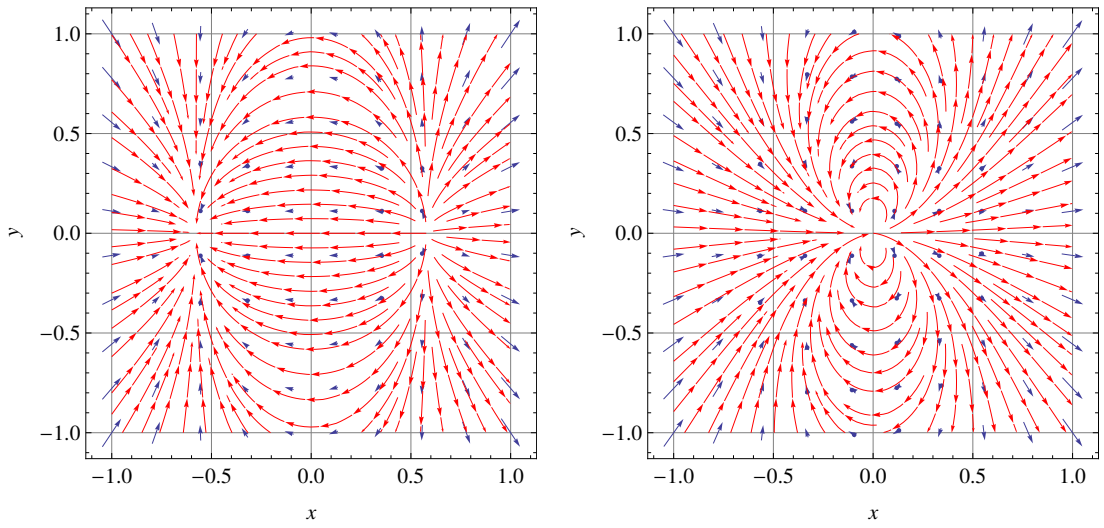

Figure 2.3: The vector field $\mathbf{F_1}(x, y)$ and the dipole-like vector field $\mathbf{F}(x, y)$

The behavior of the flow lines of the dipole-like vector field (2.8) around the origin $(0, 0)$ is the motivation for the control strategy adopted for the unicycle, see Section 4.7. To get an early grasp of the control design idea, assume that a dipole moment vector $\boldsymbol{p} = \begin{bmatrix} p_x & p_y \end{bmatrix} \in \mathbb{R}^2$ is assigned at a goal position $\boldsymbol{r_G} = \begin{bmatrix} x_G & y_G \end{bmatrix}^\top$ such that its direction $\phi_p = \mathrm{atan2}(p_y, p_x)$ coincides with a desired orientation θ_G. Then, the resulting flow lines converge to the goal position $\boldsymbol{r_G}$ with direction $\phi_p \pm \xi\pi$, $\xi = 0, 1$. Then, one could claim that the control objective for the unicycle reduces into designing a state feedback control law such that the system reaches the desired configuration $\boldsymbol{q_G} = \begin{bmatrix} x_G & y_G & \theta_G \end{bmatrix}^\top$ **by following the flow lines as reference paths**.

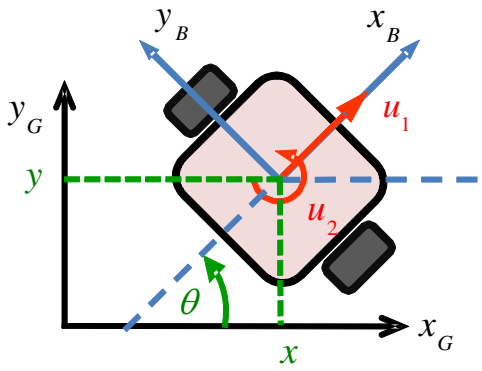

Figure 2.4: The configuration of a unicycle-like mobile robot w.r.t. a global frame $\mathcal{G}$.

2.3 Dipole-like Fields and Nonholonomic Systems

Given the n-dimensional dipole-like field (2.7), we would like to investigate whether there exists a possible relevance between the convergence properties of its flow lines, and the (single) Pfaffian constraint of a kinematic nonholonomic system. To do so, we first study the unicycle, which is frequently used to model the kinematics of underactuated systems such as wheeled mobile robots.

2.3.1 The Unicycle

Consider the motion of a robot in a workspace $\mathcal{W} \subset \mathbb{R}^2$, which is described by the unicycle kinematics

$$\begin{bmatrix} \dot{x} \\ \dot{y} \\ \dot{\theta} \end{bmatrix} = \begin{bmatrix} \cos\theta \\ \sin\theta \\ 0 \end{bmatrix} u_1 + \begin{bmatrix} 0 \\ 0 \\ 1 \end{bmatrix} u_2, \tag{2.9}$$

where $\boldsymbol{q} = \begin{bmatrix} x & y & \theta \end{bmatrix}^\top \in \mathcal{C} \subset \mathbb{R}^3$ is the configuration vector, $\mathcal{C}$ is a smooth manifold denoting the configuration space of the robot, x, y are the position coordinates and θ is the orientation of the robot with respect to a global cartesian coordinate frame $\mathcal{G}$. The control inputs of the system are the linear velocity u_1 and the angular velocity u_2 of the robot, expressed in the body-fixed frame $\mathcal{B}$. Denote $\boldsymbol{u} = \begin{bmatrix} u_1 & u_2 \end{bmatrix}^\top \in \mathcal{U} \subset \mathbb{R}^2$ the vector of control inputs, and $\mathbf{g_1}(\boldsymbol{q}) = \begin{bmatrix} \cos\theta & \sin\theta & 0 \end{bmatrix}^\top$, $\mathbf{g_2} = \begin{bmatrix} 0 & 0 & 1 \end{bmatrix}^\top$ the control vector fields.

The system (2.9) is subject to $\kappa = 1$ nonholonomic catastatic constraint

$$\underbrace{\begin{bmatrix} \sin\theta & -\cos\theta & 0 \end{bmatrix}}_{\boldsymbol{a}^\top(\boldsymbol{q})} \begin{bmatrix} \dot{x} \\ \dot{y} \\ \dot{\theta} \end{bmatrix} = 0 \Rightarrow \boldsymbol{a}^\top(\boldsymbol{q})\dot{\boldsymbol{q}} = 0, \tag{2.10}$$

which essentially expresses that the linear velocity of the robot along the body-fixed y_B axis, i.e. perpendicular to the wheels, is always equal to zero. This results from the assumption that the wheels are only rolling without slipping.

The Pfaffian form of the constraint equation implies that the vector of infinitesimal displacements $\mathrm{d}\boldsymbol{q}$ should lie tangent to the local manifestation of the constraint surface, whose normal is the constraint vector $\boldsymbol{a}^\top(\boldsymbol{q})$. Recall from Linear Algebra that the kernel (or null space) of a $k \times n$ matrix $\boldsymbol{A}$ is the set of all $\mathbf{x} \in \mathbb{R}^n$ such that $\boldsymbol{A}\mathbf{x} = \mathbf{0}$. If the matrix $\boldsymbol{A}$ has linearly independent rows and $k \leq n$, then the dimension of the null space of $\boldsymbol{A}$ is $\dim(\ker \boldsymbol{A}) = n - k$. Thus, the constraint equation implies that the subspace of the infinitesimal displacements $\mathrm{d}\boldsymbol{q}$ at a fixed $\boldsymbol{q}$ is given as the kernel of $\boldsymbol{a}^\top(\boldsymbol{q})$.

Let us now assume that the goal configuration $\boldsymbol{q_G}$ is the origin, $\boldsymbol{q_G} = \mathbf{0}$. The constraint equation at $\boldsymbol{q_G}$ reads

$$\underbrace{\begin{bmatrix} 0 & -1 & 0 \end{bmatrix}}_{\boldsymbol{a}^\top(\boldsymbol{q_G})} \begin{bmatrix} \dot{x} \\ \dot{y} \\ \dot{\theta} \end{bmatrix} = 0 \Rightarrow \langle \boldsymbol{a}^\top(\boldsymbol{q_G}), \dot{\boldsymbol{q}} \rangle = 0, \tag{2.11}$$

where $\langle \cdot, \cdot \rangle$ stands for the inner product. Then, the constraint equation (2.11) implies that the vector of generalized velocities $\dot{\boldsymbol{q}}$ at the goal configuration $\boldsymbol{q_G}$ is restricted to lie in the $n - \kappa = 2$ dimensional subspace (hyperplane) $\mathcal{V}$ of the tangent space $T_{\boldsymbol{q_G}}(\mathcal{C})$ of $\mathcal{C}$ at $\boldsymbol{q_G}$. In other words, the hyperplane $\mathcal{V}$ is the set of all $\dot{\boldsymbol{q}} = \begin{bmatrix} \dot{x} & 0 & \dot{\theta} \end{bmatrix}^\top$ satisfying the constraint at the goal configuration $\boldsymbol{q_G}$, see Fig. 2.5. Thus, only the $n - \kappa$ components of $\dot{\boldsymbol{q}}$ can be chosen

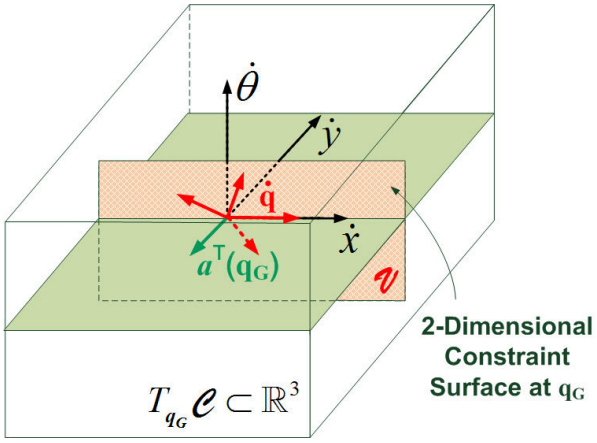

Figure 2.5: The hyperplane $\mathcal{V}$ serves locally as the $n - \kappa$ dimensional constraint surface at the goal configuration $\boldsymbol{q_G}$, whose normal is the constraint vector $\boldsymbol{a}^\top(\boldsymbol{q_G})$. The allowed generalized velocities $\dot{\boldsymbol{q}}$ at $\boldsymbol{q_G}$ lie tangent to $\mathcal{V}$.

independently, whereas the remaining κ need to be set to satisfy the Pfaffian constraints [LaV06].

Having a geometric interpretation of the Pfaffian constraint, one is interested in designing a dipole-like field $\mathbf{F}(\boldsymbol{q})$, given by (2.7), such that its flow lines

- converge to the goal configuration $\boldsymbol{q_G}$,
- are consistent with the constrained dynamics.

We call a flow line consistent if its tangent vector satisfies the Pfaffian constraint. For the unicycle, one has that the flow lines of a dipole-like vector field, taken out of (2.7) as $\mathbf{F}(x, y, \theta) = \mathrm{F}_x \hat{\boldsymbol{x}} + \mathrm{F}_y \hat{\boldsymbol{y}} + \mathrm{F}_\theta \hat{\boldsymbol{\theta}}$, should satisfy

$$\underbrace{\begin{bmatrix}\sin\theta & -\cos\theta & 0\end{bmatrix}}_{\boldsymbol{a}^\top(\boldsymbol{q})} \begin{bmatrix}\mathrm{F}_x \\ \mathrm{F}_y \\ \mathrm{F}_\theta\end{bmatrix} = 0 \Rightarrow \mathrm{F}_x \sin\theta - \mathrm{F}_y \cos\theta = 0. \tag{2.12}$$

Note that the F_θ component of the vector field *does not affect whether the constraint is satisfied*. Therefore, in this case one can define an $\mathrm{N} = 2$ dimensional dipole-like field, in terms of F_x, F_y only, with $\mathrm{F}_\theta = 0$. (This decision is system-dependent.)

The vector field $\mathbf{F}(\cdot)$ is generated by a dipole moment vector $\boldsymbol{p} \in \mathbb{R}^{\mathrm{N}}$. The vector $\boldsymbol{p}$ is required to lie on the (local manifestation of the) constraint surface at $\boldsymbol{q_G}$, in order to be consistent with the Pfaffian constraint, which reads:

$$\langle \boldsymbol{a}^\top(\boldsymbol{q_G}), \boldsymbol{p} \rangle = 0 \Rightarrow \begin{bmatrix}-\sin(0) & \cos(0) & 0\end{bmatrix} \begin{bmatrix}p_x \\ p_y \\ p_\theta\end{bmatrix} = 0, \tag{2.13}$$

where we can directly set $p_\theta = 0$, for the same reason that F_θ can be set to zero. The condition (4.9) is satisfied for any $p_x \in \mathbb{R}$ and for $p_y = 0$, but since $\boldsymbol{p}$ needs to be nonzero, we have to set $\boldsymbol{p} \triangleq \begin{bmatrix}p_x & 0\end{bmatrix}^\top$ with $p_x \neq 0$. Typically, one can set $p_x = 1$.

Thus, one can take a dipole-like vector field out of (2.6), for $\boldsymbol{p} = \begin{bmatrix}1 & 0\end{bmatrix}^\top$ and by ignoring the $\frac{1}{4\pi\varepsilon_0 r^3}$ factor, to get the following simple analytical expression in polar coordinates:

$$\mathrm{F}_x = 2\cos^2\phi - \sin^2\phi, \;\; \mathrm{F}_y = 3\sin\phi\cos\phi, \;\; \mathrm{F}_\theta = 0, \tag{2.14}$$

with (r, ϕ) being the polar representation of (x, y).[1] The flow line equation is $\frac{dr}{d\phi} = \frac{2r\cos\phi}{\sin\phi}$, and assuming that the unicycle vector field is initially aligned to the flow line tangent vector, implying $3xy\cos\theta + (y^2 - 2x^2)\sin\theta = 0$, we can verify that the flow line is consistent, by computing the derivative of the above condition and verifying that the choice of inputs

$$\begin{aligned} u_1 &= -y[(y^2 - 2x^2)\cos\theta - 3xy\sin\theta - 4x\sin\theta\cos\theta], \\ u_2 &= 2x^2\sin^2\theta + y^2\cos^2\theta + 1 \neq 0, \end{aligned}$$

keeps the system on the flow line.

Having the dipole-like vector field (2.14) at hand, one would like to design a control law so that the unicycle aligns with the dipole-like vector field, and follows the flow lines until converging to $(0, 0)$. To do so, let us first express the misalignment of the unicycle vector field $\dot{\boldsymbol{q}} \in T_{\boldsymbol{q}}(\mathcal{C})$ with the vector field $\mathbf{F}(\boldsymbol{q})$ via the projection of the vector field $\mathbf{F}(\boldsymbol{q})$ on the constraint vector $\boldsymbol{a}(\boldsymbol{q})$, and define the system output:

$$h(\boldsymbol{q}) \triangleq \langle \boldsymbol{a}^\top, \mathbf{F} \rangle = 0.5[3\sin(2\phi - \theta) - \sin\theta].$$

[1] The representation in polar coordinates in this example was chosen just to simplify the expression of the vector field $\mathbf{F}(\cdot)$, and to offer a more intuitive treatment of the control problem. The same steps can be done using cartesian coordinates as well, as shown in Chapter 4.

Then, the control design reduces into seeking a control law that stabilizes $h(\boldsymbol{q})$ to zero, which implies that the system vector field $\dot{\boldsymbol{q}}$ is aligned with $\mathbf{F}(\boldsymbol{q})$, see Fig. 2.6. To do so, one can require that the closed loop dynamics of $h(\boldsymbol{q})$ are exponentially stable: $\dot{h} = -kh$. After some algebra, one can verify that the choice of u_2

$$u_2 = \frac{2kh(\boldsymbol{q})}{3\cos(2\phi-\theta)+\cos\theta} - \frac{6u_1(x\sin\theta - y\cos\theta)\cos(2\phi-\theta)}{r^2(3\cos(2\phi-\theta)+\cos\theta)}, \tag{2.15}$$

with $k > 0$, yields $\dot{h} = -kh$. Note that in (2.15), the term $3\cos(2\phi-\theta)+\cos\theta$ appearing in

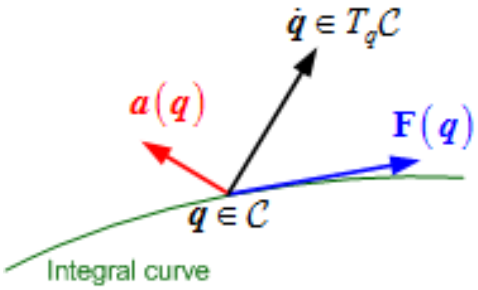

Figure 2.6: At each $\boldsymbol{q} \in \mathcal{C}$, the control design idea for the unicycle is to force the system vector field $\dot{\boldsymbol{q}} \in T_{\boldsymbol{q}}\mathcal{C}$ to align with the vector field $\mathbf{F}(\boldsymbol{q})$. When the system is aligned with $\mathbf{F}$, the output $h(\boldsymbol{q}) \triangleq \langle \boldsymbol{a}^\top, \mathbf{F}\rangle$ is equal to zero.

the denominator may become zero. To avoid this singularity one may resort to switching and set:

$$u_2 = \begin{cases} \frac{2kh(\boldsymbol{q})-6u_1 r^{-2}(x\sin\theta - y\cos\theta)\cos(2\phi-\theta)}{r^2(3\cos(2\phi-\theta)+\cos\theta)}, & |3\cos(2\phi-\theta)+\cos\theta| > \epsilon \\ k(\theta_d-\theta), & |3\cos(2\phi-\theta)+\cos\theta| \le \epsilon, \end{cases} \tag{2.16}$$

where θ_d denotes the direction of $\mathbf{F}$, and ϵ is a small constant. Setting arbitrarily a constantly positive forward speed for the unicycle, $u_1 = \tanh r$,[2] one obtains a closed loop system that converges to $\boldsymbol{q_G} = \mathbf{0}$ following the flow lines of $\mathbf{F}$ (see Fig. 2.7).

2.3.2 Brockett's Nonholonomic Double Integrator

Given the class of n-dimensional dipole-like vector fields (2.7), the procedure of defining an N = 2 dimensional dipole-like vector field for the unicycle, and the proposed control strategy for the unicycle, we would like to investigate whether this control design idea can be applied to other kinematic nonholonomic systems as well. Let us consider the nonholonomic double integrator

$$\begin{bmatrix}\dot{x}_1\\ \dot{x}_2\\ \dot{x}_3\end{bmatrix} = \begin{bmatrix}1\\ 0\\ -x_2\end{bmatrix} u_1 + \begin{bmatrix}0\\ 1\\ x_1\end{bmatrix} u_2, \tag{2.17}$$

[2]Although it is possible to set u_1 as proportional to r^2, to cancel the effect of r^2 in the denominator of (2.15), the choice made here yields faster convergence.

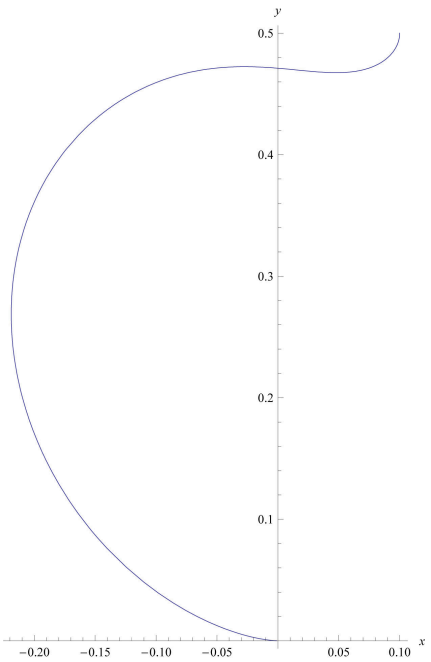

Figure 2.7: Closed loop behavior of a unicycle, initialized at $(x, y, \theta) = (0.1, 0.5, -\frac{\pi}{2})$, with a control law forcing it to follow the flow lines of a dipole-like vector field.

where $\boldsymbol{q} = \begin{bmatrix} x_1 & x_2 & x_3 \end{bmatrix}^\top$ is the state vector, $\mathbf{g_1}(\boldsymbol{q}) = \begin{bmatrix} 1 & 0 & -x_2 \end{bmatrix}^\top$ and $\mathbf{g_2}(\boldsymbol{q}) = \begin{bmatrix} 0 & 1 & x_1 \end{bmatrix}^\top$ are the control vector fields. The system is subject to $\kappa = 1$ nonholonomic constraint given as

$$\underbrace{\begin{bmatrix} x_2 & -x_1 & 1 \end{bmatrix}}_{\boldsymbol{a}^\top(\boldsymbol{q})} \begin{bmatrix} \dot{x}_1 \\ \dot{x}_2 \\ \dot{x}_3 \end{bmatrix} = 0 \Rightarrow \langle \boldsymbol{a}^\top(\boldsymbol{q}), \dot{\boldsymbol{q}} \rangle = 0. \tag{2.18}$$

The constraint vector at the origin $\boldsymbol{q_G} = \mathbf{0}$ reads $\boldsymbol{a}^\top(\boldsymbol{q_G}) = \begin{bmatrix} 0 & 0 & 1 \end{bmatrix}$. Thus, the generalized velocities $\dot{\boldsymbol{q}}$ are restricted to lie in the $n - \kappa = 2$ dimensional hyperplane $\mathcal{V}$ of the tangent space $T_{\boldsymbol{q_G}}(\mathcal{C})$ at $\boldsymbol{q_G}$, which is the set of all $\dot{\boldsymbol{q}} = \begin{bmatrix} \dot{x}_1 & \dot{x}_2 & 0 \end{bmatrix}^\top$ that satisfies (2.18), see Fig. 2.8. As done in the unicycle case, a dipole-like vector field $\mathbf{F}(\boldsymbol{q}) = \mathrm{F}_{x_1}\hat{\boldsymbol{x}}_\mathbf{1} + \mathrm{F}_{x_2}\hat{\boldsymbol{x}}_\mathbf{2} + \mathrm{F}_{x_3}\hat{\boldsymbol{x}}_\mathbf{3}$ should satisfy the constraint equation

$$\underbrace{\begin{bmatrix} x_2 & -x_1 & 1 \end{bmatrix}}_{\boldsymbol{a}^\top(\boldsymbol{q})} \begin{bmatrix} \mathrm{F}_{x_1} \\ \mathrm{F}_{x_2} \\ \mathrm{F}_{x_3} \end{bmatrix} = 0 \Rightarrow \mathrm{F}_{x_1} x_2 - \mathrm{F}_{x_2} x_1 + \mathrm{F}_{x_3} = 0. \tag{2.19}$$

In this case, all the vector field components F_{x_j}, $j = 1, 2, 3$, appear in (2.19). Thus, contrary to the unicycle case, here we can not drop any of the vector field components, and need to define an $\mathrm{N} = 3$ dimensional dipole-like field in terms of F_{x_1}, F_{x_2}, F_{x_3}, dependent on the full state vector $\boldsymbol{q}$.

The vector field will be generated by a dipole moment vector $\boldsymbol{p}$ satisfying the nonholonomic constraint at the goal configuration $\boldsymbol{q_G}$, which reads: $\langle \boldsymbol{a}^\top(\boldsymbol{q_G}), \boldsymbol{p} \rangle = 0$. This condition holds for $\boldsymbol{p} = \begin{bmatrix} p_1 & p_2 & 0 \end{bmatrix}^\top$, where $p_1, p_2 \in \mathbb{R}$. Let us take $\boldsymbol{p} = \begin{bmatrix} 1 & 0 & 0 \end{bmatrix}^\top$ and $\lambda = 1$, then one has

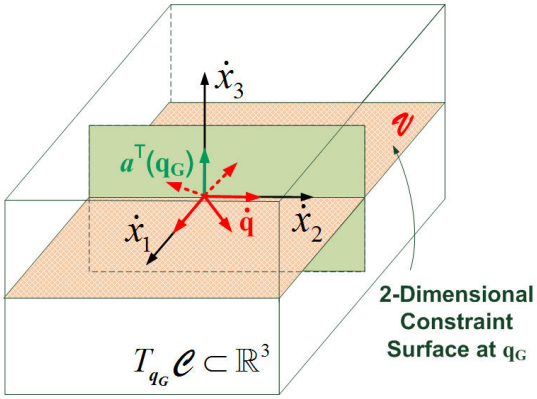

Figure 2.8: The hyperplane $\mathcal{V}$ serves locally as the $n-\kappa$ dimensional constraint surface at the goal configuration $\boldsymbol{q_G}$, whose normal is the constraint vector $\boldsymbol{a}^\top(\boldsymbol{q_G})$. The allowed generalized velocities $\dot{\boldsymbol{q}}$ at $\boldsymbol{q_G}$ lie tangent to $\mathcal{V}$.

out of (2.7) that: $\mathrm{F}_{x_1} = x_1^2 - 1 + \exp^{-(x_1^2+x_2^2+x_3^2)}$, $\mathrm{F}_{x_2} = x_1x_2$, $\mathrm{F}_{x_3} = x_1x_3$. The condition (2.19) can serve as an output to be regulated to zero, $h(\boldsymbol{q}) \to 0$, so that the system vector field is aligned with the dipole field. By substituting the field components F_{x_1}, F_{x_2}, F_{x_3} in (2.19) one has

$$h(\boldsymbol{q}) = x_1x_3 - x_2[1 - \exp^{-(x_1^2+x_2^2+x_3^2)}].$$

This condition suggests that the system can be controlled with a strategy that brings first $x_3 \to 0$ and then x_2, $x_1 \to 0$, i.e. in a way such that x_3 converges faster than x_1, x_2 to zero. This is consistent with other relevant control designs for Brockett's integrator [BD96, Ast97].

However, in this particular case the expression of $\dot{h}(\boldsymbol{q})$ is quite complex and makes it difficult to derive a control law so that $\dot{h}(\boldsymbol{q}) = -k\, h(\boldsymbol{q})$. For this reason, we consider a simplified vector field of the form $\mathbf{F}(\boldsymbol{q}) = \lambda(\boldsymbol{p}\cdot\boldsymbol{q})\boldsymbol{q}$, where $\lambda = 1$, $\mathrm{F}_{x_1} = x_1^2$, $\mathrm{F}_{x_2} = x_1x_2$, $\mathrm{F}_{x_3} = x_1x_3$, in order to enable an easier controller design, since now the output to be regulated reads: $h(\boldsymbol{q}) = x_1x_3$.

Following the strategy presented in the previous section, one would like to derive a control law so that $\dot{h} = -kh$, $k > 0$, which reads

$$\begin{aligned} \dot{x}_1x_3 + x_1\dot{x}_3 = -kx_1x_3 \Rightarrow x_3u_1 + x_1(-x_2u_1 + x_1u_2) = -kx_1x_3 \Rightarrow \\ (x_3 - x_2x_1)u_1 + x_1^2u_2 = -kx_1x_3. \end{aligned} \tag{2.20}$$

Note that the condition (2.20) includes both control inputs u_1, u_2. Therefore, one can set the control input $u_1 = -k_1x_1$, $k_1 > 0$, in order to directly regulate $x_1 \to 0$. The control input u_2 is then given out of (2.20) as

$$u_2 = -k\frac{x_3}{x_1} - \frac{x_3 - x_2x_1}{x_1^2}u_1 = -k\frac{x_3}{x_1} + k_1\frac{x_3 - x_2x_1}{x_1} = -(k-k_1)\frac{x_3}{x_1} - k_1x_2,$$

where $k > k_1$, $x_1 \neq 0$.

Consequently, the condition (2.20) suggests that one can choose $u_2 = -k\frac{x_3}{x_1} - \frac{x_3-x_2x_1}{x_1^2}u_1$, where $x_1 \neq 0$, $k > 0$, and $u_1 = -k_1x_1$, $k_1 > 0$. Finally, since $x_1 = 0$ results in $\mathbf{F} = \mathbf{0}$, a switching

strategy can be formulated as:

$$u_1 = \begin{cases} -k_1 x_1, & \text{if } x_1 \neq 0 \\ -k_3 x_3, & \text{if } x_1 = 0 \end{cases} \tag{2.21a}$$

$$u_2 = \begin{cases} -k\frac{x_3}{x_1} - \frac{x_3 - x_2 x_1}{x_1^2} u_1, & \text{if } x_1 \neq 0 \\ -k_2 x_2, & \text{if } x_1 = 0 \end{cases} \tag{2.21b}$$

where $k_2,\ k_3 > 0$.

2.4 Conclusions

The goal of this chapter is to present preliminary ideas on a framework for motion planning and control of systems with kinematic nonholonomic Pfaffian constraints, in which guidelines for the control design can be established in a uniform way across different dynamics. The control law examples presented, therefore, are preliminary and may not claim performance but rather demonstrate that the same design rules can be used for different systems. The basic idea is that one can define a dipole-like vector field, which is used as a reference for the system, and regulate to zero an output expressing the misalignment between the system vector field and the dipole-like field. Preliminary work also suggests that this idea may be compatible with artificial potential field methods used for robot navigation, in which case the development of a new, unified framework for control under combined holonomic and nonholonomic constraints may be feasible.

The systems studied in this chapter fall into the class of drift-less kinematic nonholonomic systems with catastatic Pfaffian constraints. The proposed guidelines, however, can be as well used for the control design of a class of kinematic nonholonomic systems with drift, which are subject to acatastatic Pfaffian constraints. Such an example in presented in Chapter 3.

Chapter 3

Practical Stabilization of a Unicycle with Drift via Switching Control

Abstract

This chapter presents a state feedback solution for the problem of controlling a unicycle-like robot that is subject to a non-vanishing drift vector field. The motivation for studying this problem mainly comes from the dynamic positioning [1] problem for underactuated marine vehicles (ships, surface vessels, underwater vehicles), under the influence of slowly-varying environmental currents. Although the modeling in this chapter has been chosen to be simplified and to rely on the system kinematics only, the applicability of the proposed feedback control solution is not limited, in the sense that it can be used as a velocity reference to be tracked by the system dynamics via standard techniques, like feedback linearization and backstepping.

In this chapter, we present a control solution for the dynamic positioning of a unicycle-like marine vehicle under environmental disturbances by means of switching control. Switching and hybrid control has seen an increasing amount of interest from many viewpoints, featuring thus a solid framework in control theory [YMH98, Bra98, Lib03]. When it comes to nonholonomic stabilization, hybrid controllers that combine a discrete event supervisor and a family of low-level, time-invariant feedback controllers have been presented in [BRM92,OBNtdW95,KRM96], whereas switching among time-varying feedback controllers has been presented in [SE95,KM95, KM96]. In [Mor98, HM99], nonholonomic stabilization is addressed in terms of supervisory control using logic-based switching, whereas [HLM99a, HLM02, HLM03] address the control of uncertain nonholonomic systems in the aforementioned framework. A similar approach where the switching strategy depends on the value of a Lyapunov function is given in [CAP08].

Typically, a switching control system consists of a family of candidate controllers and a switching signal (switching function) that specifies, at each time instant, the active controller that is currently being followed. Thus, switching between the candidate controllers results in a so-called *switched system*. From a control perspective, the term switched systems has been established in the past few years to differentiate this class of continuous-time systems with (isolated) discrete switching events from the wider class of *hybrid systems*, which are characterized by an interaction between continuous and discrete dynamics [Lib03].

The proposed feedback solution involves a hysteresis-based switching control strategy, which renders the system globally practically stable to a set G around a desired position. The control scheme consists of three control laws; the first one is active out of the set G and drives the system trajectories into G, based on a dipole-like vector field. The other two control laws are

[1] The term dynamic positioning refers to a computer controlled system in order to automatically maintain a vessel's position and heading by using its own propellers and thrusters. The dynamic positioning control problem thus reduces into finding a feedback control law that asymptotically stabilizes both position and orientation of the vessel to desired constant values.

active in the set G and alternately regulate the position and the orientation of the vehicle, so that the switched system is practically stable around the desired position. The overall system is shown to be robust, in the sense that the vehicle enters and remains into G even if the external current disturbance is unknown and only its maximum bound is given. The efficacy of the proposed solution is demonstrated through simulation results.

The chapter is organized as follows: Section 3.1 gives the problem formulation and Section 3.2 presents the switching control strategy. The analytic construction of the control laws, the stability analysis of the switched system and the robustness consideration are given in Section 3.3. Section 3.4 includes the simulation results. The conclusions and thoughts on future research are summarized in Section 3.5.

3.1 Problem Formulation

Modeling

Let us consider a marine vehicle which has two back thrusters for the motion on the horizontal plane, but no thruster along the lateral degree-of-freedom (d.o.f.). In general, the modeling and control of this class of marine vehicles does not rely on kinematic considerations only, since the effect of the unactuated lateral d.o.f. is often not negligible, as it is in principle assumed for wheeled mobile robots. Nevertheless, in order to get some first intuition and to simplify the control design, we preliminarily model the vehicle as a unicycle.

Let us also assume that the vehicle moves under the influence of an non-rotational current $\boldsymbol{v}$, with components v_x, v_y w.r.t. a global cartesian coordinate frame $\mathcal{G}$. Note that this is standard modeling for current-induced effects [Fos02]. The equations of motion on the horizontal plane are given as:

$$\dot{\boldsymbol{q}} = \boldsymbol{v} + \boldsymbol{G}(\boldsymbol{q})\boldsymbol{u} \Rightarrow \begin{bmatrix} \dot{x} \\ \dot{y} \\ \dot{\theta} \end{bmatrix} = \begin{bmatrix} v_x \\ v_y \\ 0 \end{bmatrix} + \begin{bmatrix} \cos\theta & 0 \\ \sin\theta & 0 \\ 0 & 1 \end{bmatrix} \begin{bmatrix} u_1 \\ u_2 \end{bmatrix}, \tag{3.1}$$

where $\boldsymbol{q} = \begin{bmatrix} x & y & \theta \end{bmatrix}^\top \in \mathbb{R}^n$ is the system configuration vector, x, y are the position coordinates of the vehicle and θ is the orientation of the vehicle w.r.t. $\mathcal{G}$, $\boldsymbol{u} = \begin{bmatrix} u_1 & u_2 \end{bmatrix}^\top$ is the vector of control inputs, u_1, u_2 are the linear and the angular velocity of the vehicle in the body-fixed frame $\mathcal{B}$ respectively, and $\boldsymbol{v} = \begin{bmatrix} v_x & v_y & 0 \end{bmatrix}^\top$ is the drift (or perturbation) vector field, see Fig. 3.1.

The system (3.1) can be seen as a perturbation (or perturbed system [Kha02]) of the unicycle (2.9), with $\boldsymbol{v}$ being the perturbation term, and the unicycle being the nominal system. Note that the perturbation term is non-vanishing at the origin $\boldsymbol{q_G} = \boldsymbol{0}$, since $\boldsymbol{v}(t, \boldsymbol{q_G}) \neq 0 \ \forall t \in [0, \infty)$.

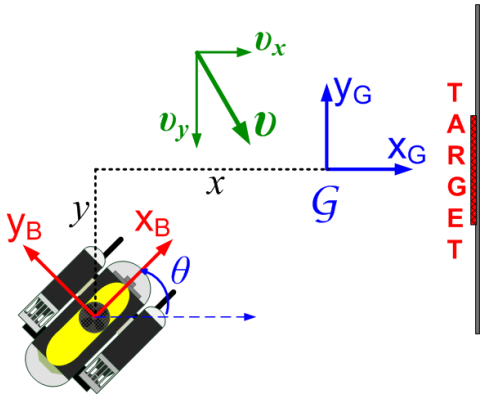

Figure 3.1: The considered scenario: The unicycle-like marine vehicle should be driven and remain into a neighborhood of the origin $\boldsymbol{q_G} = [0 \quad 0 \quad 0]^\top$, despite the effect of the current disturbance $\boldsymbol{v}$

The perturbed system is nonholonomic

The $\kappa = 1$ Pfaffian constraint of the system reads:

$$\underbrace{\begin{bmatrix} -\sin\theta & \cos\theta & 0 \end{bmatrix}}_{\boldsymbol{a}^\top(\boldsymbol{q})} \begin{bmatrix} \dot{x} \\ \dot{y} \\ \dot{\theta} \end{bmatrix} = -v_x \sin\theta + v_y \cos\theta \Rightarrow \boldsymbol{a}^\top(\boldsymbol{q})\dot{\boldsymbol{q}} = b(\boldsymbol{q}), \tag{3.2}$$

The constraint (3.2) is acatastatic, since $b(\boldsymbol{q}) \neq 0$. One can verify that the constraint is non-integrable by using the Frobenius theorem [BL05].

Theorem 1 *(**Frobenius**) A non-singular smooth distribution*[2] *is integrable if and only if it is involutive*[3].

Corollary 1 *The perturbed system* (3.1) *is nonholonomic.*

Proof Consider the distribution of the $k = 3$ smooth system vector fields $\boldsymbol{v}, \mathbf{g_1}(\boldsymbol{q}), \mathbf{g_2}$, that is $\Delta(\boldsymbol{q}) = \text{span}\{\boldsymbol{v}, \mathbf{g_1}(\boldsymbol{q}), \mathbf{g_2}\}$. The dimension of $\Delta(\boldsymbol{q})$ is the rank of $\mathbf{H}(\boldsymbol{q}) = \begin{bmatrix} \boldsymbol{v} & \mathbf{g_1}(\boldsymbol{q}) & \mathbf{g_2} \end{bmatrix}$. The rank of the matrix H$(\boldsymbol{q})$ is $\text{rank}\,(\mathbf{H}(\boldsymbol{q})) = 3, \forall \boldsymbol{q} \in \mathcal{C}$. Since $\dim(\Delta) = k, \forall \boldsymbol{q} \in \mathcal{C}$, the distribution Δ is non-singular. To determine whether Δ is involutive, one has to calculate the Lie brackets for $\boldsymbol{v}, \mathbf{g_1}, \mathbf{g_2}$: $[\mathbf{g_1}, \mathbf{g_2}] = \begin{bmatrix} \sin\theta & -\cos\theta & 0 \end{bmatrix}^\top$, $[\boldsymbol{v}, \mathbf{g_1}] = [\boldsymbol{v}, \mathbf{g_2}] = \begin{bmatrix} 0 & 0 & 0 \end{bmatrix}^\top$. Since $[\mathbf{g_1}, \mathbf{g_2}] \notin \Delta$, the distribution Δ is not involutive and thus (3.1) is nonholonomic. ■

The drift vector field violates the catastatic constraint of the unicycle

Furthermore, the term $b(\boldsymbol{q}) \neq 0$ can be seen as a violation of the catastatic constraint (2.10) of the unicycle. To illustrate this, let us consider the constraint equation evaluated at the goal

[2] Consider a distribution Δ of k smooth vector fields $\boldsymbol{w_i}(\boldsymbol{q})$, $1 \leq i \leq k$, over a smooth manifold $\mathcal{C} \subset \mathbb{R}^n$, $\Delta(\boldsymbol{q}) = \text{span}\{\boldsymbol{w_1}(\boldsymbol{q}), \ldots, \boldsymbol{w_k}(\boldsymbol{q})\}$. The distribution is said to be non-singular (or regular) if $\dim(\Delta(\boldsymbol{q})) = \dim(\Delta) = k$, $\forall \boldsymbol{q} \in \mathcal{C}$.

[3] A non-singular distribution Δ of k smooth vector fields $\boldsymbol{w}$, $\Delta = \text{span}\{\boldsymbol{w_1}, \ldots, \boldsymbol{w_k}\}$, is said to be involutive if for all $\boldsymbol{w_i}$, $\boldsymbol{w_j} \in \Delta$, $1 \leq i, j \leq k$, it follows that $[\boldsymbol{w_i}, \boldsymbol{w_j}] \in \Delta$, where $[\boldsymbol{w_i}, \boldsymbol{w_j}]$ is the Lie bracket of $\boldsymbol{w_i}, \boldsymbol{w_j}$.

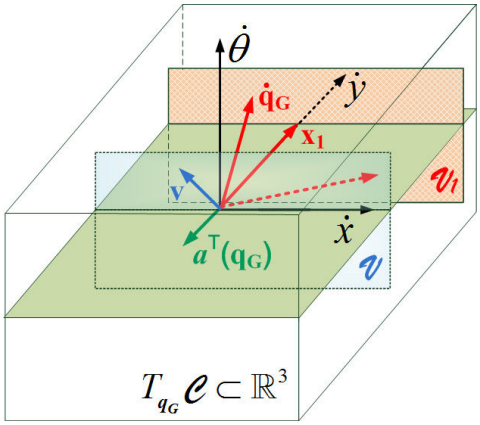

Figure 3.2: The hyperplane that lies tangent to the subspace $\mathcal{V}$ serves locally as the $n - \kappa = 2$ dimensional constraint surface at the goal configuration $\boldsymbol{q_G}$, whose normal is the constraint vector $\boldsymbol{a}^\top(\boldsymbol{q_G})$. The allowed generalized velocities $\dot{\boldsymbol{q}}$ form the affine subspace $\mathcal{V}_1$ of $T_{\boldsymbol{q_G}}(\mathcal{C})$ and *do not* lie tangent to the constraint surface.

configuration $\boldsymbol{q_G} = \mathbf{0}$, that reads

$$\underbrace{\begin{bmatrix} -\sin(0) & \cos(0) & 0 \end{bmatrix}}_{\boldsymbol{a}^\top(\mathbf{0})} \begin{bmatrix} \dot{x} \\ \dot{y} \\ \dot{\theta} \end{bmatrix} = v_y \Rightarrow \boldsymbol{a}^\top(\mathbf{0})\dot{\boldsymbol{q}} = v_y,$$

which is satisfied for all $\dot{\boldsymbol{q}} = \begin{bmatrix} \dot{x} & v_y & \dot{\theta} \end{bmatrix}^\top$. The generalized velocities $\dot{\boldsymbol{q}}$ at the origin form an affine subspace $\mathcal{V}_1$ of the tangent space $T_{\boldsymbol{q_G}}(\mathcal{C})$ at the goal configuration $\boldsymbol{q_G}$, see Fig. 3.2. Note that the subspace $\mathcal{V}_1$ is obtained by translating the null space $\mathcal{V}$ of the constraint vector $\boldsymbol{a}^\top(\boldsymbol{q_G})$, given as $\mathcal{V} = \left\{ \dot{\boldsymbol{q}} \in T_{\boldsymbol{q_G}}(\mathcal{C}) \;\middle|\; \langle \boldsymbol{a}^\top(\boldsymbol{q_G}), \dot{\boldsymbol{q}} \rangle = 0 \right\}$, by the fixed vector $\mathbf{x_1} = \begin{bmatrix} 0 & v_y & 0 \end{bmatrix}^\top \in \mathcal{V}_1$. Note also that $\mathcal{V}$ is the subspace of the generalized velocities $\dot{\boldsymbol{q}}$ that satisfy the corresponding catastatic constraint (i.e. for $b(0) = 0$) at $\boldsymbol{q_G}$. Equivalently, $\mathcal{V}_1$ is the set of all $\mathbf{x_1} + \mathbf{v}$, where $\mathbf{v} \in \mathcal{V}$, and has the same dimension with $\mathcal{V}$, $\dim \mathcal{V}_1 = \dim \mathcal{V}$, where $\dim \mathcal{V} = n - \kappa = 2$.

Recall that, in general, a nonholonomic constraint implies that it is not possible to identify a constraint surface. However, for a system subject to a catastatic nonholonomic constraint ($b(\boldsymbol{q}) = 0$), the kinematically admissible virtual displacement $\delta\boldsymbol{q}$ should satisfy $\boldsymbol{a}^\top(\boldsymbol{q}) \cdot \delta\boldsymbol{q} = 0$ [Blo03]. This is a statement that at each $\boldsymbol{q}$, the virtual displacement vector must lie in a plane whose normal is the constraint vector $\boldsymbol{a}^\top(\boldsymbol{q})$. This plane can be interpreted as the local manifestation of a constraint surface at fixed $\boldsymbol{q}$ [Gin07]. Note also that the subspace $\mathcal{V} = \left\{ \dot{\boldsymbol{q}} \in T_{\boldsymbol{q_G}}(\mathcal{C}) \;\middle|\; \langle \boldsymbol{a}^\top(\boldsymbol{q_G}), \dot{\boldsymbol{q}} \rangle = 0 \right\}$ of the allowed generalized velocities is by definition tangent to the hyperplane that is normal to $\boldsymbol{a}^\top(\boldsymbol{q_G})$; thus, this hyperplane serves as the local constraint surface at $\boldsymbol{q_G}$. Then, the condition $\langle \boldsymbol{a}^\top(\boldsymbol{q_G}), \dot{\boldsymbol{q}} \rangle = b(\boldsymbol{q_G}) \neq 0$ implies that the vector of generalized velocities $\dot{\boldsymbol{q}}$ at the goal configuration $\boldsymbol{q_G}$ *is not* tangent to the (local manifestation of the) constraint surface, see Fig. 3.2. This remark actually verifies the characterization of the term $b(\boldsymbol{q_G})$ as a violation of the catastatic constraint.

Equilibrium Point, Stability and Ultimate Boundedness

The constraint equation (3.2) implies that a configuration $\boldsymbol{q_e} = \begin{bmatrix} x_e & y_e & \theta_e \end{bmatrix}^\top$ is an equilibrium point of (3.1), i.e. that $\dot{\boldsymbol{q}}_{\boldsymbol{e}} = \boldsymbol{0}$ if and only if

$$b(\boldsymbol{q_e}) = 0 \Rightarrow -v_x \sin\theta_e + v_y \cos\theta_e = 0.$$

This condition is consistent with what one would expected from physical intuition, i.e. that the orientation θ_e at the equilibrium is dictated by the external disturbance $\boldsymbol{v} = \begin{bmatrix} v_x & v_y \end{bmatrix}^\top$. Furthermore, the origin $\boldsymbol{q_G} = \begin{bmatrix} 0 & 0 & 0 \end{bmatrix}^\top$ is an equilibrium point of (3.1) if and only if $v_y = 0$. In other words, if $v_y \neq 0$ the origin $\boldsymbol{q_G}$ is no longer an equilibrium point of (3.1), and therefore the trajectories of the closed-loop system can only be uniformly ultimately bounded in a neighborhood of the origin [Kha02].

Nevertheless, allowing the desired orientation to be ruled by external disturbances is in general not acceptable for various applications, e.g. for inspection tasks (Fig. 3.1), in the following sense: assume that the marine vehicle is equipped with an onboard camera and is used to inspect a stationary target. For the inspection task to be effective, the vehicle is required to converge to the origin $\boldsymbol{q_G} = \begin{bmatrix} 0 & 0 & 0 \end{bmatrix}^\top$ w.r.t. the global frame $\mathcal{G}$. However, the perturbation induced by the current is non-vanishing at $\boldsymbol{q_G}$, and thus the origin is not an equilibrium point. Consequently, it is meaningless to search for control laws that yield the system asymptotically stable at $\boldsymbol{q_G}$. Instead, one can aim at rendering the system uniformly ultimately bounded within a set that contains the origin, addressing thus the *practical stabilization* problem. Therefore, the control problem can be formulated as follows:

Problem Statement: Given the nonholonomic system (3.1), which is subject to a non-vanishing perturbation $\boldsymbol{v}$, design a switching signal $\sigma(\cdot) : \mathbb{R}^n \to \mathcal{I} = \{1, 2, \ldots, \chi\}$ and χ feedback control laws $\boldsymbol{u} = \boldsymbol{\psi}_\sigma(t, \boldsymbol{q})$, so that the closed-loop system is ε-practically asymptotically stable around the origin, in the sense that for given $\varepsilon > 0$ and any initial $\boldsymbol{q}_0$ the solution $\boldsymbol{q}(t) = \boldsymbol{q}(t, \boldsymbol{q}_0, \boldsymbol{u})$ exists $\forall t \geq 0$, and furthermore $\boldsymbol{q}(t) \in \mathcal{B}(\boldsymbol{0}, \varepsilon),\ \forall t \geq T$, where $T = T(\boldsymbol{q}_0) > 0$.

3.2 Switching Control Strategy

Dipole-like Vector Fields for the Nominal and the Perturbed System

The control design employs the concept of dipole-like vector fields (2.7). Recall from Chapter 2 that one can define a 2-dimensional dipole-like vector field $\mathbf{F}_{\boldsymbol{n}}$ for the unicycle, and control the system so that it follows the flow lines as reference paths, which converge to $(x, y) = (0, 0)$ with orientation $\phi_n \to 0$. The vector field $\mathbf{F}_{\boldsymbol{n}} = \mathrm{F}_{nx}\,\hat{\boldsymbol{x}} + \mathrm{F}_{ny}\,\hat{\boldsymbol{y}}$ is shown in Fig. 3.3(a) and its analytical expression is given by:

$$\mathrm{F}_{nx} = \lambda p_1 x^2 - p_1 + p_1 e^{-(x^2+y^2)}, \quad \mathrm{F}_{ny} = \lambda p_1 x y. \tag{3.3}$$

Following the ideas presented in Chapter 2, one can construct a dipole-like vector field $\mathbf{F}_{\boldsymbol{p}}$ for the perturbed system (3.1), so that the flow lines converge to the equilibrium point $\boldsymbol{q_e}$. The vector field $\mathbf{F}_{\boldsymbol{p}}$ is generated by a dipole moment vector $\boldsymbol{p_p} \in \mathbb{R}^2$ that satisfies the constraint equation (3.2) at the desired configuration $\boldsymbol{q_G} = \boldsymbol{0}$, which reads: $\begin{bmatrix} 0 & 1 \end{bmatrix} \boldsymbol{p_p} = v_y$. This condition

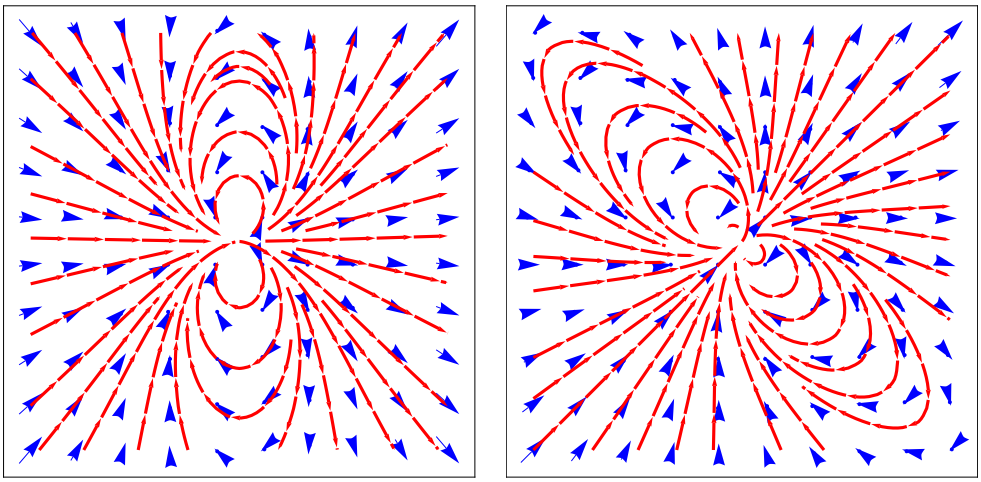

(a) The nominal field $\mathbf{F}_{\boldsymbol{n}}$ (b) The perturbed field $\mathbf{F}_{\boldsymbol{p}}$

Figure 3.3: The fields $\mathbf{F}_{\boldsymbol{n}}(x, y)$ and $\mathbf{F}_{\boldsymbol{p}}(x, y)$ for $\lambda = 3$, $\boldsymbol{p_n} = \begin{bmatrix} p_1 & 0 \end{bmatrix}^\top$, $\boldsymbol{p_p} = \begin{bmatrix} p_1 & v_y \end{bmatrix}^\top$, $p_1 = v_x = 1$ m/sec, $v_y = 1$ m/sec. The flow lines converge to $(x, y) = (0, 0)$ with the direction ϕ_n and ϕ_p of the vectors $\boldsymbol{p}_n$ and $\boldsymbol{p}_p$, respectively. In the case of the perturbed system, the flow lines can not converge to $(0, 0)$ with $\phi_p = 0$, since $v_y \neq 0$.

holds for $\boldsymbol{p_p} = \begin{bmatrix} p_1 & v_y \end{bmatrix}^\top$, where $p_1 \in \mathbb{R}$. Furthermore, note that for $p_1 = v_x$, the direction of the dipole moment is $\theta_{\boldsymbol{p}} = \arctan(\frac{v_y}{v_x}) = \theta_e$.

Consequently, taking $\boldsymbol{p_p} = \begin{bmatrix} v_x & v_y \end{bmatrix}^\top$ results in a vector field $\mathbf{F}_{\boldsymbol{p}}$ whose flow lines converge to the equilibrium of the perturbed system (3.1). The vector field $\mathbf{F}_{\boldsymbol{p}}$ is shown in Fig. 3.3(b) and the analytic form of F_{px}, F_{py} are given by (2.7) as:

$$\mathrm{F}_{px} = \lambda(v_x x + v_y y)x - v_x + v_x e^{-(x^2+y^2)}, \tag{3.4a}$$

$$\mathrm{F}_{py} = \lambda(v_x x + v_y y)y - v_y + v_y e^{-(x^2+y^2)}. \tag{3.4b}$$

Following the Vector Field $\mathbf{F}_{\boldsymbol{p}}$

Given the vector field $\mathbf{F}_{\boldsymbol{p}}$ (3.4), one can design a state feedback control law $\boldsymbol{u} = \boldsymbol{\psi}_1(\boldsymbol{q})$ that forces (3.1) to follow the flow lines. Let us denote the closed-loop system (3.1) under the control law $\boldsymbol{\psi}_1(\boldsymbol{q})$ as the subsystem $\dot{\boldsymbol{q}} = \boldsymbol{f}_1(\boldsymbol{q}, \boldsymbol{\psi}_1)$. Note that by forcing the system to follow the flow lines of $\mathbf{F}_{\boldsymbol{p}}$ the position $\boldsymbol{r} = \begin{bmatrix} x & y \end{bmatrix}^\top$ converges to the origin $(0, 0)$, however the orientation θ converges to the orientation ϕ_p of the vector field $\mathbf{F}_{\boldsymbol{p}}$.

Let us denote $\boldsymbol{q} = \begin{bmatrix} \boldsymbol{r}^\top & \theta \end{bmatrix}^\top$. Inspired by [AHP07b], we say that the subsystem $\boldsymbol{f}_1(\boldsymbol{q}, \boldsymbol{\psi}_1)$ is stable w.r.t. $\boldsymbol{r}$ and unstable w.r.t. θ, in the sense that θ does not converge to the desired value $\theta_d = 0$. In fact, since $\boldsymbol{q_G} = \boldsymbol{0}$ is not an equilibrium point of (3.1), it follows that forcing $\theta \to 0$ via a (different) control law $\boldsymbol{u} = \boldsymbol{\psi}_2(\boldsymbol{q})$ will result in a subsystem $\dot{\boldsymbol{q}} = \boldsymbol{f}_2(\boldsymbol{q}, \boldsymbol{\psi}_2)$ of stable θ, but unstable $\boldsymbol{r}$. In other words, one needs to make a trade-off between regulating the position $\boldsymbol{r}$ to a desired value $\boldsymbol{r_d}$ and regulating the orientation θ to a desired value θ_d. In this sense, one may resort to a switching control strategy between the subsystems $\boldsymbol{f}_1(\boldsymbol{q}, \boldsymbol{\psi}_1)$,

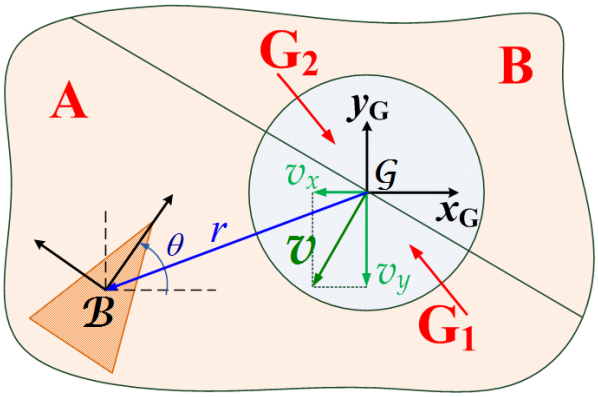

Figure 3.4: Operating regions and system description w.r.t. frame $\mathcal{G}$

$\boldsymbol{f}_2(\boldsymbol{q}, \psi_2)$, to alternately force either the position $\boldsymbol{r}$, or the orientation θ to the corresponding desired values, to eventually get an ε-practically stable system. For a thorough introduction to switching control, the reader is referred to [Lib03].

Switching Control Strategy

In order to design a (state-dependent) switching control strategy, and under the assumption that the disturbance $\boldsymbol{v} = \begin{bmatrix} v_x & v_y \end{bmatrix}^\top$ is known[4], we partition the configuration space $\mathcal{C} \subseteq \mathbb{R}^2 \times [0, 2\pi)$ into the operating regions K and G, such that $K = \left\{ \begin{bmatrix} \boldsymbol{r}^\top & \theta \end{bmatrix}^\top \in \mathcal{C} \;\middle|\; \|\boldsymbol{r}\| > r_0 \right\}$ and $G = \mathcal{C} \setminus K$, see Fig. 3.4.[5]

The region K is divided into $A = \left\{ \boldsymbol{q} \in K \;\middle|\; \langle \boldsymbol{r}, \boldsymbol{v} \rangle \geq 0 \right\}$ and $B = \left\{ \boldsymbol{q} \in K \;\middle|\; \langle \boldsymbol{r}, \boldsymbol{v} \rangle < 0 \right\}$, with $K = (A \cup B)$.

The region G is divided into G_1 and G_2, where $G_1 = \{ \boldsymbol{q} \in G \mid \langle \boldsymbol{r}, \boldsymbol{v} \rangle \geq 0 \}$, $G_2 = \{ \boldsymbol{q} \in G \mid \langle \boldsymbol{r}, \boldsymbol{v} \rangle < 0 \}$ and $G = (G_1 \cup G_2)$. The division of G is inspired by the following consideration: When $\boldsymbol{q} \in G_1$, the disturbance $\boldsymbol{v}$ forces the position trajectories $\boldsymbol{r}(t)$ of the (uncontrolled) system (3.1) away from the desired value $(0, 0)$, whereas when $\boldsymbol{q} \in G_2$, the disturbance forces the position trajectories $\boldsymbol{r}(t)$ towards the desired value $(0, 0)$.

The main idea for the control design is that if $\boldsymbol{q} \in K$, then a control law based on the dipole-like field (3.4) drives the system trajectories into the set G that contains the origin $\boldsymbol{q_G}$. Then, while $\boldsymbol{q} \in G$, the system switches to a control law that regulates the orientation $\theta \to 0$.

However, since the regulation of θ may yield instability w.r.t. the position $\boldsymbol{r}$, it is preferable to control θ when $\boldsymbol{v}$ forces $\boldsymbol{r}$ towards the origin, i.e. when $\boldsymbol{q} \in G_2$. Thus, if the system trajectory $\boldsymbol{q}(t)$ enters G_1 after leaving K, an additional control law is needed to drive $\boldsymbol{q}(t)$ into G_2. This consideration results into switching among $\chi = 3$ candidate controllers $\boldsymbol{\psi}_\sigma(\boldsymbol{q})$, $\sigma \in \{1, 2, 3\}$. Briefly,

[4] This assumption is later dropped, and only the maximum bound of $\boldsymbol{v}$ is considered to be known.

[5] The radius $r_0 > 0$ needs to satisfy the conditions (3.6) and (3.7), which guarantee that the system trajectories $\boldsymbol{r}(t)$ starting in K enter the ball $\mathcal{B}(\boldsymbol{0}, r_0)$ around the origin, i.e. enter in the set G; the detailed analysis is given in Section 3.3.1.

1. the control law $\boldsymbol{\psi}_1(\boldsymbol{q})$ forces the system into G, yielding stable position $\boldsymbol{r}$ and unstable orientation that converges to the orientation of the vector field $\mathbf{F}_{\boldsymbol{p}}$, i.e. $\theta \to \phi$,

2. the control law $\boldsymbol{\psi}_2(\boldsymbol{q})$ forces the system into G_2, in the case that $\boldsymbol{r}$ has reached G_1, yielding unstable both $\boldsymbol{r}$ and $\theta \to \theta_{\boldsymbol{p}}$, where $\theta_{\boldsymbol{p}} = \arctan(\frac{v_y}{v_x})$,

3. the control law $\boldsymbol{\psi}_3(\boldsymbol{q})$ regulates $\theta \to 0$, in the case that $\boldsymbol{r}$ has reached G_2, yielding unstable $\boldsymbol{r}$ and stable θ.

More specifically, we propose the following hysteresis-based switching logic.

- If $\boldsymbol{q}(0) \in K$, then $\sigma(\boldsymbol{q}(0)) = 1$, else $\sigma(\boldsymbol{q}(0)) = 3$.
  For all $t > 0$,
- If $\boldsymbol{q}(t) \in K$ and $\sigma(\boldsymbol{q}(t^-)) = 1$, then $\sigma(\boldsymbol{q}(t)) = 1$.
- If $\boldsymbol{q}(t) \in G_1$ and $\sigma(\boldsymbol{q}(t^-)) = 1$, then $\sigma(\boldsymbol{q}(t)) = 2$.
- If $\boldsymbol{q}(t) \in G_2$ and $\sigma(\boldsymbol{q}(t^-)) = 1$, then $\sigma(\boldsymbol{q}(t)) = 3$.
- If $\boldsymbol{q}(t) \in G$ and $\sigma(\boldsymbol{q}(t^-)) = 2$, then $\sigma(\boldsymbol{q}(t)) = 2$.
- If $\boldsymbol{q}(t) \in B$ and $\sigma(\boldsymbol{q}(t^-)) = 2$, then $\sigma(\boldsymbol{q}(t)) = 3$.
- If $\boldsymbol{q}(t) \in B$ and $\sigma(\boldsymbol{q}(t^-)) = 3$, then $\sigma(\boldsymbol{q}(t)) = 3$.
- If $\boldsymbol{q}(t) \in G$ and $\sigma(\boldsymbol{q}(t^-)) = 3$, then $\sigma(\boldsymbol{q}(t)) = 3$.
- If $\boldsymbol{q}(t) \in A$ and $\sigma(\boldsymbol{q}(t^-)) = 3$, then $\sigma(\boldsymbol{q}(t)) = 1$.

This switching logic results in a hybrid closed-loop control system, with σ being the discrete state, since the value of σ is not determined by the current value of $\boldsymbol{q}(t)$ alone, but is also depended on its previous value, $\sigma = \phi(\boldsymbol{q}, \sigma^-)$ [Lib03]. The hysteresis-based logic prevents the appearance of chattering when the state crosses the switching surfaces.

3.3 Control Design

After having defined the switching strategy, we now need to design the candidate state feedback controllers $\boldsymbol{\psi}_\sigma(\cdot)$, $\sigma \in \{1, 2, 3\}$.

3.3.1 Design of the control law $\boldsymbol{u} = \boldsymbol{\psi}_1(\boldsymbol{q})$

The control law $\boldsymbol{\psi}_1(\boldsymbol{q})$ forces the system to align with the vector field (3.4) while converging to the desired position $(0, 0)$. Define the dipole moment vector $\boldsymbol{p}_{\boldsymbol{p}} = \boldsymbol{p} = \begin{bmatrix} p_1 & p_2 \end{bmatrix}^\top$. Note that we would like the direction of the flow lines at $(0, 0)$ to be $\theta_p \in [-\pi/2, \pi/2]$, so that the vehicle faces to a target of interest as shown in Fig. 3.1. Thus, we need a vector $\boldsymbol{p}$ such that $\boldsymbol{p}^\top \hat{\boldsymbol{x}}_{\mathcal{G}} > 0 \Rightarrow p_1 > 0$. Therefore, we take $\boldsymbol{p} = \begin{bmatrix} v_x \operatorname{sgn}(v_x) & v_y \operatorname{sgn}(v_x) \end{bmatrix}^\top$, which implies that if $v_x \geq 0$, then $\boldsymbol{p} = \boldsymbol{v}$, whereas if $v_x < 0$, then $\boldsymbol{p} = -\boldsymbol{v}$.

Theorem 1 The position $\boldsymbol{r} = \begin{bmatrix} x & y \end{bmatrix}^\top$ of the perturbed system (3.1) enters a ball $\mathcal{B}(\mathbf{0}, r_0)$ of the origin for any $\boldsymbol{r}(0) \notin \mathcal{B}(\mathbf{0}, r_0)$, under the control input $\boldsymbol{\psi}_1 = \begin{bmatrix} u_1 & u_2 \end{bmatrix}^\top$,

$$u_1 = -k_1 \operatorname{sgn}\left(\boldsymbol{r}^\top \begin{bmatrix} \cos\theta \\ \sin\theta \end{bmatrix}\right) \|\boldsymbol{r}\| - \operatorname{sgn}(\boldsymbol{r}^\top \boldsymbol{v}) \operatorname{sgn}(\boldsymbol{p}^\top \boldsymbol{r}) \|\boldsymbol{v}\|, \tag{3.5a}$$

$$u_2 = -k_2(\theta - \varphi) + \dot{\varphi}, \tag{3.5b}$$

where $k_1, k_2 > 0$, $\varphi = \operatorname{atan2}(\mathrm{F}_{py}, \mathrm{F}_{px})$ is the orientation of the vector field (3.4) at (x, y), $\operatorname{sgn}(\cdot)$ is defined as

$$\operatorname{sgn}(a) = \begin{cases} 1, & \text{if } a \geq 0, \\ -1, & \text{if } a < 0, \end{cases}$$

and r_0 is chosen to satisfy the conditions (3.6) and (3.7).

Proof Define the orientation error $\eta = \theta - \varphi$, where φ is the orientation of the field (3.4) at (x, y), and consider the error dynamics $\dot{\eta} = \dot{\theta} - \dot{\varphi} \Rightarrow \dot{\eta} = u_2 - \dot{\varphi}$. Substituting the control law (3.5b) yields $\dot{\eta} = -k_2(\theta - \varphi) + \dot{\varphi} - \dot{\varphi} \Rightarrow \dot{\eta} = -k_2\eta$, which implies that θ converges exponentially to φ.

To study the convergence of the trajectories $\boldsymbol{r}(t)$ into a ball $\mathcal{B}(\mathbf{0}, r_0)$, consider the Lyapunov function $V = \frac{1}{2}(x^2 + y^2)$, which is positive definite, radially unbounded and of class C^1 and take the derivative of V along the trajectories of (3.1),

$$\dot{V} = \nabla V \begin{bmatrix} \dot{x} \\ \dot{y} \end{bmatrix} = \begin{bmatrix} x & y \end{bmatrix} \begin{bmatrix} u_1 \cos\theta + v_x \\ u_1 \sin\theta + v_y \end{bmatrix} = \boldsymbol{r}^\top \begin{bmatrix} \cos\theta \\ \sin\theta \end{bmatrix} u_1 + \boldsymbol{r}^\top \begin{bmatrix} v_x \\ v_y \end{bmatrix}.$$

Substituting the control law (3.5a) yields

$$\begin{aligned} \dot{V} = &- k_1 \left(\boldsymbol{r}^\top \begin{bmatrix} \cos\theta \\ \sin\theta \end{bmatrix}\right) \operatorname{sgn}\left(\boldsymbol{r}^\top \begin{bmatrix} \cos\theta \\ \sin\theta \end{bmatrix}\right) \|\boldsymbol{r}\| - \left(\boldsymbol{r}^\top \begin{bmatrix} \cos\theta \\ \sin\theta \end{bmatrix}\right) \operatorname{sgn}(\boldsymbol{r}^\top \boldsymbol{v}) \operatorname{sgn}(\boldsymbol{p}^\top \boldsymbol{r}) \|\boldsymbol{v}\| + \boldsymbol{r}^\top \boldsymbol{v} \Rightarrow \\ \dot{V} = &- k_1 \left|\boldsymbol{r}^\top \begin{bmatrix} \cos\theta \\ \sin\theta \end{bmatrix}\right| \|\boldsymbol{r}\| + \operatorname{sgn}(\boldsymbol{r}^\top \boldsymbol{v}) \left|\boldsymbol{r}^\top \boldsymbol{v}\right| - \left(\boldsymbol{r}^\top \begin{bmatrix} \cos\theta \\ \sin\theta \end{bmatrix}\right) \operatorname{sgn}(\boldsymbol{r}^\top \boldsymbol{v}) \operatorname{sgn}(\boldsymbol{p}^\top \boldsymbol{r}) \|\boldsymbol{v}\|. \end{aligned}$$

Check the sign of $\dot{V}$ by considering the following cases.
C1. $\operatorname{sgn}(\boldsymbol{p}^\top \boldsymbol{r}) = -1$ and $\operatorname{sgn}(\boldsymbol{r}^\top \boldsymbol{v}) = 1$, see Fig. 3.5. Then,

$$\dot{V} = -k_1 \left|\boldsymbol{r}^\top \begin{bmatrix} \cos\theta \\ \sin\theta \end{bmatrix}\right| \|\boldsymbol{r}\| + \left|\boldsymbol{r}^\top \boldsymbol{v}\right| + \left(\boldsymbol{r}^\top \begin{bmatrix} \cos\theta \\ \sin\theta \end{bmatrix}\right) \|\boldsymbol{v}\|.$$

Moreover, since under (3.5b) one has $\dot{\eta} = -k_2\eta$, one can argue that by choosing $k_2 > 0$ large enough, the orientation error $\eta \to 0 \Rightarrow \theta \to \varphi$ fast enough, compared to the rest (slow) dynamics. In this case, $\boldsymbol{r}^\top \begin{bmatrix} \cos\varphi \\ \sin\varphi \end{bmatrix} \leq 0$. Thus,

$$\dot{V} = -k_1 \left|\boldsymbol{r}^\top \begin{bmatrix} \cos\varphi \\ \sin\varphi \end{bmatrix}\right| \|\boldsymbol{r}\| + \left|\boldsymbol{r}^\top \boldsymbol{v}\right| - \left|\boldsymbol{r}^\top \begin{bmatrix} \cos\varphi \\ \sin\varphi \end{bmatrix}\right| \|\boldsymbol{v}\| = -\left|\boldsymbol{r}^\top \begin{bmatrix} \cos\varphi \\ \sin\varphi \end{bmatrix}\right| (k_1 \|\boldsymbol{r}\| + \|\boldsymbol{v}\|) + \left|\boldsymbol{r}^\top \boldsymbol{v}\right|.$$

After some algebra one can verify that

$$\left|\boldsymbol{r}^\top \begin{bmatrix} \cos\varphi \\ \sin\varphi \end{bmatrix}\right| = \|\mathbf{F}\|^{-1} \left|\boldsymbol{r}^\top \begin{bmatrix} \mathrm{F}_{px} \\ \mathrm{F}_{py} \end{bmatrix}\right| = \|\mathbf{F}\|^{-1} \left|\boldsymbol{r}^\top \boldsymbol{v}\right| \gamma_1(\|\boldsymbol{r}\|),$$

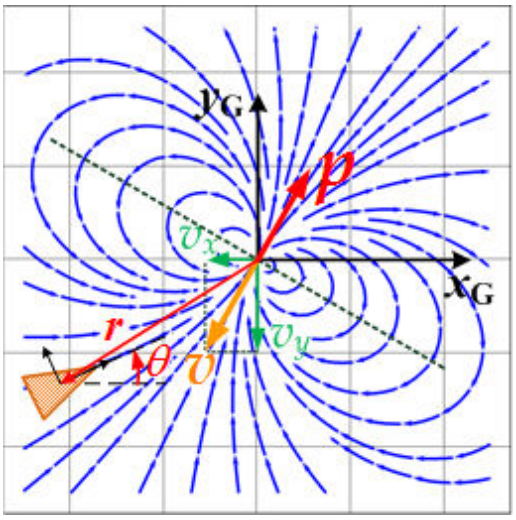

Figure 3.5: System configuration w.r.t. the dipole-like field (3.4)

where $\gamma_1(\|\boldsymbol{r}\|) = \lambda\|\boldsymbol{r}\|^2 - 1 + e^{-\|\boldsymbol{r}\|^2}$ is of class $\mathcal{K}_\infty$ for $\lambda \geq 2$, the norm $\|\mathbf{F}\| = \|\mathbf{F}_{\boldsymbol{p}}\|$ of the field is zero only at $(x, y) = (0, 0)$ and

$$\|\mathbf{F}\| = \sqrt{\lambda(\boldsymbol{r}^\top \boldsymbol{v})^2\left(\lambda\|\boldsymbol{r}\|^2 - 2(1-e^{-\|\boldsymbol{r}\|^2})\right) + \|\boldsymbol{v}\|^2\left(1-e^{-\|\boldsymbol{r}\|^2}\right)^2}.$$

Then,

$$\dot{V} = \left|\boldsymbol{r}^\top \boldsymbol{v}\right| \left(1 - \|\mathbf{F}\|^{-1}\gamma_1(\|\boldsymbol{r}\|)\left(k_1\|\boldsymbol{r}\| + \|\boldsymbol{v}\|\right)\right),$$

where the second factor is negative for

$$\|\mathbf{F}\|^{-1}\gamma_1(\|\boldsymbol{r}\|)\left(k_1\|\boldsymbol{r}\| + \|\boldsymbol{v}\|\right) > 1. \tag{3.6}$$

C2. $\text{sgn}(\boldsymbol{p}^\top \boldsymbol{r}) = -1$ and $\text{sgn}(\boldsymbol{r}^\top \boldsymbol{v}) = -1$. Then,

$$\dot{V} = -k_1 \left|\boldsymbol{r}^\top \begin{bmatrix}\cos\theta \\ \sin\theta\end{bmatrix}\right| \|\boldsymbol{r}\| - \left|\boldsymbol{r}^\top \boldsymbol{v}\right| - \left(\boldsymbol{r}^\top \begin{bmatrix}\cos\theta \\ \sin\theta\end{bmatrix}\right) \|\boldsymbol{v}\|.$$

Considering $\theta = \varphi$, in this case $\boldsymbol{r}^\top \begin{bmatrix}\cos\varphi \\ \sin\varphi\end{bmatrix} \leq 0$. Then,

$$\dot{V} = -k_1 \left|\boldsymbol{r}^\top \begin{bmatrix}\cos\varphi \\ \sin\varphi\end{bmatrix}\right| \|\boldsymbol{r}\| - \left|\boldsymbol{r}^\top \boldsymbol{v}\right| + \left|\boldsymbol{r}^\top \begin{bmatrix}\cos\varphi \\ \sin\varphi\end{bmatrix}\right| \|\boldsymbol{v}\| = -\left|\boldsymbol{r}^\top \begin{bmatrix}\cos\varphi \\ \sin\varphi\end{bmatrix}\right| \left(k_1\|\boldsymbol{r}\| - \|\boldsymbol{v}\|\right) - \left|\boldsymbol{r}^\top \boldsymbol{v}\right|.$$

Following the same analysis as above,

$$\dot{V} = -\left|\boldsymbol{r}^\top \boldsymbol{v}\right| \left(1 + \|\mathbf{F}\|^{-1}\gamma_1(\|\boldsymbol{r}\|)\left(k_1\|\boldsymbol{r}\| - \|\boldsymbol{v}\|\right)\right),$$

where the second factor is positive for

$$\|\mathbf{F}\|^{-1}\gamma_1(\|\boldsymbol{r}\|)\left(k_1\|\boldsymbol{r}\| - \|\boldsymbol{v}\|\right) > -1. \tag{3.7}$$

C3. $\text{sgn}(\boldsymbol{p}^\top \boldsymbol{r}) = 1$ and $\text{sgn}(\boldsymbol{r}^\top \boldsymbol{v}) = 1$. Then,

$$\dot{V} = -k_1 \left|\boldsymbol{r}^\top \begin{bmatrix}\cos\theta \\ \sin\theta\end{bmatrix}\right| \|\boldsymbol{r}\| + \left|\boldsymbol{r}^\top \boldsymbol{v}\right| - \left(\boldsymbol{r}^\top \begin{bmatrix}\cos\theta \\ \sin\theta\end{bmatrix}\right) \|\boldsymbol{v}\|.$$

Considering $\theta = \varphi$, in this case $\boldsymbol{r}^\top \left[\begin{smallmatrix}\cos\varphi\\ \sin\varphi\end{smallmatrix}\right] \geq 0$. Then,

$$\dot{V} = -k_1 \left|\boldsymbol{r}^\top \left[\begin{smallmatrix}\cos\varphi\\ \sin\varphi\end{smallmatrix}\right]\right| \|\boldsymbol{r}\| + \left|\boldsymbol{r}^\top \boldsymbol{v}\right| - \left|\boldsymbol{r}^\top \left[\begin{smallmatrix}\cos\varphi\\ \sin\varphi\end{smallmatrix}\right]\right| \|\boldsymbol{v}\| = -\left|\boldsymbol{r}^\top \left[\begin{smallmatrix}\cos\varphi\\ \sin\varphi\end{smallmatrix}\right]\right| (k_1\|\boldsymbol{r}\| + \|\boldsymbol{v}\|) + \left|\boldsymbol{r}^\top \boldsymbol{v}\right|,$$

i.e. $\dot{V}$ is the same as in C1, thus it is ≤ 0 if (3.6) holds.
C4. $\operatorname{sgn}(\boldsymbol{p}^\top \boldsymbol{r}) = 1$ and $\operatorname{sgn}(\boldsymbol{r}^\top \boldsymbol{v}) = -1$. Then,

$$\dot{V} = -k_1 \left|\boldsymbol{r}^\top \left[\begin{smallmatrix}\cos\theta\\ \sin\theta\end{smallmatrix}\right]\right| \|\boldsymbol{r}\| - \left|\boldsymbol{r}^\top \boldsymbol{v}\right| + \left(\boldsymbol{r}^\top \left[\begin{smallmatrix}\cos\theta\\ \sin\theta\end{smallmatrix}\right]\right) \|\boldsymbol{v}\|.$$

Considering $\theta = \varphi$, in this case $\boldsymbol{r}^\top \left[\begin{smallmatrix}\cos\varphi\\ \sin\varphi\end{smallmatrix}\right] \geq 0$. Then,

$$\dot{V} = -k_1 \left|\boldsymbol{r}^\top \left[\begin{smallmatrix}\cos\varphi\\ \sin\varphi\end{smallmatrix}\right]\right| \|\boldsymbol{r}\| - \left|\boldsymbol{r}^\top \boldsymbol{v}\right| + \left|\boldsymbol{r}^\top \left[\begin{smallmatrix}\cos\varphi\\ \sin\varphi\end{smallmatrix}\right]\right| \|\boldsymbol{v}\| = -\left|\boldsymbol{r}^\top \left[\begin{smallmatrix}\cos\varphi\\ \sin\varphi\end{smallmatrix}\right]\right| (k_1\|\boldsymbol{r}\| - \|\boldsymbol{v}\|) - \left|\boldsymbol{r}^\top \boldsymbol{v}\right|,$$

i.e. $\dot{V}$ is the same as in C2, thus it is ≤ 0 if (3.7) holds.

In summary, one has that $\dot{V} \leq 0$ for any $\boldsymbol{r}$ that satisfies (3.6) and (3.7), and that $\dot{V} = 0$ if and only if $\boldsymbol{r}^\top \boldsymbol{v} = 0$. Thus, for $\boldsymbol{r}^\top \boldsymbol{v} \neq 0$, any initial $\boldsymbol{r}(0)$ and any $0 < r_0 < \|\boldsymbol{r}(0)\|$ that satisfy (3.6) and (3.7), $\dot{V}$ is negative in the set $\{\boldsymbol{r} \mid \frac{1}{2}{r_0}^2 \leq V(\|\boldsymbol{r}\|) \leq \frac{1}{2}\|\boldsymbol{r}(0)\|^2\}$, which verifies that $\boldsymbol{r}(t)$ enters the set $\{\boldsymbol{r} \mid V(\boldsymbol{r}) \leq \frac{1}{2}{r_0}^2\}$, or equivalently, $\boldsymbol{r}(t)$ enters the ball $\mathcal{B}(\mathbf{0}, r_0)$. Equivalently, if r_0 is chosen to satisfy both (3.6) and (3.7), the system trajectory enters a ball $\mathcal{B}(\mathbf{0}, r_0)$ starting from any initial condition $\boldsymbol{r}(0) \notin \mathcal{B}(\mathbf{0}, r_0)$, under the control law (3.5a), as long as θ converges exponentially to φ under the control law (3.5b). Note that the case $\boldsymbol{r}^\top \boldsymbol{v} = 0$ does not affect the convergence of the system into $\mathcal{B}(\mathbf{0}, r_0)$. ■

3.3.2 Design of the control laws $\boldsymbol{u} = \boldsymbol{\psi}_2(\boldsymbol{q}), \boldsymbol{u} = \boldsymbol{\psi}_3(\boldsymbol{q})$

Denote ∂X_Y the boundary of a set X w.r.t. a neighbor set Y. Once $\boldsymbol{q}(t)$ has entered $G = \{\boldsymbol{q} = \begin{bmatrix}\boldsymbol{r}^\top & \theta\end{bmatrix}^\top \in \mathcal{B}(\mathbf{0}, r_0) \times [0, 2\pi)\}$, consider the following two cases:

1. Assume that $\boldsymbol{q} \in G_1 = \{G \mid \langle \boldsymbol{r}, \boldsymbol{v}\rangle \geq 0\}$, i.e. that $\boldsymbol{q}(t)$ has entered G_1, where the external disturbance $\boldsymbol{v}$ drives the system away from the origin.

   Theorem 2 The system trajectory $\boldsymbol{q}(t)$ enters G_2, where $\langle \boldsymbol{r}, \boldsymbol{v}\rangle < 0$, under the control law $\boldsymbol{\psi}_2 = \begin{bmatrix}u_1 & u_2\end{bmatrix}^\top$,

   $$u_1 = -k_3 \operatorname{sgn}(v_x)\|\boldsymbol{v}\|, \quad u_2 = -k_4(\theta - \theta_{\boldsymbol{p}}), \tag{3.8}$$

   with $k_3 > 1$, $k_4 > 0$.

   Proof Under the control law (3.8) the system trajectory hits the boundary $\partial G_{1_{G_2}}$ and then the boundary ∂G_{2_B}.

   To verify the first argument, i.e. that the system trajectory hits the boundary $\partial G_{1_{G_2}}$, consider

   $$V_{21} = \boldsymbol{r}^\top \boldsymbol{v} + \frac{1}{2}(\theta - \theta_{\mathbf{p}})^2 = x v_x + y v_y + \frac{1}{2}(\theta - \theta_{\mathbf{p}})^2,$$

which is positive for $\boldsymbol{r} \in G_1$ and zero on $\partial G_{1_{G_2}}$ with $\theta = \theta_{\mathbf{p}}$, and take its time derivative along the system trajectories:

$$\begin{aligned}\dot{V}_{21} &= \left[\begin{smallmatrix} v_x & v_y \end{smallmatrix}\right] \left[\begin{smallmatrix} \cos\theta \\ \sin\theta \end{smallmatrix}\right] u_1 + \left[\begin{smallmatrix} v_x & v_y \end{smallmatrix}\right] \left[\begin{smallmatrix} v_x \\ v_y \end{smallmatrix}\right] + (\theta - \theta_{\mathbf{p}}) u_2 = \\ &= -\boldsymbol{v}^\top \left[\begin{smallmatrix} \cos\theta \\ \sin\theta \end{smallmatrix}\right] k_3 \operatorname{sgn}(v_x) \|\boldsymbol{v}\| + \|\boldsymbol{v}\|^2 - k_4(\theta - \theta_{\mathbf{p}})^2.\end{aligned}$$

Take $\operatorname{sgn}(v_x) = -1$ and assume that the system has reached G_1 with $\boldsymbol{v}^\top \left[\begin{smallmatrix} \cos\theta \\ \sin\theta \end{smallmatrix}\right] < 0$. Then,

$$\begin{aligned}\dot{V}_{21} &= -k_3 \left| \boldsymbol{v}^\top \left[\begin{smallmatrix} \cos\theta \\ \sin\theta \end{smallmatrix}\right] \right| \|\boldsymbol{v}\| + \|\boldsymbol{v}\|^2 - k_4(\theta - \theta_{\mathbf{p}})^2 = \\ &= \|\boldsymbol{v}\| \left(\|\boldsymbol{v}\| - k_3 \left| \boldsymbol{v}^\top \left[\begin{smallmatrix} \cos\theta \\ \sin\theta \end{smallmatrix}\right] \right| \right) - k_4(\theta - \theta_{\mathbf{p}})^2,\end{aligned}$$

where the first term is < 0 for $\|\boldsymbol{v}\| < k_3 \left| \boldsymbol{v}^\top \left[\begin{smallmatrix} \cos\theta \\ \sin\theta \end{smallmatrix}\right] \right| \Rightarrow k_3 > 1$. Moreover, one has $\dot{V}_{21} = 0 \Leftrightarrow \{k_3 = 1 \text{ and } \theta = \theta_{\mathbf{p}}\}$. Therefore, for $k_3 > 1$ the system trajectory starting in G_1 enters the region G_2. Similarly one can verify the case $\operatorname{sgn}(v_x) = 1$, for $\boldsymbol{v}^\top \left[\begin{smallmatrix} \cos\theta \\ \sin\theta \end{smallmatrix}\right] > 0$.
For the second argument, i.e. that the system trajectory hits the boundary ∂G_{2_B}, consider:

$$V_{22} = {r_0}^2 - \|\boldsymbol{r}\|^2 = {r_0}^2 - (x^2 + y^2),$$

which is positive for $\boldsymbol{r} \in G_2$ and zero on ∂G_{2_B}. The time derivative of V_{22} along the system trajectories is

$$\dot{V}_{22} = -2\boldsymbol{r}^\top \left[\begin{smallmatrix} \cos\theta \\ \sin\theta \end{smallmatrix}\right] u_1 - 2\boldsymbol{r}^\top \boldsymbol{v}.$$

For $\operatorname{sgn}(v_x) = -1$: $\boldsymbol{r}^\top \boldsymbol{v} < 0$ and $\boldsymbol{r}^\top \left[\begin{smallmatrix} \cos\theta \\ \sin\theta \end{smallmatrix}\right] > 0$. Then,

$$\begin{aligned}\dot{V}_{22} &= -2k_3 \boldsymbol{r}^\top \left[\begin{smallmatrix} \cos\theta \\ \sin\theta \end{smallmatrix}\right] \|\boldsymbol{v}\| - 2\boldsymbol{r}^\top \boldsymbol{v} = -2k_3 \left| \boldsymbol{r}^\top \left[\begin{smallmatrix} \cos\theta \\ \sin\theta \end{smallmatrix}\right] \right| \|\boldsymbol{v}\| + 2 \left| \boldsymbol{r}^\top \boldsymbol{v} \right| \leq \\ &\leq -2k_3 \left| \boldsymbol{r}^\top \left[\begin{smallmatrix} \cos\theta \\ \sin\theta \end{smallmatrix}\right] \right| \|\boldsymbol{v}\| + 2\|\boldsymbol{r}\|\|\boldsymbol{v}\| = 2\|\boldsymbol{v}\| \left(\|\boldsymbol{r}\| - k_3 \left| \boldsymbol{r}^\top \left[\begin{smallmatrix} \cos\theta \\ \sin\theta \end{smallmatrix}\right] \right| \right),\end{aligned}$$

which is < 0 for $\|\boldsymbol{r}\| < k_3 \left| \boldsymbol{r}^\top \left[\begin{smallmatrix} \cos\theta \\ \sin\theta \end{smallmatrix}\right] \right| \leq \|\boldsymbol{r}\| \Rightarrow k_3 > 1$. Thus, for $k_3 > 1$, the system trajectory hits the boundary ∂G_{2_B} and enters B.
For $\operatorname{sgn}(v_x) = 1$: $\boldsymbol{r}^\top \boldsymbol{v} < 0$ and $\boldsymbol{r}^\top \left[\begin{smallmatrix} \cos\theta \\ \sin\theta \end{smallmatrix}\right] < 0$. Following the same procedure, one has that $\dot{V}_{22} < 0 \Rightarrow k_3 > 1$. ■

2. Assume that $\boldsymbol{q} \in G_2 = \{G \mid \langle \boldsymbol{r}, \boldsymbol{v} \rangle < 0\}$, i.e. that $\boldsymbol{q}(t)$ has entered G_2, where the external disturbance $\boldsymbol{v}$ drives the system towards the origin. Then $\boldsymbol{r}(t)$ enters G_1 under the control law

$$\boldsymbol{\psi}_3 = [0 \quad u_{23}]^\top, \text{ where } u_{23} = -k_5\theta, \;\; k_5 > 0. \tag{3.9}$$

Proof To verify so, consider the function $V_{31} = -\boldsymbol{r}^\top \boldsymbol{v}$, which is positive for $\boldsymbol{r} \in G_2$ and zero on $\partial G_{2_{G_1}}$. The time derivative along the system trajectories is

$$\dot{V}_{31} = -v_x(u_1 \cos\theta + v_x) - v_y(u_1 \sin\theta + v_y) = -{v_x}^2 - {v_y}^2 < 0,$$

which verifies that the system trajectory enters G_1. ■

3.3.3 Stability of the switched system $\dot{\boldsymbol{q}} = \boldsymbol{f}_\sigma(\boldsymbol{q}, \boldsymbol{\psi}_\sigma)$

Stability analysis in the case of state-dependent switching is often facilitated by the fact that properties of each subsystem $\boldsymbol{f}_\sigma(\boldsymbol{q})$ are of concern only in the regions where this system is active, and that the behavior of $\boldsymbol{f}_\sigma(\boldsymbol{q})$ in other parts of the state space has no influence on the switched system. [Lib03]

Following [Bra98], let us consider a strictly increasing sequence of times

$$\top = \{t_0, t_1, \ldots, t_n, \ldots, \},$$

the interval completion $\mathrm{I}(\top) = \bigcup_{n\in\mathbb{N}}[t_{2n}, t_{2n+1}]$ of $\top$, and the switching sequence

$$\Sigma = \{\boldsymbol{q}_0; (\iota_0, t_0), (\iota_1, t_1), \ldots, (\iota_n, t_n), \ldots \mid \iota_n \in \mathcal{I}, n \in \mathbb{N}\},$$

where t_0 is the initial time, $\boldsymbol{q}_0$ is the initial state and $\mathbb{N}$ is the set of nonnegative integers.

For $t \in [t_k, t_{k+1})$, one has $\sigma(t) = \iota_k$, that is the ι_k-th subsystem is active. For any $j \in \mathcal{I}$, denote

$$\Sigma \mid j = \{t_{j_1}, t_{j_1+1}, t_{j_2}, t_{j_2+1}, \ldots, t_{j_\nu}, t_{j_\nu+1}, \ldots\}$$

the sequence of switching times when the j-th subsystem is "switched on" or "switched off", with

$$\mathrm{E} \mid j = \{t_{j_1}, t_{j_2}, \ldots, t_{j_\nu}, \ldots\}$$

being the "switched on" times of the j-th subsystem.

Theorem 2 [ZH08, Thm 3.9] *Assume that for each $j \in \mathcal{I}$, there exists a positive definite generalized Lyapunov-like function*[6] *$V_j(\boldsymbol{q})$ with respect to $\boldsymbol{f}_j(\boldsymbol{q}, 0)$ and the associated trajectory $\boldsymbol{q}(t)$. Then the origin of the system $\dot{\boldsymbol{q}} = \boldsymbol{f}_\sigma(\boldsymbol{q}, \boldsymbol{u}_\sigma)$, with $\boldsymbol{u}_\sigma \equiv 0$, is stable if and only if there exist class $\mathcal{GK}$*[7] *functions α_j satisfying*

$$V_j\left(\boldsymbol{q}(t_{j_{k+1}})\right) - V_j\left(\boldsymbol{q}(t_{j_1})\right) \leq \alpha_j(\|\boldsymbol{q}_0\|), \quad k \geq 1, \quad j = 1, 2, \ldots, \chi. \tag{3.10}$$

This theorem states that stability is ensured as long as $V_j\left(\boldsymbol{q}(t_{j_{k+1}})\right) - V_j\left(\boldsymbol{q}(t_{j_1})\right)$, i.e. the change of V_j between any "switched on" time $t_{j_{k+1}}$ and the first active time t_{j_1}, is bounded by a class $\mathcal{GK}$ function, regardless of the initial value $V_j\left(\boldsymbol{q}(t_{j_1})\right)$ at the first active time.

Collorary 2 The position $\boldsymbol{r}$ of the switched system $\dot{\boldsymbol{q}} = \boldsymbol{f}_\sigma(\boldsymbol{q}, \boldsymbol{\psi}_\sigma)$, where $\sigma \in \mathcal{I} = \{1, 2, 3\}$, under the proposed switching logic, is Lyapunov stable.

[6] A continuous function $V : \mathbb{R}^n \to [0, \infty)$ is called a generalized Lyapunov-like function for the vector field $\boldsymbol{f}$ and the associated trajectory $\boldsymbol{q}(t)$ over a strictly increasing sequence of times $\top$, if there exists a continuous function $\phi : [0, \infty) \to [0, \infty)$ with $\phi(0) = 0$, such that $V(\boldsymbol{q}(t)) \leq \phi(V(\boldsymbol{q}(t_{2n})))$, for all $t \in (t_{2n}, t_{2n+1})$ and all $n \in \mathbb{N}$ [ZH08]

[7] A function $a : [0, \infty) \to [0, \infty)$ is called a class $\mathcal{GK}$ function if it is increasing and right continuous at the origin with $a(0) = 0$ [ZH08]

Proof The correctness of the proposed lemma can be verified by a direct application of Theorem 2. Note that the initial condition $\boldsymbol{r}(0)$ may either be in K or in G, and that all the switchings occur when the state $\boldsymbol{q}$ crosses the switching surface $\mathcal{S} : \|\boldsymbol{r}\| = r_0$.

For each subsystem $\sigma \in \{1, 2, 3\}$, consider the generalized Lyapunov-like function $V_\sigma(\boldsymbol{r}) = \|\boldsymbol{r}\|$. Note that V_σ serves as a generalized Lyapunov-like function even when $\sigma = 2$ or $\sigma = 3$ is the active subsystem, i.e. when $\boldsymbol{r}(t) \in G$, since its value is bounded in the sense that $V_\sigma(\boldsymbol{r}(t)) \leq \phi\left(V_\sigma(\boldsymbol{r}(t_k))\right) = \phi(r_0)$, where $t \in [t_k, t_{k+1})$ and $\phi(\cdot) = \|\boldsymbol{r}\|$.

At any "switched on" time instant $t_{\sigma n}$ with $n > 1$, (that is, for any "switched on" time instant after the first switch has occurred at $t_{\sigma 1}$), one has that $V_\sigma(\boldsymbol{r}(t_{\sigma n})) \leq r_\sigma$, where $r_\sigma = r_0 + \epsilon_\sigma$ and $\epsilon_\sigma > 0$ can be chosen arbitrarily small. Then, for any first active time $t_{\sigma 1}$, where clearly $V_\sigma(\boldsymbol{r}(t_{\sigma 1})) \geq 0$, one has $V_\sigma(\boldsymbol{r}(t_{\sigma n})) - V_\sigma(\boldsymbol{r}(t_{\sigma 1})) \leq r_\sigma$, that is, any growth of each V_σ is always bounded. ■

In summary, the proposed switching control strategy guarantees that the trajectory $\boldsymbol{r}(t)$ of the perturbed system (3.1) is ε-practically asymptotically stable around the origin, with $\varepsilon = r_1$, in the sense that $\boldsymbol{r}(t)$ converges into a ball $\mathcal{B}(\mathbf{0}, r_1)$ around the origin, where $r_1 = r_0 + \epsilon$, and $\epsilon > 0$ is arbitrarily small, and remains into the ball for $t > T$, whereas the orientation θ is regulated to zero, $\theta \to 0$, during the time intervals that the subsystem $\boldsymbol{f}_3(\boldsymbol{q}, \boldsymbol{\psi}_3)$ is active.

3.3.4 Robustness consideration

The control design and stability analysis has been based on the assumption that the current disturbance $\boldsymbol{v}$ is known. However, this is quite unrealistic in general, since on-line measurements of the current velocity can not be easily acquired. An estimation of the current velocity $\hat{\boldsymbol{v}} = \begin{bmatrix}\hat{v}_x & \hat{v}_y\end{bmatrix}^\top$ is usually obtained using nonlinear observers, see for example in [AP07, RSP07], and then employed into the control design. However, this approach complicates the design and analysis of the overall closed-loop system, since both the estimation error $\tilde{\boldsymbol{v}} = \hat{\boldsymbol{v}} - \boldsymbol{v}$ and the state vector $\boldsymbol{q}$ are required to be stable at zero.

Therefore, guaranteeing the robustness of the switched system in the case that the current disturbance is unknown is meaningful for the class of problems considered here. Robustness reduces into guaranteeing that the system trajectories enter and remain into a ball $\mathcal{B}(\mathbf{0}, \varepsilon)$ of the origin.

Let us assume that only a maximum bound $\|\boldsymbol{v}\|_{\max}$ on the disturbance is known, i.e. that the magnitude of the current velocity $\|\boldsymbol{v}\| = \sqrt{{v_x}^2 + {v_y}^2} \leq \|\boldsymbol{v}\|_{\max}$, while the current direction $\theta_c = \text{atan2}(v_y, v_x)$ is unknown. In this case, the vector $\boldsymbol{p}_{\boldsymbol{p}}$ which generates the vector field can not be a priori determined; let us therefore consider the nominal vector field $\mathbf{F}_{\boldsymbol{n}} = \mathbf{F}$, generated by a vector $\boldsymbol{p}_{\boldsymbol{n}} = \boldsymbol{p} = \begin{bmatrix}p & 0\end{bmatrix}^\top$, where $p > 0$. Then, applying the proposed switching control strategy is not straightforward, since the terms $\text{sgn}(\boldsymbol{r}^\top \boldsymbol{v})$ and $\text{sgn}(v_x)$ are unknown.

Nevertheless, regarding the control law $\boldsymbol{u} = \boldsymbol{\psi}_1(\boldsymbol{q})$, one can verify that by following the same analysis as in Section 3.3.1, still gets the four cases in terms of $\text{sgn}(\boldsymbol{r}^\top \boldsymbol{v})$ and $\text{sgn}(\boldsymbol{p}^\top \boldsymbol{r})$, which end up in the conditions (3.6) and (3.7). These conditions can be combined to yield

$$\left| \|\boldsymbol{v}\| - \frac{\|\mathbf{F}\|}{\gamma_1(\|\boldsymbol{r}\|)} \right| < k_1 \|\boldsymbol{r}\|, \tag{3.11}$$

which effectively means that whatever the term $\text{sgn}(\boldsymbol{r}^\top \boldsymbol{v})$ might be, if the radius r_0 is chosen to satisfy (3.11), the system trajectories enter $\mathcal{B}(\mathbf{0}, r_0)$. In other words, the position $\boldsymbol{r}$ of the system robustly converges into $\mathcal{B}(\mathbf{0}, r_0)$ under any current disturbance $\boldsymbol{v}$ such that $\|\boldsymbol{v}\| \leq \|\boldsymbol{v}_{\max}\|$, as long as r_0 satisfies (3.11).

However, controlling the switched system while being in $\mathcal{B}(\mathbf{0}, r_0)$ depends on both the $\text{sgn}(\boldsymbol{r}^\top \boldsymbol{v})$ and the $\text{sgn}(v_x)$, which is included in $\boldsymbol{u} = \boldsymbol{\psi}_2(\boldsymbol{q})$. Still, the same idea on the control design while into $\mathcal{B}(\mathbf{0}, r_0)$ can be used, where now the linear velocity controller depends on the sign of the coordinate x_{in} where the vehicle enters $\mathcal{B}(\mathbf{0}, r_0)$: while in $\mathcal{B}(\mathbf{0}, r_0)$, the vehicle is controlled with linear velocity $u_1 = -\text{sgn}(x_{\text{in}}) k_3 \|\boldsymbol{v}\|_{\max} > 0$ and angular velocity $u_2 = -k_4\theta$, $k_4 > 0$, until it reaches the boundary of $\mathcal{B}(\mathbf{0}, r_0)$. In both cases, a high gain $k_3 > 1$ on the linear velocity u_1 is needed to counteract the destabilizing effect of the unknown lateral velocity induced by the current. At any case, even if the vehicle exits $\mathcal{B}(\mathbf{0}, r_0)$, the control law $\boldsymbol{u} = \boldsymbol{\psi}_1$ guarantees that it will re-enter.

3.4 Simulation Results

The efficacy of the switching control strategy has been verified through computer simulations. Consider the red triangle in Fig. 3.6(b), 3.7(b) as a unicycle-like underwater or surface vehicle (e.g. an underactuated Remotely Operated Vehicle or a hovercraft), that is moving on the horizontal plane under the influence of an environmental disturbance $\boldsymbol{v}$. The goal configuration $\boldsymbol{q_G}$ is the origin and the black line centered at $(0.5, 0)$ is a point of interest, e.g. a target that the vehicle has to inspect through an onboard camera.

Two cases are considered; in the first one, the disturbance is known, equal to $\boldsymbol{v} = \begin{bmatrix} -0.1 & 0.2 \end{bmatrix}^\top$ m/sec; thus $\boldsymbol{p} = \begin{bmatrix} 0.1 & -0.2 \end{bmatrix}^\top$. In the second one, the same disturbance $\boldsymbol{v}$ is used for the simulation, which is assumed to be unknown; the only information which is available to the switching controller is the bound $\|\boldsymbol{v}\|_{\max}$. The region G is defined as the ball $\mathcal{B}(\mathbf{0}, r_0)$, where $r_0 = 0.1$ m satisfies the conditions (3.6) and (3.7). In both cases, the trajectories $x(t)$, $y(t)$ converge into $\mathcal{B}(\mathbf{0}, r_0)$ and remain bounded into the ball $\mathcal{B}(\mathbf{0}, r_1)$, where $r_1 = r_0 + \epsilon$, with ϵ being a small positive number, see Fig. 3.6(a), 3.6(c), 3.7(a), 3.7(c).

The main difference between the two cases is the evolution of the orientation $\theta(t)$; when the current disturbance is known, and the system has entered the set G, θ is alternately regulated between zero (when the control law $\boldsymbol{\psi}_3$ is active) and the direction $\theta_{\boldsymbol{p}}$ of the vector $\boldsymbol{p}$, which coincides with the orientation θ_e at the equilibrium (when the control law $\boldsymbol{\psi}_2$ is active). Clearly, the smaller the component $|v_y|$ is compared to $|v_x|$, the less oscillation occurs for θ. On the contrary, when the current disturbance is unknown, the orientation θ is still regulated to zero when the system has reached G, but oscillates with higher frequency. This behavior is due to the fact that the system switches more frequently between the control laws 1 and 3, since the destabilizing effect of the current-induced motion along the unactuated d.o.f. drives the vehicle faster out of the set G, compared to the first case. Still, the hysteresis-based switching prevents the appearance of chattering when crossing the switching surface.

A drawback of state-dependent switching control is that it is sensitive to measurement noise. Figure 3.8 depicts a scenario where the sensed state variables are subject to zero-mean, uniform random noise. The system still converges into $\mathcal{B}(\mathbf{0}, r_0)$, however chattering occurs during some time intervals around the switching surface. The measurement noise also affects the

angular velocity u_2, which depends on the vector field orientation $\varphi(x, y)$; for these reasons, the evolution of θ is quite oscillatory compared to the noise-free cases. Still, using some additional control logic, for instance to sample and hold each value of the controls for a long enough period of time, in order to move sufficiently away from the switching surface, may also offer robustness w.r.t. measurement errors.

The difference in the trajectories $\boldsymbol{r}(t)$ near the set G is due to the second term of the control law $\boldsymbol{\psi}_1$, that is $-\operatorname{sgn}(\boldsymbol{r}^\top \boldsymbol{v}) \operatorname{sgn}(\boldsymbol{p}^\top \boldsymbol{r}) \|\boldsymbol{v}\|$. More specifically, in the first case the vehicle moves with linear velocity $u_1 > 0$ and has to counteract the current effect at the origin with $u_1 = \|\boldsymbol{v}\|$, whereas in the second case, the vehicle moves with $u_1 > 0$ and has to counteract the current effect at the origin with $u_1 = -\|\boldsymbol{v}\|$. Furthermore, the smaller the component $|v_y|$ is compared to $|v_x|$, the less oscillation occurs for θ. Then, it remains a trade-off for the control designer to choose r_0, in order to at least specify a smaller or larger region in which θ is close to zero.

3.5 Conclusions

This chapter presented a switching control approach for the practical stabilization of a unicycle-like marine vehicle, under non-vanishing, current-induced perturbations. The control scheme is a hysteresis-based switching among three control laws.

The first control law employs a dipole-like vector field and drives the system trajectories into a set G around the origin. The other two control laws are active in G; switching between them renders the position of the vehicle practically stable, while the orientation is regulated to zero during some time intervals. The switched system is robust in the sense that the system trajectories converge and remain into the set G, even if only a bound $\|\boldsymbol{v}_{\max}\|$ on the current velocity is given.

This work is extended to the state feedback control design for a class of nonholonomic systems under the consideration of input constraints (i.e. thrust saturation) and state constraints (induced by limited sensing, i.e. limited camera field-of-view), using concepts and tools from viability theory, see Chapter 5.

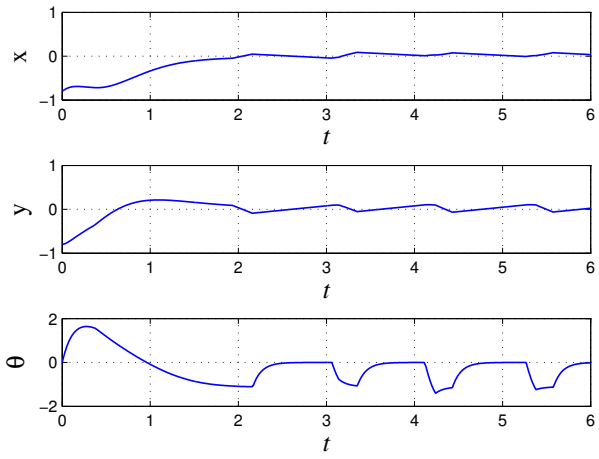

(a) The system trajectories $x(t), y(t), \theta(t)$

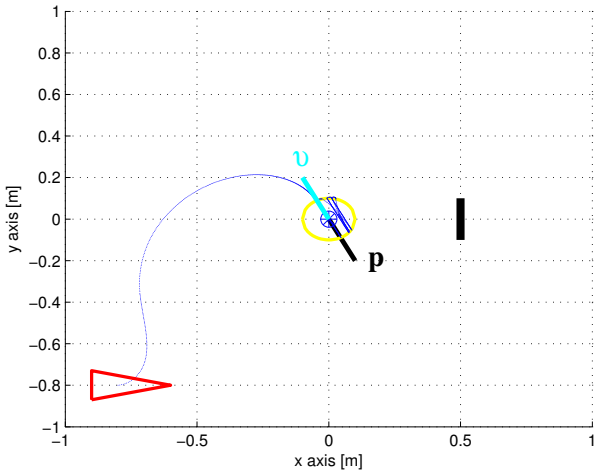

(b) The path $x(t), y(t)$ followed by the closed loop system

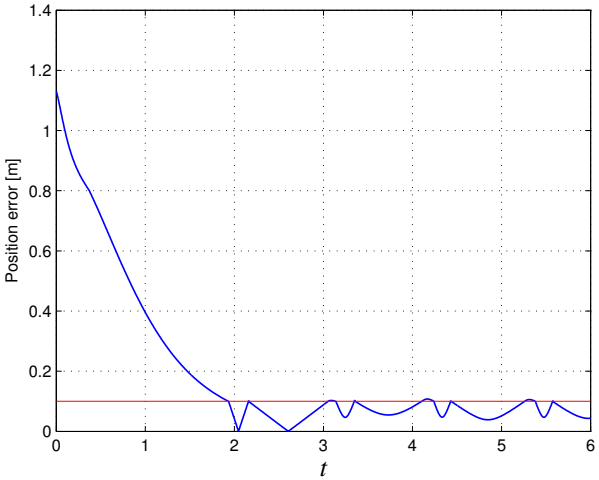

(c) The position error $e(t) = \sqrt{x(t)^2 + y(t)^2}$

Figure 3.6: System response for *known* $\boldsymbol{v} = \begin{bmatrix} -0.1 & 0.2 \end{bmatrix}^\top$

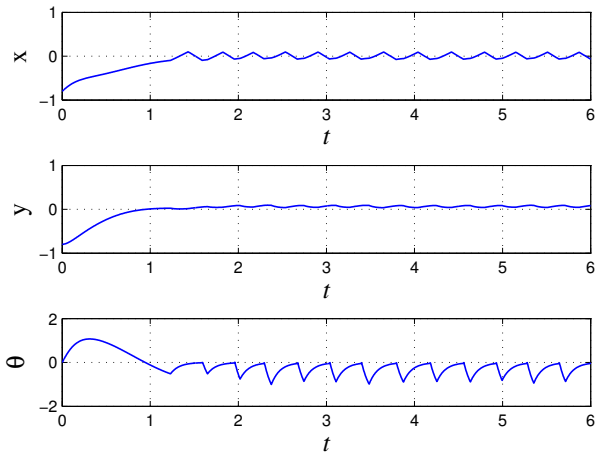

(a) The system trajectories $x(t), y(t), \theta(t)$

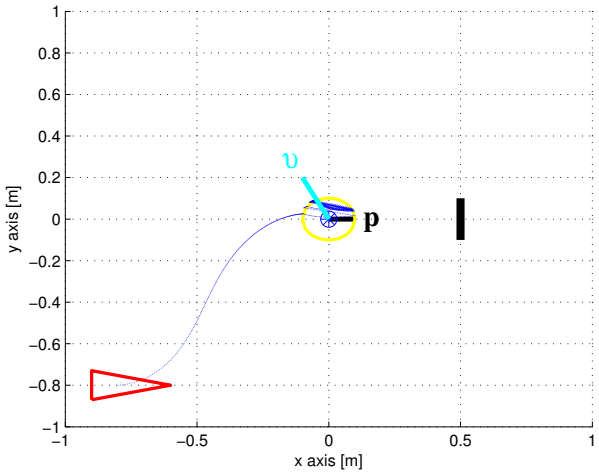

(b) The path $x(t), y(t)$ followed by the closed loop system

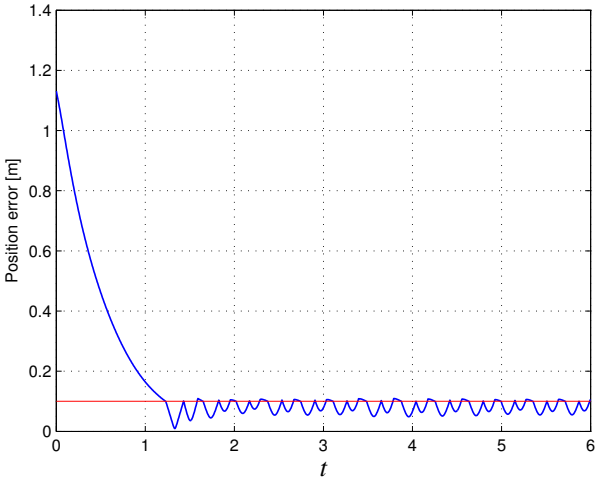

(c) The position error $e(t) = \sqrt{x(t)^2 + y(t)^2}$

Figure 3.7: System response for *unknown* $\boldsymbol{v} = \begin{bmatrix} -0.1 & 0.2 \end{bmatrix}^\top$

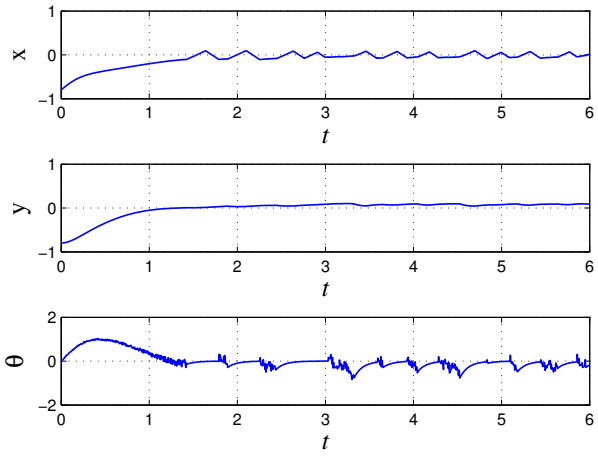

(a) The system trajectories $x(t), y(t), \theta(t)$

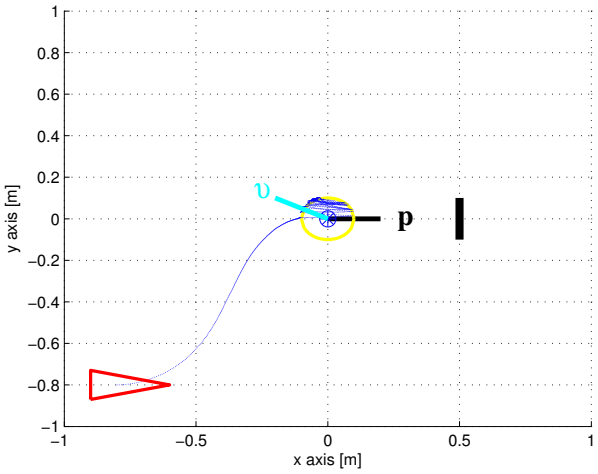

(b) The path $x(t), y(t)$ followed by the closed loop system

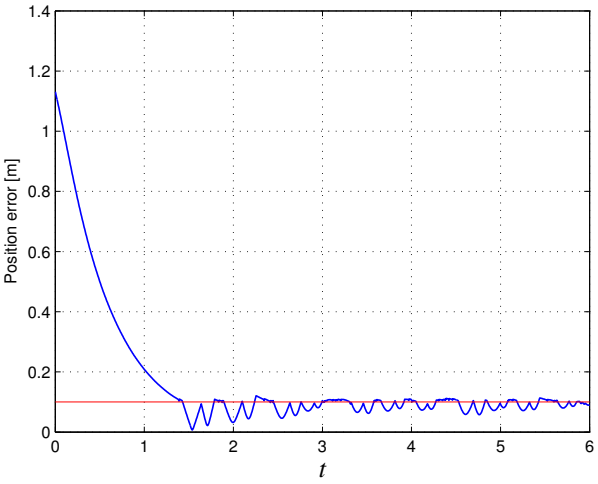

(c) The position error $e(t) = \sqrt{x(t)^2 + y(t)^2}$

Figure 3.8: System response for *unknown* $\boldsymbol{v}$ under measurement noise

Chapter 4

Nonholonomic Control Design via Reference Vector Fields and Output Regulation

Abstract

This chapter presents a control strategy comprising formal guidelines for the construction of state feedback controllers for *driftless, kinematic* nonholonomic systems, as well as *dynamic* nonholonomic systems *with drift*.

The main idea is that, given an n-dimensional *kinematic* nonholonomic system subject to κ Pfaffian constraints, one can define an N-dimensional ($\mathrm{N} \leq n$) reference vector field $\mathbf{F}(\cdot)$ on a subset $\mathcal{L}$ of the configuration space $\mathcal{C}$. The vector field $\mathbf{F}(\cdot)$ is taken out of the family of vector fields

$$\mathbf{F}(\boldsymbol{x}) = \lambda \left(\boldsymbol{p}^\top \boldsymbol{x} \right) \boldsymbol{x} - \boldsymbol{p} \left(\boldsymbol{x}^\top \boldsymbol{x} \right),$$

where $\mathrm{N} \leq n$, $\boldsymbol{x} \in \mathbb{R}^{\mathrm{N}}$ is a sub-vector of the configuration vector $\boldsymbol{q} \in \mathbb{R}^n$, $\boldsymbol{p} \in \mathbb{R}^{\mathrm{N}}$ is the dipole moment vector, and $\lambda \geq 2$, see Section 4.2. The vector field $\mathbf{F}(\cdot)$ is by construction nonsingular everywhere on $\mathcal{L}$ except for the origin $\boldsymbol{x} = \mathbf{0}$ of the local coordinate frame on $\mathcal{L}$; the origin $\boldsymbol{x} = \mathbf{0}$ is thus the unique, isolated critical point of the vector field $\mathbf{F}(\cdot)$, and is by construction of *dipole* type. This further implies that all integral curves of the vector field $\mathbf{F}(\cdot)$ begin and end at the critical point; in this sense, any of the integral curves offers a path to $\boldsymbol{x} = \mathbf{0}$.

The subspace $\mathcal{L} \subseteq \mathcal{C}$ on which the vector field $\mathbf{F}(\cdot)$ is defined is dictated by the structure of the constraint matrix $\boldsymbol{A}(\boldsymbol{q})$. In particular, the zero columns of $\boldsymbol{A}(\boldsymbol{q})$ induce a trivial foliation of the configuration space $\mathcal{C}$ into the **leaf space** $\mathcal{L}$ and the **fiber space** $\mathcal{T}$, and characterize the configuration variables $\boldsymbol{q} \in \mathbb{R}^n$ into **leafwise** coordinates $\boldsymbol{x} \in \mathbb{R}^{n-n_0}$, and **transverse** coordinates $\boldsymbol{t} \in \mathbb{R}^{n_0}$. The vector field $\mathbf{F}(\cdot)$ is then defined on the leaf space $\mathcal{L}$, in terms of the leafwise coordinates $\boldsymbol{x}$ only.

Having the vector field $\mathbf{F}(\cdot)$ at hand, the idea for the control design is that, at each $\boldsymbol{q} \in \mathcal{C}$, the system vector field $\dot{\boldsymbol{q}} \in T_{\boldsymbol{q}}\mathcal{C}$ is controlled to "align with" the vector field $\mathbf{F}(\cdot)$, i.e. is forced into the tangent space of the integral curve of $\mathbf{F}(\cdot)$ at $\boldsymbol{q} \in \mathcal{C}$.

For a nonholonomic system subject to a single Pfaffian constraint, the "misalignment" between the system vector field $\dot{\boldsymbol{q}}$ and the reference vector field $\mathbf{F}(\cdot)$ is codified via the output $h(\boldsymbol{q}) = \langle \boldsymbol{a}(\boldsymbol{q}), \mathbf{F}(\cdot) \rangle$, where $\langle \cdot, \cdot \rangle$ is the inner product. Then, forcing the system vector field $\dot{\boldsymbol{q}} \in T_{\boldsymbol{q}}\mathcal{C}$ to align with $\mathbf{F}(\cdot)$ is codified by requiring that $h \to 0$. This condition offers a way of choosing at least one of the control inputs u_i, as long as the system has relative degree 1 for the output h.

Similarly, for $\kappa > 1$ Pfaffian constraints, the misalignment of the system vector field with the vector field $\mathbf{F}(\cdot)$ is codified via the (vector) output $\boldsymbol{h}(\boldsymbol{q}) = \boldsymbol{A}(\boldsymbol{q})\mathbf{F}(\cdot)$, and the condition $\boldsymbol{h}(\boldsymbol{q}) \to 0$ is enforced, by requiring that all κ elements of the output vector $\boldsymbol{h}(\boldsymbol{q})$ vanish as $t \to \infty$.

In other words, the vector field $\mathbf{F}(\cdot)$ provides a reference direction $\dot{\boldsymbol{q}}_{\text{ref}}$ for the system vector field at each $\boldsymbol{q} \in \mathcal{C}$; this condition, along with the foliation of the configuration space into $\mathcal{L}$ and $\mathcal{T}$ suggests a choice of Lyapunov-like functions, which are further used into the control design to formally establish convergence of system trajectories $\boldsymbol{q}(t)$ to the origin $\boldsymbol{q} = \mathbf{0}$.

In this sense, the proposed approach recasts the original nonholonomic control problem into an output regulation problem, which although nontrivial, can more easily be tackled with existing design and analysis tools. Furthermore, the new perspective brings forth an interdependence between the convergence of the state variables and exposes a potential time-scale decomposition.

The methodology is also extended to the control design for a class of underactuated mechanical systems with drift, subject to dynamic Pfaffian nonholonomic constraints.

Organization and Notation

The chapter is organized as follows: Section 4.1 gives a brief introduction on vector fields and isolated critical points. In Sections 4.2 and 4.3 we consider the control design for kinematic nonholonomic systems with κ Pfaffian constraints, which fall into the class of n-dimensional, drift-free systems

$$\dot{\boldsymbol{q}} = \sum_{i=1}^{m} \mathbf{g}_i(\boldsymbol{q}) u_i, \tag{4.1}$$

where $\boldsymbol{q} \in \mathcal{C}$ is the configuration vector, or the vector of generalized coordinates, $\mathcal{C}$ is the configuration space, and for $i \in \{1, \ldots, m\}$ we have the control inputs u_i, and the control vector fields $\mathbf{g}_i(\boldsymbol{q})$. The considered nonholonomic constraints are of the form

$$\boldsymbol{A}(\boldsymbol{q})\dot{\boldsymbol{q}} = \mathbf{0}, \tag{4.2}$$

with $\boldsymbol{A}(\boldsymbol{q}) \in \mathbb{R}^{\kappa \times n}$, and $\dot{\boldsymbol{q}} \in T_{\boldsymbol{q}}\mathcal{C}$ is the vector of generalized velocities.[1]

In particular, in Section 4.2 we present the construction of the N-dimensional vector field $\mathbf{F}(\cdot)$ and the control design for the cases of the unicycle and Brockett's NDI, which are examples of kinematic systems subject to a single Pfaffian constraint equation, whereas Section 4.3 illustrates how the proposed framework extends to n-dimensional chained systems, where $\kappa \geq 1$ constraints apply. Numerical simulation examples are given alongside the technical discussion, both for the single constraint examples as well as the multiple constraint cases.

Finally, in Section 4.4 it is shown how the proposed methodology for kinematic n-dimensional nonholonomic systems can be extended to the control design of control affine underactuated mechanical systems with drift:

$$\dot{\mathbf{x}} = \mathbf{f}(\mathbf{x}) + \sum_{i=1}^{m} \mathbf{g}_i(\mathbf{x}) \mathrm{u}_i, \tag{4.3}$$

[1] In general, *kinematic* nonholonomic constraints can be written in Pfaffian form as $\boldsymbol{A}(\boldsymbol{q})\dot{\boldsymbol{q}} = \boldsymbol{b}(\boldsymbol{q})$, where $\boldsymbol{q} \in \mathbb{R}^n$ is the vector of generalized coordinates, $\boldsymbol{A}(\boldsymbol{q}) \in \mathbb{R}^{\kappa \times n}$ and $\boldsymbol{b}(\boldsymbol{q}) \in \mathbb{R}^{\kappa}$. If $\boldsymbol{b}(\boldsymbol{q}) = \mathbf{0}$ the constraints are called catastatic, otherwise they are called acatastatic.

where $\mathbf{x} = \begin{bmatrix} \boldsymbol{q}^\top & \boldsymbol{v}^\top \end{bmatrix}^\top \in \mathbb{R}^{2n}$ is the state vector including the generalized coordinates $\boldsymbol{q} \in \mathbb{R}^n$ and the system velocities $\boldsymbol{v} \in \mathbb{R}^n$, $\mathbf{f}(\mathbf{x})$ is the drift vector field and u_i, $\mathbf{g}_i(\cdot)$ are the i-th control input and control vector field, respectively. This class of systems is subject to second-order nonholonomic constraints, which essentially refer to non-integrable acceleration constraints of the form $\boldsymbol{a}(\boldsymbol{v})\dot{\boldsymbol{v}} = b(\boldsymbol{v})$. As a case study we treat the control design for the motion of an underactuated marine vehicle on the horizontal plane.

Our conclusions and our plans for future extensions are summarized in Section 4.5.

Overview of the Approach

The main idea of the approach is that, given an n-dimensional, *kinematic* nonholonomic system, one can define a smooth N-dimensional reference vector field $\mathbf{F} : \mathcal{L} \to T\mathcal{L}$ on a subset $\mathcal{L}$ of the configuration space $\mathcal{C}$, chosen from the family of vector fields (4.6), which are non-singular everywhere on $\mathcal{L}$ except for the origin $\boldsymbol{x} = \mathbf{0}$, which serves as the unique, isolated critical point of **dipole** type (see also Section 4.1).

The vector field $\mathbf{F}(\cdot)$ serves as a velocity reference for (5.1). This means that, at each $\boldsymbol{q} \in \mathcal{C}$, the system vector field $\dot{\boldsymbol{q}} \in T_{\boldsymbol{q}}\mathcal{C}$ is controlled to be made parallel to $\mathbf{F}(\cdot)$, i.e. is forced into the tangent space of the integral curve of $\mathbf{F}(\cdot)$ at $\boldsymbol{q}$.

This in turn implies that the constraint equations (4.2) (for the closed-loop system) take the form $\boldsymbol{A}(\boldsymbol{q})\mathbf{F}(\boldsymbol{q}) = \mathbf{0}$; we say in this case that $\mathbf{F}(\boldsymbol{q})$ satisfies, or is consistent with, the constraints at $\boldsymbol{q} \in \mathcal{C}$.

Definition 1 *A vector field*[2] $\mathbf{F} : \mathcal{C} \to T\mathcal{C}$ *will be said to be* consistent *with the nonholonomic constraints* (4.2) *at a point* $\boldsymbol{q} \in \mathcal{C}$*, (or that it satisfies the* consistency *condition at* $\boldsymbol{q}$*) if*

$$\boldsymbol{A}(\boldsymbol{q})\mathbf{F}(\boldsymbol{q}) = \mathbf{0}. \tag{4.4}$$

In fact, the explicit form of the condition (4.4) dictates the subset $\mathcal{L}$ of the configuration space $\mathcal{C}$ on which the vector field $\mathbf{F}(\cdot)$ is defined, and affects the analytic form of $\mathbf{F}(\cdot)$. To see how, consider the vector field $\mathbf{F} = \sum_{j=1}^{n} \mathrm{F}_j \frac{\partial}{\partial q_j}$, where $\left\{ \frac{\partial}{\partial q_1}, \ldots, \frac{\partial}{\partial q_n} \right\}$ are the unit basis vectors of the tangent space $T_{\boldsymbol{q}}\mathcal{C}$, and the resulting linear (in terms of F_j) system:

$$\begin{aligned} a_{11}\,\mathrm{F}_1 + a_{12}\,\mathrm{F}_2 + \ldots + a_{1n}\,\mathrm{F}_n &= 0, \\ a_{21}\,\mathrm{F}_1 + a_{22}\,\mathrm{F}_2 + \ldots + a_{2n}\,\mathrm{F}_n &= 0, \\ &\vdots \\ a_{\kappa 1}\,\mathrm{F}_1 + a_{\kappa 2}\,\mathrm{F}_2 + \ldots + a_{\kappa n}\,\mathrm{F}_n &= 0; \end{aligned}$$

then, if for example $\boldsymbol{A}(\boldsymbol{q})$ contains one zero column, i.e. if $\begin{bmatrix} a_{1j}(\boldsymbol{q}) & \ldots & a_{\kappa j}(\boldsymbol{q}) \end{bmatrix}^\top = \mathbf{0}$ for some $j \in \{1, \ldots, n\}$, the corresponding component F_j of the vector field *does not affect whether the consistency condition* (4.4) *is satisfied or not*, because the linear map always sends F_j to zero.

[2] Given an n-dimensional smooth manifold $\mathcal{N}$, a smooth vector field $\mathbf{F} : \mathcal{N} \to T\mathcal{N}$ is a function which, at each $\mathbf{x} \in \mathcal{N}$, assigns a vector $\mathbf{F}(\mathbf{x})$ that is tangent to $\mathcal{N}$, $\mathbf{F}(\mathbf{x}) \in T_{\mathbf{x}}\mathcal{N}$, whose components in the frames of any local coordinates (U, φ) are smooth functions on the domain U of the coordinates. A point $\mathbf{x} \in \mathcal{N}$ at which $\mathbf{F}(\mathbf{x}) = \mathbf{0}$ is called a *singular* point of the vector field, otherwise it is referred to as *regular* [Boo86]. The consistency condition (4.4) is trivially satisfied at singular points.

One could therefore define a vector field $\mathbf{F}$ in which $\mathrm{F}_j = 0$. Since reference vector field $\mathbf{F}$ has no component along q_j, may just as well be independent of this variable.

In this sense, if $\boldsymbol{A}(\boldsymbol{q})$ has $0 \leq n_0 < n$ zero columns, the dimension of the vector field $\mathbf{F}$ can be set equal to $\mathrm{N} = n - n_0$. We refer to the $n - n_0$ coordinates q_i, $i \in \{1, \ldots, n\}$, whose generalized velocities $\dot{q}_i$ are associated with the non-zero columns of $\boldsymbol{A}(\boldsymbol{q})$ as **leafwise** states $\boldsymbol{x}$, and to the remaining n_0 states whose generalized velocities are associated with the zero columns of $\boldsymbol{A}(\boldsymbol{q})$ as **transverse** states $\boldsymbol{t}$. The configuration space $\mathcal{C}$ is then trivially foliated as $\mathcal{C} = \mathcal{L} \times \mathcal{T}$, where $\mathcal{L}$ is the submanifold of the leafwise states $\boldsymbol{x}$, $\mathcal{T}$ is the submanifold of the transverse states $\boldsymbol{t}$, $\dim \mathcal{L} = n - n_0$, $\dim \mathcal{T} = n_0$.

The vector field $\mathbf{F}(\cdot)$ is then defined on the N-dimensional leaf space $\mathcal{L}$, in terms of the leafwise variables $\boldsymbol{x}$, and is non-vanishing everywhere on $\mathcal{L}$ except for the origin $\boldsymbol{x} = \mathbf{0}$ of the local coordinate system. The singularity $\boldsymbol{x} = \mathbf{0}$ is the unique, isolated critical point of the vector field $\mathbf{F}(\cdot)$, and is by construction a *rose*, i.e. all integral curves begin and end at the critical point; in that sense, any of the integral curves of $\mathbf{F}(\cdot)$ offers a path to $\boldsymbol{x} = \mathbf{0}$.

Thus, in the case that the constraint matrix $\boldsymbol{A}(\boldsymbol{q})$ has no zero columns, one takes $\mathrm{N} = n$ and $\boldsymbol{x} \triangleq \boldsymbol{q}$, i.e. the leaf space $\mathcal{L}$ coincides with the whole configuration space $\mathcal{C}$. Then, the vector field $\mathbf{F}(\cdot)$ is defined on the whole configuration space $\mathcal{C}$ and vanishes only at the origin $\boldsymbol{q} = \mathbf{0}$, see the case of NDI in Section 4.2.2.

On the other hand, if $\boldsymbol{A}(\boldsymbol{q})$ has n_0 zero columns, one can pick $\mathrm{N} = n - n_0$, $\mathbf{F}(\cdot)$ is defined on the leaf space $\mathcal{L} \subset \mathcal{C}$ in terms of the $n - n_0$ leafwise variables $\boldsymbol{x}$, and is singular on a submanifold $\mathcal{A} = \{\boldsymbol{q} \in \mathcal{C} \mid \boldsymbol{x} = \mathbf{0}\}$ that contains the origin $\boldsymbol{q} = \mathbf{0}$. Note, however, that this simplification comes at a cost: since dropping some of the configuration variables from the definition of $\mathbf{F}$ permits the latter to vanish on a whole submanifold $\mathcal{A}$ which contains the origin $\boldsymbol{q} = \mathbf{0}$, one may be forced to use switching control for the cases where the system is initiated on this submanifold, see the case of the unicycle in Section 4.2.1.

Input discontinuities are assumed to yield a closed loop vector field in (5.1) which is piecewise continuous. Solutions are then understood in the Filippov sense, i.e. $\dot{\boldsymbol{q}} \in \mathfrak{F}(\boldsymbol{q})$, where $\mathfrak{F}$ is a set valued map given by

$$\mathfrak{F}(\boldsymbol{q}) \triangleq \overline{\mathrm{co}} \left\{ \lim_{j \to \infty} \sum_{i=1}^{m} \boldsymbol{g}_i(\boldsymbol{q}_j) u_i : \boldsymbol{q}_j \to \boldsymbol{q}, \boldsymbol{q}_j \notin S_q \right\} \ ,$$

and S_q is any set of measure zero.

In this sense, the main idea of the approach is that instead of trying to stabilize (5.1) to the origin, one can use the available control authority to steer the system vector field onto the tangent bundle of the integral curves of $\mathbf{F}(\cdot)$, and "flow" along the reference vector field on its way to the origin $\boldsymbol{q} = \mathbf{0}$. In the sections that follow we show that these two objectives suggest the choice of particular Lyapunov-like functions in terms of the leafwise states $\boldsymbol{x} \in \mathbb{R}^{\mathrm{N}}$ and the transverse states $\boldsymbol{t} \in \mathbb{R}^{n-\mathrm{N}}$, and enable one to establish convergence to the origin based on standard techniques.

Thus, the control strategy we consider involves two steps:

1. find an N-dimensional vector field $\mathbf{F}(\cdot) : \mathcal{L} \to T\mathcal{L}$, the integral curves of which contain the origin $\boldsymbol{x} = \mathbf{0}$ of the local coordinate system on $\mathcal{L}$;

2. design a feedback control scheme to first align the system's vector field $\dot{\boldsymbol{q}} \in T_{\boldsymbol{q}}\mathcal{C}$ with $\mathbf{F}(\cdot)$, and "flow" along $\mathbf{F}(\cdot)$ ensuring that $\dot{\boldsymbol{q}}$ is non-vanishing everywhere but the origin $\boldsymbol{q} = \mathbf{0}$.

Guidelines for Control Design

For *kinematic* nonholonomic systems in particular, the above process can be described in more detail as follows: Given (5.1) subject to (4.2),

- Consider the constraint matrix $\boldsymbol{A}(\boldsymbol{q}) \in \mathbb{R}^{\kappa \times n}$, which has $0 \leq n_0 < n$ zero columns, where n is the number of generalized velocities $\dot{\boldsymbol{q}}$. Refer to the $n - n_0$ states (coordinates) q_i, $i \in \{1, \ldots, n\}$, whose generalized velocities $\dot{q}_i$ are associated with the non-zero columns of $\boldsymbol{A}(\boldsymbol{q})$ as *leafwise* states $\boldsymbol{x}$, and to the remaining n_0 states whose generalized velocities are associated with the zero columns of $\boldsymbol{A}(\boldsymbol{q})$ as *transverse* states $\boldsymbol{t}$.
- Foliate[3] the configuration space $\mathcal{C}$ as $\mathcal{F} = \mathcal{L} \times \mathcal{T}$, where $\mathcal{L}$ is the submanifold of the leafwise states $\boldsymbol{x}$, $\mathcal{T}$ is the submanifold of the transverse states $\boldsymbol{t}$, and $\dim \mathcal{L} = n - n_0$, $\dim \mathcal{T} = n_0$.
- Pick a reference vector field $\mathbf{F}(\cdot)$ from the family of vector fields given by (4.6), dependent only on the leafwise states $\boldsymbol{x}$, so that its tangent vectors are tangent to $\mathcal{L} \subseteq \mathcal{C}$.
- Verify that all integral curves of $\mathbf{F}(\cdot)$ contain the origin $\boldsymbol{x} = \mathbf{0}$ of the local coordinate system of the leafwise submanifold $\mathcal{L}$.
- Define a κ-dimensional system output as $\boldsymbol{h}(\cdot) = \boldsymbol{A}(\boldsymbol{q})\ \mathbf{F}$ and force the right hand side of (5.1) to align with $\mathbf{F}$ by selecting control inputs to make all elements of $\boldsymbol{h}(\cdot)$ converge to zero. To do this, you may want to define a number of "consistency error"' variables s_j, that measure how far away the components of $\boldsymbol{h}$ are from zero.
- Establish formally convergence of the trajectories of (5.1) to the origin by selecting a Lyapunov-like function V of the form $V = \frac{1}{2}(\sum_{j=1}^{\kappa} {s_j}^2 + \ldots + \|\boldsymbol{x}\|^2)$, or employ a singular perturbation analysis considering the dynamics of $\boldsymbol{t}$ as part of the boundary layer subsystem.

4.1 Vector Fields and Isolated Critical Points

As already mentioned in Chapter 2, our inspiration for addressing the steering problem of the **unicycle** to the origin using a reference vector field comes from the form of the integral curves of the electric point dipole.

[3] An m-dimensional foliation $\mathcal{F}$ of an n-dimensional manifold $\mathcal{N}$ is a collection of disjoint, connected, immersed m-dimensional submanifolds of $\mathcal{N}$ (called the leaves of the foliation), whose union is $\mathcal{N}$, with the following property: Every point in $\mathcal{N}$ has a neighborhood U and a system of local coordinates $x = (x^1, \ldots, x^n) : U \to \mathbb{R}^n$ such that each leaf of the foliation intersects U in either the empty set, or a countable union of m-dimensional slices of the form $x^{m+1} = \text{constant}, \ldots, x^n = \text{constant}$ [Lee02]. Intuitively, an m-dimensional foliation $\mathcal{F}$ of $\mathcal{N}$ looks locally like a decomposition $\mathcal{N} = B \times F$, where $B \subseteq \mathbb{R}^m$ and $F \subseteq \mathbb{R}^{n-m}$. The set B is spanned by all "leafwise" directions while the set F is spanned by the "transverse" directions.

In order to formally describe the behavior of the integral curves of a vector field, let us first briefly mention some related notions. For more information please refer to [Boo86, Hen94, Lee02].

4.1.1 Critical Points of Vector Fields

Definition 1 *A vector field on an open subset $U \subset \mathbb{R}^n$ is a function which assigns to each point $p \in U$ a vector $X_p \in T_p(\mathbb{R}^n)$. A vector field on $\mathbb{R}^n$ is C^∞ (smooth) if its components relative to the canonical basis are C^∞ functions on U.*

Definition 2 *Given a (smooth) vector field X on $\mathbb{R}^n$, we say that a curve $t \to F(t)$ defined on an open interval J of $\mathbb{R}$ is an integral curve of X if $\frac{dF}{dt} = X_{F(t)}$ on J.*[4] *By definition, an integral curve is connected.*

Remark 1 *A point p of U at which $X_p = 0$ is called a **singular**, or **critical** point of the vector field, and any other point is referred to as **regular**.*

In the neighborhood of a regular point the integral curves are - within diffeomorphism - the family of parallel lines $x^2 = c^2, \ldots, x^n = c^n$ in $\mathbb{R}^n$, where $(x^1, x^2, \ldots, x^n)$ is a (local) coordinate frame in U [Boo86]. On the other hand, the pattern of integral curves at an isolated singularity can take many forms, even in the two-dimensional case.

Singular points are typically distinguished to those that are reached by no integral curve (called **center** type) and those that are reached by at least one integral curve (called **non-center** type).

In the case of a **center** type singularity, one can find a neighborhood of the singular point where all integral curves are closed, inside one another, and contain the singular point into their interior. A focus is an example of a center-type singular point.

In the case of **non-center** type singularities, one actually has that *at least two* integral curves converge to the singular point. To analyze the local structure of non-center type singularities, one has to consider the behavior of all the integral curves that pass through the neighborhood of the critical point [TSH00]. This neighborhood is typically made of several curvilinear sectors; a curvilinear sector is defined as the region bounded by a circle C with arbitrary small radius, and two integral curves, S and S', which both converge (for either $t \to +\infty$, or $t \to -\infty$) towards the critical point O (Fig. 4.1(a)). Then, one considers the integral curves passing through the *open* sector g, in order to distinguish between the following three possible types of curvilinear sectors.

1. S tends to O for $t \to +\infty$ and S' tends to O for $t \to -\infty$, and every integral curve through the open sector g leaves g for both $t \to +\infty$ and $t \to -\infty$. Then, the sector is called a **hyperbolic** sector (Fig. 4.1(b)).

2. S and S' both tend to O for $t \to +\infty$ (resp. $t \to -\infty$), and every integral curve through the open sector g tends to O for $t \to \infty$ (resp. $t \to -\infty$) without leaving g, and leaves g for $t \to -\infty$ (resp. $t \to \infty$): Then, the sector is called a **parabolic** sector (Fig. 4.2(a)).

[4] The same definition holds in general for a vector field X on a manifold M.

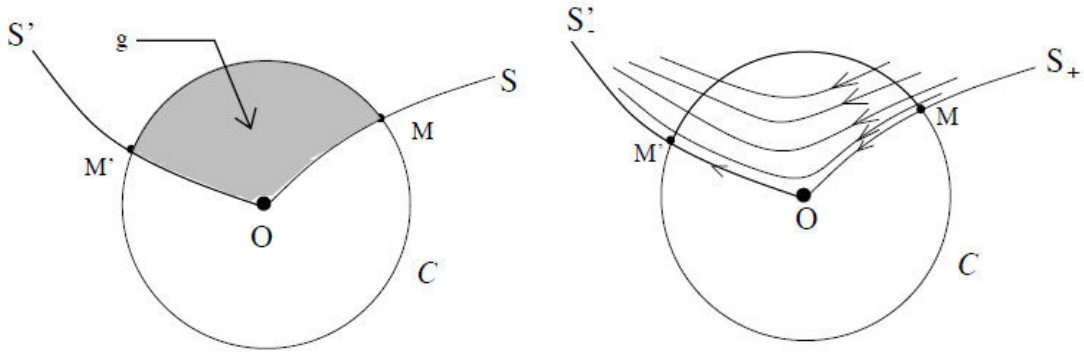

(a) A curvilinear sector (b) A hyperbolic sector

Figure 4.1: A curvilinear sector (left) and a hyperbolic sector (right). Images are taken from [TSH00].

3. S and S' are two semi-integral curves on the same integral curve: All the paths through a point inside this loop form nested loops tending to O for both $t \to \infty$ and $t \to -\infty$: Then, the sector is called an **elliptic** sector (Fig. 4.2(b)).

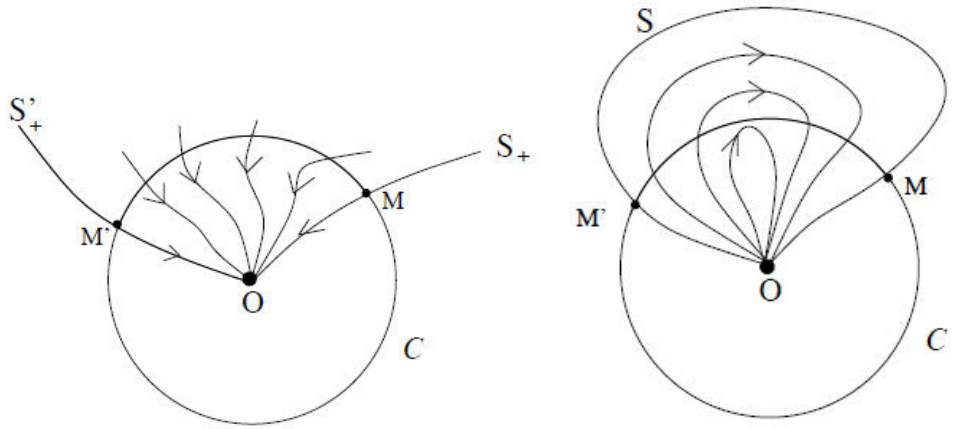

(a) A parabolic sector (b) An elliptic sector

Figure 4.2: A parabolic sector (left) and an elliptic sector (right). Images are taken from [TSH00].

In other words, a critical point of *non-center* type may be made up of either:

- elliptic sectors, where all paths begin and end at the critical point,
- parabolic sectors, where just one end of the path is at the critical point, and
- hyperbolic sectors, where the paths do not reach the critical point at all.

A typical (non-center) critical point might have sectors of all three types (Fig. 4.3). The paths that separate each sector from the next are called *separatrixes*. It may happen that a critical point has only one type of sector.

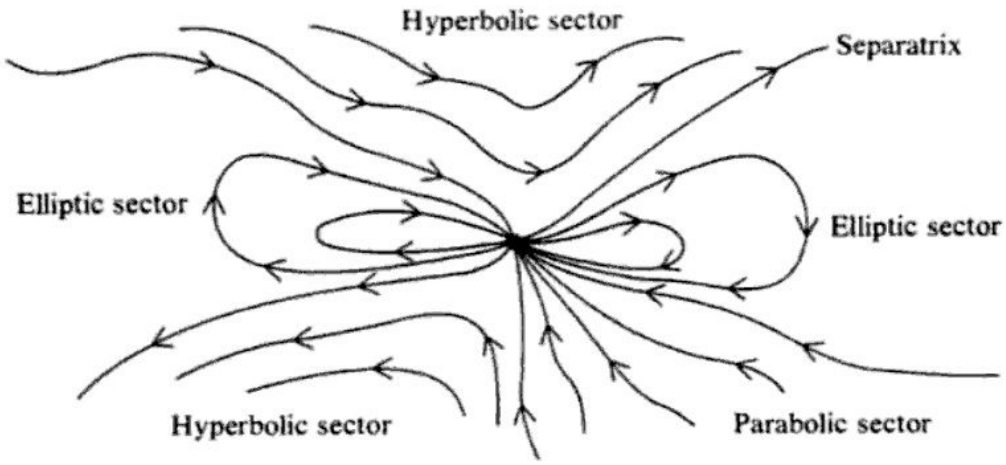

Figure 4.3: A typical isolated critical point. Image taken from [Hen94].

- A critical point with only parabolic sectors is called a **node**.
- A critical point with only elliptic sectors is called a **rose**; an example is the dipole.
- A critical point with only hyperbolic sectors is called a **cross point**; saddle points are cross points with four sectors.

4.1.2 The critical point of the 2-dimensional dipolar vector field

As mentioned in Chapter 2, the point electric dipole in a 2-dimensional Euclidean space is realized as a physical electric dipole of two opposite charges of equal magnitude, which lie at an infinitesimal distance between them. The vector field of the physical electric dipole has two critical points (nodes); one stable (the negative charge) and one unstable (the positive charge). As the distance between the charges tends to zero, the nodes of the original vector field join to form a single critical point, which is a dipole [Hen94]. Since the critical point of the resulting vector field is of elliptic type, all integral curves begin at, and end at, the critical point. *In this sense, any of the integral curves offers a path to the critical point.*

Inspired by the expression of the vector field of the point electric dipole in a 2-dimensional Euclidean space, we introduce the **dipolar** vector field:

$$\mathbf{F}(\boldsymbol{r}) = \lambda(\boldsymbol{p}^\top \boldsymbol{r})\boldsymbol{r} - \boldsymbol{p}(\boldsymbol{r}^\top \boldsymbol{r}), \tag{4.5}$$

where $\boldsymbol{r} = \begin{bmatrix} x & y \end{bmatrix}^\top$ is the vector of position coordinates w.r.t. to a frame $\mathcal{G}$ in $\mathbb{R}^2$, and $\boldsymbol{p}$ stands for the dipole moment vector, which can be thought as the quantity that generates the field. The vector field components F_x, F_y of $\mathbf{F} = \mathrm{F}_x \frac{\partial}{\partial x} + \mathrm{F}_y \frac{\partial}{\partial y}$ for $\boldsymbol{p} = \begin{bmatrix} 1 & 0 \end{bmatrix}^\top$ read:

$$\begin{aligned} \mathrm{F}_x &= (\lambda - 1)x^2 - y^2, \\ \mathrm{F}_y &= \lambda xy. \end{aligned}$$

For $\lambda \neq 1$ the vector field $\mathbf{F}(\cdot)$ is non-vanishing everywhere but the origin $\boldsymbol{r} = \mathbf{0}$, which is the unique, isolated critical point of the vector field, while for $\lambda > 1$ the critical point $\boldsymbol{r} = \mathbf{0}$ is a *dipole*, see Fig. 4.4(a).

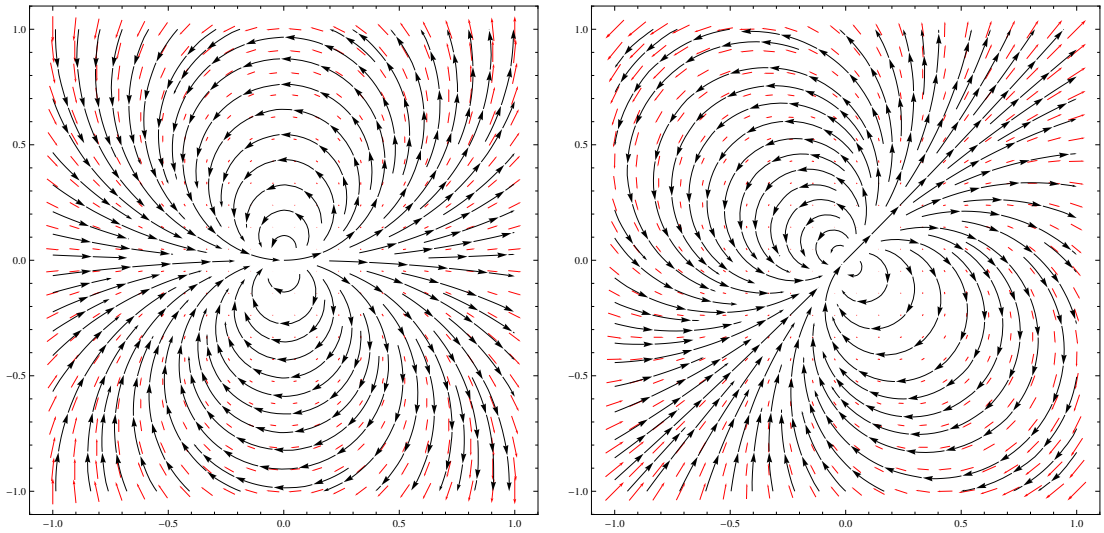

Figure 4.4: Vector Field $\mathbf{F}(\cdot)$ for **(a)** $\boldsymbol{p} = [1\ 0]$ (left) and **(b)** $\boldsymbol{p} = \frac{1}{\sqrt{2}}[1\ 1]$ (right).

Furthermore, the integral curves are symmetric with respect to the axis of the vector $\boldsymbol{p}$, see Fig. 4.4(b) the vector field $\mathbf{F}(\cdot)$ given by (4.5), for $\lambda = 2$, $\boldsymbol{p} = \frac{1}{\sqrt{2}}\begin{bmatrix}1 & 1\end{bmatrix}^\top$. In that sense, any of the integral curves of $\mathbf{F}(\cdot)$ offers a path to $\boldsymbol{r} = \mathbf{0}$, while $\boldsymbol{p}$ dictates the orientation of the integral curves w.r.t. the global frame $\mathcal{G}$.

Thus, the idea for the control design of the unicycle is, at each $\boldsymbol{q} \in \mathcal{C}$, to force the system vector field $\dot{\boldsymbol{q}} \in T_{\boldsymbol{q}}\mathcal{C}$ to "align with" the dipolar vector field $\mathbf{F}(\cdot)$, which by construction offers a path to the critical point $\boldsymbol{r} = \mathbf{0}$. Furthermore, note that by picking a (unit) dipole moment vector $\boldsymbol{p}$ that satisfies the constraint equations *at the origin*, i.e. such that $\boldsymbol{A}(\mathbf{0})\boldsymbol{p} = \mathbf{0}$, one gets a dipolar vector field $\mathbf{F}(\cdot)$ whose integral curves can serve to indirectly control the orientation of the unicycle as well, since they converge to $\boldsymbol{x} = \mathbf{0}$ parallel to the x_G axis.

Inspired by this, we propose the following general class of N-dimensional vector fields

$$\mathbf{F}(\boldsymbol{x}) = \lambda\left(\boldsymbol{p}^\top\boldsymbol{x}\right)\boldsymbol{x} - \boldsymbol{p}\left(\boldsymbol{x}^\top\boldsymbol{x}\right), \tag{4.6}$$

where $\mathrm{N} \leq n$, $\boldsymbol{x} \in \mathbb{R}^{\mathrm{N}}$ is the vector of the leafwise states, $\boldsymbol{p} \in \mathbb{R}^{\mathrm{N}}$ such that $\boldsymbol{A}(\mathbf{0})\boldsymbol{p} = \mathbf{0}$, and $\lambda \geq 2$. In the following sections, we show that (4.6) can be used to design controllers for a wide class of nonholonomic systems.

4.2 Systems with a single Pfaffian constraint

In this section we present the construction of the reference vector field and the proposed control strategy for two systems that are subject to a single Pfaffian constraint, namely the unicycle and the NDI.

Although the unicycle and the NDI are globally diffeomorphic, we use both examples to demonstrate how the approach applies in any given coordinates, without the need of finding transformations into new, convenient coordinates, as often encountered in the literature. Moreover,

the NDI case is indicative of how the approach applies to a system where the constraint matrix $\boldsymbol{A}(\boldsymbol{q})$ in the given coordinates has no zero columns.

4.2.1 The unicycle: a first example

To illustrate the proposed control strategy, let us first consider the unicycle, given by

$$\begin{bmatrix}\dot{x}\\ \dot{y}\\ \dot{\theta}\end{bmatrix} = \begin{bmatrix}\cos\theta\\ \sin\theta\\ 0\end{bmatrix} u_1 + \begin{bmatrix}0\\ 0\\ 1\end{bmatrix} u_2, \tag{4.7}$$

where $\boldsymbol{q} = \begin{bmatrix}x & y & \theta\end{bmatrix}^\top \in \mathcal{C}$ is the configuration vector, $\mathcal{C}$ is a 3-dimensional smooth manifold denoting the configuration space, x, y, θ are the generalized coordinates with x and y being the position coordinates and θ the orientation with respect to some global cartesian coordinate frame $\mathcal{G}$, and u_1, u_2 are the control inputs. The $\kappa = 1$ nonholonomic constraint for (4.7) is written in Pfaffian form as

$$\underbrace{\begin{bmatrix}-\sin\theta & \cos\theta & 0\end{bmatrix}}_{\boldsymbol{a}^\top(\boldsymbol{q})} \begin{bmatrix}\dot{x}\\ \dot{y}\\ \dot{\theta}\end{bmatrix} = 0 \;\Leftrightarrow\; \langle \boldsymbol{a}^\top(\boldsymbol{q}), \dot{\boldsymbol{q}}\rangle = 0,$$

where $\langle\cdot,\cdot\rangle$ stands for the inner product.[5]

For a vector field $\mathbf{F} = \mathrm{F}_x \frac{\partial}{\partial x} + \mathrm{F}_y \frac{\partial}{\partial y} + \mathrm{F}_\theta \frac{\partial}{\partial \theta}$ to satisfy the consistency condition (4.4) at a point $\boldsymbol{q}$, it needs to be orthogonal to $\boldsymbol{a}(\boldsymbol{q})$:

$$\underbrace{\begin{bmatrix}-\sin\theta & \cos\theta & 0\end{bmatrix}}_{\boldsymbol{a}^\top(\boldsymbol{q})} \begin{bmatrix}\mathrm{F}_x\\ \mathrm{F}_y\\ \mathrm{F}_\theta\end{bmatrix} = 0 \Rightarrow \mathrm{F}_y \cos\theta - \mathrm{F}_x \sin\theta = 0. \tag{4.8}$$

In this case, the constraint matrix (vector) $\boldsymbol{a}^\top(\boldsymbol{q})$ contains $n_0 = 1$ zero column (element) and thus the component F_θ does not affect whether the consistency condition (4.8) is satisfied. Thus, one can define $\mathrm{F}_\theta = 0$, and search for an $\mathrm{N} = n - n_0 = 2$ dimensional vector field $\mathbf{F}(\cdot)$, in terms of F_x, F_y only. The position coordinates x, y are the leafwise states, and the orientation θ is the transverse state.

From a geometric point of view, setting $\mathrm{F}_\theta = 0$ implies that, for each $\boldsymbol{q} \in \mathcal{C}$, the vector field $\mathbf{F}(\cdot)$ should lie in the subspace $\mathcal{W} = \left\{\boldsymbol{w} \in T_{\boldsymbol{q}}\mathcal{C} \mid \boldsymbol{w} = \begin{bmatrix}w_x & w_y & 0\end{bmatrix}^\top\right\}$ of the tangent space $T_{\boldsymbol{q}}\mathcal{C}$ of $\mathcal{C}$. The vector field $\mathbf{F}(\cdot)$ should be tangent to the submanifold[6] $\mathcal{S} = \mathbb{R}^2$ at $\boldsymbol{q}$, (Fig. 4.5).[7]

[5] The notation $\langle \boldsymbol{w}, \boldsymbol{v}\rangle := \boldsymbol{w}(\boldsymbol{v})$, where $\boldsymbol{w}(\cdot) \in W^\star$, $\boldsymbol{v} \in W$ and $W^\star$ is the dual space of the vector space W, stands for the duality pairing, that is a bilinear map $\langle\cdot,\cdot\rangle : W^\star \times W \to \mathbb{F}$, where $\mathbb{F}$ is a (real or complex) field. Nevertheless, it often occurs in the literature that the "value" of the linear functional $\boldsymbol{w}(\cdot)$ at $\boldsymbol{v} \in W$ is represented by an inner product [Isi95]. Here we adopt this notation and treat $\boldsymbol{w}(\cdot)$ as co-vectors rather than linear maps.

[6] A subset $\mathcal{M} \subset \mathcal{N}$, where $\mathcal{N}$ is a smooth manifold of dimension n, is said to have the submanifold property if there exists an integer $0 \le m \le n$ such that for each $p \in \mathcal{M}$ there is a coordinate neighborhood U and a (local) coordinate function $\varphi : U \to \mathbb{R}^n$ of $\mathcal{N}$ such that $\varphi(p) = (0,0,0,\ldots,0), \varphi(U \cap \mathcal{M}) = \{x \in \varphi(U) \mid x_{m+1} = x_{m+2} = \ldots = x_n = 0\}$ if $m < n$, or $(U \cap \mathcal{M}) = U$ if $m = n$ [Boo86]. A subset $\mathcal{M} \subset \mathcal{N}$ with the submanifold property for some $m \le n$ is a (regular or embedded) submanifold of $\mathcal{N}$ of dimension m and of codimension $n - m$ [Lee02].

[7] A vector field X on $\mathcal{N}$ is said to be tangent to $\mathcal{S}$ if $X_p \in T_p\mathcal{S} \subset T_p\mathcal{N}$, for each $p \in \mathcal{S}$ [Lee02].

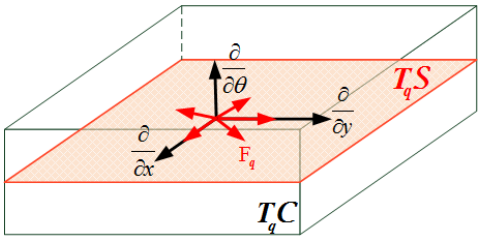

Figure 4.5: The vector field $\mathbf{F}(\boldsymbol{q})$ is by definition restricted to lie in the tangent space $T_{\boldsymbol{q}}\mathcal{S} \subset T_{\boldsymbol{q}}\mathcal{C}$, for each $\boldsymbol{q} \in \mathcal{S}$.

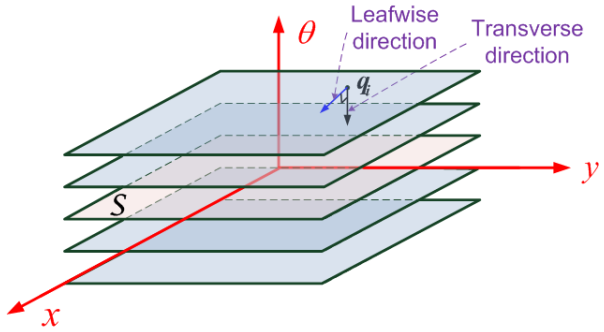

Figure 4.6: The foliation $\mathcal{F}$ of the 3-dimensional configuration space $\mathcal{C}$ of the unicycle into $\mathcal{C} = \mathbb{R}^2 \times \mathbb{S}^1$.

The submanifold $\mathcal{S}$ is a 2-dimensional leaf of a codimension-1 foliation $\mathcal{F} = \mathcal{L} \times \mathcal{T}$ of the configuration space into $\mathcal{C} = \mathbb{R}^2 \times \mathbb{S}^1$ (Fig. 4.6). Consequently, as expected, the vector field $\mathbf{F}(\cdot)$ is tangent to the leafwise directions $\mathcal{L} = \mathbb{R}^2$ of $\mathcal{F}$. Its analytic form is given out of (4.5), where the vector $\boldsymbol{p}$ is selected based on the structure of $\boldsymbol{a}(\boldsymbol{q})$ at the origin: $\boldsymbol{p}$ is required to lie on the (local manifestation of the) constraint surface at the origin, in order to be consistent with the constraints:

$$\langle \boldsymbol{a}^\top(\mathbf{0}), \boldsymbol{p} \rangle = 0 \Rightarrow \begin{bmatrix} -\sin(0) & \cos(0) & 0 \end{bmatrix} \begin{bmatrix} p_x \\ p_y \\ p_\theta \end{bmatrix} = 0, \tag{4.9}$$

where $p_\theta = 0$, for the same reason that F_θ can be set to zero. Condition (4.9) is satisfied for any $p_x \in \mathbb{R}$ and for $p_y = 0$, but since $\boldsymbol{p}$ needs to be nonzero we have to set $\boldsymbol{p} \triangleq \begin{bmatrix} p_x & 0 \end{bmatrix}^\top$ with $p_x \neq 0$. For $p_x = 1$ and $\lambda = 3$, the vector field components F_x, F_y in (4.5) take the form

$$\mathrm{F}_x = 2x^2 - y^2 = 3x^2 - (x^2 + y^2), \quad \mathrm{F}_y = 3xy. \tag{4.10}$$

The resulting field is shown in Fig. 4.7(a). Since $\mathrm{F}_\theta = 0$, the vector field (4.10) on $\mathcal{C}$ does not vary along the transverse direction of the foliation $\mathcal{F}$, see Fig. 4.7(b).

Given the decomposition $\mathcal{F} = \mathcal{L} \times \mathcal{T}$ and the vector field $\mathbf{F}(\cdot) : \mathcal{L} \to T\mathcal{L}$, the control objective is thus to find a control law $\boldsymbol{u} = \boldsymbol{\gamma}(\boldsymbol{q})$ such that, starting from any initial configuration $\boldsymbol{q_i} \in \mathcal{C}$, the system trajectories $\boldsymbol{q}(t)$ evolve along both the transverse direction and the leafwise direction, until they converge to the origin $\boldsymbol{q} = \mathbf{0}$. We refer to the evolution along the transverse direction as motion *from leaf to leaf*, and the evolution on the leafwise direction as motion *on the leaf*.

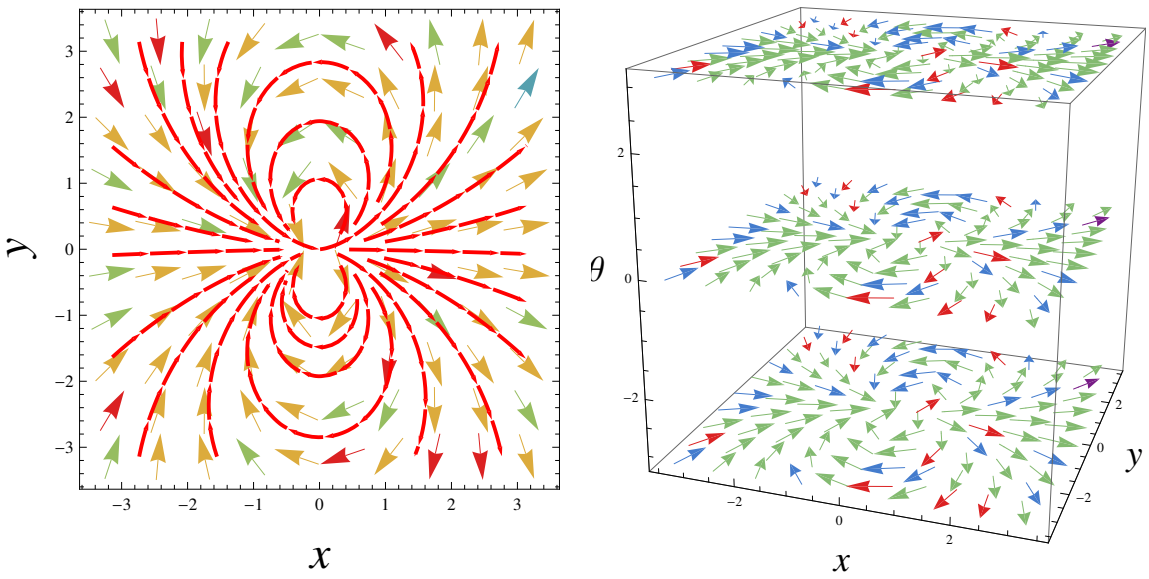

(a) The vector field $\mathbf{F}(\boldsymbol{r})$ on $\mathbb{R}^2$

(b) The vector field $\mathbf{F}(\boldsymbol{r})$ on $\mathcal{C}$

Figure 4.7: The vector field $\mathbf{F}(\boldsymbol{r})$ in the case of the unicycle.

At this point, note also that for each $\theta \in \mathbb{S}^1$, the condition (4.8) is a linear equation in F_x and F_y. We can set $\mathrm{F}_x = \|\mathbf{F}\| \cos\phi$ and $\mathrm{F}_y = \|\mathbf{F}\| \sin\phi$, where $\|\mathbf{F}\|$ is the Euclidean norm of the vector field at $\boldsymbol{q} \in \mathcal{C}$, and ϕ is the direction of the vector $\mathbf{F}(\boldsymbol{q})$ with respect to a global frame $\mathcal{G}$. The consistency condition (4.8) then becomes

$$\langle \boldsymbol{a}^\top(\boldsymbol{q}), \mathbf{F} \rangle = \|\mathbf{F}\| \sin(\phi - \theta) = 0. \tag{4.11}$$

For a nonsingular vector field $\mathbf{F}$, the consistency condition (4.11) holds as long as $\sin(\phi - \theta) = 0 \Rightarrow \phi - \theta = \xi\pi$, with $\xi \in \mathbb{Z}$, i.e. as long as the system vector field $\dot{\boldsymbol{q}}$ w.r.t. the global frame $\mathcal{G}$ is collinear (or aligns) with the vector field $\mathbf{F}(\cdot)$.

To enable the alignment of the system's vector field with (4.10), we define the map $h(\cdot) : \mathcal{C} \to \mathbb{R}$

$$h(\boldsymbol{q}) = \langle \boldsymbol{a}^\top(\boldsymbol{q}), \mathbf{F} \rangle. \tag{4.12}$$

When $h(\boldsymbol{q}) = 0$, $\mathbf{F}(\boldsymbol{q})$ is in the null space of the constraint co-vector $\boldsymbol{a}^\top(\boldsymbol{q})$ at $\boldsymbol{q}$, and can be locally realized as a linear combination of the control vector fields $\mathbf{g}_i(\boldsymbol{q})$. We treat $h(\boldsymbol{q}) \neq 0$ as an error variable, or output which should be regulated to zero. For a nonsingular vector field $\mathbf{F}$, $h(\boldsymbol{q}) = 0 \overset{(4.11)}{\Leftrightarrow} \{\theta - \phi = 0 \text{ or } \theta - \phi = \pm\pi\}$. In this case, the orientation θ of the unicycle is tangent to the integral line of the vector field (4.10).

Getting $h(\boldsymbol{q}) \to 0$ in the case of the unicycle is realized by making $\theta \to \phi + \xi\pi$, $\xi \in \mathbb{Z}$. Let us define the consistency error $s = \theta - \phi$ and force the dynamics $\dot{s} = -ks, k > 0$, by choosing u_2

$$\dot{\theta} - \dot{\phi} = -k(\theta - \phi) \Rightarrow u_2 = -k(\theta - \phi) + \dot{\phi}. \tag{4.13}$$

With this choice of u_2, the dynamics of the reference vector field $\mathbf{F}$ orientation angle, ϕ become

$$\dot{\phi} \overset{(4.7)}{=} \frac{(3y\,\mathrm{F}_x - 4x\,\mathrm{F}_y)\cos\theta + (3x\,\mathrm{F}_x + 2y\,\mathrm{F}_y)\sin\theta}{\mathrm{F}_x{}^2 + \mathrm{F}_y{}^2}\, u_1.$$

The quantity $\dot{\phi}$ is not defined when $\|\mathbf{F}\| = 0$, i.e., at the singular points of $\mathbf{F}$ on the submanifold

$$\mathcal{A} = \left\{ \boldsymbol{q} \in \mathcal{C} \mid \boldsymbol{q} = \begin{bmatrix} 0 & 0 & \theta \end{bmatrix}^\top \right\}, \theta \in \mathbb{S}^1.$$

Thus, if $\boldsymbol{q}(0) \in \mathcal{A}$, a different control law should be applied; for instance, one can set $u_1 = 0$, $u_2 = -k\ \theta$. Note that this choice renders $\mathcal{A}$ positively invariant and forces the system to approach the origin exponentially while staying in $\mathcal{A}$. No control switching is needed.

The conditions (4.12), (4.13) determine the motion of the system in the transverse direction. With the choice of (4.13), the unicycle aligns itself with $\mathbf{F}$ as it moves *from leaf to leaf*. Along the leaves, on the other hand, the system should be driven to the origin of each local (x, y) coordinate system. In order to analyze the dynamics on the leaves, we consider a smooth, positive definite function V in terms of the leafwise states x, y and the consistency error s

$$V = \frac{1}{2}(x^2 + y^2 + s^2) = \frac{1}{2}\left(x^2 + y^2 + (\theta - \phi)^2\right),$$

and take its time derivative along the system trajectories,

$$\dot{V} = (x\cos\theta + y\sin\theta)u_1 + (\theta - \phi)(u_2 - \dot{\phi}) = (x\cos\theta + y\sin\theta)u_1 - k(\theta - \phi)^2.$$

Then, choosing the control input u_1 as

$$u_1 = -k_1 \operatorname{sgn}(x\cos\theta + y\sin\theta)\|\boldsymbol{r}\|, \quad k_1 > 0, \tag{4.14}$$

where $\operatorname{sgn}(a) = 1$ for $a \geq 0$, and $\operatorname{sgn}(a) = -1$ for $a < 0$. This choice of input renders the right hand side of (4.7) *piecewise* continuous, and solutions are considered in the Filippov sense:

$$\dot{\boldsymbol{q}} \in \overline{\text{co}} \left\{ \lim \begin{bmatrix} \cos\theta_i \\ \sin\theta_i \\ 0 \end{bmatrix} u_1(\boldsymbol{q}_i) + \begin{bmatrix} 0 \\ 0 \\ 1 \end{bmatrix} u_2(\boldsymbol{q}_i) : \boldsymbol{q}_i \to \boldsymbol{q}, \boldsymbol{q}_i \notin S_q \right\}$$

If we now define the set-valued (time) derivative of V as [BC99]

$$\dot{\tilde{V}} \triangleq \left\{ a \in \mathbb{R} \mid \exists v \in \mathfrak{F}(\boldsymbol{q}) : v^T \cdot \nabla V = a \right\} \ ,$$

we can invoke the nonsmooth version of the invariance principle of [BC99, Thm 3] to conclude that $\boldsymbol{q}(t) \to \mathbf{0}$ as $t \to \infty$.

To this end, note first that away from the discontinuity one has $\dot{V} = -k_1(x\cos\theta + y\sin\theta)\operatorname{sgn}(x\cos\theta + y\sin\theta)\|\boldsymbol{r}\| - k(\theta - \phi)^2 \leq 0$. The set $\Omega = \{\boldsymbol{q} \in \mathcal{C} \mid \dot{V}(\boldsymbol{q}) = 0\}$ is given as the union $\Omega_1 \cup \Omega_2$, where $\Omega_1 = \{\boldsymbol{q} \in \mathcal{C} \mid \{x\cos\theta + y\sin\theta = 0\} \wedge \{\theta = \phi\}\}$ and $\Omega_2 = \{\boldsymbol{q} \in \mathcal{C} \mid \{x = y = 0\} \wedge \{\theta = \phi\}\}$. After some algebra, and since $\phi\big|_{x=0,y=0} = 0$, one gets $\Omega_1 = \{\boldsymbol{q} \in \mathcal{C} \mid \{x = 0\} \wedge \{\theta = \pi\}\}$, and $\Omega_2 = \{\boldsymbol{q} = \mathbf{0}\}$. One can easily verify that Ω_1 is not an invariant set, since for $\boldsymbol{q_i} = \begin{bmatrix} 0 & y & \pi \end{bmatrix}^\top$ the system has $u_1 \neq 0$ and thus escapes Ω_1, whereas Ω_2 is an invariant set.

On the other hand, at the discontinuity we can write $u_1 = -k_1\|\boldsymbol{r}\|\ \zeta$, for some $\zeta \in [-1, 1]$. Then, since $x\cos\theta + y\sin\theta = 0$ there, we can verify that $\dot{\tilde{V}}$ remains a singleton and is equal to $-k(\theta - \phi)^2$ for any $\zeta \in [-1, 1]$.[8] Note now that when $\theta = \phi$, and therefore at the discontinuity, it should be $x\cos\phi + y\sin\phi = 0$. It can be verified that $\mathbf{F}$ satisfies this only along the hyperplane $x = 0$, and that the largest invariant set there is the origin. Recall now that V is positive definite, which implies that its level sets are compact, and with $\dot{\tilde{V}} \leq 0$ they are also positively invariant. This completes the convergence proof. The closed-loop trajectories are depicted in Fig. 4.8(a).

[8] This is because it is the same ζ that appears in all the terms when $\dot{\tilde{V}}$ is expanded.

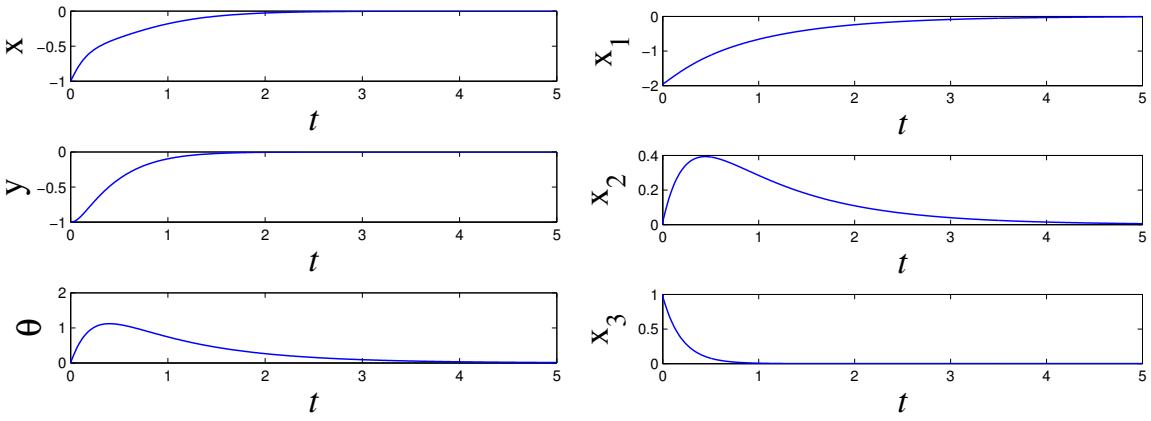

(a) Unicycle trajectories

(b) NDI trajectories. $k_1 = 5$, $k_2 = 1$

Figure 4.8: Closed-loop system response for the unicycle and the NDI.

4.2.2 Brockett's Nonholonomic Double Integrator

In this section we implement the strategy to the case of the NDI. Although the unicycle and the NDI are globally diffeomorphic, we use this example to demonstrate how the approach applies in any given coordinates, without the need of finding transformations into new, convenient system, as often encountered in the literature. Moreover, this case is indicative of how the methodology applies to a system where the constraint matrix $\boldsymbol{A}(\boldsymbol{q})$ in the given coordinates has no zero columns. The dynamics of the integrator is

$$\begin{bmatrix} \dot{x}_1 \\ \dot{x}_2 \\ \dot{x}_3 \end{bmatrix} = \begin{bmatrix} 1 \\ 0 \\ -x_2 \end{bmatrix} u_1 + \begin{bmatrix} 0 \\ 1 \\ x_1 \end{bmatrix} u_2 \ , \tag{4.15}$$

where $\boldsymbol{q} = \begin{bmatrix} x_1 & x_2 & x_3 \end{bmatrix}^\top \in \mathbb{R}^3$ is the state vector and u_1, u_2 are the controls. The nonholonomic constraint ($\kappa = 1$) is

$$\underbrace{\begin{bmatrix} x_2 & -x_1 & 1 \end{bmatrix}}_{\boldsymbol{a}^\top(\boldsymbol{q})} \begin{bmatrix} \dot{x}_1 \\ \dot{x}_2 \\ \dot{x}_3 \end{bmatrix} = 0 \ \Leftrightarrow \ \langle \boldsymbol{a}^\top(\boldsymbol{q}), \dot{\boldsymbol{q}} \rangle = 0 \ .$$

In this case, for a reference vector field $\mathbf{F}(\cdot)$ to satisfy the consistency condition (4.4) the following equation should hold

$$\underbrace{\begin{bmatrix} x_2 & -x_1 & 1 \end{bmatrix}}_{\boldsymbol{a}^\top(\boldsymbol{q})} \begin{bmatrix} \mathrm{F}_{x_1} \\ \mathrm{F}_{x_2} \\ \mathrm{F}_{x_3} \end{bmatrix} = 0 \Rightarrow \mathrm{F}_{x_1} x_2 - \mathrm{F}_{x_2} x_1 + \mathrm{F}_{x_3} = 0.$$

The constraint vector $\boldsymbol{a}^\top(\boldsymbol{q})$ contains no zero elements and consequently, *all* the components of an $\mathrm{N} = 3$ dimensional vector field $\mathbf{F}(\cdot) = \mathrm{F}_{x_1} \frac{\partial}{\partial x_1} + \mathrm{F}_{x_2} \frac{\partial}{\partial x_2} + \mathrm{F}_{x_3} \frac{\partial}{\partial x_3}$ affect the consistency condition and all the system states are leafwise.

To select $\mathbf{F}$ from the family of vector fields defined by (4.6), one needs to first pick $\boldsymbol{p}$ so that

$$\langle \boldsymbol{a}^\top(\mathbf{0}), \boldsymbol{p} \rangle = 0 \Rightarrow \begin{bmatrix} 0 & 0 & 1 \end{bmatrix} \begin{bmatrix} p_1 \\ p_2 \\ p_3 \end{bmatrix} = 0 \Rightarrow \boldsymbol{p} = \begin{bmatrix} p_1 & p_2 & 0 \end{bmatrix}^\top,$$

where p_1, $p_2 \in \mathbb{R}$. Take $\boldsymbol{p} = \begin{bmatrix} 1 & 0 & 0 \end{bmatrix}^\top$ and let $\lambda = 3$. Then,

$$\mathrm{F}_{x_1} = 2{x_1}^2 - {x_2}^2 - {x_3}^2, \ \mathrm{F}_{x_2} = 3x_1x_2, \ \mathrm{F}_{x_3} = 3x_1x_3. \tag{4.16}$$

The vector field $\mathbf{F}(\boldsymbol{q})$ on $\mathbb{R}^3$ is shown in Fig. 4.9, and is axial-symmetric with respect to the x_1 axis. For $x_3 = 0$, $\mathbf{F}(\boldsymbol{q})$ is as shown in Fig. 4.7(a), with $x_1 = x$ and $x_2 = y$.

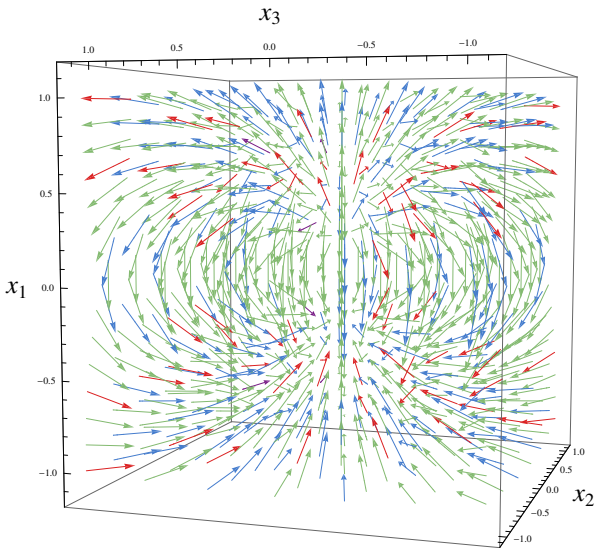

Figure 4.9: The vector field $\mathbf{F}(\boldsymbol{q})$ on $\mathbb{R}^3$ for the NDI, given by (4.16).

To align the system's vector field with the reference field $\mathbf{F}$, let us consider the map $h(\cdot) : \mathbb{R}^3 \to \mathbb{R}$, given as

$$h(\boldsymbol{q}) = \langle \boldsymbol{a}^\top(\boldsymbol{q}), \mathbf{F} \rangle = 3x_1x_3 - x_2\left({x_1}^2 + {x_2}^2 + {x_3}^2\right) \tag{4.17}$$

where $h(\boldsymbol{q}) \neq 0$ is an error which should be regulated to zero, so that the consistency condition is satisfied. By an appropriate choice of one of the control inputs, it is possible to set the dynamics of h to $\dot{h}(\boldsymbol{q}) = -k\, h(\boldsymbol{q})$; however, in this particular case, $\dot{h}(\boldsymbol{q})$ is quite complex and makes it difficult to derive the control law for the other input.

Alternatively, one can still guarantee that $h(\boldsymbol{q}) \to 0$ by making first $x_3 \to 0$, and then let x_2, x_1 tend to zero. To do this, define the consistency errors $s_1 = x_3$ and $s_2 = x_2$, since if $s_1 = s_2 = 0$ then automatically $h(\boldsymbol{q}) = 0$, which means that the consistency condition is satisfied. Now choose u_1, so that $s_1 \to 0$ exponentially: $\dot{s}_1 = -k_1 s_1$, for $k_1 > 0$. This is achieved by solving the following equation for u_1:

$$-x_2u_1 + x_1u_2 = -k_1x_3 \quad \Leftrightarrow \quad u_1 = k_1\frac{x_3}{x_2} + \frac{x_1}{x_2}u_2. \tag{4.18}$$

To design the other control input u_2 so that both s_2 and the the remaining (leafwise) states converge to zero, consider a smooth function V, similar in form to the one used in the case of the unicycle,

$$V = \frac{1}{2}\left({x_1}^2 + {s_1}^2 + {s_2}^2\right) = \frac{1}{2}\left({x_1}^2 + {x_3}^2 + {x_2}^2\right).$$

The time derivative of V along the system trajectories is

$$\dot{V} = \nabla V \dot{\boldsymbol{q}} \overset{(4.15),(4.18)}{\Rightarrow} \dot{V} = k_1 \frac{x_3}{x_2} x_1 + \frac{{x_1}^2}{x_2} u_2 + x_2 u_2 - k_1 {x_3}^2.$$

Then, choosing

$$u_2 = -k_2 x_2 - k_1 \frac{x_3 x_1}{{x_1}^2 + {x_2}^2} \tag{4.19}$$

results in

$$u_1 \overset{(4.19)}{=} -k_2 x_1 + k_1 \frac{x_3 x_2}{{x_1}^2 + {x_2}^2} \tag{4.20}$$

and yields $\dot{V} = -k_2 {x_1}^2 - k_2 {x_2}^2 - k_1 {x_3}^2$. Control law (4.19)-(4.20) is not defined on the submanifold $\mathcal{A} = \{\boldsymbol{q} \in \mathbb{R}^3 \mid \boldsymbol{q} = \begin{bmatrix} 0 & 0 & x_3 \end{bmatrix}^\top$. With this noted, the closed loop system reads

$$\dot{x}_1 = -k_2 x_1 + k_1 \frac{x_3 x_2}{{x_1}^2 + {x_2}^2}, \quad \dot{x}_2 = -k_2 x_2 - k_1 \frac{x_3 x_1}{{x_1}^2 + {x_2}^2}, \quad \dot{x}_3 = -k_1 x_3,$$

verifying that x_3 is exponentially stable to zero, irrespectively of x_1, x_2. For initial conditions $\boldsymbol{q_i} \notin \mathcal{A}$, one can invoke once more the invariance principle to establish that the system trajectories converge to the largest invariant set contained in the set $\Omega = \{\boldsymbol{q} \in \mathcal{C} \mid \dot{V} = 0\}$, which is the origin $\boldsymbol{q} = \boldsymbol{0}$.[9]

For initial conditions $\boldsymbol{q_i} \in \mathcal{A}$ one needs to use a different strategy to steer the system away from $\mathcal{A}$, and then switch to the control law given by (4.20), (4.19) [Lib03]; one option is $u_1(t) = u_2(t) = -k x_3(t) \neq 0$ for $t < T$, $T > 0$. Chattering does not occur, since once $\boldsymbol{q} \notin \mathcal{A}$, the system is guaranteed to converge to the origin. Note also that the second consistency error converges exponentially once the first one settles, since once $x_3 = 0$, (4.19) yields $u_2 = -k_2 x_2$. The closed-loop trajectories are depicted in Fig. 4.8(b).

Is also of interest that this system can be decomposed into two subsystems with different time scales, with the $x_3 \triangleq \boldsymbol{z}$ dynamics in the role of the boundary-layer (fast) system, and $\begin{bmatrix} x_1 & x_2 \end{bmatrix}^\top \triangleq \boldsymbol{w}$ in that of the reduced (slow) system. Assuming that $k_1 > k_2$ and defining $\varepsilon = \frac{1}{k_1}$, we can rewrite the closed-loop dynamics as

$$\dot{x}_1 = -k_2 x_1 + k_1 \frac{x_3 x_2}{{x_1}^2 + {x_2}^2}, \quad \dot{x}_2 = -k_2 x_2 - k_1 \frac{x_3 x_1}{{x_1}^2 + {x_2}^2}, \quad \varepsilon \dot{x}_3 = -x_3 \ .$$

The equilibria of the boundary layer system are given for $\varepsilon = 0$; thus, the unique equilibrium of the fast system is $x_3 = 0$. The reduced system then reads $\dot{x}_1 = -k_2 x_1$, $\dot{x}_2 = -k_2 x_2$, which is exponentially stable as well.

[9] Lyapunov's second method should not be used because the origin is not stable in the sense of Lyapunov.

4.3 Chained Systems

Consider the n-dimensional chained system

$$\begin{bmatrix} \dot{x}_1 \\ \dot{x}_2 \\ \dot{x}_3 \\ \vdots \\ \dot{x}_n \end{bmatrix} = \begin{bmatrix} 1 \\ 0 \\ x_2 \\ \vdots \\ x_{n-1} \end{bmatrix} u_1 + \begin{bmatrix} 0 \\ 1 \\ 0 \\ \vdots \\ 0 \end{bmatrix} u_2, \tag{4.21}$$

where $\boldsymbol{q} = \begin{bmatrix} x_1 & x_2 & x_3 & \dots & x_n \end{bmatrix}^\top \in \mathbb{R}^n$ is the state vector and u_1, u_2 are the control inputs. The system is subject to $\kappa = n - 2$ nonholonomic constraints, written in Pfaffian form

$$\underbrace{\begin{bmatrix} -x_2 & 0 & 1 & 0 & \dots & 0 \\ -x_3 & 0 & 0 & 1 & \dots & 0 \\ \vdots & \vdots & \vdots & \vdots & \ddots & \vdots \\ -x_{n-1} & 0 & 0 & 0 & \dots & 1 \end{bmatrix}}_{\boldsymbol{A}(\boldsymbol{q})} \begin{bmatrix} \dot{x}_1 \\ \dot{x}_2 \\ \vdots \\ \dot{x}_n \end{bmatrix} = \begin{bmatrix} 0 \\ 0 \\ \vdots \\ 0 \end{bmatrix}, \tag{4.22}$$

where $\boldsymbol{A}(\boldsymbol{q}) \in \mathbb{R}^{(n-2)\times n}$. This constraint matrix has $n_0 = 1$ zero column, associated with the generalized coordinate x_2. In this case, one can define $\mathrm{F}_{x_2} = 0$, and look for an $\mathrm{N} = (n-1)$ dimensional vector field $\mathbf{F}(\cdot)$, in terms of F_{x_j}, where $j \in \{1, 3, \dots, n\}$. The configuration space of (4.21) will then be foliated into $\mathbb{R}^{\mathrm{N}} \times \mathbb{R}$, where $\begin{bmatrix} x_1 & x_3 & \dots & x_n \end{bmatrix}^\top \in \mathbb{R}^{\mathrm{N}}$ are the leafwise states and $x_2 \in \mathbb{R}$ is the transverse state (Fig. 4.10).

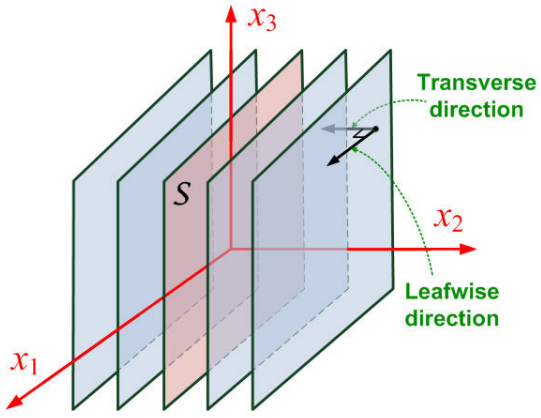

Figure 4.10: The trivial $\mathbb{R}^2 \times \mathbb{R}$ foliation $\mathcal{F}$ for a 3-dimensional chained system.

For $\boldsymbol{p} \in \mathbb{R}^{\mathrm{N}}$ to satisfy the constraints at the origin,

$$\underbrace{\begin{bmatrix} 0 & 0 & 1 & 0 & \dots & 0 \\ 0 & 0 & 0 & 1 & \dots & 0 \\ \vdots & \vdots & \vdots & \vdots & \ddots & \vdots \\ 0 & 0 & 0 & 0 & \dots & 1 \end{bmatrix}}_{\boldsymbol{A}(\boldsymbol{0}) \in \mathbb{R}^{\kappa \times n}} \begin{bmatrix} p_1 \\ 0 \\ p_3 \\ \vdots \\ p_n \end{bmatrix} = \begin{bmatrix} 0 \\ 0 \\ \vdots \\ 0 \end{bmatrix} \Rightarrow p_1 \neq 0, \quad p_3 = \dots = p_n = 0,$$

where by definition $p_2 = 0$. Take $\boldsymbol{p} = \begin{bmatrix} 1 & 0 & \dots & 0 \end{bmatrix}^\top$ and $\lambda = 3$; then (4.6) yields

$$\begin{aligned} \mathrm{F}_{x_1} &= 2{x_1}^2 - {x_3}^2 - {x_4}^2 - \ldots - {x_n}^2, \\ \mathrm{F}_{x_3} &= 3x_1x_3, \\ &\vdots \\ \mathrm{F}_{x_n} &= 3x_1x_n. \end{aligned} \tag{4.23}$$

Define the $\kappa = (n-2)$ maps $h_k(\cdot) : \mathbb{R}^n \to \mathbb{R}$ as $h_k(\boldsymbol{q}) = \langle \boldsymbol{a}_{\boldsymbol{k}}^\top(\boldsymbol{q}), \mathbf{F} \rangle$, where $\boldsymbol{a}_{\boldsymbol{k}}^\top(\boldsymbol{q})$, $k = 1, \ldots, \kappa$ are the constraint vectors. This results to

$$h_1(\boldsymbol{q}) = -x_2\,\mathrm{F}_{x_1} + \mathrm{F}_{x_3}, \;\; \ldots \;\; , h_\kappa(\boldsymbol{q}) = -x_{n-1}\,\mathrm{F}_{x_1} + \mathrm{F}_{x_n}\,.$$

Each $h_k(\boldsymbol{q}) \neq 0$ is an output which should be regulated to zero. This can be achieved if $x_{n-1} \to \frac{\mathrm{F}_{x_n}}{\mathrm{F}_{x_1}}$, $\forall n \geq 3$.

4.3.1 Example: The case $n = 3$

The derivation of the control laws u_1, u_2 can be simplified if one considers the analytic expressions of the outputs $h_k(\boldsymbol{q})$. Take for instance the $n = 3$ dimensional chained system, and the corresponding $\kappa = n - 2 = 1$ map

$$h_1(\boldsymbol{q}) = -3x_1(x_1x_2 - x_3) + x_2({x_1}^2 + {x_3}^2)\;. \tag{4.24}$$

As in the case of the nonholonomic double integrator, one can require that each one of the terms of h_1 converges to zero. This occurs if, for instance, $s_1 \triangleq x_1x_2 - x_3 \to 0$ and $s_2 \triangleq {x_1}^2 + {x_3}^2 \to 0$. Then, one can define a continuously differentiable function of the errors s_1, s_2 and the leafwise states[10] x_1, x_3 as

$$V = \frac{1}{2}\left(x_1x_2 - x_3\right)^2 + \frac{1}{2}\left({x_1}^2 + {x_3}^2\right).$$

The time derivative of V along the system trajectories is

$$\dot{V} = (x_1x_2 - x_3)(\dot{x}_1x_2 + x_1\dot{x}_2 - \dot{x}_3) + x_1\dot{x}_1 + x_3\dot{x}_3 \overset{(4.21)}{=} x_1(x_1x_2 - x_3)u_2 + (x_1 + x_3x_2)u_1.$$

We would like to render $\dot{V}$ negative semidefinite, and render the origin the largest invariant set contained in the set $\Omega = \{\boldsymbol{q} \in \mathbb{R}^3 \mid \dot{V} = 0\}$. Then convergence of the system trajectories to the origin can be established via LaSalle's invariance principle [Kha02], with the following caveat: the use of the invariance principle requires that system trajectories evolve in a compact invariant set. In this case this condition is not automatically satisfied, since the level surfaces of V are not compact sets: for $x_1 = x_3 = 0$, $|x_2| \to \infty \Rightarrow V = 0$.

However, V is in indeed radially unbounded so long as x_1 remains nonzero. Thus, if $x_1(0) \neq 0$, and the system is controlled so that x_1 maintains its sign and varies at a much slower time scale compared to x_2, x_3, then the negative definiteness of $\dot{V}$ ensures the inclusion of the trajectories in some compact set (i.e. a level set of V for $x_1 \neq 0$). Note that the requirement for a slowly-convergent x_1 is frequently used in the literature of chained systems [LOS98,MA03].

[10] Here the error s_2 directly includes the quadratic terms of the leafwise states x_1, x_3.

With x_1 assumed nonzero along the trajectories of (4.21), the following positive definite function V_1 on $\mathbb{R}^3 \setminus \{\boldsymbol{q} : x_1 = 0\}$ can be used instead

$$V_1 = \frac{1}{2}\left(x_1 x_2 - x_3\right)^2 + \frac{1}{2}{x_3}^2, \tag{4.25}$$

whose time derivative along the system trajectories is

$$\dot{V}_1 = (x_1 x_2 - x_3)(\dot{x}_1 x_2 + x_1 \dot{x}_2 - \dot{x}_3) + x_3 \dot{x}_3 \overset{(4.21)}{=} x_1 (x_1 x_2 - x_3) u_2 + x_3 x_2 u_1. \tag{4.26}$$

Then, if the control inputs u_1, u_2 are chosen so that the state x_1 converges to zero slowly and

$$\dot{V}_1 = -k_2 (x_1 x_2 - x_3)^2 - k_3 {x_3}^2, \tag{4.27}$$

for $x_1 \neq 0$ and $k_2,\ k_3 > 0$, then the set where $\dot{V}_1$ vanishes is

$$\Omega_1 = \{\boldsymbol{q} | x_1 x_2 = x_3 \wedge x_3 = 0\} \Leftrightarrow \Omega_1 = \{\boldsymbol{q} \mid x_2 = x_3 = 0\}.$$

To this end, one can first choose $u_1 = -k_1 x_1$, where k_1 is a small positive scalar, and then pick u_2 by combining (4.26) and (4.27):

$$\begin{aligned} x_1 (x_1 x_2 - x_3) u_2 + x_3 x_2 u_1 = -k_2 (x_1 x_2 - x_3)^2 - k_3 {x_3}^2 \Rightarrow \\ u_2 = -k_2 (x_2 - \frac{x_3}{x_1}) + \frac{k_1 x_3 (x_1 x_2 - \frac{k_3}{k_1} x_3)}{x_1 (x_1 x_2 - x_3)}. \end{aligned} \tag{4.28}$$

With $k_3 = k_1$, (4.28) further simplifies to

$$u_2 = -k_2 x_2 + (k_2 + k_1) \frac{x_3}{x_1},\ \text{for } x_1 \neq 0. \tag{4.29}$$

Given $x_1(0) \neq 0$, and with x_1 converging to zero slower than x_2, one can show that $\boldsymbol{q}(t)$ converges to Ω_1. To pick the gains k_1, k_2 so that this condition applies, consider that the derivative (4.27) for the closed loop system ($k_3 = k_1$) reads

$$\dot{V}_1 = -k_2 (x_2 x_1 - x_3)^2 - k_1 {x_3}^2 \leq -2 \min\{k_2, k_1\} V_1,$$

while the dynamics of x_1 read $\dot{x}_1 = -k_1 x_1$. Thus picking $k_2 > k_1$ ensures that V_1 vanishes at least twice faster than x_1.

If $x_1(0) = 0$, then one needs to switch to a different control strategy to drive the system away from the $x_1 = 0$ surface; for instance use $u_1 = \text{const}$, $u_2 = 0$ for some time $t < T$ just as in the case of the NDI, and then apply the scheme described above. The closed-loop system trajectories of the three-dimensional chained system are shown in Fig. 4.11.

4.3.2 Chained systems with more than 3 states

The same guidelines can be followed for systems with $\kappa > 1$ constraint equations. Consider the $n = 4$ dimensional chained system, and the $\mathrm{N} = n - 1 = 3$ dimensional vector field $\mathbf{F}(\cdot) = \mathrm{F}_{x_1} \frac{\partial}{\partial x_1} + \mathrm{F}_{x_3} \frac{\partial}{\partial x_3} + \mathrm{F}_{x_4} \frac{\partial}{\partial x_4}$,

$$\mathrm{F}_{x_1} = 2{x_1}^2 - {x_3}^2 - {x_4}^2,\ \mathrm{F}_{x_3} = 3 x_1 x_3,\ \mathrm{F}_{x_4} = 3 x_1 x_4.$$

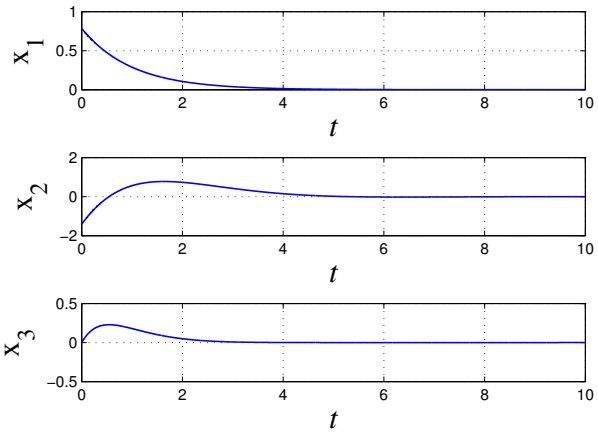

Figure 4.11: The state trajectories of a 3-d chained system for $k_1 = 1$, $k_2 = 2.5$.

Then, the corresponding $\kappa = n - 2 = 2$ maps are

$$h_1(\boldsymbol{q}) = -3x_1(x_1x_2 - x_3) + x_2({x_1}^2 + {x_3}^2 + {x_4}^2),$$
$$h_2(\boldsymbol{q}) = -3x_1(x_1x_3 - x_4) + x_3({x_1}^2 + {x_3}^2 + {x_4}^2).$$

Recalling the (simpler) structure of the outputs h_k in the $n = 3$ dimensional case, one could try to design a stabilizing control law by exploiting the existing lower dimensional solution. Note that for $x_4 = 0$, $h_1(\boldsymbol{q})$ reduces to (4.24), while $h_2(\boldsymbol{q})$ becomes $-x_3(2{x_1}^2 - {x_3}^2)$; then $x_3 \to 0$ implies that $h_2 \to 0$. Consequently, one could resort to finding a way to force $x_4 \to 0$, while keeping the same structure of the control law as in the $n = 3$ case.

For the convergence of x_4 to zero, one can require that $\dot{x}_4 = -k_4x_4$, $k_4 > 0$. Then (4.21) implies $x_3u_1 = -k_4x_4$, which for the control input $u_1 = -k_1x_1$ reads $k_1x_3x_1 = k_4x_4$. Assuming $x_1 \neq 0$ just as in $n = 3$ case, one gets $k_1\frac{x_3}{x_1} = k_4\frac{x_4}{{x_1}^2}$; if this condition holds, then $x_4 \to 0$.

The objective of the control can then be to bring the "error" $s = k_1\frac{x_3}{x_1} - k_4\frac{x_4}{{x_1}^2}$ to zero, while letting x_1 converge slowly using $u_1 = -k_1x_1$ with a small $k_1 > 0$. Let us use the same control architecture as in the three-dimensional case, and take $u_2|_{n=4} = u_2|_{n=3} + s$:

$$u_2 = -k_2x_2 + (k_2 + k_1)\frac{x_3}{x_1} + k_1\frac{x_3}{x_1} - k_4\frac{x_4}{{x_1}^2} \Rightarrow$$
$$u_2 = -k_2x_2 + k_3\frac{x_3}{x_1} - k_4\frac{x_4}{{x_1}^2}, \text{ for } x_1 \neq 0, \tag{4.30}$$

where $k_4 > k_3 > k_2$. Then one has the lower dimensional chained system, perturbed by $-k_4\frac{x_4}{{x_1}^2}$.

In order to study the convergence of the overall system to the origin one can employ a singular perturbation argument, and think of the system as decomposed into two subsystems with different time scales, where the states $\boldsymbol{z} \triangleq \begin{bmatrix} x_2 & x_3 & x_4 \end{bmatrix}^\top$ constitute the boundary-layer (fast) system, and the state $\boldsymbol{x} \triangleq x_1$ constitutes the reduced (slow) system. Then, the closed-loop dynamics of the overall system can be written as a singular perturbation model by considering

the (small) parameter $\varepsilon = \frac{1}{k_4}$ as

$$\begin{aligned}
\varepsilon \dot{x}_2 &= -(1 - a_1\varepsilon)x_2 + (1 - a_2\varepsilon)\,\frac{x_3}{x_1} - \frac{x_4}{{x_1}^2} \\
\varepsilon \dot{x}_3 &= -\varepsilon k_1 x_1 x_2 \\
\varepsilon \dot{x}_4 &= -\varepsilon k_1 x_1 x_3 \\
\dot{x}_1 &= -k_1 x_1,
\end{aligned}$$

where $k_2 = k_4 - a_1$, $k_3 = k_4 - a_2$, and a_1, a_2 are positive constants. The boundary-layer system has one isolated root, given for $\varepsilon = 0$ as $x_2 = \frac{x_3}{x_1} - \frac{x_4}{{x_1}^2}$. Taking $y = x_2 - (\frac{x_3}{x_1} - \frac{x_4}{{x_1}^2})$, one can easily verify that $\frac{dy}{d\tau} = -y$, which implies that x_2 converges exponentially and at a very fast time scale (significantly faster than x_3, x_4), to $\frac{x_3}{x_1} - \frac{x_4}{{x_1}^2}$. The remaining dynamics of the boundary layer system then read

$$\dot{x}_3 = -k_1 x_1 x_2 = -k_1 x_1 \left(\frac{x_3}{x_1} - \frac{x_4}{{x_1}^2} \right) = -k_1 x_3 + k_1 \frac{x_4}{x_1}, \quad \dot{x}_4 = -k_1 x_1 x_3;$$

for $x_1 \neq 0$ a "frozen" parameter, the resulting linear subsystem of x_3, x_4 has eigenvalues of negative real part, which are independent of x_1. Thus, with an appropriate choice of the control gains where k_4 sufficiently large so that $\varepsilon \to 0$, one has that the (reduced) boundary layer system states converge to zero. To tune the control gains, one can write the dynamics of the boundary-layer states in matrix form

$$\begin{bmatrix} \dot{x}_2 \\ \dot{x}_3 \\ \dot{x}_4 \end{bmatrix} = \begin{bmatrix} -k_2 & \frac{k_3}{x_1} & -\frac{k_4}{{x_1}^2} \\ -k_1 x_1 & 0 & 0 \\ 0 & -k_1 x_1 & 0 \end{bmatrix} \begin{bmatrix} x_2 \\ x_3 \\ x_4 \end{bmatrix} \Rightarrow \dot{\boldsymbol{z}} = \boldsymbol{A_1}(x_1)\boldsymbol{z},$$

and choose k_1, k_2, k_3, k_4 so that $\boldsymbol{A_1}(x_1)$ is a Hurwitz matrix, and its eigenvalues are sufficiently small compared to the eigenvalue of the slow subsystem.[11] The closed-loop system trajectories are shown in Fig. 4.12. Note that the same procedure applies for $\forall\, n > 4$ as well.

4.4 Nonholonomic systems with drift

This section demonstrates how the proposed methodology for kinematic nonholonomic systems can be extended to the control design of a class of dynamic nonholonomic systems with drift. As an example, we consider the motion control on the horizontal plane for an underactuated marine vehicle, which has two back thrusters for moving along the surge and the yaw degree of freedom, but no side (lateral) thruster for moving along the sway degree of freedom.

Following [Fos02], the kinematic and dynamic equations of motion are analytically written as:

[11] Note that a direct application of slowly-varying system approach [Kha02] is not possible due to the unboundedness of the slowly varying term in the neighborhood of the origin.

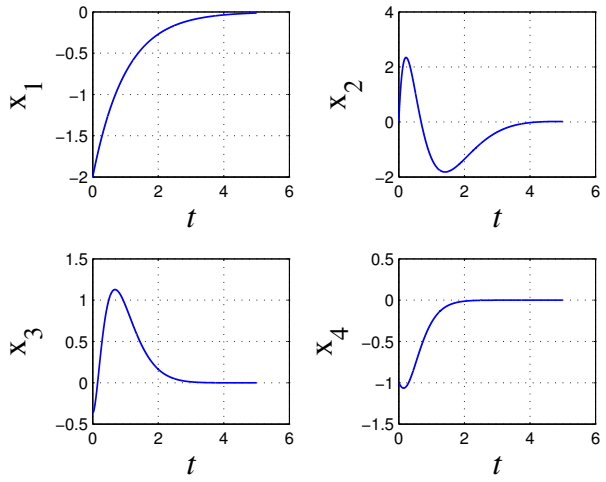

Figure 4.12: The state trajectories of a 4-d chained system for $k_1 = 1$, $k_2 = 10$, $k_3 = 42$, $k_4 = 75$. The eigenvalues of the matrix $\boldsymbol{A_1}(x_1)$ are -4.2819, $-2.8591 \pm 3.0564i$.

$$\dot{x} = u\cos\psi - v\sin\psi \tag{4.31a}$$

$$\dot{y} = u\sin\psi + v\cos\psi \tag{4.31b}$$

$$\dot{\psi} = r \tag{4.31c}$$

$$\dot{u} = \frac{m_{22}}{m_{11}}vr + \frac{X_u}{m_{11}}u + \frac{X_{u|u|}}{m_{11}}|u|\,u + \frac{1}{m_{11}}\tau_u \tag{4.31d}$$

$$\dot{v} = -\frac{m_{11}}{m_{22}}ur + \frac{Y_v}{m_{22}}v + \frac{Y_{v|v|}}{m_{22}}|v|\,v \tag{4.31e}$$

$$\dot{r} = \frac{m_{11} - m_{22}}{m_{33}}uv + \frac{N_r}{m_{33}}r + \frac{N_{r|r|}}{m_{33}}|r|\,r + \frac{1}{m_{33}}\tau_r, \tag{4.31f}$$

where $\boldsymbol{q} = \begin{bmatrix} x & y & \psi \end{bmatrix}^\top$ is the pose vector of the vehicle with respect to a global frame $\mathcal{G}$, $\boldsymbol{\nu} = \begin{bmatrix} u & v & r \end{bmatrix}^\top$ is the vector of linear and angular velocities in the body-fixed coordinate frame $\mathcal{B}$, m_{11}, m_{22}, m_{33} are the inertia matrix terms (including the "added mass" effect) along the axes of the body-fixed frame, X_u, Y_v, N_r are the linear drag terms, $X_{u|u|}$, $Y_{v|v|}$, $N_{r|r|}$ are the nonlinear drag terms, and τ_u, τ_r are the control inputs along the surge and yaw degree of freedom.

The system (4.31) falls into the class (4.3) of control affine underactuated mechanical systems with drift:

$$\dot{\mathbf{x}} = \mathbf{f}(\mathbf{x}) + \sum_{i=1}^{m} \mathbf{g}_i(\mathbf{x})\mathrm{u}_i,$$

where here $\mathbf{x} = \begin{bmatrix} x & y & \psi & u & v & r \end{bmatrix}^\top$ is the state vector, including the generalized coordinates $\boldsymbol{q}$ and the body-fixed velocities $\boldsymbol{\nu}$. The dynamics (4.31e) along the sway degree of freedom serve as a second-order (dynamic) nonholonomic constraint, which involves the velocities $\boldsymbol{\nu}$ of the vehicle, but not the generalized coordinates $\boldsymbol{q}$. Since the constraint equation is *not* of the form $\boldsymbol{a}^\top(\boldsymbol{q})\dot{\boldsymbol{q}} = 0$, the approach presented so far can not be directly applied.

However, if we only consider the kinematic subsystem for a moment, we see that (4.31a), (4.31b) are combined into

$$\underbrace{\begin{bmatrix}-\sin\psi & \cos\psi & 0\end{bmatrix}}_{\boldsymbol{a}^\top(\boldsymbol{q})}\begin{bmatrix}\dot{x}\\ \dot{y}\\ \dot{\psi}\end{bmatrix} = v \Rightarrow \boldsymbol{a}^\top(\boldsymbol{q})\dot{\boldsymbol{q}} = v, \tag{4.32}$$

which for $v \neq 0$ can be seen as a non-catastatic Pfaffian constraint on the unicycle. Equation (4.32) implies that $\boldsymbol{q} = \boldsymbol{0}$ is an equilibrium point if and only $v\,|_{\boldsymbol{q}=\boldsymbol{0}} = 0$, i.e., when (4.32) turns into catastatic constraint at $\boldsymbol{q} = \boldsymbol{0}$.

With this insight, one can try to steer the kinematic subsystem augmented with the constraint (4.31e) to $\boldsymbol{q} = \boldsymbol{0}$ using the velocities u, r as virtual control inputs, while ensuring that the velocity v along the sway degree of freedom vanishes at $\boldsymbol{q} = \boldsymbol{0}$. The constraint equation (4.32) can now be used to apply the steps of the methodology presented in Section 4.2: similarly to the unicycle case, the structure of the vector $\boldsymbol{a}^\top(\boldsymbol{q})$ implies that x, y are the leafwise states and ψ is the transverse state. Thus, an $\mathrm{N} = 2$ dimensional reference vector field given by (4.6) can be defined, where $\boldsymbol{x} = \begin{bmatrix}x & y\end{bmatrix}^\top$, $\lambda = 2$ and $\boldsymbol{p} = \begin{bmatrix}1 & 0\end{bmatrix}^\top$; the vector field components F_x, F_y read

$$\mathrm{F}_x = x^2 - y^2, \quad \mathrm{F}_y = 2xy. \tag{4.33}$$

To enable the alignment of the system's vector field with (4.10), we define the output

$$h(\boldsymbol{q}) = \langle \boldsymbol{a}^\top(\boldsymbol{q}), \mathbf{F}\rangle = -\sin\psi\,\mathrm{F}_x + \cos\psi\,\mathrm{F}_y$$

and require that $h(\boldsymbol{q}) \neq 0$ should be regulated to zero, which for a non-vanishing vector field $\mathbf{F}(\cdot)$ reads $h(\boldsymbol{q}) = 0 \Rightarrow \psi = \arctan\frac{\mathrm{F}_y}{\mathrm{F}_x} \triangleq \phi$, where ϕ is the orientation of the vector field $\mathbf{F}(\cdot)$ with respect to the global frame $\mathcal{G}$.

In order to design a feedback control law $r = \gamma_2(\cdot)$ for stabilizing the consistency error $s = \psi - \phi$ to zero, one can require that $\dot{s} = -k_2 s$, where $k_2 > 0$, that reads

$$\dot{\psi} - \dot{\phi} = -k_2(\psi - \phi) \overset{(4.31c)}{\Rightarrow} r = -k_2(\psi - \phi) + \dot{\phi}. \tag{4.34}$$

Then, one can take a function V in terms of the leafwise states x, y and the consistency error $s = \psi - \phi$ as

$$V = \frac{1}{2}(x^2 + y^2 + s^2) = \frac{1}{2}\left(x^2 + y^2 + (\psi - \phi)^2\right),$$

which is positive definite with respect to $\begin{bmatrix}x & y & s\end{bmatrix}^\top$ and radially unbounded, and take its time derivative as

$$\dot{V} \overset{(4.34)}{=} \begin{bmatrix}x & y\end{bmatrix}\begin{bmatrix}\cos\psi\\ \sin\psi\end{bmatrix}u + \begin{bmatrix}x & y\end{bmatrix}\begin{bmatrix}-\sin\psi\\ \cos\psi\end{bmatrix}v - k_2 s^2. \tag{4.35}$$

The behavior of $\dot{V}$ depends on the velocity v. If v is seen as a bounded perturbation that vanishes at $\begin{bmatrix}x & y & s\end{bmatrix}^\top = \boldsymbol{0}$, then this point is an equilibrium of the kinematic subsystem (in the sense that, at $x = y = 0$, one has $s = 0 \Rightarrow \psi = \phi|_{x=y=0} = 0$).

With this insight, consider in isolation the subsystem (4.31e) with ur in the role of input, and apply the following ISS argument: take $V_v = \frac{1}{2}v^2$ as an ISS-Lyapunov function, and expand its time derivative

$$\dot{V}_v = -\frac{m_{11}}{m_{22}}v(ur) - \left(\frac{|Y_v|}{m_{22}}v^2 + \frac{|Y_{v|v|}|}{m_{22}}|v|\,v^2\right)$$

where by definition $Y_v, Y_{v|v|} < 0$, and $w(v) = \frac{|Y_v|}{m_{22}}v^2 + \frac{|Y_{v|v|}|}{m_{22}}|v|\,v^2$ is a continuous, positive definite function. Take $0 < \theta < 1$, then $\dot{V}_v = -\frac{m_{11}}{m_{22}}v(ur) - (1-\theta)w(v) - \theta w(v) \Rightarrow$

$$\dot{V}_v \leq -(1-\theta)w(v),\ \forall v : -\frac{m_{11}}{m_{22}}v(ur) - \theta w(v) < 0.$$

If the control input $\zeta = ur$ is bounded, $|\zeta| \leq \zeta_b$, then

$$\dot{V}_v \leq -(1-\theta)w(v),\ \forall |v| : |Y_v||v| + |Y_{v|v|}||v|^2 \geq \frac{m_{11}}{\theta}\zeta_b.$$

Then, the subsystem (4.31e) is ISS [Kha02, Thm 4.19]. Thus, for any bounded input $\zeta = ur$, the linear velocity $v(t)$ will be ultimately bounded by a class $\mathcal{K}$ function of $\sup_{t>0}|\zeta(t)|$. If furthermore $\zeta(t) = u(t)r(t)$ converges to zero as $t \to \infty$, then $v(t)$ converges to zero as well [Kha02].

Consequently, if the control inputs $u = \gamma_1(\cdot)$, $r = \gamma_2(\cdot)$ are bounded functions which converge to zero as $t \to \infty$, then one has that $v(t)$ is bounded and furthermore, $v(t) \to 0$ as $t \to \infty$.

For analyzing the behavior of the kinematic trajectories $x(t)$, $y(t)$, $\psi(t)$, let us define the metric [Tan04]

$$V_\mu = \frac{1}{2}\frac{x^2+y^2}{\cos^2(\arctan(\frac{y}{x}))} + \frac{1}{2}s^2, \tag{4.36}$$

and take its time derivative as

$$\begin{aligned}\dot{V}_\mu = \frac{x^2+y^2}{x^4}\left((x^3-xy^2)\dot{x} + 2x^2y\dot{y}\right) + s\dot{s} = \frac{x^2+y^2}{x^4}\begin{bmatrix}x^3-xy^2 & 2x^2y\end{bmatrix}\begin{bmatrix}\cos\psi\\ \sin\psi\end{bmatrix}u + \\ + \frac{x^2+y^2}{x^4}\begin{bmatrix}x^3-xy^2 & 2x^2y\end{bmatrix}\begin{bmatrix}-\sin\psi\\ \cos\psi\end{bmatrix}v - k_2 s^2.\end{aligned} \tag{4.37}$$

Then, one can pick the control law $u = \gamma_1(\cdot)$ as

$$u = -k_1\,\mathrm{sgn}(x)\left((x^2-y^2)\cos\psi + 2xy\sin\psi\right), \tag{4.38}$$

which basically projects the vector field $\mathbf{F}(\cdot)$ on the vehicle's direction, and assigns the sign based on the side of the x axis: if the vehicle is on the right, it goes to zero in reverse; otherwise it goes forward. Then, the time derivative of V_μ reads:

$$\dot{V}_\mu = -k_1\frac{x^2+y^2}{|x|^3}\left(\begin{bmatrix}x^2-y^2 & 2xy\end{bmatrix}\begin{bmatrix}\cos\psi\\ \sin\psi\end{bmatrix}\right)^2 - k_2 s^2 + \frac{x^2+y^2}{x^4}\begin{bmatrix}x^3-xy^2 & 2x^2y\end{bmatrix}\begin{bmatrix}-\sin\psi\\ \cos\psi\end{bmatrix}v. \tag{4.39}$$

Take $\theta \in (0,1)$, then one has

$$\begin{aligned}\dot{V}_\mu \leq -k_2(1-\theta)s^2 - k_2\theta\sin^2 s - k_1\frac{x^2+y^2}{|x|^3}\left(\begin{bmatrix}x^2-y^2 & 2xy\end{bmatrix}\begin{bmatrix}\cos\psi\\ \sin\psi\end{bmatrix}\right)^2 + \\ + \frac{x^2+y^2}{x^4}\begin{bmatrix}x^3-xy^2 & 2x^2y\end{bmatrix}\begin{bmatrix}-\sin\psi\\ \cos\psi\end{bmatrix}v.\end{aligned}$$

Substitute $s = \psi - \phi$, $\cos\phi = \frac{\mathrm{F}_x}{\|\mathbf{F}\|} = \frac{x^2-y^2}{x^2+y^2}$, $\sin\phi = \frac{\mathrm{F}_y}{\|\mathbf{F}\|} = \frac{2xy}{x^2+y^2}$, then one has:

$$
\begin{aligned}
\dot{V}_\mu &\leq -k_2(1-\theta)s^2 - \frac{k_2\theta}{(x^2+y^2)^2}\left(\begin{bmatrix} x^2-y^2 & 2xy\end{bmatrix}\begin{bmatrix}-\sin\psi\\ \cos\psi\end{bmatrix}\right)^2 - \\
&- k_1\frac{x^2+y^2}{|x|^3}\left(\begin{bmatrix} x^2-y^2 & 2xy\end{bmatrix}\begin{bmatrix}\cos\psi\\ \sin\psi\end{bmatrix}\right)^2 + \frac{x^2+y^2}{x^4}\begin{bmatrix} x^3-xy^2 & 2x^2y\end{bmatrix}\begin{bmatrix}-\sin\psi\\ \cos\psi\end{bmatrix} v \\
&\leq -k_2(1-\theta)s^2 - \min\left\{\frac{k_2\theta}{(x^2+y^2)^2}, k_1\frac{x^2+y^2}{|x|^3}\right\}\|(\mathrm{F}_x,\mathrm{F}_y)\|^2 + \\
&+ \frac{x^2+y^2}{x^4}\begin{bmatrix} x^3-xy^2 & 2x^2y\end{bmatrix}\begin{bmatrix}-\sin\psi\\ \cos\psi\end{bmatrix} v \\
&= -k_2(1-\theta)s^2 - \min\left\{\frac{k_2\theta}{(x^2+y^2)^2}, k_1\frac{x^2+y^2}{|x|^3}\right\}\frac{x^6}{(x^2+y^2)^2}\left\|\left(\frac{\partial V_\mu}{\partial x}, \frac{\partial V_\mu}{\partial y}\right)\right\|^2 + \\
&+ \frac{x^2+y^2}{x^4}\begin{bmatrix} x^3-xy^2 & 2x^2y\end{bmatrix}\begin{bmatrix}-\sin\psi\\ \cos\psi\end{bmatrix} v \\
&= -k_2(1-\theta)s^2 - \min\left\{\frac{k_2\theta x^6}{(x^2+y^2)^4}, \frac{k_1|x|^3}{x^2+y^2}\right\}\left\|\left(\frac{\partial V_\mu}{\partial x}, \frac{\partial V_\mu}{\partial y}\right)\right\|^2 + \\
&+ \frac{x^2+y^2}{x^4}\begin{bmatrix} x^3-xy^2 & 2x^2y\end{bmatrix}\begin{bmatrix}-\sin\psi\\ \cos\psi\end{bmatrix} v \\
&= -k_2(1-\theta)s^2 - \min\left\{\frac{k_2\theta x^6}{(x^2+y^2)^4}, \frac{k_1|x|^3}{x^2+y^2}\right\}\frac{x^2+y^2}{\cos^2\left(\arctan(\frac{y}{x})\right)} + \\
&+ \frac{x^2+y^2}{x^4}\begin{bmatrix} x^3-xy^2 & 2x^2y\end{bmatrix}\begin{bmatrix}-\sin\psi\\ \cos\psi\end{bmatrix} v \Rightarrow \\
\dot{V}_\mu &\leq -2\min\left\{k_2(1-\theta), \frac{\theta k_2 x^6}{(x^2+y^2)^4}, \frac{k_1|x|^3}{x^2+y^2}\right\} V_\mu + \underbrace{\frac{x^2+y^2}{x^4}\begin{bmatrix} x^3-xy^2 & 2x^2y\end{bmatrix}\begin{bmatrix}-\sin\psi\\ \cos\psi\end{bmatrix} v}_{A},
\end{aligned}
$$

where $A \leq \frac{x^2+y^2}{x^4}|x|\|\mathbf{F}\||v_b| = \left(\frac{x^2+y^2}{x^2}\right)^2|x||v_b|$. Then, the trajectories of the kinematic subsystem are ISS with respect to the metric V_μ and the input $v(t)$ [Tan04].

Consequently, the system (4.31a)-(4.31c), (4.31e) can be seen as an interconnection of the kinematic subsystem (4.31a)-(4.31c) and the subsystem (4.31e) (Fig. 4.13), where each one of the subsystems is ISS. This suggests that the coupled system is ISS. Then, applying

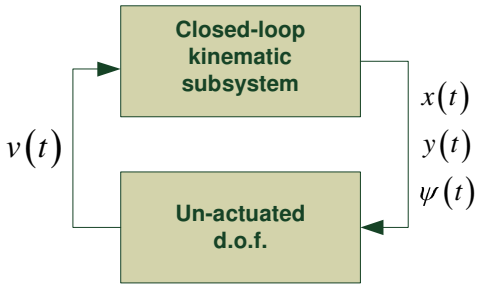

Figure 4.13: The system (4.31a)-(4.31c), (4.31e) as an interconnection of two ISS subsystems.

[HW07, Thm IV.1] one can conclude that for suitable gain selection (see Appendix 4.6), the

interconnected system is globally asymptotically stable with respect to the metric V_μ, i.e. the trajectories $x(t)$, $y(t)$, $\psi(t)$, $v(t)$ globally asymptotically converge to zero. Note that the choice of the metric V_μ is critical, since a typical one equivalent to the Euclidean would not work.

Finally, for the design of the control inputs τ_u, τ_r, one can use a feedback linearization transformation for the dynamic subsystems (4.31d), (4.31f) given as

$$\tau_u = m_{11}\alpha - m_{22}vr - X_u u - X_{u|u|}|u|u, \tag{4.40a}$$

$$\tau_r = m_{33}\beta - (m_{11} - m_{22})ur - N_r r - N_{r|r|}|r|r, \tag{4.40b}$$

that yields $\dot{u} = \alpha$, $\dot{r} = \beta$, where α, β are the new control inputs. Thus, the system should be controlled so that the velocities u, r track the virtual control inputs $\gamma_1(\cdot)$, $\gamma_2(\cdot)$. To design the control laws $\alpha(\cdot)$, $\beta(\cdot)$, consider the candidate Lyapunov function

$$V_\tau = \frac{1}{2}\left(u - \gamma_1(\cdot)\right)^2 + \frac{1}{2}\left(r - \gamma_2(\cdot)\right)^2$$

and take its time derivative as

$$\dot{V}_\tau = \left(u - \gamma_1(\cdot)\right)\left(\dot{u} - \frac{\partial \gamma_1}{\partial \boldsymbol{\eta}}\dot{\boldsymbol{\eta}}\right) + \left(r - \gamma_2(\cdot)\right)\left(\dot{r} - \frac{\partial \gamma_2}{\partial \boldsymbol{\eta}}\dot{\boldsymbol{\eta}}\right).$$

Then, under the control inputs

$$\alpha = -k_u(u - \gamma_1(\cdot)) + \frac{\partial \gamma_1}{\partial \boldsymbol{\eta}}\dot{\boldsymbol{\eta}}, \;\; \beta = -k_r(r - \gamma_2(\cdot)) + \frac{\partial \gamma_2}{\partial \boldsymbol{\eta}}\dot{\boldsymbol{\eta}},$$

where k_u, $k_r > 0$, one gets $\dot{V}_\tau = -k_u(u - \gamma_1(\cdot))^2 - k_r(r - \gamma_2(\cdot))^2$, which verifies that the velocities u, r are globally asymptotically stable to $\gamma_1(\cdot)$, $\gamma_2(\cdot)$, respectively.

The system trajectories $x(t)$, $y(t)$, $\psi(t)$, $u(t)$, $v(t)$, $r(t)$ under the control laws (4.38), (4.34), (5.21) are shown in Fig. 4.14. The inertia and hydrodynamic parameters of the system's dynamic model were taken from [WC06].

4.5 Conclusions

This chapter addressed the control design for a class of n-dimensional nonholonomic systems, subject to $\kappa \geq 1$ constraints in Pfaffian form, within a unified framework.

In this framework, one designs an N-dimensional vector field $\mathbf{F}(\cdot)$ of the general form (4.6), and then aligns the system vector field with $\mathbf{F}(\cdot)$. In this way the problem of steering the states to the origin is reduced into an output regulation problem, in which the outputs are functions that quantify the "misalignment" between $\mathbf{F}$ and the system's vector field. The outputs can directly suggest Lyapunov-like functions V that are employed into the control design and analysis.

The control laws derived unavoidably have singularities, which necessitate switching to alternative control functions when the system is initialized on the singularity manifolds, but away from the latter there is no need for switching. The proposed methodology offers a uniform logic into the control design of n-dimensional nonholonomic systems, by providing guidelines for the construction of state feedback controllers, and leads to control designs which may be preliminary, but form a good basis for further refinement. The unicycle, the nonholonomic double integrator, the n-dimensional chained systems and an underactuated marine vehicle have been considered as illustrative examples, and feedback control laws have been constructed following the same guidelines.

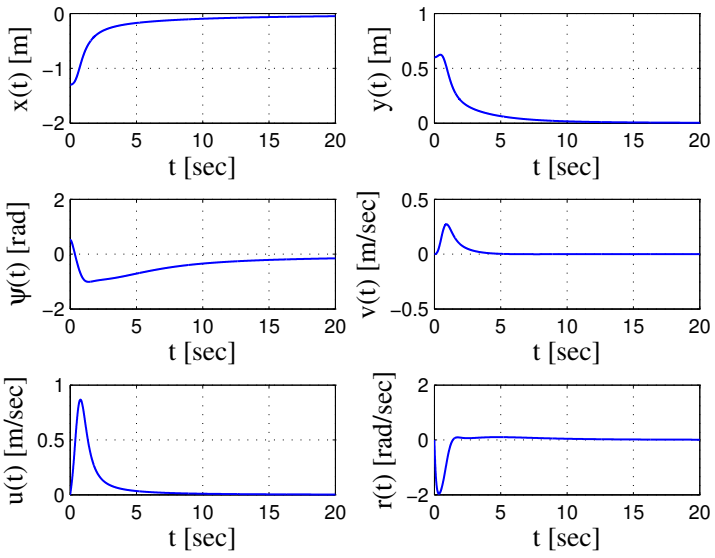

Figure 4.14: The system trajectories $\mathbf{x}(t)$ under the control laws (4.38), (4.34), (5.21).

4.6 Appendix

The subsystem (4.31e) describing the dynamics of v is ISS from input $\zeta = u(x, y, \psi)\ r(x, y, \psi)$ to state v with ultimate bound $\gamma_1(|\zeta|) = \frac{m_{11}}{\theta}|\zeta|$. For the subsystem describing the evolution of the kinematic states x, y, ψ, consider (4.40a): given a $\theta_1 \in (0, 1)$ and that $k_1 << k_2$, one has that $\dot{V}_\mu \leq -2(1-\theta_1)\frac{k_1|x|^3}{x^2+y^2}V_\mu$ as long as

$$-\frac{2\theta_1 k_1|x|^3}{x^2+y^2}V_\mu \leq -\left(\frac{x^2+y^2}{x^2}\right)^2|x||v| \Rightarrow V_\mu \geq \frac{(x^2+y^2)^3}{2\theta_1 k_1 x^6}|v| = \frac{1}{2k_1\theta_1}\frac{1}{\cos^6(\text{atan}(\frac{y}{x}))}|v|.$$

Note that as $(x, y) \to (0, 0)$ one has $\cos(\arctan(\frac{y}{x})) \to 1$. Thus the kinematic subsystem is ISS from input v to the metric V_μ with ultimate bound $\gamma_2(|v|) = \frac{1}{2k_1\theta_1}\frac{1}{\cos^6(\text{atan}(\frac{y}{x}))}|v|$.

Consequently, the interconnected system is asymptotically stable with respect to the metric V_μ for $\gamma_2(\gamma_1(r)) < r,\ \forall r > 0$, which yields $\frac{1}{2\theta_1}\frac{1}{\cos^6(\text{atan}(\frac{y}{x}))}\frac{m_{11}}{\theta} < k_1$.

Chapter 5

Viable Control Design for Nonholonomic Systems

Abstract

This chapter addresses the feedback control design for a class of nonholonomic systems which are subject to inequality state constraints defining a constrained (viability) set K. Based on concepts from viability theory, the necessary conditions for selecting viable controls for a nonholonomic system are given, so that system trajectories starting in K always remain in K. Furthermore, a class of state feedback control solutions for a class of nonholonomic systems are redesigned by means of switching control, so that system trajectories starting in K converge to a goal set G in K, without ever leaving K. The proposed approach can be applied in various problems, whose objective can be recast as controlling a nonholonomic system so that the resulting trajectories remain for ever in a subset K of the state space, until they converge into a goal (target) set G in K. The motion control for an underactuated marine vehicle in a constrained configuration set K is treated as a case study; the set K essentially describes the limited sensing area of a vision-based sensor system, and viable control laws which establish convergence to a goal set G in K are constructed. The robustness of the proposed control approach under a class of bounded external perturbations is also considered. The efficacy of the methodology is demonstrated through simulation results.

Contributions

Control of systems which are subject to both nonholonomic and state (configuration) constraints is a challenging problem, often encountered within the fields of robotics and multiagent systems, ranging from the classical motion planning problem [CLH+05] to maintaining connectivity in robotic networks [BCM09].

This chapter proposes a control design methodology for a class of nonholonomic systems which are subject to hard state constraints. The state constraints are realized as nonlinear inequalities w.r.t. the state variables, which constitute a closed subset K of the state space $\mathcal{Q}$. The set K is thus the subset of state space in which the system trajectories should evolve $\forall t \geq 0$. System trajectories which either start out of K, or escape K for some $t > 0$ immediately violate the state constraints and thus are not acceptable. Therefore, the control objective reduces into finding a (possibly switching) state feedback control law, so that system trajectories starting in K converge to a goal set G in K without ever leaving K.

The proposed approach combines concepts from viability theory[1] and results from our earlier work on the state feedback control of n-dimensional nonholonomic systems with Pfaffian con-

[1] Viability theory describes the evolution of systems under the consideration that for different reasons, not all system evolutions are acceptable or possible. The system must obey state (viability) constraints, and system solutions should be viable in the sense that they must satisfy, at each time instant, these constraints [Aub91].

straints [PTK11] (Section 5.1). In the sequel, following [Aub91], state constraints are called *viability* constraints, the set K is called the *viability set* of the system, and system trajectories that remain in K $\forall t \geq 0$ are called *viable* (Section 5.2).

In particular, we adopt the concept of tangency to a set K defined by inequality constraints [Aub91], and provide the necessary conditions under which the admissible velocities of a kinematic nonholonomic system are viable in K, as well as the necessary conditions for selecting viable controls (Section 5.3). In addition, given the control solutions in [PTK11], we propose a way of redesigning them by means of switching control, so that the resulting trajectories are viable in K and furthermore converge to a goal set $G \subset K$. As a case study, we consider the motion planning for an underactuated marine vehicle which is subject to configuration constraints because of limited sensing (Section 5.4); the onboard sensor system consists of a camera with limited angle-of-view and two laser pointers of limited range. The task is defined as to control the vehicle so that it converges to a desired configuration w.r.t. a target of interest, while the target is always visible in the camera f.o.v.; in that sense, this is also a problem of maintaining visibility. The visibility maintenance requirement, along with limited sensing, impose a set of configuration constraints that define a viability set K. The robustness of the proposed control approach under a class of bounded perturbations is studied in Section 5.5. Our conclusions and plans for future extensions are summarized in Section 4.5.

The problem formulation is similar to the characterization of viable capture basins of a target set C in a constrained set K [Aub01], which is based on the Frankowska method that characterizes the backward invariance and (local) forward viability of subsets by means of the value function of an optimal control problem. However, in this paper we rather address the problem in terms of set invariance [Bla99, BM08], where the objective is to render the viability set K a positively invariant (or controlled invariant) set, and the goal set G the largest invariant set of the system by means of state feedback control.[2]

The notion of controlled invariance for linear systems has been utilized for the control design of systems with first-order (kinematic) nonholonomic constraints, after linearizing the nonlinear system equations around the equilibrium [MBP11]; compared to this work, here we present a method which addresses a wider class of constrained underactuated systems, including the class of nonholonomic systems with second-order (dynamic) nonholonomic constraints, without the need for linearizing the system equations, but rather working in the initial coordinates.

The motion control of underactuated marine (underwater, surface) vehicles and ships has been treated in the past using various control design techniques, see for instance [Leo95, PE99, PF00, AP02a, DJPN04]; however, to the best of our knowledge, none of the relevant work considers any additional state (configuration) constraints on the system. Furthermore, in this paper we present a novel motion control scheme for the considered class of underactuated marine vehicles, based on our methodology for the state feedback control for n-dimensional nonholonomic systems [PTK11].

In relation to our prior work in [PMS$^+$09], here we do not adopt an optimal control formulation, and propose control solutions that not only remain in K, but also converge to a goal set $G \subset K$. Compared to [PK11], we consider a wider class of viability constraints, while we further address the viable robust control design of underactuated systems w.r.t. a class of bounded external perturbations.

[2]The viability property has been introduced as "controlled invariance" for linear and smooth nonlinear systems [Aub91].

Overview

We consider the class of nonlinear systems described by

$$\dot{\boldsymbol{q}} = \boldsymbol{f}(\boldsymbol{q}, \boldsymbol{u}), \quad \boldsymbol{u} \in \boldsymbol{U}(\boldsymbol{q}), \tag{5.1}$$

where $\boldsymbol{q} \in \mathcal{Q}$ is the state vector, $\mathcal{Q} \subset \mathbb{R}^n$ is the state space (a normed space), $\boldsymbol{u} \in \mathcal{U}$ is the vector of $m < n$ control inputs, $\mathcal{U} \subset \mathbb{R}^m$ is the control space, $\boldsymbol{U} : \mathcal{Q} \rightsquigarrow \mathcal{U}$ is a feedback set-valued map associating with any state $\boldsymbol{q}$ the (possibly empty) subset $\boldsymbol{U}(\boldsymbol{q})$ of feasible controls at $\boldsymbol{q}$ and $\boldsymbol{f} : \text{Graph}(\boldsymbol{U}) \mapsto \mathcal{Q}$ is a continuous single-valued map, which assigns to each state-control pair $(\boldsymbol{q}, \boldsymbol{u}) \in \text{Graph}(\boldsymbol{U})$ the velocity $\boldsymbol{f}(\boldsymbol{q}, \boldsymbol{u})$ of the state, i.e. the (tangent) vector $\dot{\boldsymbol{q}} \in \mathcal{Q}$.

Nonholonomic constraints

The system (5.1) is subject to $\kappa < n$ nonholonomic constraint equations.[3] Each constraint $i \in \{1, \dots, \kappa\}$ is written in Pfaffian form as

$$\textstyle\sum_{j=1}^{n} a_{ij}(\boldsymbol{q})\dot{q}_j = 0 \Rightarrow \langle \boldsymbol{a_i}, \dot{\boldsymbol{q}} \rangle = 0, \tag{5.2}$$

where $\langle \cdot, \cdot \rangle$ stands for the duality pairing, a bilinear map $(\boldsymbol{w}, \boldsymbol{v}) \in \mathcal{Q}^\star \times \mathcal{Q} \mapsto \langle \boldsymbol{w}, \boldsymbol{v} \rangle := \boldsymbol{w}(\boldsymbol{v})$, where $\mathcal{Q}^\star$ is the dual space of $\mathcal{Q}$, $\boldsymbol{w} \in \mathcal{Q}^\star$ is a linear functional $\boldsymbol{w} : \mathcal{Q} \mapsto \mathbb{R}$ and $\boldsymbol{v} \in \mathcal{Q}$ [AF90]. Since any element $\boldsymbol{w} \in \mathcal{Q}^\star$ is a linear map from the n-dimensional space $\mathcal{Q}$ to the 1-dimensional space $\mathbb{R}$, it can be represented by means of a row vector [Isi95]. In this sense, the value $\langle \boldsymbol{a_i}, \dot{\boldsymbol{q}} \rangle$ of the functional $\boldsymbol{a_i}(\cdot)$ at $\dot{\boldsymbol{q}}$ is given by the dot product $\boldsymbol{a_i}\dot{\boldsymbol{q}} = \sum_{j=1}^{n} a_{ij}(\boldsymbol{q})\dot{q}_j = \boldsymbol{a_i}^\top(\boldsymbol{q})\dot{\boldsymbol{q}}$, where $\boldsymbol{a_i}^\top(\boldsymbol{q}) = \begin{bmatrix} a_{i1}(\boldsymbol{q}) & a_{i2}(\boldsymbol{q}) & \dots & a_{in}(\boldsymbol{q}) \end{bmatrix}$ is called the constraint vector. Thus, a nonholonomic constraint (5.2) can be written as

$$\underbrace{\begin{bmatrix} a_{i1}(\boldsymbol{q}) & \dots & a_{in}(\boldsymbol{q}) \end{bmatrix}}_{\boldsymbol{a_i}^\top(\boldsymbol{q})} \begin{bmatrix} \dot{q}_1 \\ \vdots \\ \dot{q}_n \end{bmatrix} = 0 \Rightarrow \boldsymbol{a_i}^\top(\boldsymbol{q})\dot{\boldsymbol{q}} = 0,$$

while $\kappa > 1$ constraints are written in matrix form as

$$\boldsymbol{A}(\boldsymbol{q})\dot{\boldsymbol{q}} = \boldsymbol{0}, \tag{5.3}$$

where $\boldsymbol{A}(\boldsymbol{q}) \in \mathbb{R}^{\kappa \times n}$. Each row i of the constraint matrix $\boldsymbol{A}(\boldsymbol{q})$ is a constraint vector $\boldsymbol{a_i}^\top(\boldsymbol{q})$.

State (viability) constraints

The system (5.1) is additionally subject to μ nonlinear inequalities w.r.t. the state variables. Consider the continuous map $\boldsymbol{c} = (c_1, c_2, \dots, c_\mu) : Q \to \mathbb{R}^\mu$; then, the subset K of Q defined by the inequality constraints

$$K := \{\boldsymbol{q} \in Q \mid c_j(\boldsymbol{q}) \leq 0, \;\; j = 1, 2, \dots, \mu\}, \tag{5.4}$$

is the viability set of the system, where $\mathcal{J}(\boldsymbol{q}) = \{j = 1, 2, \dots, \mu \mid c_j(\boldsymbol{q}) = 0\}$ is the subset of active constraints.

[3] Typically, *kinematic* nonholonomic constraints can be written in Pfaffian form as $\boldsymbol{A}(\boldsymbol{q})\dot{\boldsymbol{q}} = \boldsymbol{b}(\boldsymbol{q})$, where $\boldsymbol{q} \in \mathbb{R}^n$ is the vector of generalized coordinates, $\boldsymbol{A}(\boldsymbol{q}) \in \mathbb{R}^{\kappa \times n}$ and $\boldsymbol{b}(\boldsymbol{q}) \in \mathbb{R}^\kappa$. If $\boldsymbol{b}(\boldsymbol{q}) = \boldsymbol{0}$ the constraints are called catastatic, otherwise they are called acatastatic.

5.1 Nonholonomic Control Design

The control design is based on our methodology [PTK11] (Chapter 4) on the state feedback control for drift-free, kinematic nonholonomic systems of the form

$$\dot{\boldsymbol{q}} = \sum_{i=1}^{m} \boldsymbol{g}_i(\boldsymbol{q}) u_i, \tag{5.5}$$

which are subject to kinematic Pfaffian constraints (5.3), where the state vector $\boldsymbol{q} \in \mathbb{R}^n$ includes the system generalized coordinates, $\boldsymbol{g}_i(\boldsymbol{q})$ are the control vector fields and u_i are the control inputs.[4] Recall that the main idea of our approach is to define a smooth N-dimensional reference vector field $\mathbf{F}(\cdot)$ for (5.5), given by

$$\mathbf{F}(\boldsymbol{x}) = \lambda \left(\boldsymbol{p}^\top \boldsymbol{x} \right) \boldsymbol{x} - \boldsymbol{p} \left(\boldsymbol{x}^\top \boldsymbol{x} \right), \tag{5.6}$$

where $\mathrm{N} \leq n$, $\lambda \geq 2$, $\boldsymbol{x} \in \mathbb{R}^{\mathrm{N}}$ is a (particular) subvector of the configuration vector $\boldsymbol{q} \in \mathbb{R}^n$ and $\boldsymbol{p} \in \mathbb{R}^{\mathrm{N}}$ is a vector that "generates" the vector field $\mathbf{F}(\cdot)$, defined such that $\boldsymbol{A}(\mathbf{0})\boldsymbol{p} = \mathbf{0}$.

The dimension N of the vector field $\mathbf{F}(\cdot)$ is specified by the explicit form of the constraint equations, in the following sense: depending on the structure of $\boldsymbol{A}(\boldsymbol{q})$, the state space $\mathcal{Q}$ is trivially decomposed into $\mathcal{L} \times \mathcal{T}$, where $\mathcal{L}$ is the "leaf" space, $\mathcal{T}$ is the "fiber" space, $\dim \mathcal{L} = \mathrm{N}$, $n = \dim \mathcal{L} + \dim \mathcal{T}$. The local coordinates $\boldsymbol{x} \in \mathbb{R}^{\mathrm{N}}$ on the leaf are called leafwise states and the local coordinates $\boldsymbol{t} \in \mathbb{R}^{n-\mathrm{N}}$ on the fiber are called transverse states. The vector field $\mathbf{F}(\cdot)$ is defined tangent to $\mathcal{L}$ in terms of the leafwise states $\boldsymbol{x}$, and is non-vanishing everywhere on $\mathcal{L}$ except for the origin $\boldsymbol{x} = \mathbf{0}$, which is of *dipole* type by construction; thus, all integral curves of $\mathbf{F}(\boldsymbol{x})$ begin and end at the origin $\boldsymbol{x} = \mathbf{0}$.

In the case that $\mathbf{A}(\boldsymbol{q})$ has at least one zero column, i.e. in the case that $\mathrm{N} < n$, the vector field $\mathbf{F}(\cdot)$ is singular (vanishes) on the subset $\mathcal{A} = \{\boldsymbol{q} \in \mathbb{R}^n \mid \boldsymbol{x} = \mathbf{0}\}$; this singularity may necessitate switching for initial conditions $\boldsymbol{q_0} \in \mathcal{A}$.Input discontinuities are assumed to yield a closed loop vector field in (5.5) which is piecewise continuous. Solutions are then understood in the Filippov sense, i.e. $\dot{\boldsymbol{q}} \in \mathfrak{F}(\boldsymbol{q})$, where $\mathfrak{F}$ is a set valued map given by

$$\mathfrak{F}(\boldsymbol{q}) \triangleq \overline{\mathrm{co}} \left\{ \lim_{j \to \infty} \sum_{i=1}^{m} \boldsymbol{g}_i(\boldsymbol{q}_j) u_i : \boldsymbol{q}_j \to \boldsymbol{q}, \boldsymbol{q}_j \notin S_q \right\}$$

and S_q is any set of measure zero.

Away from the singularity subset $\mathcal{A}$, $\mathbf{F}(\cdot)$ serves as a velocity reference for (5.5). This means that, at each $\boldsymbol{q} \in \mathcal{Q}$, the system vector field $\dot{\boldsymbol{q}} \in T_{\boldsymbol{q}}\mathcal{Q}$ is controlled to "align with" $\mathbf{F}(\cdot)$, i.e. is forced into the tangent space $T_{\boldsymbol{q}}\mathcal{L}$ of the integral curve of $\mathbf{F}(\cdot)$ at $\boldsymbol{q} \in \mathcal{Q}$.

In this sense, one can use the available control authority to steer the system vector field into the tangent bundle of the integral curves of $\mathbf{F}$, and "flow" in the direction of the vector field on its way to the origin. In [PTK11] we show that these two objectives suggest the choice of particular Lyapunov-like functions V, and enable one to establish convergence of the system trajectories $\boldsymbol{q}(t)$ to the origin based on standard design and analysis techniques. In particular,

[4] The method can be extended to the control of underactuated systems with dynamic Pfaffian constraints as well, see Section 5.4.

one can find a smooth function $V(\boldsymbol{q}) : \mathbb{R}^n \to \mathbb{R}$ of compact level sets, and a state feedback control law $\boldsymbol{\gamma}(\cdot) = (\gamma_1(\cdot), \ldots, \gamma_m(\cdot)) : \mathbb{R}^n \to \mathbb{R}^m$ such that

$$\dot{V} \leq 0 \quad \Leftrightarrow \quad \nabla V \, \dot{\boldsymbol{q}} = \nabla V \sum_{i=1}^{m} \boldsymbol{g}_i(\boldsymbol{q}) \gamma_i(\cdot) \leq 0, \tag{5.7}$$

where $\nabla V \triangleq \left[\frac{\partial V}{\partial q_1} \quad \ldots \quad \frac{\partial V}{\partial q_n} \right]$ the gradient of V at $\boldsymbol{q}$. Then, using standard tools, one can formally establish the convergence of the system trajectories $\boldsymbol{q}(t)$ to the origin.[5]

5.2 Tools from Viability Theory

This section gives a brief description of concepts from viability theory [Aub91, AF90] that are used in the chapter.

Consider the dynamics of a system described by a (single-valued) map f from some open subset Ω of X to X, $f : \Omega \mapsto X$, where X is a finite dimensional vector space, and the initial value problem associated with the differential equation:

$$\forall t \in [0, T], \quad \dot{x}\,(t) = f\big(x(t)\big), \quad x(0) = x_0. \tag{5.8}$$

Definition 1 (*Viable Functions*) Let K be a subset of X. A function $x(\cdot)$ from $[0, T]$ to X is viable in K on $[0, T]$, if $x(t) \in K \ \forall t \in [0, T]$.

Definition 2 (*Viability Property*) Let K be a subset of Ω. K is said to be locally viable under f if, for any initial state $x_0 \in K$, there exist $T > 0$ and a viable solution on $[0, T]$ to the differential equation (5.8) starting at x_0. It is said to be (globally) viable under f if $T = \infty$.

The characterization of viable sets K under f is based on the concept of tangency: A subset K is viable under f if at each state x of K the velocity $f(x)$ is "tangent" to K at x, for bringing back a solution to the differential equation inside K. An adequate concept of tangency is realized via the concept of the contingent cone.

Definition 3 (*Contingent Cone*) Let X be a normed space, K be a nonempty subset of X and x belong to K. The contingent cone to K at x is the set

$$T_K(x) = \left\{ \upsilon \in X \mid \liminf_{h \to 0+} \frac{d_K(x + h\upsilon)}{h} = 0 \right\},$$

where $d_K(y)$ denotes the distance of y to K, $d_K(y) := \inf_{z \in K} \|y - z\|$. Note that $\forall \ x \in \mathrm{Int}(K)$, $T_K(x) = X$. Thus, if K is an open set, the contingent cone $T_K(x)$ to K at any $x \in K$, is always equal to the whole space.

[5] The convergence to the origin under the control law $\boldsymbol{\gamma}(\boldsymbol{q})$ holds for "almost all" initial conditions, in the sense that $\boldsymbol{\gamma}(\boldsymbol{q})$ is undefined on particular singularity subsets $\mathcal{A}$.

(*Contingent Cone at a Fréchet differentiable point*) Consider the continuous real-valued map $g = (g_1, g_2, \ldots, g_p) : X \to \mathbb{R}^p$ and the subset K of X defined as

$$K = \{x \in X \mid g_i(x) \geq 0, \;\; i = 1, 2, \ldots, p\}, \tag{5.9}$$

where $g_i(\cdot)$ are Fréchet differentiable at x. For $x \in K$, denote

$$I(x) = \{i = 1, 2, \ldots, p \mid g_i(x) = 0\} \tag{5.10}$$

the subset of active constraints. The contingent cone $T_K(x)$ to K is $T_K(x) = X$ whenever $I(x) = \emptyset$, otherwise

$$T_K(x) = \left\{\upsilon \in X \mid \forall i \in I(x), \; \langle g_i'(x), \upsilon\rangle \geq 0\right\},$$

where $g_i'(x) \in X^\star$ is the gradient of g_i at x, and $\langle \cdot, \cdot \rangle$ stands for the duality pairing.

Definition 4 (*Viability Domain*) Let K be a subset of Ω, then K is a viability domain of the map $f : \Omega \mapsto X$ if $\forall \; x \in K, \; f(x) \in T_K(x)$.

Definition 5 Consider a control system (U, f), defined by a feedback set-valued map $U : X \rightsquigarrow Z$, where X the state space and Z the control space, and a map $f : \mathrm{Graph}(U) \to X$, describing the dynamics of the system:

$$\dot{x}(t) = f(x(t), u(t)), \;\; \text{where } u(t) \in U(x(t)).$$

We associate with any subset $K \subset \mathrm{Dom}(U)$ the regulation map $R_K := K \rightsquigarrow Z$ defined by

$$\forall x \in K, \;\; R_K(x) := \{u \in U(x) \mid f(x, u) \in T_K(x)\}.$$

Controls u belonging to $R_K(x)$ are called viable, and K is a viability domain if and only if the regulation map $R_K(x)$ has nonempty values.

If the subset K is given by (5.9)*, the set of active constraints is as in* (5.10)*, and for every $x \in K$, $\exists \upsilon_0 \in X$ such that $\forall i \in I(x)$, $\langle g_i'(x), \upsilon_0\rangle \geq 0$, then the regulation map $R_K(x)$ is*

$$R_K(x) := \{u \in U(x) \mid \forall i \in I(x), \; \langle g_i'(x), f(x, u)\rangle \geq 0\}.$$

5.3 Viable Nonholonomic Controls

Consider a nonholonomic system of the form (5.5) subject to μ inequality state constraints determining a viability set K of the form (5.4), where $c_j(\cdot) : Q \to \mathbb{R}$ are continuously differentiable maps, $j \in \mathcal{J} = \{1, \ldots, \mu\}$.

Assume that at some $\boldsymbol{q} \in K$ one has that $\mathcal{J}(\boldsymbol{q}) = \emptyset$, i.e. none of the constraints is active; then obviously $\boldsymbol{q} \in \mathrm{Int}(K)$, and the contingent cone of K at $\boldsymbol{q}$ coincides with the state space Q, $T_K(\boldsymbol{q}) = Q$.[6] This implies that the system can evolve along any direction $\dot{\boldsymbol{q}} \in T_{\boldsymbol{q}}Q$ without violating the viability constraints. For a nonholonomic system (5.5) with Pfaffian constraints

[6] If K is a differentiable manifold, then the contingent cone $T_K(\boldsymbol{q})$ coincides with the tangent space to K at $\boldsymbol{q}$.

(5.3), the admissible velocities $\dot{\boldsymbol{q}} \in T_{\boldsymbol{q}}Q$ belong into the null space of the constraint matrix $\boldsymbol{A}(\boldsymbol{q})$, which is an $(n-\kappa)$ dimensional subspace of the tangent space $T_{\boldsymbol{q}}Q$. Thus, at each $\boldsymbol{q} \in \mathrm{Int}(K)$, the viable admissible velocities $\dot{\boldsymbol{q}}$ for a nonholonomic system are tangent to an $(n-\kappa)$ dimensional subspace of the contingent cone $T_K(\boldsymbol{q})$.

Assume now that the j-th constraint becomes active at some point $\boldsymbol{z} \in \partial K$: $c_j(\boldsymbol{z}) = 0$, $j \in \mathcal{J}$. The viable system velocities belong into the contingent cone of K at $\boldsymbol{z}$, $\dot{\boldsymbol{z}} \in T_K(\boldsymbol{z})$, which now is a subset (not necessarily a vector space but rather a cone) of the tangent space $T_{\boldsymbol{z}}Q$. Thus, an admissible velocity for a nonholonomic system (5.5) is viable at $\boldsymbol{z}$ if and only if

$$\dot{\boldsymbol{z}} \in \Big(\mathrm{Null}(\boldsymbol{A}(\boldsymbol{z})) \bigcap T_K(\boldsymbol{z})\Big) \neq \emptyset.$$

Based on these, we are able to characterize the conditions for selecting viable controls (if any) for the system (5.5).

For $\boldsymbol{q} \in \mathrm{Int}(K)$, an admissible control $\boldsymbol{u} = (u_1, \ldots, u_m) : \mathbb{R}^n \to \mathbb{R}^m$ for (5.5) is viable at $\boldsymbol{q}$ if and only if

$$\boldsymbol{u} \in \boldsymbol{U}(\boldsymbol{q}), \quad \dot{\boldsymbol{q}} = \sum_{i=1}^{m} \boldsymbol{g}_i(\boldsymbol{q}) u_i \in T_K(\boldsymbol{q}) \triangleq T_{\boldsymbol{q}}Q,$$

which essentially implies that a control law $\boldsymbol{u}(\cdot)$ is viable at $\boldsymbol{q}$ as long as the control inputs u_i belong into the subset $\boldsymbol{U}(\boldsymbol{q})$ of feasible controls.

Assume now that $\boldsymbol{z} \in \partial K$ so that a single constraint is active: $c_j(\boldsymbol{z}) = 0$ for some $j \in \mathcal{J}$. The map of viable controls for a system (5.1) at $\boldsymbol{z}$ is:

$$R_K(\boldsymbol{z}) = \{\boldsymbol{u} \in \boldsymbol{U}(\boldsymbol{z}) \mid \langle c_j'(\boldsymbol{z}), \boldsymbol{f}(\boldsymbol{z}, \boldsymbol{u})\rangle \leq 0\},$$

where c_j' is the gradient of $c_j(\cdot)$ at $\boldsymbol{z}$, and $\langle \cdot, \cdot \rangle$ is the duality pairing. Following [Isi95], the value of the duality pairing at $\boldsymbol{z}$ can be essentially expressed by the dot product $\nabla c_j \, \boldsymbol{f}(\boldsymbol{z}, \boldsymbol{u})$, where $\nabla c_j = \begin{bmatrix} \frac{\partial c_j}{\partial q_1} & \ldots & \frac{\partial c_j}{\partial q_n} \end{bmatrix}$ at $\boldsymbol{z} \in \partial K$. The regulation map then reads:

$$R_K(\boldsymbol{z}) = \{\boldsymbol{u} \in \boldsymbol{U}(\boldsymbol{z}) \mid \nabla c_j \boldsymbol{f}(\boldsymbol{z}, \boldsymbol{u}) \leq 0\}.$$

Thus, an admissible control $\boldsymbol{u} = (u_1, \ldots, u_m) : \mathbb{R}^n \to \mathbb{R}^m$ for (5.5) is viable at $\boldsymbol{z} \in \partial K$ if and only if

$$\boldsymbol{u}(\boldsymbol{z}) \in \boldsymbol{U}(\boldsymbol{z}), \ \begin{bmatrix} \frac{\partial c_j}{\partial q_1} & \ldots & \frac{\partial c_j}{\partial q_n} \end{bmatrix} \sum_{i=1}^{m} \boldsymbol{g}_i(\boldsymbol{z}) u_i \leq 0. \tag{5.11}$$

It immediately follows that if more than one constraints $c_j(\cdot) : Q \to \mathbb{R}$ are simultaneously active at some $\boldsymbol{z} \in \partial K$, then a control law $\boldsymbol{u}(\cdot)$ is viable at $\boldsymbol{z}$ if the condition (5.11) is satisfied for each one of the active constraints. If *all* μ constraints are active at $\boldsymbol{z}$, the viability conditions are written in matrix form as

$$\boldsymbol{u}(\boldsymbol{z}) \in \boldsymbol{U}(\boldsymbol{z}), \quad \mathbf{J}_{\boldsymbol{c}}(\boldsymbol{z}) \sum_{i=1}^{m} \boldsymbol{g}_i(\boldsymbol{z}) u_i \leq \mathbf{0}, \tag{5.12}$$

where $\mathbf{J}_{\boldsymbol{c}}(\boldsymbol{z})$ is the Jacobian matrix of the map $\boldsymbol{c} = (c_1(\cdot), \ldots, c_\mu(\cdot)) : Q \to \mathbb{R}^\mu$, evaluated at $\boldsymbol{z} \in \partial K$.

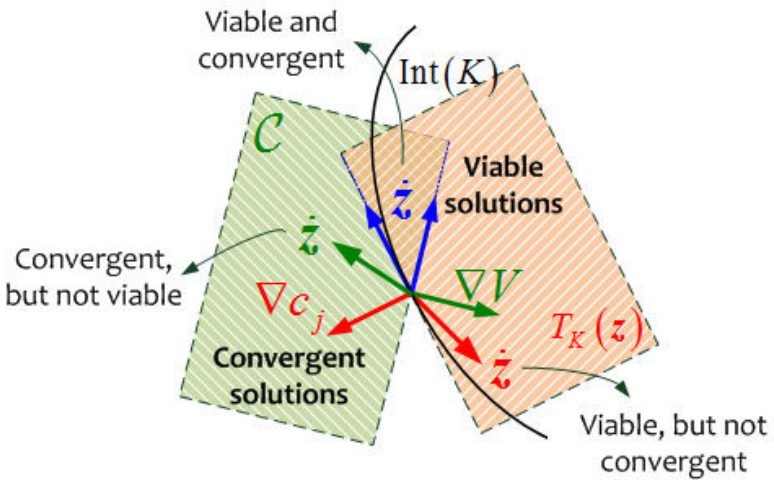

Figure 5.1: Any control law $\boldsymbol{\gamma}(\cdot) = (\gamma_1(\cdot), \ldots, \gamma_m(\cdot)) : \mathbb{R}^n \to \mathbb{R}^m$ such that $\boldsymbol{\gamma}(\boldsymbol{z}) \in \boldsymbol{U}(\boldsymbol{z})$, $\dot{\boldsymbol{z}} = \sum_{i=1}^m \boldsymbol{g}_i(\boldsymbol{z})\gamma_i(\cdot) \in (\mathcal{C} \bigcap T_K(\boldsymbol{z}))$ is also viable at $\boldsymbol{z} \in \partial K$, bringing the system trajectories into the interior of K.

Consequently, a control law $\boldsymbol{\gamma}(\cdot) = (\gamma_1(\cdot), \ldots, \gamma_m(\cdot)) : \mathbb{R}^n \to \mathbb{R}^m$ is viable at $\boldsymbol{z} \in \partial K$ if and only if

$$\boldsymbol{\gamma}(\boldsymbol{z}) \in \boldsymbol{U}(\boldsymbol{z}), \ \left[\frac{\partial c_j}{\partial q_1} \ \ \ldots \ \ \frac{\partial c_j}{\partial q_n}\right] \sum_{i=1}^m \boldsymbol{g}_i(\boldsymbol{z})\gamma_i(\boldsymbol{z}) \leq 0, \tag{5.13}$$

for each one of the active constraints $c_j(\boldsymbol{z}) = 0$, where $\boldsymbol{U}(\boldsymbol{z}) \subseteq \mathbb{R}^m$ is the subset of feasible controls at $\boldsymbol{z}$.

To illustrate the viability condition (5.11) let us consider the case when a single constraint is active: $c_j(\boldsymbol{z}) = 0$, $\boldsymbol{z} \in \partial K$ (Fig. 5.1). The viable system velocities $\dot{\boldsymbol{z}}$ belong into the contingent cone $T_K(\boldsymbol{z})$ at $\boldsymbol{z}$; thus, any control $\boldsymbol{u} = (u_1, \ldots, u_m) \in \boldsymbol{U}(\boldsymbol{z})$ such that $\dot{\boldsymbol{z}} = \sum_{i=1}^m \boldsymbol{g}_i(\boldsymbol{z})u_i \in T_K(\boldsymbol{z})$ is viable. Furthermore, following [PTK11], the system velocities that establish asymptotic convergence to the origin define the subset $\mathcal{C} = \{\dot{\boldsymbol{z}} \in T_{\boldsymbol{z}}Q \mid \nabla V \dot{\boldsymbol{z}} \leq 0\}$. Thus, a convergent control law $\boldsymbol{\gamma}(\cdot)$ is also viable at $\boldsymbol{z} \in \partial K$ if and only if $\boldsymbol{\gamma}(\boldsymbol{z}) \in \boldsymbol{U}(\boldsymbol{z})$ and furthermore the system velocity $\dot{\boldsymbol{z}} = \sum_{i=1}^m \boldsymbol{g}_i(\boldsymbol{z})\gamma_i(\boldsymbol{z})$ belongs into the intersection $(\mathcal{C} \bigcap T_K(\boldsymbol{z}))$; if this intersection is empty, then any convergent solution $\boldsymbol{\gamma}(\cdot)$ steers the system trajectories out of K.

Therefore, given the state feedback control solutions in [PTK11], the idea for designing viable feedback control laws for the class of nonholonomic systems (5.1) reduces into redesigning (if necessary) the convergent control laws $\boldsymbol{\gamma}(\cdot) : \mathbb{R}^n \to \mathbb{R}^m$ by means of switching control, so that they yield viable control inputs $\boldsymbol{u}(\boldsymbol{z})$, $\forall \boldsymbol{z} \in \partial K$. The proposed control design is illustrated via the following example.

5.4 An underactuated marine vehicle with limited sensing

We consider the motion control on the horizontal plane for an underactuated marine vehicle subject to configuration constraints, which mainly arise because of the onboard vision-based

sensor system. The sensor suite consists of a camera and two laser pointers mounted on the vehicle, and provides the vehicle's position and orientation (pose) vector $\boldsymbol{\eta} = \begin{bmatrix} x & y & \psi \end{bmatrix}^\top$ w.r.t. a global coordinate frame $\mathcal{G}$, which lies on the center of a target on a vertical surface (Fig. 5.2). The target and the two laser dots projected on the surface are tracked using computer

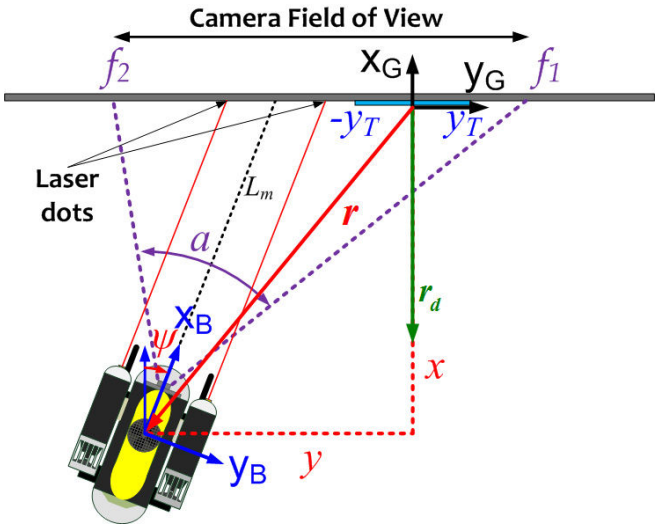

Figure 5.2: Modeling of the state constraints

vision algorithms and this information is used to estimate the pose vector $\boldsymbol{\eta}$ [KPK06]. Thus, the target and the laser dots should always be visible in the camera f.o.v., for the sensor system to be effective.

These requirements impose a set of nonlinear inequality constraints w.r.t. $\boldsymbol{\eta}$, which are treated as viability constraints that define a viability set K for the system. The control objective is thus defined as to control the vehicle so that it converges into a set $G \subset K$ of desired configurations $\boldsymbol{\eta_d} \in G$, while the system trajectories $\boldsymbol{\eta}(t)$ never escape K.

5.4.1 Mathematical Modeling

The marine vehicle has two back thrusters for moving along the surge and the yaw d.o.f., but no side (lateral) thruster for moving along the sway d.o.f.. Typically, the motion along roll and pitch d.o.f. is negligible for this class of vehicles, since roll and pitch angles are stable because of the mass configuration. The vehicle is assumed to move on the horizontal plane; thus the heave d.o.f. is not taken into account. Following [Fos02] the kinematic and dynamic equations

of motion are analytically written as:

$$\dot{x} = u\cos\psi - v\sin\psi \tag{5.14a}$$

$$\dot{y} = u\sin\psi + v\cos\psi \tag{5.14b}$$

$$\dot{\psi} = r \tag{5.14c}$$

$$\dot{u} = \frac{m_{22}}{m_{11}}vr + \frac{X_u}{m_{11}}u + \frac{X_{u|u|}}{m_{11}}|u|\,u + \frac{\tau_u}{m_{11}} \tag{5.14d}$$

$$\dot{v} = -\frac{m_{11}}{m_{22}}ur + \frac{Y_v}{m_{22}}v + \frac{Y_{v|v|}}{m_{22}}|v|\,v \tag{5.14e}$$

$$\dot{r} = \frac{m_{11}-m_{22}}{m_{33}}uv + \frac{N_r}{m_{33}}r + \frac{N_{r|r|}}{m_{33}}|r|\,r + \frac{\tau_r}{m_{33}}, \tag{5.14f}$$

where $\boldsymbol{\eta} = \begin{bmatrix}\boldsymbol{r}^\top & \psi\end{bmatrix}^\top = \begin{bmatrix}x & y & \psi\end{bmatrix}^\top$ is the pose vector of the vehicle w.r.t. the global frame $\mathcal{G}$, $\boldsymbol{r} = \begin{bmatrix}x & y\end{bmatrix}^\top$ is the position vector and ψ is the orientation of the vehicle w.r.t. $\mathcal{G}$, $\boldsymbol{\nu} = \begin{bmatrix}u & v & r\end{bmatrix}^\top$ is the vector of linear and angular velocities in the body-fixed coordinate frame $\mathcal{B}$, m_{11}, m_{22}, m_{33} are the inertia matrix terms (including the "added mass" effect) along the axes of frame $\mathcal{B}$, X_u, Y_v, N_r are the linear drag terms, $X_{u|u|}$, $Y_{v|v|}$, $N_{r|r|}$ are the nonlinear drag terms, and τ_u, τ_r are the control inputs along the surge and yaw d.o.f.. Furthermore, the thrust allocation implies that

$$\tau_u = F_p + F_{st} \text{ and } \tau_r = l\,(F_p - F_{st})\,,$$

where $F_p \in [-f_p, f_p]$, $F_{st} \in [-f_{st}, f_{st}]$ are the port and starboard thrust forces, respectively, f_p, $f_{st} > 0$ are the bounds of the thrust forces and $2l$ is the distance between the two thrusters.

5.4.2 Nonholonomic control design

The system (5.14) falls into the class of control affine underactuated systems with drift:

$$\dot{\mathbf{x}} = \mathbf{f}(\mathbf{x}) + \sum_{i=1}^{m}\mathbf{g}_i(\mathbf{x})\mathrm{u}_i,$$

where $\mathbf{x} = \begin{bmatrix}x & y & \psi & u & v & r\end{bmatrix}^\top$ is the state vector, including the generalized coordinates $\boldsymbol{\eta}$ and the body-fixed velocities $\boldsymbol{\nu}$, and $\mathrm{u}_1 = \tau_u$, $\mathrm{u}_2 = \tau_r$ are the control inputs, respectively.

The dynamics of the sway d.o.f. (5.14e) serve as a second-order (dynamic) nonholonomic constraint, which involves the velocities $\boldsymbol{\nu}$, but not the generalized coordinates $\boldsymbol{\eta}$. Since the constraint equation is *not* of the form $\boldsymbol{a}^\top(\boldsymbol{\eta})\dot{\boldsymbol{\eta}} = 0$, the approach in [PTK11] on the control design for kinematic systems can not be directly applied.

System decomposition into subsystems Σ_1, Σ_2

Nevertheless, if we only consider the kinematic subsystem for a moment, we see that (5.14a), (5.14b) are combined into $-\dot{x}\sin\psi + \dot{y}\cos\psi = v \Rightarrow$

$$\underbrace{\begin{bmatrix}-\sin\psi & \cos\psi & 0\end{bmatrix}}_{\boldsymbol{a}^\top(\boldsymbol{\eta})}\begin{bmatrix}\dot{x}\\ \dot{y}\\ \dot{\psi}\end{bmatrix} = v \Rightarrow \boldsymbol{a}^\top(\boldsymbol{\eta})\dot{\boldsymbol{\eta}} = v, \tag{5.15}$$

which for $v \neq 0$ can be seen as a non-catastatic Pfaffian constraint on the unicycle. The constraint equation (5.15) implies that $\boldsymbol{\eta} = \mathbf{0}$ is an equilibrium point if and only if $v\,|_{\boldsymbol{\eta}=\mathbf{0}} = 0$, i.e. if and only if (5.15) turns into catastatic at the origin $\boldsymbol{\eta} = \mathbf{0}$.

With this insight, one can try to steer the kinematic subsystem augmented with the second order constraint (5.14e) to the origin $\boldsymbol{\eta} = \mathbf{0}$, using the velocities u, r as virtual control inputs, while ensuring that the velocity v vanishes at $\boldsymbol{\eta} = \mathbf{0}$.

Thus, the system (5.14) can be divided into two subsystems Σ_1, Σ_2, where Σ_1 consists of the kinematic equations (5.14a)-(5.14c) and the sway dynamics (5.14e), while the dynamic equations (5.14d), (5.14f) constitute the subsystem Σ_2. The velocities u, r are considered as virtual control inputs for Σ_1, while the actual control inputs τ_u, τ_r are used to control Σ_2.

The constraint (5.15) can now be used to apply the steps presented in Chapter 4, in order to design the virtual control inputs for Σ_1: based on the structure of the constraint vector $\boldsymbol{a}^\top(\boldsymbol{\eta})$, the states $\boldsymbol{r} = \begin{bmatrix} x & y \end{bmatrix}^\top \triangleq \boldsymbol{x}$ are the *leafwise* states while ψ is the *transverse* state. Thus, an $\mathrm{N} = 2$ dimensional reference vector field $\mathbf{F}(\cdot) = \mathrm{F}_x \frac{\partial}{\partial x} + \mathrm{F}_y \frac{\partial}{\partial y}$ can be picked out of (4.6), in terms of the leafwise states x, y. For $\lambda = 3$ and $\boldsymbol{p} = \begin{bmatrix} 1 & 0 \end{bmatrix}^\top$, the vector field components read:

$$\mathrm{F}_x = 2x^2 - y^2, \quad \mathrm{F}_y = 3xy. \tag{5.16}$$

The vector field (5.16) is non-vanishing everywhere in $\mathbb{R}^2$ except for the origin $\boldsymbol{r} = \mathbf{0}$ and has integral curves that all converge to $\boldsymbol{r} = \mathbf{0}$ with direction $\phi \to 0$. Thus, the idea for the kinematic control design is that the vehicle can be controlled so that it "aligns with" the direction and flows along the integral curves of the vector field $\mathbf{F}(\cdot)$, until it converges to $\boldsymbol{\eta} = \mathbf{0}$.

Finally, since in the considered scenario the desired configuration $\boldsymbol{\eta_d} = \begin{bmatrix} x_d & y_d & 0 \end{bmatrix}^\top$ does not coincide with the origin $\boldsymbol{\eta} = \mathbf{0}$, the reference vector field $\mathbf{F}(\cdot)$ is defined out of (4.6) in terms of the position error $\boldsymbol{r_1} = \boldsymbol{r} - \boldsymbol{r_d}$; thus, the integral curves converge to $\boldsymbol{r_d}$. Then, for $\boldsymbol{p} = \begin{bmatrix} 1 & 0 \end{bmatrix}^\top$ and $\lambda = 3$ the vector field components read:

$$\mathrm{F}_x = 2{x_1}^2 - {y_1}^2, \quad \mathrm{F}_y = 3x_1 y_1, \tag{5.17}$$

where $\boldsymbol{r_1} = \begin{bmatrix} x_1 & y_1 \end{bmatrix}^\top$, $x_1 = x - x_d$, $y_1 = y - y_d$.

We are now ready to state the following theorems, which establish the asymptotic convergence of system trajectories $\mathbf{x}(t)$ to the desired state $\mathbf{x_d} = \begin{bmatrix} x_d & y_d & 0 & 0 & 0 & 0 \end{bmatrix}^\top$.

Control design for the subsystem Σ_1

Theorem 1 The trajectories $\boldsymbol{\eta}(t) = \begin{bmatrix} x(t) & y(t) & \psi(t) \end{bmatrix}^\top$ of the subsystem Σ_1 globally asymptotically converge to the desired configuration $\boldsymbol{\eta_d} = \begin{bmatrix} x_d & y_d & 0 \end{bmatrix}^\top$ under the control laws $u = \gamma_1(\cdot)$, $r = \gamma_2(\cdot)$ given as

$$\gamma_1(\cdot) = -k_1 \operatorname{sgn}\left(\boldsymbol{r_1}^\top \begin{bmatrix} \cos\psi \\ \sin\psi \end{bmatrix}\right) \tanh\left(\mu \|\boldsymbol{r_1}\|\right), \tag{5.18a}$$

$$\gamma_2(\cdot) = -k_2(\psi - \phi) + \dot{\phi}, \tag{5.18b}$$

where $k_1, k_2 > 0$, $\phi = \operatorname{atan2}(\mathrm{F}_y, \mathrm{F}_x)$ is the orientation of the vector field (4.33) at (x, y) and the function $\operatorname{sgn}(\cdot) : \mathbb{R} \to \{-1, 1\}$ is defined as: $\operatorname{sgn}(a) = \begin{cases} 1, & \text{if } a \geq 0, \\ -1, & \text{if } a < 0. \end{cases}$.

Proof of Theorem 1

Let us first prove the following lemma:

Lemma 1 *The orientation error $e = \psi - \phi$ is exponentially stable to zero under the control law* (5.18b)*.*

Proof Take the positive definite, radially unbounded function $V_e = \frac{1}{2}e^2$, then its time derivative reads

$$\dot{V}_e = e\,\dot{e} \overset{(4.31c)}{=} (\psi - \phi)(r - \dot{\phi}) \overset{(5.18b)}{=} -k_2(\psi - \phi)^2 = -2k_2 V_e.$$

Thus, the ψ is globally exponentially stable to the orientation $\phi(x, y) \triangleq \text{atan2}(\text{F}_y, \text{F}_x)$ of the vector field $\mathbf{F}(\cdot)$, where F_y, F_x are given by (5.17). ■

In order to study the convergence of the trajectories $\boldsymbol{\eta}(t)$ to $\boldsymbol{\eta_d}$, one can take a function V in terms of the position errors $x_1 = x - x_d$, $y_1 = y - y_d$ and the orientation error $e = \psi - \phi$ as

$$V = \frac{1}{2}({x_1}^2 + {y_1}^2) + \frac{1}{2}e^2 = V_1 + \frac{1}{2}e^2,$$

which is positive definite w.r.t. $\begin{bmatrix} x_1 & y_1 & e \end{bmatrix}^\top$ and radially unbounded, and take its time derivative as

$$\dot{V} = \dot{V}_1 + e\,\dot{e} \overset{(5.14),(5.18b)}{=} -k_2 e^2 + \begin{bmatrix} x_1 & y_1 \end{bmatrix} \begin{bmatrix} \cos\psi \\ \sin\psi \end{bmatrix} u + \begin{bmatrix} x_1 & y_1 \end{bmatrix} \begin{bmatrix} -\sin\psi \\ \cos\psi \end{bmatrix} v. \tag{5.19}$$

The behavior of $\dot{V}$ depends on the velocity v. If v can be seen as a bounded perturbation that vanishes at $\begin{bmatrix} x_1 & y_1 & e \end{bmatrix}^\top = \mathbf{0}$, then this point is an equilibrium of the kinematic subsystem Σ_1, (in the sense that, for $x_1 = y_1 = 0$, one has $e = 0 \Rightarrow \psi = \phi|_{x_1 = y_1 = 0} = 0$) and therefore it is meaningful to analyze its (asymptotic) stability. Since v comes from the control input $\zeta = ur$, one should study its evolution in an ISS framework.

With this insight, consider the candidate ISS-Lyapunov function

$$V_v = \frac{1}{2}v^2$$

and take its time derivative:

$$\dot{V}_v = -\frac{m_{11}}{m_{22}} v(ur) - \left(\frac{|Y_v|}{m_{22}} v^2 + \frac{|Y_{v|v|}|}{m_{22}} |v|\, v^2 \right),$$

where by definition $Y_v, Y_{v|v|} < 0$ and $w(v) = \frac{|Y_v|}{m_{22}} v^2 + \frac{|Y_{v|v|}|}{m_{22}} |v|\, v^2$ is a continuous, positive definite function. Take $0 < \theta < 1$, then:

$$\begin{aligned} &\dot{V}_v = -\frac{m_{11}}{m_{22}} v(ur) - (1 - \theta)w(v) - \theta w(v) \Rightarrow \\ &\dot{V}_v \leq -(1 - \theta)w(v),\ \forall v : -\frac{m_{11}}{m_{22}} v(ur) - \theta w(v) < 0. \end{aligned}$$

If the control input $\zeta = ur$ is bounded, $|\zeta| \leq \zeta_b$, then

$$\dot{V}_v \leq -(1 - \theta)w(v),\ \forall |v| : |Y_v||v| + |Y_{v|v|}||v|^2 > \frac{m_{11}}{\theta}\zeta_b.$$

Then, the subsystem (5.14e) is ISS [Kha02, Thm 4.19]. Thus, for any bounded input $\zeta = ur$, the linear velocity $v(t)$ will be ultimately bounded by a class $\mathcal{K}$ function of $\sup_{t>0}|\zeta(t)|$. If furthermore $\zeta(t) = u(t)r(t)$ converges to zero as $t \to \infty$, then $v(t)$ converges to zero as well [Kha02].

Consequently, if the control inputs $u = \gamma_1(\cdot)$, $r = \gamma_2(\cdot)$ are bounded functions which converge to zero as $t \to \infty$, then one has that $v(t)$ is bounded and furthermore, $v(t) \to 0$ as $t \to \infty$. Therefore, first note that the control input $u(t)$ is bounded by construction. Furthermore, one has out of (5.18b) that the control input $r(t)$ is bounded as well, since e, $\dot{\phi}$ are bounded. Thus, $v(t)$ is bounded: $|v(t)| \leq v_b$.

Going back to (5.19), substituting $u = \gamma_1(x, y)$ by (5.18a) yields:

$$\dot{V} = \dot{V}_1 - k_2 e^2 = -k_1 \left| \begin{bmatrix} x_1 & y_1 \end{bmatrix} \begin{bmatrix} \cos\psi \\ \sin\psi \end{bmatrix} \right| \tanh(\mu\|\boldsymbol{r_1}\|) + \begin{bmatrix} x_1 & y_1 \end{bmatrix} \begin{bmatrix} \cos(\frac{\pi}{2}-\psi) \\ \sin(\frac{\pi}{2}-\psi) \end{bmatrix} v(t) - k_2 e^2.$$

Since $|v(t)| \leq v_b$, the derivative $\dot{V}$ reads:

$$\dot{V} \leq -k_1 \left| \begin{bmatrix} x_1 & y_1 \end{bmatrix} \begin{bmatrix} \cos\psi \\ \sin\psi \end{bmatrix} \right| \tanh(\mu\|\boldsymbol{r_1}\|) + \|\boldsymbol{r_1}\| v_b - k_2 e^2.$$

Thus, a sufficient condition for $\dot{V}_1 \leq 0$ can be taken as:

$$\begin{aligned} \|\boldsymbol{r_1}\| v_b \leq k_1 \left| \boldsymbol{r_1}^\top \begin{bmatrix} \cos\psi \\ \sin\psi \end{bmatrix} \right| \tanh(\mu\|\boldsymbol{r_1}\|) \leq k_1 \|\boldsymbol{r_1}\| \tanh(\mu\|\boldsymbol{r_1}\|) \Rightarrow \\ v_b \leq k_1 \tanh(\mu\|\boldsymbol{r_1}\|) \Rightarrow \|\boldsymbol{r_1}\| \geq \frac{1}{\mu} \text{artanh}(\frac{v_b}{k_1}), \end{aligned} \tag{5.20}$$

where artanh$(\cdot)$ is the inverse hyperbolic tangent function. This condition essentially expresses that $\dot{V}_1 \leq 0$ for any position vector $\boldsymbol{r_1} = \begin{bmatrix} x_1 & y_1 \end{bmatrix}^\top$ that satisfies (5.20).

Consequently, for any initial position $\boldsymbol{r_1}(0)$ and for any $0 \leq r_0 \leq \|\boldsymbol{r_1}(0)\|$ that satisfies (5.20), $\dot{V}_1$ is negative in the set $\{\boldsymbol{r_1} \mid \frac{1}{2}{r_0}^2 \leq V_1(\|\boldsymbol{r_1}\|) \leq \frac{1}{2}\|\boldsymbol{r_1}(0)\|^2\}$, which verifies that the trajectories $\boldsymbol{r_1}(t)$ enter and remain bounded in the set $\{\boldsymbol{r_1} \mid V_1(\boldsymbol{r_1}) \leq \frac{1}{2}{r_0}^2\}$, i.e. that $\boldsymbol{r_1}(t)$ enters and remains into the ball $\mathcal{B}(\boldsymbol{0}, r_0)$; equivalently, the trajectories $\boldsymbol{r}(t)$ enter and remain into the ball $\mathcal{B}(\boldsymbol{r_d}, r_0)$.

Note also that within the ball $\mathcal{B}(\boldsymbol{r_d}, r_0)$ the solution $\boldsymbol{r}(t)$ is bounded and belongs into $\mathcal{B}(\boldsymbol{r_d}, r_0)$ $\forall t > t_1$. Then, it follows that its positive limit set L^+ is a non-empty, compact invariant set; furthermore, $\boldsymbol{r}(t)$ approaches L^+ as $t \to \infty$ [Kha02, Lemma 4.1].

Lemma 2 *The trajectories $\psi(t)$ of the kinematic subsystem Σ_1 globally asymptotically converge to the equilibrium $\psi_e = 0$ under the control law* (5.18b).

Proof Consider the time derivative $\dot{V}_e = -k_2 e^2 \leq 0$, and denote

$$\Omega = \{e \mid \dot{V}_e = 0\} \Rightarrow \Omega = \{e \mid \psi = \phi(x, y)\}.$$

Then, the trajectories $e(t)$ converge to the largest invariant set M included in Ω.

To identify the largest invariant set M in Ω, note first that the control input $r = \gamma_2(\cdot)$, given by (5.18b), vanishes for $\dot{\phi} = 0$, given that the tracking error $e = \psi - \phi(x, y)$ is globally exponentially stable to zero.

The dynamics of $\phi = \arctan\left(\frac{\mathrm{F}_y}{\mathrm{F}_x}\right)$ is $\dot{\phi} = \frac{\partial \phi}{\partial x}(x,y)\dot{x} + \frac{\partial \phi}{\partial y}(x,y)\dot{y}$. One can verify out of the analytic expressions of $\frac{\partial \phi}{\partial x}$, $\frac{\partial \phi}{\partial y}$ that $\dot{\phi}$ vanishes at the set $\mathrm{M} = (\mathrm{M}_1 \vee \mathrm{M}_2 \vee \mathrm{M}_3)$, where:

$$\begin{aligned}
\mathrm{M}_1 &= \{\mathbf{x} \mid x_1 = y_1 = 0 \wedge \psi = \phi\big|_{x_1=0, y_1=0} = 0\}, \\
\mathrm{M}_2 &= \{\mathbf{x} \mid x_1 \neq 0 \wedge y_1 = 0 \wedge \dot{y} = 0\}, \\
\mathrm{M}_3 &= \{\mathbf{x} \mid y_1 \neq 0 \wedge x_1 = 0 \wedge \dot{x} = 0\}.
\end{aligned}$$

For angular velocity $r = 0$, the sets further read:

$$\begin{aligned}
\mathrm{M}_1 &= \{\mathbf{x} \mid x_1 = y_1 = \psi = 0 \wedge u = v = 0\}, \\
\mathrm{M}_2 &= \{\mathbf{x} \mid x_1 \neq 0 \wedge y_1 = 0 \wedge \psi = 0 \wedge v = 0\}, \\
\mathrm{M}_3 &= \{\mathbf{x} \mid y_1 \neq 0 \wedge x_1 = 0 \wedge \psi = \pi \wedge u = 0\}.
\end{aligned}$$

However, if the system trajectories start on or enter the set M_3, one has $u = \gamma_1(\cdot) \neq 0$, which implies that the trajectories escape M_3. On the other hand, it is easy to verify that the sets M_1, M_2 are invariant w.r.t. the trajectories $\psi(t)$; the set M_1 corresponds to the trivial solution $\mathbf{x}(t) = \mathbf{0}$, whereas M_2 corresponds to the system moving along the x_G axis with $u \neq 0$, $r = 0$. Thus, $\dot{\phi}$ vanishes at the set $(\mathrm{M}_1 \vee \mathrm{M}_2)$. Consequently, the largest invariant set M in Ω reduces to $(\mathrm{M}_1 \vee \mathrm{M}_2)$, where the orientation $\psi = 0$, since in any other case the control input (5.18b) yields $r \neq 0$, which implies that $\psi = \phi(x,y)$ does not identically stay in Ω. Consequently, the orientation trajectories $\psi(t)$ globally asymptotically converge to $\psi_e = 0$. ■

Going back to the evolution of the position trajectories $\boldsymbol{r}(t)$, note that, within the ball $\mathcal{B}(\boldsymbol{r_d}, r_0)$, the control input $\zeta = ur$ vanishes as $r \to 0$. According to the above analysis, the control input $r(t)$ vanishes as $(\psi \to \phi(x,y)) \wedge (\psi \to 0)$. Since the dynamics of the linear velocity v are ISS, one has out of $\zeta(t) \to 0$ that $v(t) \to 0$ as well.

Consequently, one gets out of (5.20) that the system trajectories $\boldsymbol{r}(t)$ approach the ball $\mathcal{B}(\boldsymbol{r_d}, r_b)$ of radius:

$$r_b = \frac{1}{\mu} \operatorname{artanh}\left(\frac{v(t)}{k_1}\right),$$

where r_b is the ultimate bound of the system, $r_b < r_0$.

Then, as $v(t) \to 0$, one also gets that the ultimate bound $r_b \to 0$, i.e. that the trajectories $\boldsymbol{r}(t) \to \boldsymbol{r_d}$. ■

Control design for the subsystem Σ_2

Finally, the control inputs τ_u, τ_r of the subsystem Σ_2 should be designed so that the actual velocities $u(t)$, $r(t)$ track the virtual control inputs $\gamma_1(\cdot)$, $\gamma_2(\cdot)$.

Theorem 2 The actual velocities $u(t)$, $r(t)$ globally exponentially track the virtual control inputs $\gamma_1(\cdot)$, $\gamma_2(\cdot)$, respectively, under the control laws $\tau_u = \xi_1(\cdot)$, $\tau_r = \xi_2(\cdot)$ given as:

$$\tau_u = m_{11}\alpha - m_{22}vr - X_u u - X_{u|u|}|u|u, \tag{5.21a}$$

$$\tau_r = m_{33}\beta - (m_{11} - m_{22})uv - N_r r - N_{r|r|}|r|r, \tag{5.21b}$$

where

$$\alpha = -k_u(u - \gamma_1(\cdot)) + (\nabla\gamma_1)\dot{\boldsymbol{\eta}}, \quad k_u > 0, \tag{5.22a}$$

$$\beta = -k_r(r - \gamma_2(\cdot)) + (\nabla\gamma_2)\dot{\boldsymbol{\eta}}, \quad k_r > 0, \tag{5.22b}$$

and $\nabla\gamma_{\mathtt{k}} = \left[\frac{\partial\gamma_{\mathtt{k}}}{\partial x} \quad \frac{\partial\gamma_{\mathtt{k}}}{\partial y} \quad \frac{\partial\gamma_{\mathtt{k}}}{\partial\psi}\right]$ is the gradient of $\gamma_{\mathtt{k}}$, $\mathtt{k} = 1, 2$.

Proof of Theorem 2

Proof Under the feedback linearization transformation (5.21) the dynamic subsystem (5.14d), (5.14f) reads $\dot{u} = \alpha$, $\dot{r} = \beta$, where α, β are the new control inputs. Consider the candidate Lyapunov function:

$$V_\tau = \frac{1}{2}\left(u - \gamma_1(\boldsymbol{\eta})\right)^2 + \frac{1}{2}\left(r - \gamma_2(\boldsymbol{\eta})\right)^2,$$

and take its time derivative as

$$\dot{V}_\tau = \left(u - \gamma_1(\boldsymbol{\eta})\right)\left(\dot{u} - (\nabla\gamma_1)\dot{\boldsymbol{\eta}}\right) + \left(r - \gamma_2(\boldsymbol{\eta})\right)\left(\dot{r} - (\nabla\gamma_2)\dot{\boldsymbol{\eta}}\right),$$

where $\nabla\gamma_{\mathtt{k}} = \left[\frac{\partial\gamma_{\mathtt{k}}}{\partial x} \quad \frac{\partial\gamma_{\mathtt{k}}}{\partial y} \quad \frac{\partial\gamma_{\mathtt{k}}}{\partial\psi}\right]$, $\mathtt{k} = 1, 2$. Under the control inputs (5.22) one gets

$$\dot{V}_\tau = -k_u(u - \gamma_1(\cdot))^2 - k_r(r - \gamma_2(\cdot))^2 \leq -2\min\{k_u, k_r\}V_\tau,$$

where $k_u, k_r > 0$, which verifies that the actual velocities u, r globally exponentially track the virtual controls $\gamma_1(\cdot)$, $\gamma_2(\cdot)$, respectively. ■

The system trajectories $\mathbf{x}(t)$ under the control law (5.21), (5.22), (5.18) are shown in Fig. 5.3, whereas the control inputs τ_u, τ_r and the resulting thrust forces F_p, F_{st} are shown in Fig. 5.4(a) and Fig. 5.4(b), respectively.

5.4.3 Viable nonholonomic control design

The viability set K of the system (5.14) is determined by the following requirements (Fig. 5.2):

- The target should always be in the camera f.o.v., $[-y_T, y_T] \subseteq [f_2, f_1]$, so that sensing is effective.
- The laser range L_m must be within given bounds, $L_{\min} \leq L_m \leq L_{\max}$, so that the laser dots on the surface can be effectively detected.

These specifications impose $\mu = 4$ nonlinear inequality constraints of the form $c_j(x, y, \psi) \leq 0$, $j \in \mathcal{J} = \{1, 2, 3, 4\}$, written analytically as

$$c_1 : y - x\tan(\psi - \alpha) + y_T \leq 0, \tag{5.23a}$$

$$c_2 : y_T - y + x\tan(\psi + \alpha) \leq 0, \tag{5.23b}$$

$$c_3 : L_{\min} + \frac{x}{\cos\psi} \leq 0, \tag{5.23c}$$

$$c_4 : -\frac{x}{\cos\psi} - L_{\max} \leq 0. \tag{5.23d}$$

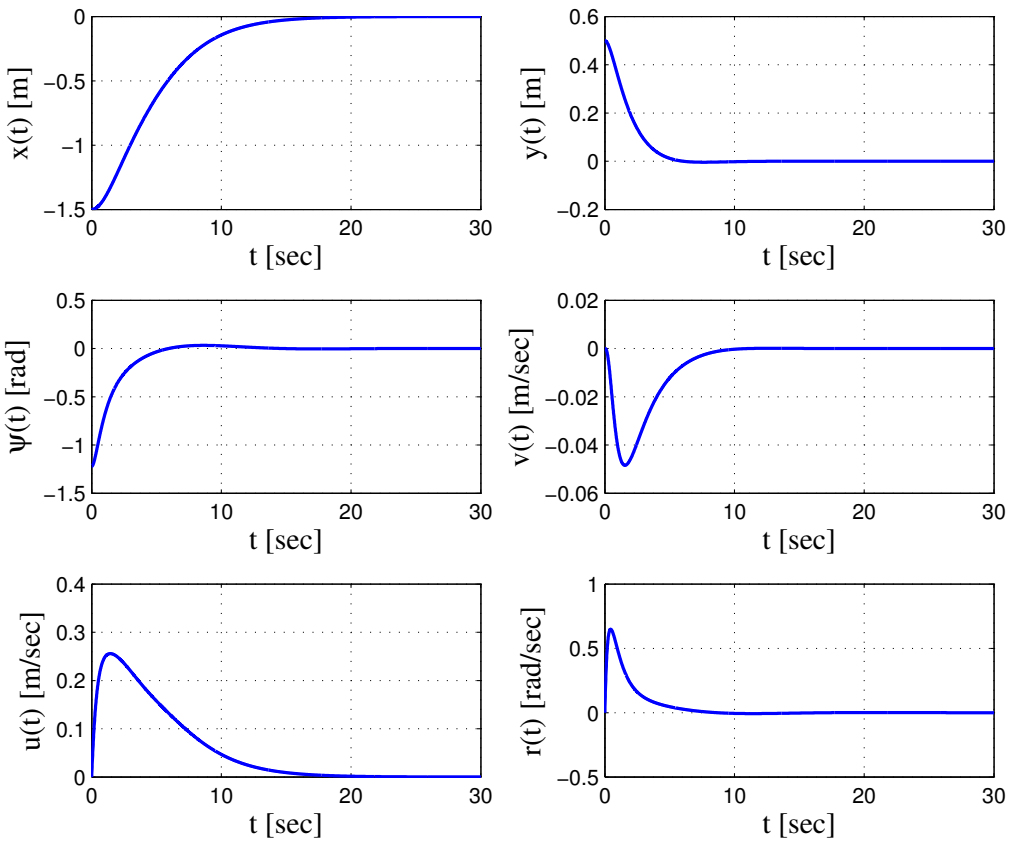

Figure 5.3: Response of the system trajectories $\mathbf{x}(t)$.

Note that the control law (5.18) yields solutions that, starting from any initial configuration $\boldsymbol{\eta_0}$ in K converge to (any) desired configuration $\boldsymbol{\eta_d}$ in K. Nevertheless, the convergent trajectories $\boldsymbol{\eta}(t)$ may not be viable in K, in the sense that the control inputs may steer the trajectories $\boldsymbol{\eta}(t)$ out of K during some finite time.

Such an example is shown in Fig. 5.5. Assume for now that only the constraint $c_1(\cdot)$ given by (5.23a) is of interest. The vehicle starts on a configuration $\boldsymbol{\eta_0} \in K$; however, tracking the reference vector field $\mathbf{F}(\cdot)$ under the control law (5.18) on its way to $\boldsymbol{\eta_d} = \begin{bmatrix} -0.5 & 0 & 0 \end{bmatrix}^\top$ implies that the convergent trajectories $\boldsymbol{\eta}(t)$ are driven out of K for some finite time, where the target is no longer in the camera f.o.v.. More specifically, the constraint $c_1(\cdot)$ becomes active when the target lies on the left boundary of the f.o.v., where $f_2 = -y_T$ (Fig. 5.5, dashed line). This condition defines a subset $\mathcal{Z}_1 = \{\boldsymbol{z} \in \partial K \mid c_1(\cdot) = y - x\tan(\psi - \alpha) + y_T = 0\}$ of ∂K.

From the definition of the regulation map $R_K(\cdot)$ (Section 5.2) one has that the viable system velocities at $\boldsymbol{z} \in \mathcal{Z}_1$ satisfy $\nabla c_1 \dot{\boldsymbol{z}} \leq 0 \Rightarrow \begin{bmatrix} -\tan(\psi-\alpha) & 1 & -x\sec^2(\psi-\alpha) \end{bmatrix} \begin{bmatrix} \dot{x} \\ \dot{y} \\ \dot{\psi} \end{bmatrix} \leq 0$. Substituting the system equations yields:

$$[-\tan(\psi-\alpha)\cos\psi + \sin\psi]\, u + [\tan(\psi-\alpha)\sin\psi + \cos\psi]\, v - x\sec^2(\psi-\alpha) r \leq 0. \qquad (5.24)$$

The viability condition (5.24) verifies that the control inputs (5.18) violate the constraint $c_1(\boldsymbol{z}) = 0$: at $\boldsymbol{z} \in \mathcal{Z}_1$ the vehicle moves with $u, r, \psi > 0$, thus the first and third term are

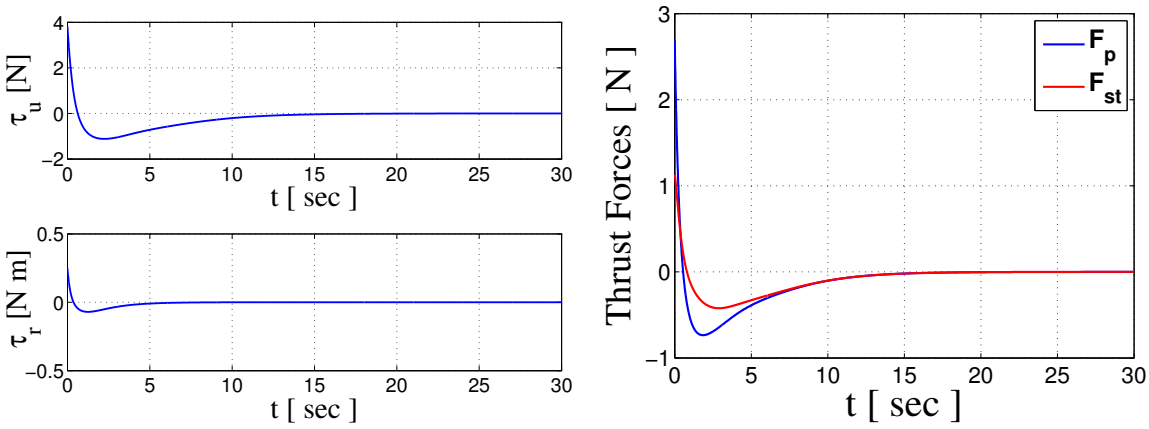

(a) The control inputs (5.21)

(b) Thrust Forces

Figure 5.4: The resulting control inputs and thrust forces.

> 0, whereas the (in general indefinite) velocity v is not negative enough to satisfy (5.24). Therefore, the control laws $u = \gamma_1(\cdot)$, $r = \gamma_2(\cdot)$ should be redesigned so that (5.24) holds $\forall \boldsymbol{z} \in \mathcal{Z}_1$.

To this end, the condition (5.24) offers the way to select viable control inputs when $\boldsymbol{z} \in \mathcal{Z}_1$. If the system starts at $\boldsymbol{z}$ with zero linear and angular velocities, then a viable option is to set $u(\boldsymbol{z}) = 0$ and $r(\boldsymbol{z}) < 0$; then, one has $v = 0$ since (5.14e) reduces to $\dot{v} = 0$, and the condition (5.24) is satisfied, since always $x < 0$.[7]

For picking a viable control input $r(\boldsymbol{z})$, one can choose to regulate the orientation ψ of the vehicle to the angle $\phi_t = \text{atan2}(-y, -x)$, which essentially is the orientation of the vector $-\boldsymbol{\eta}$ that connects the vehicle with the target via the angular velocity $r_{viab_1} = -k(\psi - \phi_t)$. In this way, the system is controlled so that target is centered in the camera f.o.v., avoiding thus the left boundary.

Similarly, the viability conditions when the remaining constraints become active at some $\mathcal{Z}_j = \{\boldsymbol{z} \mid c_j(\boldsymbol{z}) = 0\}$, $j \in \{2, 3, 4\}$, are analytically written as:

$$\nabla c_2 \dot{\boldsymbol{\eta}} \leq 0 \Rightarrow \begin{bmatrix} \tan(\psi+\alpha) & -1 & x\sec^2(\psi+\alpha) \end{bmatrix} \dot{\boldsymbol{\eta}} \leq 0 \overset{(5.14)}{\Rightarrow}$$
$$[\tan(\psi+\alpha)\cos\psi - \sin\psi]\, u + x\sec^2(\psi+\alpha) r - [\tan(\psi+\alpha)\sin\psi + \cos\psi]\, v \leq 0, \tag{5.25a}$$

$$\nabla c_3 \dot{\boldsymbol{\eta}} \leq 0 \Rightarrow \begin{bmatrix} \sec\psi & 0 & x \end{bmatrix} \dot{\boldsymbol{\eta}} \leq 0 \overset{(5.14)}{\Rightarrow} u + x\, r - \tan\psi\, v \leq 0, \tag{5.25b}$$

$$\nabla c_4 \dot{\boldsymbol{\eta}} \leq 0 \Rightarrow \begin{bmatrix} -\sec\psi & 0 & -x \end{bmatrix} \dot{\boldsymbol{\eta}} \leq 0 \overset{(5.14)}{\Rightarrow} \tan\psi\, v - u - x\, r \leq 0, \tag{5.25c}$$

and indicate how to select viable control laws for the case that the corresponding constraint becomes active.

Thus, if $\boldsymbol{z} \in \mathcal{Z}_2$, i.e. if the target is adjacent to the right boundary of the f.o.v., the system can be as well controlled so that the target is centered in the camera f.o.v. via $r_{viab_2} = -k(\psi - \phi_t)$; in this case the resulting angular velocity is $r_{viab_2} > 0$; given that $x < 0$ and by choosing the

[7] This is not the only viable option; any control input $\begin{bmatrix} u & r \end{bmatrix}^\top \in \boldsymbol{U}(\boldsymbol{z})$ such that $\nabla c_1 \dot{\boldsymbol{z}} \leq 0$ implies that the constraint $c_1(\boldsymbol{z})$ is not violated.

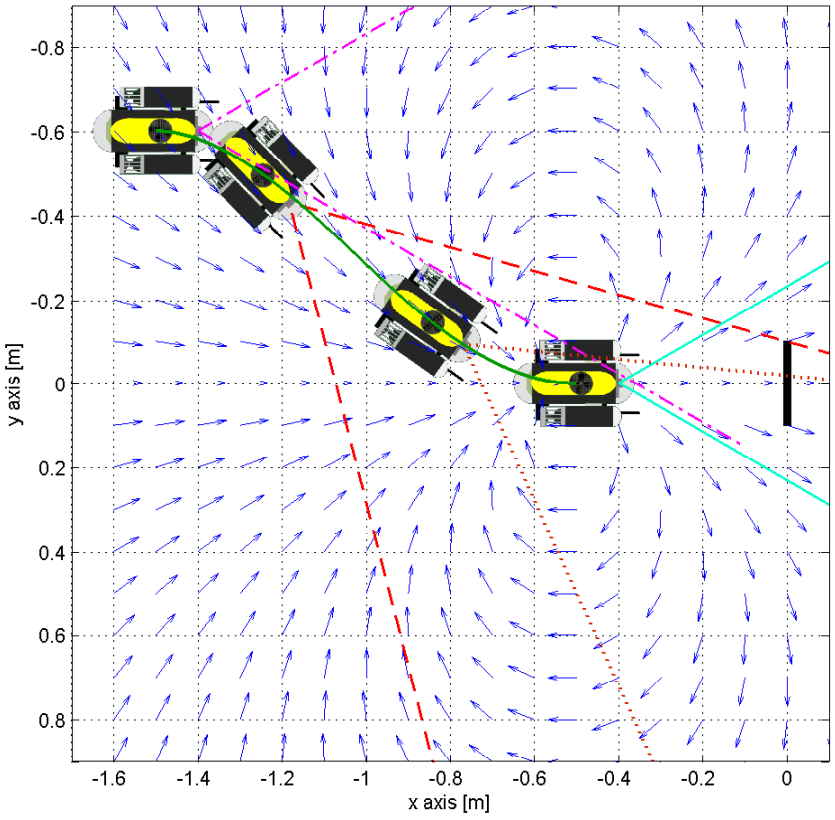

Figure 5.5: A convergent solution $\boldsymbol{\eta}(t)$ given by the control law (5.18) may violate viability during some (finite) time interval.

control gain k large enough, the term involving r is negative and dominates the remaining terms in (5.25a).

In the same spirit, for the remaining constraints one can verify that by setting $r_{viab_{3,4}} = 0$ and $u_{viab_{3,4}}$ by (5.18a) the term involving u is negative, implying that viability is maintained.

Thus, for redesigning the control laws (5.18) so that they are viable at $\boldsymbol{z} \in \mathcal{Z}_j$, $j \in \mathcal{J}$, one can consider the continuous switching signal

$$\sigma_j(c_j) = \begin{cases} 0, & \text{if } c_{j\,\min} < c_j \leq 0 \\ \frac{c_j - c_{j\,\max}}{c_{j\,\min} - c_{j\,\max}}, & \text{if } c_{j\,\max} \leq c_j \leq c_{j\,\min} \\ 1, & \text{if } c_j < c_{j\,\max} \end{cases} \tag{5.26}$$

shown in Fig. 5.4.3, and use the control law:

$$u = \sigma_j(c_j) u_{conv} + (1 - \sigma_j(c_j)) u_{viab_j}, \tag{5.27a}$$

$$r = \sigma_j(c_j) r_{conv} + (1 - \sigma_j(c_j)) r_{viab_j}, \tag{5.27b}$$

where $c_{j\,\min}$, $c_{j\,\max}$ are a priori defined values for the constraint $c_j(\cdot)$, u_{conv}, r_{conv} are the convergent to the origin control laws given by (5.18) and u_{viab_j}, r_{viab_j} are viable control laws at $\boldsymbol{z} \in \mathcal{Z}_j$. Then, if $c_j(\boldsymbol{z}) = 0$ one has $\sigma_j(c_j) = 0$, which ensures that the control laws given by (5.27) at $\boldsymbol{z} \in \mathcal{Z}_j$ are viable.

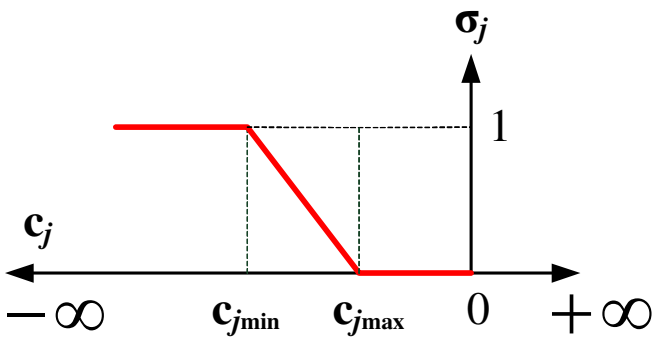

Figure 5.6: The switching signal $\sigma_j(c_j)$.

Under this control setting, if the system trajectories $\boldsymbol{\eta}(t)$ evolve away from the subset $\mathcal{Z}_j \in \partial K$ so that $c_j(\boldsymbol{\eta}(t)) < c_{j\,\min}(\boldsymbol{\eta}(t))\ \forall j \in \mathcal{J}\ \forall t \geq 0$, then the viable controls are never activated and the system is guaranteed to converge to the desired configuration $\boldsymbol{\eta_d}$ under the convergent control law (5.18).

On the other hand, if the switch $\sigma_j(\cdot)$ is activated at some $t \geq 0$, then the vehicle does not track the convergent to $(x, y) = (0, 0)$ integral curves of the vector field $\mathbf{F}$ during the time interval that $\sigma_j(c_j) \neq 1$. If furthermore the corresponding viable control laws are not convergent to $\boldsymbol{\eta_d}$, then the system is no longer guaranteed to converge to $\boldsymbol{\eta_d}$. In this case, one can relax the requirement on the convergence to a single point, and rather choose to establish convergence to a goal set $G \subset K$ of desired configurations, given as

$$G = \left\{ \boldsymbol{\eta_d} \in K \;\middle|\; {x_d}^2 + {y_d}^2 = d^2, \psi_d = \text{atan2}(-y_d, -x_d) \right\},$$

where d is a desired distance w.r.t. the target. The viable linear velocity controller is given as

$$u_{viab} = -k_1 \,\text{sgn}\left(\begin{bmatrix} x_1 & y_1 \end{bmatrix} \begin{bmatrix} \cos\psi \\ \sin\psi \end{bmatrix} \right) \tanh(\mu \|\boldsymbol{r_1}\|), \tag{5.28}$$

where $\boldsymbol{r_1} = \begin{bmatrix} x_1 & y_1 \end{bmatrix}^\top$, $x_1 = x - x_d$, $y_1 = y - y_d$, $x_d = d\cos\psi_d$, $y_d = d\sin\psi_d$, $\psi_d = \text{atan2}(-y, -x)$.

The orchestration of the switching between convergent and viable control laws taking into consideration all j constraints can be implemented by replacing the switching signal $\sigma_j(c_j)$ with the switching signal $\sigma^* := \min(\sigma_j)$, $j \in \mathcal{J}$;

$$u = \min(\sigma_j) u_{conv} + (1 - \min(\sigma_j)) u_{viab_j}, \tag{5.29a}$$

$$r = \min(\sigma_j) r_{conv} + (1 - \min(\sigma_j)) r_{viab_j}, \tag{5.29b}$$

In this way, the system switches when necessary to the viable controls u_{viab_j}, r_{viab_j} that correspond to the constraint j which is closer to be violated.

Finally, note that the control gains k_1, k_2, k_u, k_r can be properly tuned so that the virtual control inputs u, r correspond to thrust forces F_p, F_{st} that belong into the compact set $\mathcal{U} = [-f_p, f_p] \times [-f_{st}, f_{st}]$.

To evaluate the efficacy of the methodology, let us consider the scenario shown in Fig. 5.7. The vehicle initiates on a configuration $\boldsymbol{\eta_0}$ where both the constraints $c_2(\cdot)$, $c_4(\cdot)$ are active.

Thus, a viable control law that does not violate both (5.25a), (5.25c) is active at $t = 0$; in this case, we chose to use the convergent control law (5.18) as a viable control law, with the control gains k_1, k_2 tuned so that none of the constraints is violated. The vehicle moves towards the nominal desired configuration $\boldsymbol{\eta_d}$ under (5.29); note that the constraints $c_4(\cdot)$, $c_1(\cdot)$ become nearly active during some time intervals, activating the corresponding viable control laws. The vehicle approaches the goal set G under (5.29) for $j = 1$, i.e. by regulating the orientation ψ so that the target is always visible (red path). In this scenario the effect of the viable control law for $c_1(\cdot)$ does not vanish, and thus the vehicle does not converge to $\boldsymbol{\eta_d} = \begin{bmatrix} -0.5 & 0 & 0 \end{bmatrix}^\top$, but rather to a configuration in G. Finally, to ensure that the vehicle will stabilize at some point in G, the system switches to the viable control law corresponding to $j = 1$ in a small ball around $\boldsymbol{r_d}$ (blue path).

The evolution of the constraint functions $c_j(\boldsymbol{\eta}(t))$, $j \in \mathcal{J}$ is shown in Fig. 5.8; the value of $c_j(\cdot)$ is always non-positive which implies that viability is always maintained.

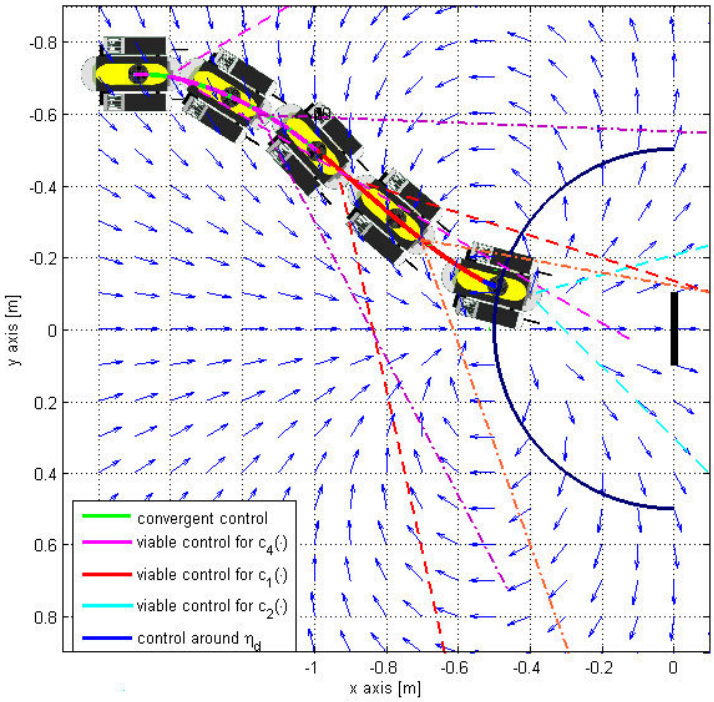

Figure 5.7: The path $x(t)$, $y(t)$ under the control scheme (5.29). The vehicle converges into a point of the goal set G.

Finally, Fig. 5.9 shows the resulting path under (5.29) for a case that the vehicle starts on a point in K, so that the viable control laws are not active (green path). As the vehicle moves towards $\boldsymbol{\eta_d}$ the switching signal $\sigma^* = \sigma_2$ becomes < 1, activating the corresponding viable control law for some finite time interval (red path). The vehicle moves away from the corresponding boundary $\mathcal{Z}_2$ of the set K, yielding $\sigma^* = 1$, and thus eventually converges to $\boldsymbol{\eta_d}$ under the convergent control law.

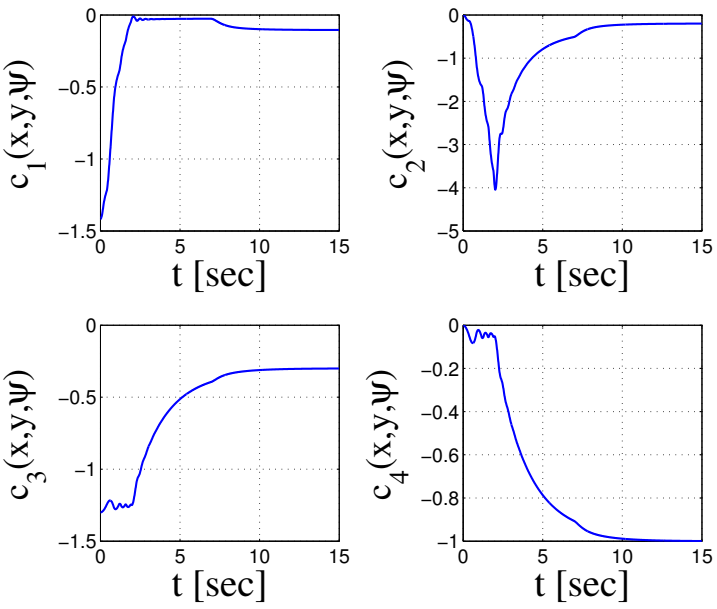

Figure 5.8: The value of the constraints remains always negative.

5.5 Viable control under a class of bounded disturbances

5.5.1 Robust nonholonomic control design

Let us now assume that the vehicle moves in the presence of an irrotational current of velocity V_c and direction β_c w.r.t. the global frame $\mathcal{G}$. As it will be shown later, the current V_c, β_c does not have to be explicitly known or constant, but rather to correspond to a class of bounded perturbations so that the velocity is at most equal to a known upper bound.

Following [Fos02], the kinematic and dynamic equations of motion are rewritten including the current effect as:

$$\dot{x} = u_r \cos\psi - v_r \sin\psi + V_c \cos\beta_c \tag{5.30a}$$

$$\dot{y} = u_r \sin\psi + v_r \cos\psi + V_c \sin\beta_c \tag{5.30b}$$

$$\dot{\psi} = r \tag{5.30c}$$

$$\dot{u}_r = \frac{m_{22}}{m_{11}} v_r r + \frac{X_u}{m_{11}} u_r + \frac{X_{u|u|}}{m_{11}} |u_r|\, u_r + \frac{\tau_u}{m_{11}} \tag{5.30d}$$

$$\dot{v}_r = -\frac{m_{11}}{m_{22}} u_r r + \frac{Y_v}{m_{22}} v_r + \frac{Y_{v|v|}}{m_{22}} |v_r|\, v_r \tag{5.30e}$$

$$\dot{r} = \frac{m_{11} - m_{22}}{m_{33}} u_r v_r + \frac{N_r}{m_{33}} r + \frac{N_{r|r|}}{m_{33}} |r|\, r + \frac{\tau_r}{m_{33}}, \tag{5.30f}$$

where $\boldsymbol{\nu_r} = \begin{bmatrix} u_r & v_r & r \end{bmatrix}^\top$ is the vector of the relative velocities in the body-fixed frame $\mathcal{B}$, $\boldsymbol{\nu_r} \triangleq \boldsymbol{\nu} - \boldsymbol{\nu_c}$ and $\boldsymbol{\nu_c} = \begin{bmatrix} V_c \cos(\beta_c - \psi) & V_c \sin(\beta_c - \psi) & 0 \end{bmatrix}^\top$ are the current velocities w.r.t. frame $\mathcal{B}$.

The system is written as a control affine system with drift vector field $\mathbf{f}(\mathbf{x})$ and additive

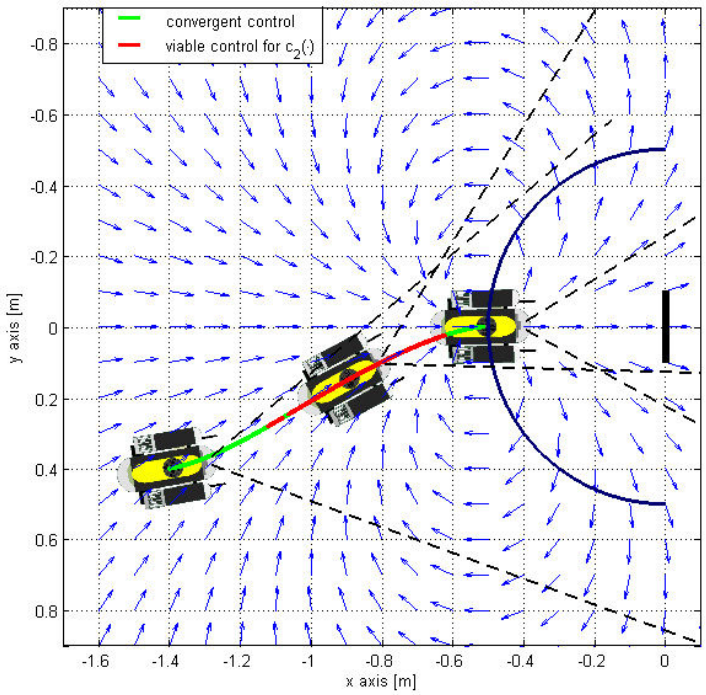

Figure 5.9: The vehicle starts moving under the control law (5.27) where $\sigma^* = 1$, i.e. the convergent control law (5.18) is active (green path). When the constraint $c_2(\cdot)$ is nearly violated the corresponding switching signal σ_2 becomes < 1 for some time interval (red path). The vehicle eventually converges to $\boldsymbol{\eta_d} = [-0.5 \;\; 0 \;\; 0]^\top$.

perturbations $\boldsymbol{\delta}(\cdot)$ as:

$$\dot{\mathbf{x}} = \mathbf{f}(\mathbf{x}) + \sum_{i=1}^{2} \mathbf{g}_i(\mathbf{x})\mathrm{u}_i + \boldsymbol{\delta}(\cdot),$$

where $\mathbf{x} = \begin{bmatrix}\boldsymbol{\eta}^\top & \boldsymbol{\nu_r}^\top\end{bmatrix}^\top = \begin{bmatrix}x & y & \psi & u_r & v_r & r\end{bmatrix}^\top$ is the state vector, $\mathbf{g}_i(\cdot)$ are the control vector fields and $\boldsymbol{\delta}(\cdot) = \begin{bmatrix}V_c\cos\beta_c & V_c\sin\beta_c & \mathbf{0}_{1\times 4}\end{bmatrix}^\top$ is the perturbation vector field.

Note that one gets out of the dynamic nonholonomic constraint (5.30e) that $\mathbf{x_e} = \mathbf{0}$ is an equilibrium point of (5.30) if $v_r = 0$ and $u_r r = 0$. The first condition reads $v = v_c$. Then, given that the linear velocity v of the vehicle along the sway d.o.f. should be zero at the equilibrium, it follows that $v_c = 0 \Rightarrow V_c \sin(\beta_c - \psi_e) = 0 \Rightarrow V_c = 0$ or $\psi_e = \beta_c + \kappa\pi$, $\kappa \in \mathbb{Z}$. Thus, the desired orientation $\psi_e = 0$ can be an equilibrium of (5.30) if $V_c = 0$, which corresponds to the nominal case, or if $\beta_c = 0$, i.e. if the current is parallel to the x-axis of the global frame $\mathcal{G}$.

Consequently, in the general case that $\beta_c \neq 0$, the current serves as a non-vanishing perturbation at the equilibrium $\boldsymbol{\eta_e} = \mathbf{0}$, and therefore the closed-loop trajectories of (5.30) can only be rendered ultimately bounded in a neighborhood of $\boldsymbol{\eta_e} = \mathbf{0}$.

Thus, the control design for (5.30) reduces into addressing the *practical* stabilization problem, i.e. to find state feedback control laws so that the system trajectories $\boldsymbol{\eta}(t)$ remain bounded around the desired configuration $\boldsymbol{\eta_d}$. Following the control design ideas used in the nominal case, the system (5.30) is divided into two subsystems Σ_1, Σ_2, where Σ_1 consists of the kine-

matic equations (5.30a)-(5.30c) and the sway dynamics (5.30e), while the dynamic equations (5.30d), (5.30f) constitute the subsystem Σ_2. The velocities u_r, r are considered as virtual control inputs for the subsystem Σ_1, while the actual control inputs τ_u, τ_r are used to control the subsystem Σ_2.

We are now ready to study the robustness of the control laws for the nominal system, under the class of bounded velocity disturbances $\boldsymbol{\delta}(\cdot)$.

Control design for the subsystem Σ_1

Theorem 3 The trajectories $\boldsymbol{r}(t) = \begin{bmatrix} x(t) & y(t) \end{bmatrix}^\top$ of the subsystem Σ_1 approach the ball $\mathcal{B}(\boldsymbol{r_d}, r_b)$, while the trajectories $\psi(t)$ globally asymptotically converge to the equilibrium $\psi_e = \beta_c + \kappa\pi$, $\kappa \in \mathbb{Z}$, under the control law $u_r = \gamma_1(\cdot)$, $r = \gamma_2(\cdot)$ given as:

$$\gamma_1(\cdot) = -k_1 \operatorname{sgn}\left(\boldsymbol{r_1}^\top \begin{bmatrix} \cos\psi \\ \sin\psi \end{bmatrix}\right) \tanh\left(\mu \|\boldsymbol{r_1}\|\right), \tag{5.31a}$$

$$\gamma_2(\cdot) = -k_2(\psi - \phi) + \dot{\phi}, \tag{5.31b}$$

where r_b is the ultimate bound given by (5.35).

Proof of Theorem 3

Proof The analysis on the trajectories of the perturbed system is along the same lines as the one for the nominal one. First, let us prove the following lemma:

Lemma 3 *The orientation error $e = \psi - \phi$ is exponentially stable to zero under the control law* (5.31b).

Proof Take the positive definite, radially unbounded function $V_e = \frac{1}{2}e^2$; then its time derivative reads $\dot{V}_e = e\dot{e} \overset{(5.30c)}{=} (\psi - \phi)(r - \dot{\phi}) \overset{(5.31b)}{=} -k_2(\psi - \phi)^2 = -2k_2 V_e$. Thus, ψ is exponentially stable to the orientation $\phi(x, y)$ of the vector field $\mathbf{F}(\boldsymbol{r})$. ■

To study the behavior of the system trajectories $\boldsymbol{r}(t)$ under (5.31), consider the Lyapunov function candidate

$$V_r = \frac{1}{2}\left((x - x_d)^2 + (y - y_d)^2\right) = \frac{1}{2}\left({x_1}^2 + {y_1}^2\right), \tag{5.32}$$

which is positive definite, radially unbounded and of class C^∞, and take the derivative of V_r along the trajectories of (5.30), given that $\dot{x}_d = 0$, $\dot{y}_d = 0$:

$$\dot{V}_r = \begin{bmatrix} x_1 & y_1 \end{bmatrix} \begin{bmatrix} \cos\psi \\ \sin\psi \end{bmatrix} u_r + \begin{bmatrix} x_1 & y_1 \end{bmatrix} \begin{bmatrix} -\sin\psi \\ \cos\psi \end{bmatrix} v_r + \begin{bmatrix} x_1 & y_1 \end{bmatrix} \begin{bmatrix} \cos\beta_c \\ \sin\beta_c \end{bmatrix} V_c. \tag{5.33}$$

The behavior of $\dot{V}_r$ depends on the linear velocity v_r along the sway d.o.f., as well as on the external perturbation. Since v_r comes from the control input $\zeta = u_r r$, one should study its evolution in an ISS framework.

With this insight, consider the candidate ISS-Lyapunov function $V_v = \frac{1}{2}{v_r}^2$ and take its time derivative

$$\dot{V}_v = -\frac{m_{11}}{m_{22}} v_r (u_r r) - \left(\frac{|Y_v|}{m_{22}} {v_r}^2 + \frac{|Y_{v|v|}|}{m_{22}} |v_r| \, {v_r}^2 \right).$$

Following the same analysis as in the nominal case, and given that the control input ζ is bounded, $|\zeta| \leq \zeta_b$, one eventually gets for some $\theta \in (0,1)$ that:

$$\dot{V}_v \leq -(1-\theta) w(v_r), \; \forall |v_r| : |Y_v||v_r| + |Y_{v|v|}||v_r|^2 \geq \frac{m_{11}}{\theta} \zeta_b.$$

Thus the subsystem (5.30e) is ISS w.r.t. ζ [Kha02, Thm 4.19], which essentially expresses that for any bounded input $\zeta = u_r r$, the linear velocity $v_r(t)$ will be ultimately bounded by a class $\mathcal{K}$ function of $\sup_{t>0} |\zeta(t)|$. Furthermore, if $\zeta(t) = u_r(t) r(t)$ converges to zero as $t \to \infty$, then $v_r(t)$ converges to zero as well [Kha02].

Remark 2 Note that the control input $\zeta(t)$ should vanish at the equilibrium $\boldsymbol{\eta_e} = \begin{bmatrix} x_e & y_e & \psi_e \end{bmatrix}^\top$, which is dictated by the direction β_c of the external disturbance, since $\psi_e = \beta_c + \kappa\pi$, $\kappa \in \mathbb{Z}$. Nevertheless, assuming that the current V_c, β_c is known and constant is unrealistic; thus, knowing a priori the equilibrium $\boldsymbol{\eta_e}$ is in general infeasible. For this reason we assume that only the bound $\|\boldsymbol{\delta}\|_{\max}$ of the current velocity is known, while the direction β_c is arbitrary, so that

$$\|\boldsymbol{\delta}\| = \sqrt{(V_c \cos\beta_c)^2 + (V_c \sin\beta_c)^2} = |V_c| \leq \|\boldsymbol{\delta}\|_{\max}.$$

This practically means that the current disturbance can be of any, *not necessarily constant* direction β_c, as long as $|V_c| \leq \|\boldsymbol{\delta}\|_{\max}$.

Substituting the control law (5.31a) into (5.33) yields

$$\begin{aligned} \dot{V}_r =& -k_1 \left| \boldsymbol{r_1}^\top \begin{bmatrix} \cos\psi \\ \sin\psi \end{bmatrix} \right| \tanh\left(\mu \|\boldsymbol{r_1}\|\right) + \begin{bmatrix} x_1 & y_1 \end{bmatrix} \begin{bmatrix} -\sin\psi \\ \cos\psi \end{bmatrix} v_r + \begin{bmatrix} x_1 & y_1 \end{bmatrix} \begin{bmatrix} \cos\beta_c \\ \sin\beta_c \end{bmatrix} V_c \Rightarrow \\ \dot{V}_r \leq& -k_1 \left| \boldsymbol{r_1}^\top \begin{bmatrix} \cos\psi \\ \sin\psi \end{bmatrix} \right| \tanh\left(\mu \|\boldsymbol{r_1}\|\right) + \|\boldsymbol{r_1}\| \left(v_{rb} + \|\boldsymbol{\delta}\|_{\max}\right), \end{aligned}$$

where v_{rb} is the ultimate bound of the linear velocity v_r. Thus, a sufficient condition for $\dot{V}_r < 0$ can be taken as

$$\begin{aligned} &\|\boldsymbol{r_1}\|(v_{rb} + \|\boldsymbol{\delta}\|_{\max}) < k_1 \left| \boldsymbol{r_1}^\top \begin{bmatrix} \cos\psi \\ \sin\psi \end{bmatrix} \right| \tanh\left(\mu \|\boldsymbol{r_1}\|\right) \leq k_1 \|\boldsymbol{r_1}\| \tanh\left(\mu \|\boldsymbol{r_1}\|\right) \\ &\quad \Rightarrow v_{rb} + \|\boldsymbol{\delta}\|_{\max} < k_1 \tanh\left(\mu \|\boldsymbol{r_1}\|\right) \Rightarrow \|\boldsymbol{r_1}\| > \frac{1}{\mu} \operatorname{artanh}\left(\frac{v_{rb} + \|\boldsymbol{\delta}\|_{\max}}{k_1} \right), \end{aligned} \tag{5.34}$$

where $\operatorname{artanh}(\cdot)$ is the inverse hyperbolic tangent function.

This condition essentially expresses that one has $\dot{V}_r < 0$ for any position vector $\boldsymbol{r_1} = \begin{bmatrix} x_1 & y_1 \end{bmatrix}^\top$ that satisfies (5.34). Thus, for any initial position $\boldsymbol{r_1}(0)$ and for any $r_0 < \|\boldsymbol{r_1}(0)\|$ that satisfies (5.34), $\dot{V}_r$ is negative in the set $\{\boldsymbol{r_1} \mid \frac{1}{2}{r_0}^2 \leq V_r(\|\boldsymbol{r_1}\|) \leq \frac{1}{2}\|\boldsymbol{r_1}(0)\|^2\}$, which verifies that the trajectories $\boldsymbol{r}(t)$ enter and remain bounded into the ball $\mathcal{B}(\boldsymbol{r_d}, r_0)$.

Note also that within the ball $\mathcal{B}(\boldsymbol{r_d}, r_0)$ the solution $\boldsymbol{r}(t)$ is bounded and belongs into $\mathcal{B}(\boldsymbol{r_d}, r_0)$ $\forall t > t_1$. Then, it follows that its positive limit set L^+ is a non-empty, compact invariant set; furthermore, $\boldsymbol{r}(t)$ approaches L^+ as $t \to \infty$ [Kha02, Lemma 4.1].

Lemma 4 *The trajectories $\psi(t)$ of the subsystem Σ_1 globally asymptotically converge to the equilibrium $\psi_e = \beta_c \pm \pi$ under the control law* (5.31b).

Proof To verify the argument, consider the time derivative $\dot{V}_e = -k_2 e^2 \leq 0$ of the positive definite, radially unbounded function $V_e = \frac{1}{2}e^2$. Denote

$$\Omega = \{e \mid \dot{V}_e = 0\} \Rightarrow \Omega = \{e \mid \psi = \phi(x, y)\}.$$

Then, the trajectories $e(t)$ converge to the largest invariant set M included in Ω.

For identifying the largest invariant set in Ω, note first that the control input (5.31b) vanishes when $\dot{\phi} = 0$, given that the tracking error $e = \psi - \phi(x, y)$ is globally exponentially stable to zero. Taking the dynamics of $\phi = \arctan(\frac{\mathrm{F}_y}{\mathrm{F}_x})$ yields that $\dot{\phi} = \mathrm{f}_1(x, y)\dot{x} + \mathrm{f}_2(x, y)\dot{y}$. The functions $\mathrm{f}_1(x, y)$, $\mathrm{f}_2(x, y)$ vanish only at $x = x_d$, $y = y_d$; nevertheless, it was shown that the system trajectories $\boldsymbol{r}(t)$ never reach the desired position $\boldsymbol{r_d}$, unless the perturbation is vanishing. Thus, $\dot{\phi}$ vanishes only when $\dot{x} = \dot{y} = 0$, i.e. at the equilibrium of (5.30), at which the vehicle's orientation is $\psi_e = \beta_c \pm \pi$. Therefore, the largest invariant set M reduces to $\psi_e = \beta_c \pm \pi$, since if $\psi = \phi(x, y) \neq \psi_e$, the control input (5.31b) yields $r \neq 0$, which implies that ψ does not identically stay in Ω. ■

Going back to the position trajectories $\boldsymbol{r}(t)$, one has that within the ball $\mathcal{B}(\boldsymbol{r_d}, r_0)$ the control input $\zeta(t) = u_r(t)\ r(t)$ vanishes as $r(t) \to 0$.[8] According to the above analysis, this occurs when $\{\psi = \phi(x, y)\} \wedge \{\psi = \beta_c \pm \pi\}$, i.e. when the orientation ψ of the vehicle is aligned with the direction of the current, at a point (x, y) where the reference orientation $\phi(x, y)$ coincides with the direction of the current as well; then out of (5.31b) one has $r = 0$. Since the dynamics of v_r are ISS, it follows that as $\zeta(t) \to 0$, then $v_r(t) \to 0$ as well.

Consequently, one gets out of (5.34) that the system trajectories $\boldsymbol{r}(t)$ eventually approach the ball $\mathcal{B}(\boldsymbol{r_d}, r_b)$ of radius $r_b < r_0$, given as:

$$r_b = \frac{1}{\mu}\ \mathrm{artanh}\left(\frac{\|\boldsymbol{\delta}\|_{\max}}{k_1}\right), \tag{5.35}$$

where r_b is the ultimate bound of the system.

Note that the ultimate bound r_b depends on the norm of the perturbation $\|\boldsymbol{\delta}\|_{\max}$, as well as on the control gain k_1 on the linear velocity, as one would expect from physical intuition. ■

At this point, recall that the evolution of the trajectories $\boldsymbol{\eta}(t)$ should respect the configuration constraints imposed by limited sensing, for the sensor system to be effective. Thus, for the scenario considered here, the vehicle is restricted to move on the left hyperplane w.r.t. the global y_G axis (see Fig. 5.10), while its orientation $\psi(t)$ should (roughly) be in $\left[-\frac{\pi}{2}, \frac{\pi}{2}\right]$, so that the vehicle faces the target.

In this sense, consider the case in Fig. 5.10, where $\boldsymbol{r_1}^\top \boldsymbol{r_d} > 0$. Then:

- Under the control law (5.31a), the vehicle tracks the vector field $\mathbf{F}(\cdot)$ and enters the ball $\mathcal{B}(\boldsymbol{r_d}, r_0)$, with linear relative velocity $u_r > 0$ and $\boldsymbol{r_1}^\top \begin{bmatrix} \cos\psi \\ \sin\psi \end{bmatrix} < 0$.

[8] It is easy to verify that $u_r(t)$ given by (5.31a) never vanishes, since $\boldsymbol{r_1}(t)$ does not converge to zero.

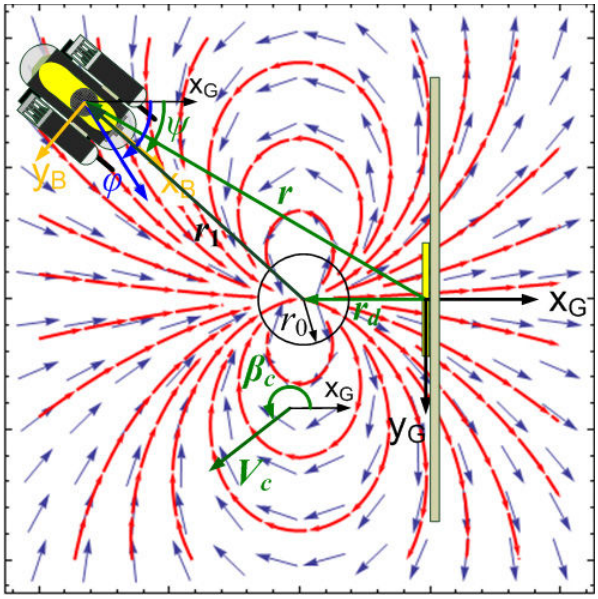

Figure 5.10: The marine vehicle is controlled so that it aligns with the direction ϕ and flows along the integral curves of the vector field $\mathbf{F}(\cdot)$, until its trajectories $\boldsymbol{r}(t)$ remain bounded into a ball $\mathcal{B}(\boldsymbol{r_d}, r_0)$ and approach the ball $\mathcal{B}(\boldsymbol{r_d}, r_b)$.

- According to Lemma 4, within the ball $\mathcal{B}(\boldsymbol{r_d}, r_0)$, the orientation trajectories $\psi(t)$ converge to the equilibrium $\boldsymbol{\eta_e}$.
- The linear velocity of the vehicle along the surge d.o.f. at the equilibrium is $u = 0$, which out of $u_r \triangleq u - u_c$ yields: $u_r = -u_c = -V_c \cos(\beta_c - \psi_e)$.
- The control input u_r given by (5.31a) at the equilibrium should be > 0 as well; otherwise one has out of (5.31a) that $\boldsymbol{r_1}^\top \begin{bmatrix} \cos\psi_e \\ \sin\psi_e \end{bmatrix} > 0$, i.e. that the vehicle does not face towards the target, which is undesirable.
- Then, it follows that $\cos(\beta_c - \psi_e) < 0$. Given that $\psi_e = \beta_c + \kappa\pi$, this further reads: $\cos(\beta_c - \psi_e) = -1 \Rightarrow \cos(\beta_c - \psi_e) = \cos\pi \Rightarrow \psi_e = \beta_c - \pi$.
- Consequently, in order to have: $\psi_e \in \left[-\frac{\pi}{2}, \frac{\pi}{2}\right]$, so that the vehicle faces the target, it follows that $\beta_c \in \left[\frac{\pi}{2}, \frac{3\pi}{2}\right]$, i.e. that $\boldsymbol{r_1}^\top \begin{bmatrix} \cos\beta_c & \sin\beta_c \end{bmatrix} > 0$.

Remark 3 In the remaining of the paper we consider the class of bounded perturbations

$$\boldsymbol{\delta} = \begin{bmatrix} V_c \cos\beta_c & V_c \sin\beta_c & \mathbf{0}_{1\times 4} \end{bmatrix}, \quad \|\boldsymbol{\delta}\| \leq \|\boldsymbol{\delta}\|_{\max}, \quad \text{such that} \quad \boldsymbol{r_1}^\top \begin{bmatrix} \cos\beta_c & \sin\beta_c \end{bmatrix} > 0,$$

as the one shown in Fig. 5.10. For $\boldsymbol{r_1}^\top \boldsymbol{r_d} > 0$ in particular, i.e. for the vehicle starting at a position $\boldsymbol{r_1}$ "behind" the desired position $\boldsymbol{r_d}$, it follows that the current direction should be so that $\cos\beta_c < 0$.

Control design for the subsystem Σ_2

Theorem 4 The actual velocities $u_r(t)$, $r(t)$ globally exponentially track the virtual control inputs $\gamma_1(\cdot)$, $\gamma_2(\cdot)$, respectively, under the control laws $\tau_u = \xi_1(\cdot)$, $\tau_r = \xi_2(\cdot)$ given as

$$\tau_u = m_{11}\alpha - m_{22}v_r r - X_u u_r - X_{u|u|}|u_r|u_r, \tag{5.36a}$$

$$\tau_r = m_{33}\beta - (m_{11} - m_{22})u_r v_r - N_r r - N_{r|r|}|r|r \tag{5.36b}$$

where

$$\alpha = -k_u(u_r - \gamma_1(\cdot)) + (\nabla\gamma_1)\dot{\boldsymbol{\eta}}, \;\; k_u > 0, \tag{5.37a}$$

$$\beta = -k_r(r - \gamma_2(\cdot)) + (\nabla\gamma_2)\dot{\boldsymbol{\eta}}, \;\; k_r > 0. \tag{5.37b}$$

Proof of Theorem 4

Proof Under the feedback linearization transformation (5.36), the corresponding dynamic equations (5.30d), (5.30f) read $\dot{u}_r = \alpha$, $\dot{r} = \beta$, respectively, where α, β are the new control inputs.

Consider the candidate Lyapunov function

$$V_\tau = \frac{1}{2}\left(u_r - \gamma_1(\cdot)\right)^2 + \frac{1}{2}\left(r - \gamma_2(\cdot)\right)^2$$

and take its time derivative as

$$\dot{V}_\tau = \left(u_r - \gamma_1(\cdot)\right)\left(\dot{u}_r - \frac{\partial\gamma_1}{\partial\boldsymbol{\eta}}\dot{\boldsymbol{\eta}}\right) + \left(r - \gamma_2(\cdot)\right)\left(\dot{r} - \frac{\partial\gamma_2}{\partial\boldsymbol{\eta}}\dot{\boldsymbol{\eta}}\right).$$

Then, under the control inputs (5.37) one gets

$$\dot{V}_\tau = -k_u(u_r - \gamma_1(\cdot))^2 - k_r(r - \gamma_2(\cdot))^2 \leq -2\min\{k_u, k_r\}V_\tau,$$

which verifies that the actual velocities $u_r(t)$, $r(t)$ are globally exponentially stable to the virtual velocities $\gamma_1(\cdot)$, $\gamma_2(\cdot)$, respectively. ■

5.5.2 Viable controls in the set K

Assume that the vehicle is at a configuration $\boldsymbol{z} \in \mathcal{Z}_j$ where $\mathcal{Z}_j = \{\boldsymbol{z} \in \partial K \mid c_j(\cdot) = 0\}$, i.e. that j-th constraint becomes active. The map of viable controls at $\boldsymbol{z} \in \mathcal{Z}_j$ is given as

$$R_K(\boldsymbol{z}) := \{\boldsymbol{\tau} \in \mathcal{T}(\boldsymbol{z}) \mid \nabla c_j(\cdot)\,\dot{\boldsymbol{\eta}} \leq 0\},$$

where $\nabla c_j(\cdot) = \left[\frac{\partial c_j}{\partial x} \quad \frac{\partial c_j}{\partial y} \quad \frac{\partial c_j}{\partial \psi}\right]^\top$ is the gradient of $c_j(\boldsymbol{\eta})$. Thus, the necessary conditions for selecting viable controls when the j-th constraint becomes active are analytically written as:

$$\nabla c_1 \dot{\boldsymbol{\eta}} \leq 0 \Rightarrow \left[-\tan(\psi-\alpha) \quad 1 \quad -x\sec^2(\psi-\alpha)\right] \dot{\boldsymbol{\eta}} \leq 0 \overset{(5.30)}{\Rightarrow} \left[-\tan(\psi-\alpha)\cos\psi + \sin\psi\right] u_r - x\sec^2(\psi-\alpha) r + \left[\tan(\psi-\alpha)\sin\psi + \cos\psi\right] v_r - \tan(\psi-\alpha) V_c \cos\beta_c + V_c \sin\beta_c \leq 0, \tag{5.38a}$$

$$\nabla c_2 \dot{\boldsymbol{\eta}} \leq 0 \Rightarrow \left[\tan(\psi+\alpha) \quad -1 \quad x\sec^2(\psi+\alpha)\right] \dot{\boldsymbol{\eta}} \leq 0 \overset{(5.30)}{\Rightarrow} \left[\tan(\psi+\alpha)\cos\psi - \sin\psi\right] u_r + x\sec^2(\psi+\alpha) r - \left(\tan(\psi+\alpha)\sin\psi + \cos\psi\right) v_r + \tan(\psi+\alpha) V_c \cos\beta_c - V_c \sin\beta_c \leq 0, \tag{5.38b}$$

$$\nabla c_3 \dot{\boldsymbol{\eta}} \leq 0 \Rightarrow \left[\sec\psi \quad 0 \quad x\right] \dot{\boldsymbol{\eta}} \leq 0 \overset{(5.30)}{\Rightarrow} u_r + x\, r - \tan\psi\, v_r + \sec\psi V_c \cos\beta_c \leq 0, \tag{5.38c}$$

$$\nabla c_4 \dot{\boldsymbol{\eta}} \leq 0 \Rightarrow \left[-\sec\psi \quad 0 \quad -x\right] \dot{\boldsymbol{\eta}} \leq 0 \overset{(5.30)}{\Rightarrow} \tan\psi\, v_r - u_r - x\, r - \sec\psi V_c \cos\beta_c \leq 0. \tag{5.38d}$$

Given that the velocities u_r, r serve as the control inputs, one should check whether the convergent control law (5.31) satisfies the viability conditions (5.38) at $\boldsymbol{z} \in \mathcal{Z}_j$. If this is not the case, then the control law should be re-designed so that the viability conditions are met at $\boldsymbol{z} \in \mathcal{Z}_j$. Clearly, if more than one constraints become active at the same time at some $\boldsymbol{z} \in \bigcap_{j\in\mathcal{J}} \mathcal{Z}_j$, the corresponding conditions should hold at the same time.

The conditions (5.38) offer the way to select viable control inputs at $\boldsymbol{z} \in \mathcal{Z}_j$. Consider, for instance, that $\boldsymbol{z} \in \mathcal{Z}_1$, which corresponds to the target being adjacent to the left boundary of the f.o.v.; then one can choose to regulate the orientation ψ to the angle $\phi_t = \text{atan2}(-y, -x)$ via the angular velocity $r_{viab_1} = -k(\psi - \phi_t)$, as one did for the nominal case. In this way, the vehicle is controlled so that target is centered in the camera f.o.v.. To select the gain k in a robust, yet conservative, way one can resort to picking k so that the resulting r_{viab_1} dominates the *worst-case* remaining terms in (5.24), i.e. the worst-case terms involving the upper bounds $|u_r|$, v_{r_b}, $\|\boldsymbol{\delta}\|$. Similarly, if $\boldsymbol{z} \in \mathcal{Z}_2$, i.e. if the target is adjacent to the right boundary of the f.o.v., the system can be as well controlled so that the target is centered in the camera f.o.v., via $r_{viab_2} = -k(\psi - \phi_t)$. In the same spirit, for the remaining constraints and for the class of perturbations considered in this paper (see the previous section) one can verify that by setting $r_{viab_{3,4}} = 0$ and $u_{r,viab_{3,4}}$ by (5.31a), where $k_1 \geq V_c$, the term involving u_r is negative and dominates the worst-case term involving V_c, implying that viability is maintained.

Therefore, for redesigning the control laws (5.31a), (5.31b) so that they are viable at $\boldsymbol{z} \in \mathcal{Z}_j$ one can consider the continuous switch (5.26) and use the control law

$$u_r = \sigma_j(c_j) u_{r,conv} + (1 - \sigma_j(c_j)) u_{r,viab_j}, \tag{5.39a}$$

$$r = \sigma_j(c_j) r_{conv} + (1 - \sigma_j(c_j)) r_{viab_j}, \tag{5.39b}$$

where $u_{r,conv}$, r_{conv} are given by (5.31), and $u_{r,viab_j}$, r_{viab_j} are control inputs satisfying the corresponding condition out of (5.25) at $\boldsymbol{z} \in \mathcal{Z}_j$. The orchestration of the switching between convergent and viable control laws taking into consideration all j constraints can be implemented similarly to the nominal case, by replacing the switching signal $\sigma_j(c_j)$ with $\sigma^* = \min(\sigma_j)$, $j \in \mathcal{J}$:

$$u_r = \min(\sigma_j) u_{r,conv} + (1 - \min(\sigma_j)) u_{r,viab_j}, \tag{5.40a}$$

$$r = \min(\sigma_j) r_{conv} + (1 - \min(\sigma_j)) r_{viab_j}, \tag{5.40b}$$

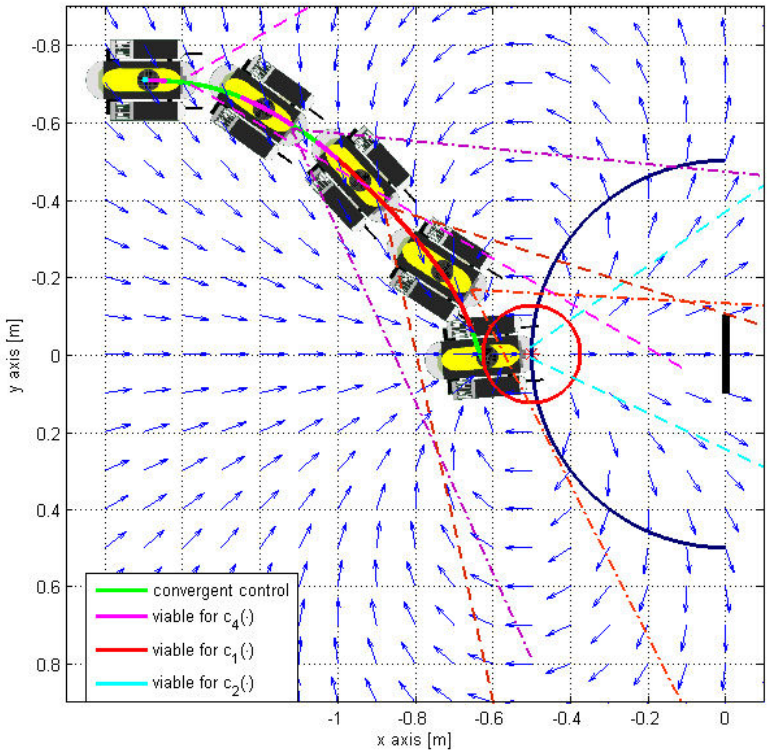

Figure 5.11: The path $x(t)$, $y(t)$ under the control scheme (5.40). The vehicle converges into a point of the goal set G.

so that the system switches when necessary to the viable controls $u_{r,viab_j}$, r_{viab_j} that correspond to the constraint j which is closer to be violated.

In the case that the control laws $u_{r,viab}$, r_{viab} are not convergent into the ball $\mathcal{B}(\boldsymbol{r_d}, r_0)$, the switching control law (5.39) does not any longer guarantee the convergence of the system trajectories $\boldsymbol{r}(t)$ into $\mathcal{B}(\boldsymbol{r_d}, r_0)$. In this case, one can relax the requirement on the convergence into $\mathcal{B}(\boldsymbol{r_d}, r_0)$ where $\boldsymbol{r_d}$ a single point, and rather consider a set $C \subset K$ of desired configurations as

$$C = \left\{ \boldsymbol{\eta_d} \in K \;\middle|\; {x_d}^2 + {y_d}^2 = d^2, \psi_d = \operatorname{atan2}(-y_d, -x_d) \right\},$$

where d is the desired distance w.r.t. the target, which define a circle of center $(x, y) = (0, 0)$ and radius d. Then, the vehicle can be controlled to converge into the set G, defined as the union of the balls $\mathcal{B}(\boldsymbol{r_d}, r_0)$, $\boldsymbol{r_d} \in C$ (Fig. 5.13). To do so, the viable velocities in (5.39) are chosen as

$$u_{r,viab} = -k_1 \operatorname{sgn}\left(\boldsymbol{r_1}^\top \begin{bmatrix} \cos\psi \\ \sin\psi \end{bmatrix} \right) \tanh(\mu \|\boldsymbol{r_1}\|), \tag{5.41a}$$

$$r_{viab} = -k(\psi - \phi_t), \tag{5.41b}$$

where $\phi_t = \operatorname{atan2}(-y, -x)$, $x_1 = x - x_d$, $x_d = d\cos\psi_d$, $y_1 = y - y_d$, $y_d = d\sin\psi_d$. Following the analysis in the previous sections, one has that the vehicle approaches the ball of radius $r_b = \frac{1}{\mu} \operatorname{artanh}\left(\frac{\|\boldsymbol{\delta}\|_{\max}}{k_1} \right)$ around some $\boldsymbol{r_d} \in C$. If the current direction β_c belongs into the cone

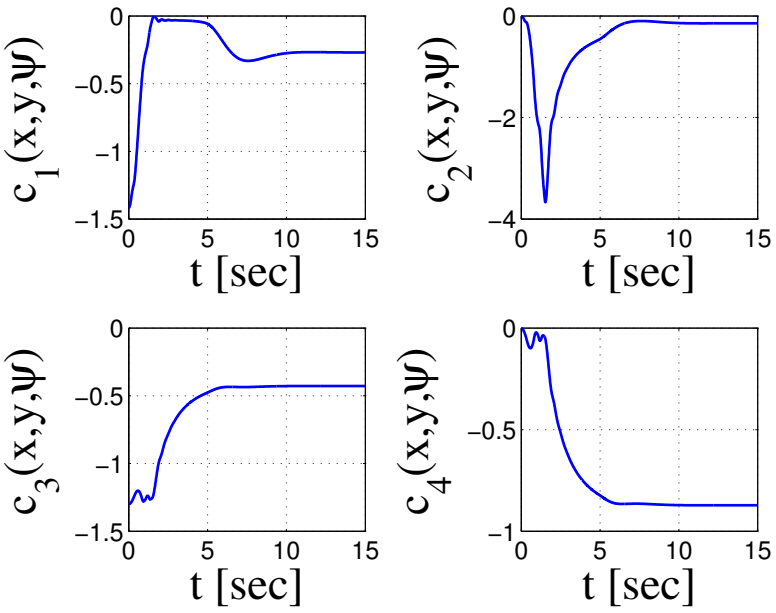

Figure 5.12: The value of the constraints remains always negative.

of angle δ shown in Fig. 5.13, then the vehicle converges into the "nominal" ball $\mathcal{B}(\boldsymbol{r_d}, r_0)$, shown in red.

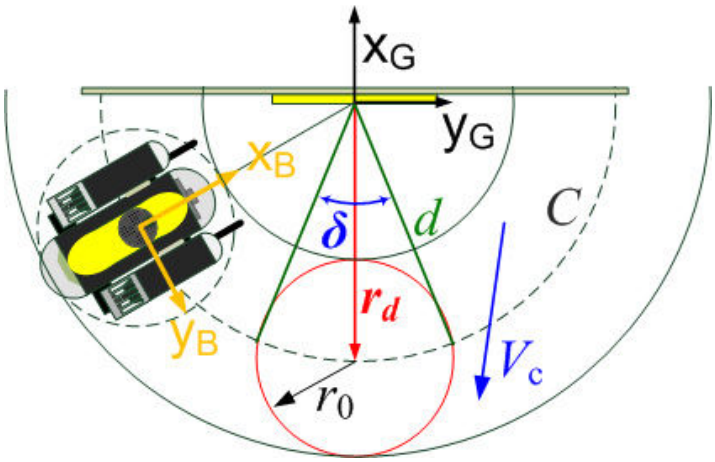

Figure 5.13: The vehicle is forced to converge into a goal set $G \subset K$, defined as the union of the balls $\mathcal{B}(\boldsymbol{r_d}, r_0)$, where $\boldsymbol{r_d}$ belong to the circle C.

Finally, the control gains k_1, k_2, k_u, k_r can be properly tuned so that the "virtual" control inputs u_r, r correspond to thrust forces F_p, F_{st} that belong into the compact set $\mathcal{U} = [-f_p, f_p] \times [-f_{st}, f_{st}]$.

5.6 Conclusions

This chapter presented a method for the feedback control design of nonholonomic systems which are subject to state constraints defining a viability set K. Using concepts from viability theory, the necessary conditions for selecting viable control laws for a nonholonomic system were given. Furthermore, a class of nonholonomic control solutions were redesigned in a switching control scheme, so that system trajectories starting in K converge to a goal set G in K, without ever leaving K. As a case study, the control design for an underactuated marine vehicle subject to configuration constraints due to limited visibility, as well as to a class of bounded external disturbances, was treated. Viable state feedback control laws in the constrained set K, which furthermore establish convergence to a goal set $G \subset K$ were constructed. Future extensions include the consideration of a wider class of external perturbations.

Chapter 6

Maintaining visibility for leader-follower formations in obstacle environments

Abstract

This chapter addresses the problem of controlling a leader-follower formation of two unicycle mobile robots, that move under visibility constraints in a known obstacle environment. Visibility constraints are realized as nonlinear inequality state constraints, that determine a visibility set K. Maintaining visibility is thus translated into controlling the robots so that system trajectories starting in K always remain in K. We provide the necessary and sufficient conditions under which visibility is maintained, as well as a control scheme that forces the follower to converge and remain into a set of desired configurations with respect to the leader, while maintaining visibility. Based on these results, we also propose a cooperative control scheme for the motion of the formation in a known obstacle environment, so that both collision avoidance and maintaining visibility are ensured. The proposed control schemes are decentralized, in the sense that there is no direct communication between the robots, nor global state feedback is available to them. The efficacy of our algorithms is evaluated through computer simulations.

6.1 Introduction

Control of leader-follower ($\mathrm{L}-\mathrm{F}$) formations has seen an increasing interest during the past few years, stimulated in part by the recent technological advances in communications and computation, which have allowed for the development of multi-agent systems that accomplish tasks effectively and reliably. Within the field of mobile robotics in particular, $\mathrm{L}-\mathrm{F}$ formations arise in applications ranging from surveillance and inspection to exploration and coverage. From a practical point of view, the case when limited sensing and/or limited communication among the robots are imposed is of particular interest; for instance, a very likely scenario for mobile robots operating in indoor environments is that global state feedback is not available to all robots, or that communication among them is restricted. These specifications impose various types of constraints to each robot, extending to the whole system, and should be taken into account during the control design.

In this chapter we consider the case of two mobile robots with unicycle kinematics that have to operate in a known environment with obstacles, while communication between them is not available. Assume that one of the robots (the leader L) is given a high-level motion plan for moving from an initial to a goal state in the free space. The task for the second robot (the follower F) is to move while keeping a fixed distance and orientation w.r.t. L, using the information from an onboard camera only, while also avoiding collisions.

The problem of maintaining formations using vision-based control is quite popular in the literature [DFK+02, CSVS03, MMP+09]; in these contributions the robots are assumed to have omnidirectional cameras, and that the leader's linear and angular velocities are either communicated to, or estimated by the follower.

However, when communication is absent and the onboard sensors have limited capabilities (e.g. limited range and/or angle-of-view), the robots can stay connected if and only if L is always visible in the f.o.v. of F. The latter specification imposes a set of visibility constraints, which should never be violated so that F always maintains visibility with L. The problem of controlling a nonholonomic robot so that it maintains visibility with either a fixed target (e.g. a landmark), or a moving target (e.g. an agent), has recently seen an increasing interest, see [KR05, BMCH07, SFPB10, MBP11] and the references therein. Moreover, when the robots have to operate in obstacle environments, avoiding collisions with obstacles, as well as between robots should be guaranteed.

This chapter proposes a feedback control solution for an $\mathrm{L}-\mathrm{F}$ formation of two unicycle mobile robots, that move in a known obstacle environment under visibility constraints and without explicit communication between them. Visibility constraints are realized as nonlinear inequalities in terms of the system states, that determine a closed subset K of the state space, called the visibility set K. Maintaining visibility can thus be translated into controlling the robots so that system trajectories starting in K always remain in K (Section 6.2). Inspired by ideas from viability theory [Aub91], we provide the conditions for visibility maintenance, as well as a control scheme that forces F to converge and remain into a set of desired configurations w.r.t. L while maintaining visibility (Sections 6.3, 6.4). We also propose a cooperative control scheme for the $\mathrm{L}-\mathrm{F}$ motion in a known obstacle environment, so that both collision avoidance and maintaining visibility are ensured (Section 6.5). The proposed control schemes are decentralized, in the sense that there is no direct communication between the robots, nor global state feedback is available to them. The follower is localized w.r.t. L, however is aware neither of the leader's navigation plan, nor of its velocities at each time instant. The leader is not aware of the follower's state, but rather moves in a way that indirectly ensures collision avoidance for both of them. The efficacy of our algorithms is evaluated through simulations.

6.2 Mathematical Modeling

6.2.1 Leader-Follower Kinematics

Consider two unicycle mobile robots moving in $\mathrm{L}-\mathrm{F}$ formation. The motion of each one of the robots L, F, w.r.t. a global frame $\mathcal{G}$ is described by

$$\dot{\boldsymbol{q}}_{\boldsymbol{i}} = \boldsymbol{G}(\boldsymbol{q}_{\boldsymbol{i}})\boldsymbol{v}_{\boldsymbol{i}} \Rightarrow \begin{bmatrix} \dot{x}_i \\ \dot{y}_i \\ \dot{\theta}_i \end{bmatrix} = \begin{bmatrix} \cos\theta_i & 0 \\ \sin\theta_i & 0 \\ 0 & 1 \end{bmatrix} \begin{bmatrix} u_i \\ w_i \end{bmatrix}, \tag{6.1}$$

where $i \in \{\mathrm{L}, \mathrm{F}\}$, $\boldsymbol{q}_{\boldsymbol{i}} = \begin{bmatrix} x_i & y_i & \theta_i \end{bmatrix}^\top$ is the configuration vector of i, $\boldsymbol{r}_{\boldsymbol{i}} = \begin{bmatrix} x_i & y_i \end{bmatrix}^\top$ is the position vector and θ_i is the orientation of i w.r.t. frame $\mathcal{G}$, u_i, w_i are the linear and angular velocity of i in the body-fixed frame ($\mathcal{L}$ or $\mathcal{F}$).

To describe the motion of F w.r.t. the leader frame $\mathcal{L}$, consider the position vector $\boldsymbol{r} = \begin{bmatrix} x & y \end{bmatrix}^\top$ of F w.r.t. $\mathcal{L}$, given as $\boldsymbol{r} = \mathbf{R}(-\theta_\mathrm{L})\,(\boldsymbol{r_F} - \boldsymbol{r_L})$, and take the time derivative as

$$\dot{\boldsymbol{r}} = \dot{\mathbf{R}}(-\theta_\mathrm{L})\,(\boldsymbol{r_F} - \boldsymbol{r_L}) + \mathbf{R}(-\theta_\mathrm{L})\,(\dot{\boldsymbol{r}}_\mathbf{F} - \dot{\boldsymbol{r}}_\mathbf{L})\,, \tag{6.2}$$

where

$$\mathbf{R}(-\theta_\mathrm{L}) = \begin{bmatrix} \cos(-\theta_\mathrm{L}) & -\sin(-\theta_\mathrm{L}) \\ \sin(-\theta_\mathrm{L}) & \cos(-\theta_\mathrm{L}) \end{bmatrix} = \begin{bmatrix} \cos\theta_\mathrm{L} & \sin\theta_\mathrm{L} \\ -\sin\theta_\mathrm{L} & \cos\theta_\mathrm{L} \end{bmatrix} \tag{6.3}$$

is the rotation matrix of the frame $\mathcal{L}$ w.r.t. frame $\mathcal{G}$, and

$$\dot{\mathbf{R}}(-\theta_\mathrm{L}) = \begin{bmatrix} 0 & w_\mathrm{L} \\ -w_\mathrm{L} & 0 \end{bmatrix} \mathbf{R}(-\theta_\mathrm{L}). \tag{6.4}$$

Substituting (6.3), (6.4), (6.1) into (6.2) and after some algebra one eventually gets

$$\begin{bmatrix} \dot{x} \\ \dot{y} \end{bmatrix} = \begin{bmatrix} -1 & y \\ 0 & -x \end{bmatrix} \begin{bmatrix} u_\mathrm{L} \\ w_\mathrm{L} \end{bmatrix} + \begin{bmatrix} \cos(\theta_\mathrm{F} - \theta_\mathrm{L}) \\ \sin(\theta_\mathrm{F} - \theta_\mathrm{L}) \end{bmatrix} u_\mathrm{F}. \tag{6.5}$$

Define $\beta = \theta_\mathrm{F} - \theta_\mathrm{L}$; then differentiating w.r.t. time yields

$$\dot{\beta} = \dot{\theta}_\mathrm{F} - \dot{\theta}_\mathrm{L} = w_\mathrm{F} - w_\mathrm{L}. \tag{6.6}$$

Combining equations (6.5) and (6.6) yields the system equations

$$\begin{bmatrix} \dot{x} \\ \dot{y} \\ \dot{\beta} \end{bmatrix} = \underbrace{\begin{bmatrix} \cos\beta & 0 \\ \sin\beta & 0 \\ 0 & 1 \end{bmatrix} \begin{bmatrix} u_\mathrm{F} \\ w_\mathrm{F} \end{bmatrix}}_{\boldsymbol{f}(\boldsymbol{q},\boldsymbol{v_F})} + \underbrace{\begin{bmatrix} -1 & y \\ 0 & -x \\ 0 & -1 \end{bmatrix} \begin{bmatrix} u_\mathrm{L} \\ w_\mathrm{L} \end{bmatrix}}_{\boldsymbol{g}(\boldsymbol{q},\boldsymbol{v_L})}, \tag{6.7}$$

where $\boldsymbol{q} = \begin{bmatrix} x & y & \beta \end{bmatrix}^\top \in \mathcal{C}$ is the state vector, including the position $\boldsymbol{r} = \begin{bmatrix} x & y \end{bmatrix}^\top$ and orientation β of F w.r.t. the leader frame $\mathcal{L}$, $\mathcal{C}$ is the state space, $\boldsymbol{v_F} = \begin{bmatrix} u_\mathrm{F} & w_\mathrm{F} \end{bmatrix}^\top \in \mathcal{U}_\mathrm{F}$ is the vector of control inputs, $\mathcal{U}_\mathrm{F} \subset \mathbb{R}^2$ is a compact set denoting the control space, and $\boldsymbol{g}(\boldsymbol{q}, \boldsymbol{v_L}) \in \mathbb{R}^3$ can be seen as a perturbation vector field, where $\boldsymbol{v_L} = \begin{bmatrix} u_\mathrm{L} & w_\mathrm{L} \end{bmatrix}^\top \in \mathcal{U}_\mathrm{L} \subset \mathbb{R}^2$ is the vector of control inputs of L.

Note that the perturbation is vanishing if and only if $\boldsymbol{g}(\boldsymbol{q}, \boldsymbol{v_L}) = \mathbf{0}$, which occurs if and only if $\boldsymbol{v_L} = \mathbf{0}$. Consequently, the motion of L can be thought as a non-vanishing perturbation to F.

6.2.2 Visibility constraints

The follower F is assumed to have an onboard camera with angle-of-view $2\alpha < \pi$, and that it can reliably detect objects which are within a maximum range L_s as shown in Fig. 6.1. These specifications define a "cone-of-view" for F, which essentially is an isosceles triangle (in obstacle-free environments). Assume also that F is localized w.r.t. L, i.e. that the distance $r = \sqrt{x^2 + y^2}$, as well as the bearing angle $\phi \in (-\pi, \pi]$ are measured. Consequently, at each time instant t, F can detect L if and only L is in the cone-of-view, i.e.

$$|\phi| \leq \alpha \;\text{ and }\; r \leq L_s(\phi) = \frac{L_s \cos\alpha}{\cos\phi}. \tag{6.8}$$

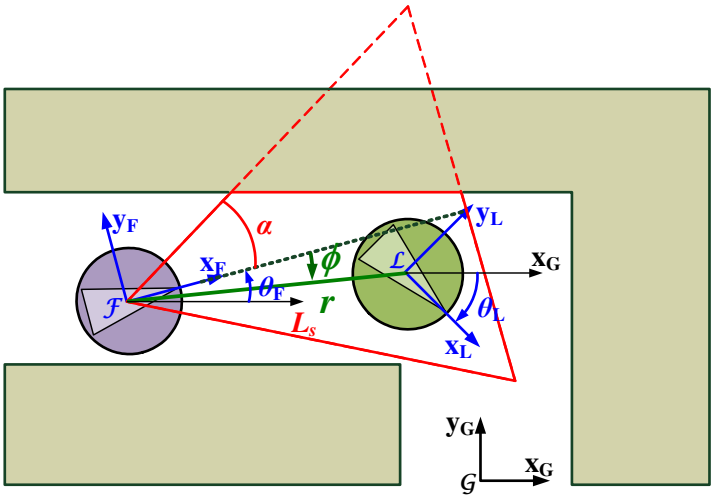

Figure 6.1: The system setup in an obstacle environment.

These constraints define a closed subset K of $\mathcal{C}$, given as

$$K = \{\boldsymbol{q} \in \mathcal{C} \mid h_k(\boldsymbol{q}) \leq 0,\ k = 1, 2\}\,, \tag{6.9}$$

where $h_1 = |\phi| - \alpha$ and $h_2 = r - L_s(\phi)$, which we call the *visibility set* K. The set K includes every configuration $\boldsymbol{q}$ for which visibility is maintained. Then, controlling F, L so that the resulting trajectories $\boldsymbol{q}(t)$ never escape K, implies that visibility is always maintained.

Consequently, the problem of maintaining visibility for (6.7) reduces into finding control inputs $\boldsymbol{v_F} \in \mathcal{U}_F$ for F, such that the visibility constraints (6.8) are met $\forall t \geq 0$, despite the (non-vanishing) perturbation $\boldsymbol{g}(\boldsymbol{q}, \boldsymbol{v_L})$ that is induced by L.

6.3 Control Design for the Nominal System

Consider the nominal system (6.7), given for $\boldsymbol{g}(\boldsymbol{q}, \boldsymbol{v_L}) = \boldsymbol{0}$, i.e. for $u_L = w_L = 0$, in an obstacle-free environment. Setting the global frame $\mathcal{G} \triangleq \mathcal{L}$ yields $\boldsymbol{q_L} \triangleq \boldsymbol{0}$, $\boldsymbol{q} \triangleq \boldsymbol{q_F}$.

The task for F is defined as to converge to a distance r_d w.r.t. L with angle $\phi = 0$, where $2r_0 \leq r_d \leq L_s \cos\alpha$, r_0 is the radius of the robots; in that way, L is centered in the camera f.o.v.. This requirement specifies a manifold $\mathcal{M}$ of desired configurations: $\boldsymbol{q_d} = \begin{bmatrix} x_d & y_d & \theta_d \end{bmatrix}^\top$ for F,

$$\mathcal{M} = \left\{\boldsymbol{q_d} \in \mathcal{C} \;\middle|\; {x_d}^2 + {y_d}^2 = {r_d}^2, \theta_d = \operatorname{atan2}(y_d, x_d) + \operatorname{sign}(y_d)\pi\right\}.$$

Thus, the control design for F reduces into finding a feedback control law $\boldsymbol{v_F} = \boldsymbol{\gamma}(\boldsymbol{q})$ such that F converges to the manifold $\mathcal{M}$, while the trajectories $\boldsymbol{q}(t) \triangleq \boldsymbol{q_F}(t)$ satisfy the visibility constraints (6.8) $\forall t \geq 0$, so that they always remain into K.

6.3.1 Convergence to a desired configuration

A control solution yielding global asymptotic convergence to a desired configuration $\boldsymbol{q_d} \in \mathcal{M}$ for the unicycle can be given using the concept of *dipolar* vector fields. A dipolar vector field

$\mathbf{F}: \mathbb{R}^2 \to \mathbb{R}^2$ has integral lines that all lead to the origin $(x, y) = (0, 0)$ of the global frame $\mathcal{G}$, is non-vanishing everywhere in $\mathbb{R}^2$ except for the origin, and is given as

$$\mathbf{F}(\boldsymbol{r}) = \lambda(\boldsymbol{p}^\top \boldsymbol{r})\boldsymbol{r} - \boldsymbol{p}(\boldsymbol{r}^\top \boldsymbol{r}), \tag{6.10}$$

where $\lambda \geq 2$, $\boldsymbol{p} \in \mathbb{R}^2$ and $\boldsymbol{r} = \begin{bmatrix} x & y \end{bmatrix}^\top$ is the position vector w.r.t. $\mathcal{G}$.

The main characteristic of a dipolar vector field (6.10) is that its integral lines converge to the origin $(0, 0)$ with the direction φ_p of the vector $\boldsymbol{p}$. Then, choosing the vector $\boldsymbol{p} = \begin{bmatrix} p_x & p_y \end{bmatrix}^\top$ such that $\varphi_p = \text{atan2}(p_y, p_x) \triangleq \theta_d$, reduces the orientation control of the unicycle into forcing it to align with the integral curves of the dipolar vector field.

Thus, if the vector $\boldsymbol{p}$ is assigned on a desired position $\boldsymbol{r_d} = \begin{bmatrix} x_d & y_d \end{bmatrix}^\top \in \mathcal{M}$, then one gets a dipolar vector field whose integral lines converge to $\boldsymbol{r_d}$ having the desired orientation $\varphi_p \triangleq \theta_d$. The analytic form of $\mathbf{F} = \mathrm{F}_x \frac{\partial}{\partial x} + \mathrm{F}_y \frac{\partial}{\partial y}$ for $\boldsymbol{p} = \begin{bmatrix} p_x & p_y \end{bmatrix}^\top$ is given by (6.10) and reads:

$$\mathrm{F}_x = 2p_x {x_1}^2 - p_x {y_1}^2 + 3p_y x_1 y_1, \tag{6.11a}$$

$$\mathrm{F}_y = 2p_y {y_1}^2 - p_y {x_1}^2 + 3p_x x_1 y_1. \tag{6.11b}$$

where $\boldsymbol{r}$ in (6.10) has been substituted by $\boldsymbol{r_1} = \begin{bmatrix} x_1 & y_1 \end{bmatrix}^\top$, $\boldsymbol{r_1} = \boldsymbol{r} - \boldsymbol{r_d}$.

Theorem 1 The trajectories $\boldsymbol{q}(t) = \begin{bmatrix} x(t) & y(t) & \theta_{\mathrm{F}}(t) \end{bmatrix}^\top$ of the nominal system (6.7) globally asymptotically converge to the desired configuration $\boldsymbol{q_d}$ under the control law $\boldsymbol{v_F} = \begin{bmatrix} u_{\mathrm{F}} & w_{\mathrm{F}} \end{bmatrix}^\top$ given as

$$u_{\mathrm{F}} = -k_1 \,\mathrm{sgn}\left(\boldsymbol{r_1}^\top \begin{bmatrix} \cos\theta_{\mathrm{F}} \\ \sin\theta_{\mathrm{F}} \end{bmatrix}\right) \|\boldsymbol{r_1}\|, \tag{6.12a}$$

$$w_{\mathrm{F}} = -k_2(\theta_{\mathrm{F}} - \varphi) + \dot{\varphi}, \tag{6.12b}$$

where $k_1, k_2 > 0$, $\varphi = \text{atan2}(\mathrm{F}_y, \mathrm{F}_x)$ is the orientation of the vector field at (x, y), $\mathrm{sgn}(\cdot)$ is defined as $\mathrm{sgn}(a) = 1$, if $a \geq 0$ and $\mathrm{sgn}(a) = -1$, if $a < 0$. The proof follows the same pattern as in the case of the unicycle in Chapter 4.

6.3.2 Maintaining Visibility

The control law (6.12) forces F to converge to a desired configuration $\boldsymbol{q_d} \in \mathcal{M}$, which belongs to the visibility set K. However, the trajectories $\boldsymbol{q}(t)$ do not necessarily belong to the visibility set K $\forall t \geq 0$, i.e. L may not be visible to F at least during some finite time interval. This mainly depends on the choice of $\boldsymbol{q_d} \in \mathcal{M}$, which specifies the vector $\boldsymbol{p}$ for the reference vector field (6.10), i.e. the reference orientation $\varphi(t)$ that the robot has to track via (6.12b).

Thus, given an initial condition $\boldsymbol{q_F}(0) \in K$, one should first select a $\boldsymbol{q_d} \in \mathcal{M}$ that ensures visibility maintenance under (6.12). In this respect, note that not all possible desired positions $\boldsymbol{r_d}$ belong to the cone-of-view at each time instant t; see Fig. 6.2 and assume that $t = 0$: the desired positions $\boldsymbol{r_d} \in \mathbb{R}^2$ belong to the circle $c = \{\boldsymbol{r} \in \mathbb{R}^2 \mid x^2 + y^2 = {r_d}^2\}$, centered at the origin (i.e. at L); however, only the positions on the arc $\mathcal{V}$ shown in bold belong to the cone-of-view of F. Thus, it makes sense to pick some $\boldsymbol{r_d} \in \mathcal{V}$.

Furthermore, out of the available options, it makes sense to pick the position $\boldsymbol{r_d} \in \mathcal{V}$ which lies on the line that connects the two robots. In this case, the orientation error to be regulated via the control input w_{F} is $e = \theta_{\mathrm{F}} - \varphi(x_1, y_1)$, where $\varphi(x_1, y_1) = \varphi_p = \theta_d$ (Fig. 6.2), while $\phi = \varphi_p - \theta_{\mathrm{F}} = -e$. Moreover, one has that e is exponentially stable to zero, since

$$\dot{e} = \dot{\theta}_{\mathrm{F}} - \dot{\varphi}_p \overset{(6.12b)}{=} -k_2(\theta_{\mathrm{F}} - \varphi_p) = -k_2 e,$$

which in turn implies that $\dot{\phi} = -k_2\phi$. Consequently, by choosing the desired configuration $\boldsymbol{q_d}$ as described above and under the control input (6.12b), any initial angle $\phi(0) \in K$ is exponentially stable to $\phi = 0$. This condition is substantial for ensuring that visibility is maintained, since it implies that the constraint $h_1(\cdot) \leq 0$ is forced to its minimum.

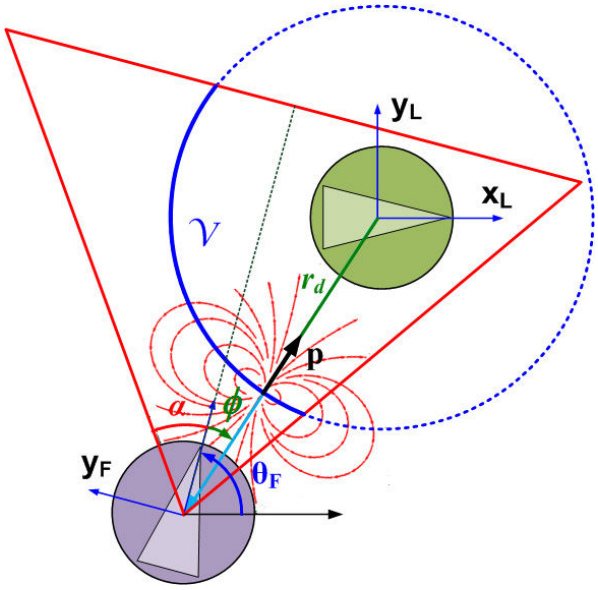

Figure 6.2: Determining the vector $\boldsymbol{p}$ and the desired position $\boldsymbol{r_d}$ on $\mathbb{R}^2$

In order to ensure that the system trajectories $\boldsymbol{q}(t)$ never escape the visibility set K, one has to consider how the system behaves on the boundary ∂K of K, where at least one of the constraints becomes active: $h_k(\boldsymbol{q}) = 0$ for some k. In particular, for $\boldsymbol{q} \in \partial K$ one has to check whether the system vector field $\dot{\boldsymbol{q}} = \boldsymbol{G}(\boldsymbol{q})\boldsymbol{v}_{\mathbf{F}}(\boldsymbol{q})$ is "tangent" to K, for bringing the solution $\boldsymbol{q}(t)$ back in the interior of K.[1] Thus, given that the constraints $h_k(\cdot) : \mathbb{R}^3 \to \mathbb{R}$ are continuously differentiable functions, one has thus to check whether

$$\dot{h}_k(\boldsymbol{q}) = \nabla h_k(\boldsymbol{q})\dot{\boldsymbol{q}} = \nabla h_k(\boldsymbol{q})\boldsymbol{G}(\boldsymbol{q})\boldsymbol{v}_{\mathbf{F}}(\boldsymbol{q}) < 0, \tag{6.13}$$

for the points where $h_k(\boldsymbol{q}) = 0$, for each k. If (6.13) holds, then the value of $h_k(\boldsymbol{q})$ is forced to decrease, bringing the trajectory $\boldsymbol{q}(t)$ into the visibility set K.[2] In other words, visibility is

[1] This "tangency" condition is the main concept in viability theory, and is realized via the concept of the contingent cone $T_K(x)$ to a set K defined by inequality constraints [Aub91, AF90].

[2] For linear and smooth nonlinear systems, the viability property has been introduced as "controlled invariance". The reader is referred to [Aub91] for a thorough introduction to viability theory.
If (6.13) holds with $\leq$ instead of $<$, then the system trajectories are forced either on the boundary, or in the interior of K.

maintained if and only if the condition (6.13) holds $\forall k$. Consequently, if (6.13) does not hold for some k, switching to a different control $\boldsymbol{v}_{\mathbf{F}}(\boldsymbol{q})$ that satisfies (6.13) should occur.

Similarly, the necessary conditions for maintaining visibility when *all* the constraints are active *at the same time* are written using the Jacobian matrix $\boldsymbol{J_h}(\boldsymbol{q})$ of the map $\boldsymbol{h} = (h_1(\cdot), h_2(\cdot)) : \mathbb{R}^3 \to \mathbb{R}^2$ as

$$\boldsymbol{J_h}(\boldsymbol{q})\dot{\boldsymbol{q}} < \mathbf{0}, \text{ where } \boldsymbol{J_h}(\boldsymbol{q}) = \begin{bmatrix} \frac{\partial h_1}{\partial x} & \frac{\partial h_1}{\partial y} & \frac{\partial h_1}{\partial \theta_{\mathrm{F}}} \\ \frac{\partial h_2}{\partial x} & \frac{\partial h_2}{\partial y} & \frac{\partial h_2}{\partial \theta_{\mathrm{F}}} \end{bmatrix}. \tag{6.14}$$

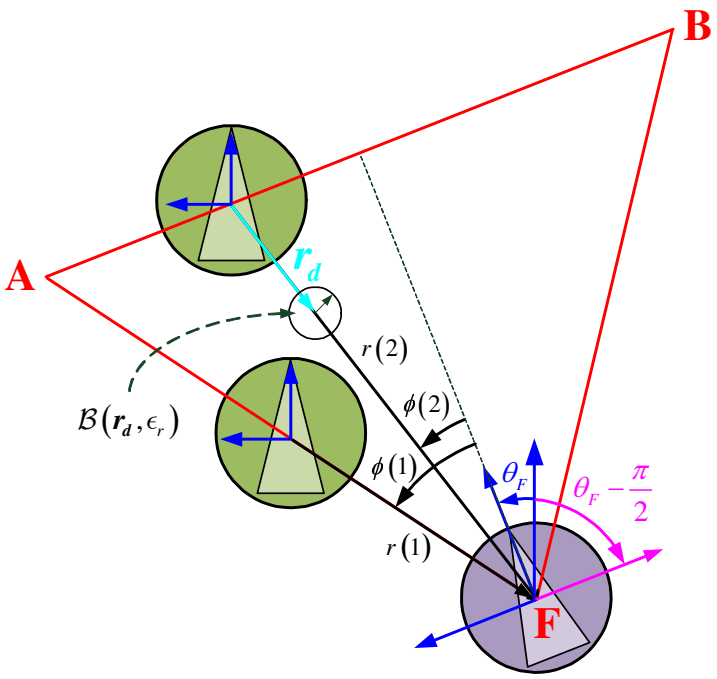

Figure 6.3: In an obstacle-free environment, the viability constraints are nearly violated on the boundary of the cone of view (visibility at stake)

The first visibility constraint is active: $h_1(\cdot) = 0$

To illustrate this, consider the boundary configurations of the system shown in Fig. 6.3. The first visibility constraint is active when $h_1(\boldsymbol{q}) = 0 \Leftrightarrow \phi = \pm\alpha$; in this case, the leader L lies on either the side AF, or the side BF of the cone of view. The second visibility constraint is active when $h_2(\boldsymbol{q}) = 0 \Leftrightarrow r = L\frac{\cos\alpha}{\cos\phi}$; in this case, L lies on the side AB. The visibility constraints are both active at the same time when L lies on either A or B.

In order to determine the conditions under which the first visibility constraint $h_1(\boldsymbol{q}) = |\phi| - \alpha$ is not violated, consider $\phi \geq 0$ and take the time derivative as

$$\dot{h}_1 = \begin{bmatrix} -\frac{y}{x^2+y^2} & \frac{x}{x^2+y^2} & -1 \end{bmatrix} \begin{bmatrix} u_{\mathrm{F}} \cos\theta_{\mathrm{F}} \\ u_{\mathrm{F}} \sin\theta_{\mathrm{F}} \\ w_{\mathrm{F}} \end{bmatrix} = \frac{u_{\mathrm{F}}}{x^2+y^2}(x\sin\theta_{\mathrm{F}} - y\cos\theta_{\mathrm{F}}) - w_{\mathrm{F}}. \tag{6.15}$$

Substituting the control law (6.12) into (6.15) yields

$$\dot{h}_1 = \frac{-k_1 \operatorname{sgn}\left(\boldsymbol{r_1}^\top \begin{bmatrix}\cos\theta_\mathrm{F}\\ \sin\theta_\mathrm{F}\end{bmatrix}\right)\|\boldsymbol{r}_1\|}{x^2+y^2}\left(\begin{bmatrix}x & y\end{bmatrix}\begin{bmatrix}\cos(\theta_\mathrm{F}-\frac{\pi}{2})\\ \sin(\theta_\mathrm{F}-\frac{\pi}{2})\end{bmatrix}\right) - k_2\phi - \dot{\varphi}_p,$$

where the first term is >0 and $-k_2\phi - \dot{\varphi}_p < 0$. Thus, the control gains k_1, k_2 should be chosen so that $\dot{h}_1 < 0$. Similarly, one can verify the same result for $\phi < 0$.

The second visibility constraint is active: $h_2(\cdot) = 0$

For the second visibility constraint, take the time derivative of $h_2(\boldsymbol{q}) = r - L\frac{\cos\alpha}{\cos\phi}$ for $\phi \geq 0$, as

$$\dot{h}_2 = \frac{u_\mathrm{F}}{\sqrt{x^2+y^2}}\left(\begin{bmatrix}x & y\end{bmatrix}\begin{bmatrix}\cos\theta_\mathrm{F}\\ \sin\theta_\mathrm{F}\end{bmatrix} + \frac{L\cos\alpha\tan\phi}{\sqrt{x^2+y^2}\cos\phi}\begin{bmatrix}x & y\end{bmatrix}\begin{bmatrix}-\sin\theta_\mathrm{F}\\ \cos\theta_\mathrm{F}\end{bmatrix}\right) + \frac{L\cos\alpha\tan\phi}{\cos\phi}w_\mathrm{F}. \tag{6.16}$$

Substituting the control law (6.12) into (6.16) yields

$$\dot{h}_2 = \frac{-k_1 \operatorname{sgn}\left(\begin{bmatrix}x_1 & y_1\end{bmatrix}\begin{bmatrix}\cos\theta_\mathrm{F}\\ \sin\theta_\mathrm{F}\end{bmatrix}\right)\|\boldsymbol{r}_1\|}{\sqrt{x^2+y^2}}\Bigg(\underbrace{\begin{bmatrix}x & y\end{bmatrix}\begin{bmatrix}\cos\theta_\mathrm{F}\\ \sin\theta_\mathrm{F}\end{bmatrix}}_{<0} + \frac{L\cos\alpha\tan\phi}{(x^2+y^2)\cos\phi}\underbrace{\begin{bmatrix}x & y\end{bmatrix}\begin{bmatrix}-\sin\theta_\mathrm{F}\\ \cos\theta_\mathrm{F}\end{bmatrix}}_{<0}\Bigg) + \underbrace{\frac{L\cos\alpha\tan\phi}{\cos\phi}w_\mathrm{F}}_{>0},$$

and the control gains k_1, k_2 should be such that $\dot{h}_2 < 0$.

Finally, if both constraints are active, one has to pick the control gains so that (6.14) is satisfied, as follows:

Both visibility constraints are active: $h_1(\cdot) = 0 \wedge h_2(\cdot) = 0$

Assume that the system starts on an initial position so that L lies at point A (Fig. 6.3), where $\phi = \alpha$, $x^2+y^2 = {L_s}^2$, $\|\boldsymbol{r_1}\| = L_s - r_d$, $\dot{\varphi}_p = 0$. The first visibility condition reads

$$\begin{aligned}\dot{h}_1 &= \frac{k_1\|\boldsymbol{r}_1\|}{{L_s}^2}\left(\begin{bmatrix}x & y\end{bmatrix}\begin{bmatrix}\cos(\theta_\mathrm{F}-\frac{\pi}{2})\\ \sin(\theta_\mathrm{F}-\frac{\pi}{2})\end{bmatrix}\right) - k_2\alpha\\ &\leq \frac{k_1\|\boldsymbol{r}_1\|}{x^2+y^2}\sqrt{x^2+y^2} - k_2\alpha = \frac{k_1(L_s-r_d)}{L_s} - k_2\alpha = k_1\left(1-\frac{r_d}{L_s}\right) - k_2\alpha.\end{aligned}$$

Thus a sufficient condition so that the constraint $h_1(\cdot) = 0$ is guaranteed not to increase is:

$$k_1\left(1-\frac{r_d}{L_s}\right) \leq k_2\alpha. \tag{6.17}$$

The second visibility condition reads:

$$\begin{aligned}\dot{h}_2 &= \frac{k_1\|\boldsymbol{r}_1\|}{\sqrt{x^2+y^2}}\left(\underbrace{\begin{bmatrix}x & y\end{bmatrix}\begin{bmatrix}\cos\theta_\mathrm{F}\\ \sin\theta_\mathrm{F}\end{bmatrix}}_{<0} + \frac{L_s\tan\alpha}{(x^2+y^2)}\underbrace{\begin{bmatrix}x & y\end{bmatrix}\begin{bmatrix}-\sin\theta_\mathrm{F}\\ \cos\theta_\mathrm{F}\end{bmatrix}}_{<0}\right)\underbrace{+L_s\tan\alpha\ k_2\alpha}_{>0} =\\ &= -\frac{k_1\|\boldsymbol{r}_1\|}{\sqrt{x^2+y^2}}\left|\begin{bmatrix}x & y\end{bmatrix}\begin{bmatrix}\cos\theta_\mathrm{F}\\ \sin\theta_\mathrm{F}\end{bmatrix} + \frac{L_s\tan\alpha}{(x^2+y^2)}\begin{bmatrix}x & y\end{bmatrix}\begin{bmatrix}-\sin\theta_\mathrm{F}\\ \cos\theta_\mathrm{F}\end{bmatrix}\right| + L_s\tan\alpha\ k_2\alpha.\end{aligned}$$

Thus a sufficient condition so that the constraint $h_2(\cdot) = 0$ is guaranteed not to increase is:

$$\begin{aligned} L_s \tan\alpha \, k_2\alpha &\leq \frac{k_1\|\boldsymbol{r}_1\|}{\sqrt{x^2+y^2}} \left| \begin{bmatrix} x & y \end{bmatrix} \begin{bmatrix} \cos\theta_{\mathrm{F}} \\ \sin\theta_{\mathrm{F}} \end{bmatrix} + \frac{L_s \tan\alpha}{(x^2+y^2)} \begin{bmatrix} x & y \end{bmatrix} \begin{bmatrix} -\sin\theta_{\mathrm{F}} \\ \cos\theta_{\mathrm{F}} \end{bmatrix} \right| \\ &\leq \frac{k_1\|\boldsymbol{r}_1\|}{\sqrt{x^2+y^2}} \left(\sqrt{x^2+y^2} + \frac{L_s \tan\alpha}{(x^2+y^2)} \sqrt{x^2+y^2} \right) \\ &= \frac{k_1(L_s - r_d)}{L_s} (L_s + \tan\alpha) = k_1 \left(1 - \frac{r_d}{L_s}\right) (L_s + \tan\alpha) \Rightarrow \\ k_2\alpha &\leq k_1 \left(1 - \frac{r_d}{L_s}\right) \frac{L_s + \tan\alpha}{L_s \tan\alpha}. \end{aligned} \tag{6.18}$$

Combining (6.17) and (6.18) yields:

$$k_1 \left(1 - \frac{r_d}{L_s}\right) \leq k_2\alpha \leq k_1 \left(1 - \frac{r_d}{L_s}\right) \frac{L_s + \tan\alpha}{L_s \tan\alpha}.$$

Note that this condition is sufficient for maintaining visibility for the **worst-case** initial configuration (i.e. on the boundary of the visibility set K where both constraints are active). Thus, picking the control gains k_1, k_2 so that this condition holds implies also that visibility is maintained for any other initial configuration as well.

6.4 Control Design for the Perturbed System

Let us now consider the perturbed system (6.7), where L is moving with $u_{\mathrm{L}} \neq 0$, $w_{\mathrm{L}} \neq 0$ in an obstacle-free environment. Assume that F is still localized w.r.t. the L, i.e. the position (x, y) and orientation β w.r.t. the leader frame $\mathcal{L}$ is available to F; however F is neither aware of the leader's navigation plan, nor of the velocities $u_{\mathrm{L}}(t)$, $w_{\mathrm{L}}(t)$ at each time instant t.

Therefore, it is reasonable to assume that F has some "a priori" knowledge on the velocity bounds $u_{\mathrm{L}\,\mathrm{M}}$, $w_{\mathrm{L}\,\mathrm{M}}$ of L, in the sense that L is restricted to move at most with velocities $|u_{\mathrm{L}}| \leq u_{\mathrm{L}\,\mathrm{M}}$, $|w_{\mathrm{L}}| \leq w_{\mathrm{L}\,\mathrm{M}}$.

Furthermore, since the perturbation $\boldsymbol{g}(\boldsymbol{q}, \boldsymbol{v}_{\mathbf{L}})$ is non-vanishing $\forall \boldsymbol{q} \in \mathcal{C}$, the desired configuration $\boldsymbol{q_d} \in \mathcal{M}$ is no longer an equilibrium point of (6.7). In that case, the best one can hope for is that the system trajectories $\boldsymbol{q}(t)$ will be ultimately bounded by a small bound, given that the perturbation is small in some sense [Kha02].

Therefore, the task for F is defined as to converge and remain into a ball $\mathcal{B}(\boldsymbol{r_d}, \epsilon_r)$ of radius $\epsilon_r > 0$ around the nominal desired position $\boldsymbol{r_d}$, where $\boldsymbol{r_d} \in \mathcal{M}$. The control design is based on the same ideas as for the nominal system: at each time instant t, a vector $\boldsymbol{p} = \begin{bmatrix} p_x & p_y \end{bmatrix}^\top$ is assigned on the position $\boldsymbol{r_d} \in \mathcal{V}$ which lies on the line that connects the two robots, such that $\varphi_p = \mathrm{atan2}(p_y, p_x) = \theta_d$. F is then controlled to align with and flow along the integral lines of the resulting vector field, until it converges into $\mathcal{B}(\boldsymbol{r_d}, \epsilon_r)$. Clearly, ϵ_r depends on the perturbation norm $\|\boldsymbol{g}(\boldsymbol{q}, \boldsymbol{v}_{\mathbf{L}})\|$.

6.4.1 Ultimate boundedness

Theorem 2 The trajectories $\boldsymbol{r}(t) = \begin{bmatrix} x(t) & y(t) \end{bmatrix}^\top$ of the perturbed system (6.7) enter and remain into a ball $\mathcal{B}(\boldsymbol{r_d}, \epsilon_r)$ around the desired position $\boldsymbol{r_d}$ (Fig. 6.3), under the control law

$\boldsymbol{v_F} = \begin{bmatrix} u_F & w_F \end{bmatrix}^\top$ where

$$u_F = -k_1 \operatorname{sgn}\left(\boldsymbol{r_1}^\top \begin{bmatrix}\cos\beta \\ \sin\beta\end{bmatrix}\right) \|\boldsymbol{r_1}\| - \operatorname{sgn}(\boldsymbol{p}^\top \boldsymbol{r_1}) u_{L\,M}, \tag{6.19a}$$

$$w_F = -k_2(\beta - \varphi) + \dot{\varphi}, \tag{6.19b}$$

where $k_1, k_2 > 0$, $\varphi = \operatorname{atan2}(F_y, F_x)$ is the orientation of the vector field at (x, y), $u_{L\,M}$ is the upper bound of the leader's linear velocity, and $\epsilon_r > \frac{|w_L|}{\sqrt{k_1 k_2}}$. A (conservative) estimation for ϵ_r can be taken for the bound $w_{L\,M}$ of the leader's angular velocity. Note also that if $w_L \to 0$, then $\epsilon_r \to 0$ as well.

Proof of Theorem 2

Proof Consider the function V of the nominal system in terms of the position errors $x_1 = x - x_d$, $y_1 = y - y_d$ and the orientation error $\eta = \beta - \varphi$, as

$$V = V_1 + \frac{1}{2}(\beta - \varphi)^2 = \frac{1}{2}\left({x_1}^2 + {y_1}^2\right) + \frac{1}{2}(\beta - \varphi)^2,$$

and take its time derivative along the system trajectories as

$$\begin{aligned}
\dot{V} &\overset{(6.7)}{=} x_1(u_F \cos\beta - u_L + y w_L) + y_1(u_F \sin\beta - x w_L) + (\beta - \varphi)(w_F - w_L - \dot{\varphi}) = \\
&= \begin{bmatrix} x_1 & y_1 \end{bmatrix} \begin{bmatrix}\cos\beta \\ \sin\beta\end{bmatrix} u_F + \begin{bmatrix} x_1 & y_1 & \beta - \varphi \end{bmatrix} \begin{bmatrix} -u_L + y w_L \\ -x w_L \\ -w_L \end{bmatrix} + (\beta - \varphi)(w_F - \dot{\varphi}) = \\
&\overset{(6.19b)}{=} \underbrace{\boldsymbol{r}_1^\top \begin{bmatrix}\cos\beta \\ \sin\beta\end{bmatrix} u_F + \boldsymbol{q}_1^\top \boldsymbol{g}(\boldsymbol{q}, \boldsymbol{v_L})}_{P(\boldsymbol{q}_1)} - k_2(\beta - \varphi)^2,
\end{aligned}$$

where $\boldsymbol{r_1} = \begin{bmatrix} x_1 & y_1 \end{bmatrix}^\top$, $\boldsymbol{q_1} = \begin{bmatrix} \boldsymbol{r_1}^\top & \beta - \varphi \end{bmatrix}^\top$.

Note that in this case, the dynamics of the orientation error $\eta = \beta - \varphi$ read

$$\dot{\eta} = \dot{\beta} - \dot{\varphi} \Rightarrow \dot{\eta} = w_F - w_L - \dot{\varphi} \Rightarrow \dot{\eta} = -k_2 \eta - w_L.$$

Thus, if $w_L = 0$, it follows that $\eta \to 0$ exponentially, i.e. that $\beta \to \varphi$. However, w_L is not in general equal to zero.[3] Let us assume that w_L is *slowly-varying*, i.e. that w_L is continuously differentiable and $\|\dot{w}_L\|$ is sufficiently small [Kha02]. Then, w_L can be treated as a frozen parameter, and the frozen system $0 = -k_2\eta - w_L$ has a continuously differentiable isolated root $\eta = -\frac{1}{k_2} w_L = h(w_L)$, for which $\|\frac{\partial h}{\partial w_L}\| = \frac{1}{k_2} \leq K$. To analyze the stability properties of the frozen equilibrium $z = \eta + \frac{1}{k_2} w_L$, take $\dot{z} = -k_2(z - \frac{1}{k_2} w_L) - w_L = -k_2 z$. Then, z is exponentially stable, i.e. $\eta \to -\frac{1}{k_2} w_L$.

Then, the term $P(\boldsymbol{q}_1)$ in $\dot{V}$ reads

$$P(\boldsymbol{q}_1) \overset{(6.19a)}{=} -k_1 \left|\boldsymbol{r}_1^\top \begin{bmatrix}\cos\beta \\ \sin\beta\end{bmatrix}\right| \|\boldsymbol{r_1}\| - \operatorname{sgn}(\boldsymbol{p}^\top \boldsymbol{r_1}) |u_L| \boldsymbol{r}_1^\top \begin{bmatrix}\cos\beta \\ \sin\beta\end{bmatrix} + \boldsymbol{q}_1^\top \boldsymbol{g}(\boldsymbol{q}, \boldsymbol{v_L}),$$

[3] It can be set though very small by forcing the leader L to move in obstacle environments as described in Section 6.5.

where

$$\boldsymbol{q}_1^\top \boldsymbol{g}(\boldsymbol{q}, \boldsymbol{v_L}) = -x_1 u_\mathrm{L} + \begin{bmatrix} x_1 & y_1 \end{bmatrix} \begin{bmatrix} y \\ -x \end{bmatrix} w_\mathrm{L} - (\beta - \varphi) w_\mathrm{L}.$$

For $\eta = -\frac{1}{k_2} w_\mathrm{L}$ one has:

$$\boldsymbol{q}_1^\top \boldsymbol{g}(\boldsymbol{q}, \boldsymbol{v_L}) = -x_1 u_\mathrm{L} + \frac{1}{k_2} {w_\mathrm{L}}^2,$$

since $\begin{bmatrix} x_1 & y_1 \end{bmatrix} \begin{bmatrix} y \\ -x \end{bmatrix} = 0$. Then, one gets:

$$\boldsymbol{q}_1^\top \boldsymbol{g}(\boldsymbol{q}, \boldsymbol{v_L}) = \begin{bmatrix} x_1 & y_1 \end{bmatrix} \begin{bmatrix} -u_\mathrm{L} \\ 0 \end{bmatrix} + \frac{{w_\mathrm{L}}^2}{k_2} \leq \|\boldsymbol{r_1}\| |u_\mathrm{L}| + \frac{{w_\mathrm{L}}^2}{k_2}.$$

To check the signum of $P(\boldsymbol{q}_1)$, consider the following cases:
C1. $\mathrm{sgn}(\boldsymbol{p}^\top \boldsymbol{r_1}) = -1$ and $\boldsymbol{r_1}^\top \begin{bmatrix} \cos\beta \\ \sin\beta \end{bmatrix} < 0$. Then,

$$\begin{aligned} P(\boldsymbol{q}_1) &= -\left| \boldsymbol{r_1}^\top \begin{bmatrix} \cos\beta \\ \sin\beta \end{bmatrix} \right| (k_1 \|\boldsymbol{r_1}\| + |u_\mathrm{L}|) + \boldsymbol{q}_1^\top \boldsymbol{g}(\boldsymbol{q}, \boldsymbol{v_L}) \\ &\leq -\left| \boldsymbol{r_1}^\top \begin{bmatrix} \cos\beta \\ \sin\beta \end{bmatrix} \right| (k_1 \|\boldsymbol{r_1}\| + |u_\mathrm{L}|) + \|\boldsymbol{r_1}\| |u_\mathrm{L}| + \frac{{w_\mathrm{L}}^2}{k_2}. \end{aligned}$$

The term $P(\boldsymbol{q}_1)$ is < 0 if

$$\begin{aligned} \left| \boldsymbol{r_1}^\top \begin{bmatrix} \cos\beta \\ \sin\beta \end{bmatrix} \right| (k_1 \|\boldsymbol{r_1}\| + |u_\mathrm{L}|) > \|\boldsymbol{r_1}\| |u_\mathrm{L}| + \frac{{w_\mathrm{L}}^2}{k_2} \Rightarrow \\ k_1 \|\boldsymbol{r_1}\|^2 + \|\boldsymbol{r_1}\| |u_\mathrm{L}| > \|\boldsymbol{r_1}\| |u_\mathrm{L}| + \frac{{w_\mathrm{L}}^2}{k_2} \Rightarrow \\ \|\boldsymbol{r_1}\|^2 > \frac{{w_\mathrm{L}}^2}{k_1 k_2} \Rightarrow \|\boldsymbol{r_1}\| > \frac{|w_\mathrm{L}|}{\sqrt{k_1 k_2}}. \end{aligned} \tag{6.20}$$

Note that (6.20) is sufficient, not necessary.
C2. $\mathrm{sgn}(\boldsymbol{p}^\top \boldsymbol{r_1}) = -1$ and $\boldsymbol{r_1}^\top \begin{bmatrix} \cos\beta \\ \sin\beta \end{bmatrix} \geq 0$. This case can be dropped, since it violates the visibility constraints.
C3. $\mathrm{sgn}(\boldsymbol{p}^\top \boldsymbol{r_1}) = 1$ and $\boldsymbol{r_1}^\top \begin{bmatrix} \cos\beta \\ \sin\beta \end{bmatrix} > 0$. Then,

$$P(\boldsymbol{q}_1) = -\left| \boldsymbol{r_1}^\top \begin{bmatrix} \cos\beta \\ \sin\beta \end{bmatrix} \right| (k_1 \|\boldsymbol{r_1}\| + |u_\mathrm{L}|) + \boldsymbol{q}_1^\top \boldsymbol{g}(\boldsymbol{q}, \boldsymbol{v_L}),$$

and thus a sufficient condition for $P(\boldsymbol{q}_1) < 0$ is acquired as in case **C1**.
C4. $\mathrm{sgn}(\boldsymbol{p}^\top \boldsymbol{r_1}) = 1$ and $\boldsymbol{r_1}^\top \begin{bmatrix} \cos\beta \\ \sin\beta \end{bmatrix} \leq 0$. This case can be dropped, since it violates the visibility constraints.

Consequently, one has $P(\boldsymbol{q}_1) < 0$ for any $\boldsymbol{r_1}$ that satisfies (6.20), yielding

$$\dot{V} = P(\boldsymbol{q}_1) - k_2 (\beta - \varphi)^2 < 0.$$

Consequently, for any initial $\boldsymbol{r_1}(0)$ and any $0 < \epsilon_r < \|\boldsymbol{r_1}(0)\|$ that satisfies (6.20), $\dot{V}$ is negative in the set

$$\{\boldsymbol{r_1} \mid \frac{1}{2} {\epsilon_r}^2 \leq V(\|\boldsymbol{r_1}\|) \leq \frac{1}{2} \|\boldsymbol{r_1}(0)\|^2\},$$

which verifies that $\boldsymbol{r_1}(t)$ enters the set $\{\boldsymbol{r_1} \mid V(\boldsymbol{r_1}) \leq \frac{1}{2}{\epsilon_r}^2\}$, or equivalently, $\boldsymbol{r_1}(t)$ enters the ball $\mathcal{B}(\mathbf{0}, \epsilon_r)$.

Equivalently, if ϵ_r is chosen to satisfy (6.20), the system trajectories $\boldsymbol{r}(t)$ enter and remain into the ball $\mathcal{B}(\boldsymbol{r_d}, \epsilon_r)$. A conservative estimation for ϵ_r can be taken for $|w_{\mathrm{L}}| = w_{\mathrm{L\,M}}$. Note also that if $w_{\mathrm{L}} \to 0$, then $\epsilon_r \to 0$ as well. ■

6.4.2 Maintaining Visibility

Visibility is maintained for the perturbed system as long as the condition (6.13) holds at $\boldsymbol{q} \in \partial K$, $\forall k$.

To illustrate this, consider the time derivative of $h_1(\cdot)$ for $\phi \geq 0$, that reads:

$$\begin{aligned}\dot{h}_1 &= \begin{bmatrix} -\frac{y}{x^2+y^2} & \frac{x}{x^2+y^2} & -1 \end{bmatrix} \begin{bmatrix} u_{\mathrm{F}}\cos\beta - u_{\mathrm{L}} + y w_{\mathrm{L}} \\ u_{\mathrm{F}}\sin\beta - x w_{\mathrm{L}} \\ w_{\mathrm{F}} - w_{\mathrm{L}} \end{bmatrix} = \\ &= \frac{u_{\mathrm{F}}}{x^2+y^2}(x\sin\beta - y\cos\beta) - w_{\mathrm{F}} + \frac{y u_{\mathrm{L}}}{x^2+y^2}, \end{aligned} \tag{6.21}$$

and the time derivative of $h_2(\cdot)$ for $\phi \geq 0$, that reads

$$\begin{aligned}\dot{h}_2 = \; & \tfrac{u_{\mathrm{F}}}{\sqrt{x^2+y^2}} \left(\begin{bmatrix} x & y \end{bmatrix} \begin{bmatrix} \cos\beta \\ \sin\beta \end{bmatrix} + \tfrac{L_s \cos\alpha \tan\phi}{\sqrt{x^2+y^2}\cos\phi} \begin{bmatrix} x & y \end{bmatrix} \begin{bmatrix} -\sin\beta \\ \cos\beta \end{bmatrix} \right) + \\ & + \tfrac{L_s \cos\alpha \tan\phi}{\cos\phi} w_{\mathrm{F}} + \left| \tfrac{x}{\sqrt{x^2+y^2}} + \tfrac{y L_s \cos\alpha \tan\phi}{(x^2+y^2)\cos\phi} \right| u_{\mathrm{L}}. \end{aligned} \tag{6.22}$$

Then, the control gains k_1, k_2 should be chosen such that the constraints are not violated in the worst-case scenario, where both constraints are active. This in turn yields the following sufficient condition:

$$\begin{aligned} A + \frac{u_{\mathrm{LM}}\sin\alpha}{L_s} \leq w_{\mathrm{F}} \leq A + \frac{u_{\mathrm{F}}}{{L_s}^2\tan\alpha}\left|x\cos\beta + y\sin\beta\right| - \\ - \frac{u_{\mathrm{LM}}}{L_s\sin\alpha}, \quad \text{where } A = \frac{u_{\mathrm{F}}}{{L_s}^2}\left|x\sin\beta - y\cos\beta\right|. \end{aligned}$$

Remark 4 *The above discussion implies that if the control gains k_1, k_2 in* (6.19) *are such that $\dot{h}_k(\boldsymbol{q}) < 0$, $\forall \boldsymbol{q} \in \partial K$, $\forall k$, then* F *is guaranteed to maintain visibility w.r.t.* L*, and furthermore to converge and remain into the ball $\mathcal{B}(\boldsymbol{r_d}, \epsilon_r)$. The orientation control (via w_{F}) for* F *ensures that ϕ is exponentially stable to $-\frac{1}{k_2}|w_{\mathrm{L}}|$, which can be tuned to be $\leq \alpha$, i.e. $h_1(\cdot)$ is always forced to be negative. This in turn implies that the system trajectories are forced as far as possible from the boundary of K that corresponds to $h_1 = 0$. Furthermore, one has from the convergence analysis of the system trajectories into the ball $\mathcal{B}(\boldsymbol{r}_d, \epsilon_r)$ that $\dot{V}_1$ is negative in the set $\{\boldsymbol{r_1} \mid \frac{1}{2}{\epsilon_r}^2 \leq V_1(\|\boldsymbol{r_1}\|) \leq \frac{1}{2}\|\boldsymbol{r_1}(0)\|^2\}$, where $V_1 = \frac{1}{2}({x_1}^2 + {y_1}^2)$, which implies that the distance $\|\boldsymbol{r_1}\|$ decreases under the control law u_{F}; this implies that $h_2(\cdot)$ is forced to decrease. These two conditions verify that if* F *starts somewhere in the interior of K, or on the boundary ∂K, it never reaches again the boundary ∂K on its way to $\boldsymbol{r_d}$. Finally, collision avoidance between the two robots is ensured since $\dot{V}_1$ is negative out of the ball $\mathcal{B}(\boldsymbol{r_d}, \epsilon_r)$.*

6.5 Motion Planning in Obstacle Environments

The L − F formation is assumed to move in a structured workspace $\mathcal{W} \subset \mathbb{R}^2$ with known obstacles (e.g. an indoor corridor environment), where F is controlled by the control law (6.19). Note that the obstacle environment may affect the cone-of-view at each time instant (Fig. 6.4), limiting thus the valid initial conditions in the sense that if L is not visible to F at $t = 0$, then no solution exists.

The motion of both robots is restricted due to the obstacles, and therefore the trajectories $\boldsymbol{q}_{\mathbf{L}}(t)$, $\boldsymbol{q}_{\mathbf{F}}(t)$ should be collision-free. Given that the robots can be represented as circular disks of radius r_0, the obstacles are inflated as shown in Fig. 6.4. Then, the dark grey region around each obstacle reduces the free space of the robots, while it does not affect visibility; F can still detect L through this region, but both F, L should not enter into it. This requirement can be encoded as additional constraint inequalities, so that the same analysis on the boundary of the viability (safe) set can be applied, as for the visibility constraints.

Consider for instance the boundary AB in Fig. 6.4. The trajectories of F remain safe as long as F does not cross AB, which reads $x_{\mathrm{F}} \leq -(b + r_0)$, encoded as the constraint $h_{01} = x_{\mathrm{F}} + b + r_0 \leq 0$, $b > 0$. Thus, if $h_{01} = 0$, safety w.r.t. collision is ensured as long as $\dot{h}_{01} \leq 0 \Rightarrow \dot{x}_{\mathrm{F}} = u_{\mathrm{F}} \cos\theta_{\mathrm{F}} \leq 0$. If $\cos\theta_{\mathrm{F}} \leq 0$, i.e. if $\begin{bmatrix}\cos\theta_{\mathrm{F}} & \sin\theta_{\mathrm{F}}\end{bmatrix} \boldsymbol{n} \geq 0$, where $\boldsymbol{n} = \begin{bmatrix}-1 & 0\end{bmatrix}^\top$ is normal to $(\vec{\mathrm{AB}})$, the system should be controlled so that $u_{\mathrm{F}} \geq 0$. This condition reads $\begin{bmatrix}u_{\mathrm{F}}\cos\theta_{\mathrm{F}} & u_{\mathrm{F}}\sin\theta_{\mathrm{F}}\end{bmatrix} \boldsymbol{n} \geq 0 \Rightarrow \begin{bmatrix}\dot{x}_{\mathrm{F}} & \dot{y}_{\mathrm{F}}\end{bmatrix} \boldsymbol{n} \geq 0 \Rightarrow \langle \dot{\boldsymbol{r}}_{\mathbf{F}}, \boldsymbol{n}\rangle \geq 0$, which expresses that the safe system velocities $\dot{\boldsymbol{r}}_{\mathbf{F}}$ should point towards the obstacle-free space. Similarly, if $\cos\theta_{\mathrm{F}} > 0$, i.e. if $\begin{bmatrix}\cos\theta_{\mathrm{F}} & \sin\theta_{\mathrm{F}}\end{bmatrix} \boldsymbol{n} < 0$, the constraint is not violated for $u_{\mathrm{F}} < 0$, which also reads $\langle \dot{\boldsymbol{r}}_{\mathbf{F}}, \boldsymbol{n}\rangle > 0$.[3]

The worst-case initial condition for the system would be to lie on the boundary of the viability set where *all* constraints are active; in that case, one has to pick the control inputs $\boldsymbol{v}_{\mathbf{F}}$, $\boldsymbol{v}_{\mathbf{L}}$ for F, L such that $\boldsymbol{J}_{\boldsymbol{v}}(\boldsymbol{q})\dot{\boldsymbol{q}} < \boldsymbol{0}$, where $\boldsymbol{J}_{\boldsymbol{v}}(\boldsymbol{q})$ is the Jacobian matrix of the map $\boldsymbol{v} = (h_1(\cdot), h_2(\cdot), h_{0j}) : \mathbb{R}^3 \to \mathbb{R}^{j+2}$, $h_{0j}(\cdot)$ are the j active constraints due to obstacles. If no control inputs satisfy this condition, then the system should not be allowed to start from, or reach these points.

6.5.1 Control design

In order to design a state feedback control scheme for an L − F formation that has to move through a corridor environment, we first decompose the free space into rectangular cells. L is assigned a global high-level discrete motion plan, which indicates the successive order of cells that L has go through in order to converge to a goal state $\boldsymbol{q}_{\boldsymbol{d}\,\mathbf{L}}$. Then, a dipolar vector field (6.10) of certain desired properties is defined into each one of the cells. The desired properties are specified by the motion plan: the vector field in a cell i is constructed so that its integral curves point into the interior of the successor cell $i + 1$ on the exit face of the cell i, while pointing into the interior of the cell i on each one of the remaining faces (Fig. 6.5). This approach is similar in spirit with the one in [LL09]. The difference is that the vector fields defined in each cell i are dipolar, so that the integral curves converge to the midpoint of the exit face of cell i.

[3] In general, the safe system velocities on the boundary of obstacles should satisfy $\boldsymbol{n}\dot{\boldsymbol{r}}_{\mathbf{F}} \geq 0$, where $\boldsymbol{n}$ is the normal vector to the supporting hyperplane of the boundary, which reads $\nabla h_{0j}\dot{\boldsymbol{r}}_{\mathbf{F}} \leq 0$. This condition represents the contingent cone at the boundary of the safe set.

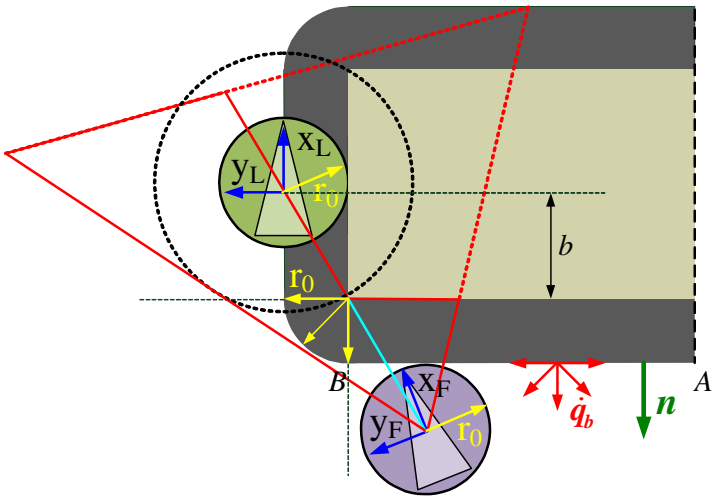

Figure 6.4: In an obstacle environment, the "viability" constraints are active on the boundary of the cone of view (visibility at stake) and on the boundary of the inflated obstacles (safety due to collisions at stake)

The feedback plan for L is defined as to orient with and flow along the integral curves of the vector field in each cell. To do so, the control inputs for L are defined as

$$u_{\mathrm{L}} = \mathrm{const} \leq u_{\mathrm{L\,M}}, \tag{6.23a}$$

$$w_{\mathrm{L}} = -k_{\mathrm{L}}(\theta_{\mathrm{L}} - \varphi_{\mathrm{L}\,i}) + \dot{\varphi}_{\mathrm{L}\,i}, \tag{6.23b}$$

where $\varphi_{\mathrm{L}\,i}$ is the orientation of the vector field in cell i, $k_{\mathrm{L}} > 0$. Collision avoidance for L is ensured since by definition each vector field points into the interior of the free space.

The trajectories of L essentially dictate the desired position $\boldsymbol{r_d}(t) \in \mathcal{V}$ (Fig. 6.2) that F has to track at each t; clearly $\boldsymbol{r_d}(t)$ should always lie in the free space. To see if this is always the case, let us first assume that L, F start in the same cell i, at initial distance $r > r_d$. Initial configurations that violate visibility are excluded. In the worst case, both robots start on the boundary of the free space. It is easy to verify that if the initial orientations θ_{L}, θ_{F} point into the interior of the cell i, then under the control laws (6.23), (6.19) both robots move into the cell i, and thus collisions with obstacles are avoided. Inter-robot collision avoidance is also guaranteed, as shown in Section 6.4; therefore, their motion in cell i is guaranteed to be collision-free.

However, when L enters cell $i+1$ while F is still in cell i, it is likely that the trajectory $\boldsymbol{q_{\mathrm{L}}}(t)$ will force the desired position $\boldsymbol{r_d}$ to eventually enter the obstacle space. To see how, consider Fig. 6.5: if L is allowed to accurately track the vector field in cell $i+1$ after exiting cell i, it will move in the free space but very close to the obstacle, forcing F to eventually collide with the obstacle.

This remark implies that L should move with a minimum turning radius R_{L} when entering into cell $i+1$, such that the trajectories $\boldsymbol{q_{\mathrm{F}}}(t)$ do not enter the obstacle space. Note also that after F has converged into $\mathcal{B}(\boldsymbol{r_d}, \epsilon_r)$, where $\epsilon_r \to 0$, the L $-$ F formation essentially behaves as a tractor (L) pulling a trailer (F) with axle-to-axle hitching of length r_d [BMSS94].[5] Then, if L

[5]Equivalently, the formation can be kinematically seen as a front-wheel driven car, where $\beta = \theta_{\mathrm{F}} - \theta_{\mathrm{L}}$ is

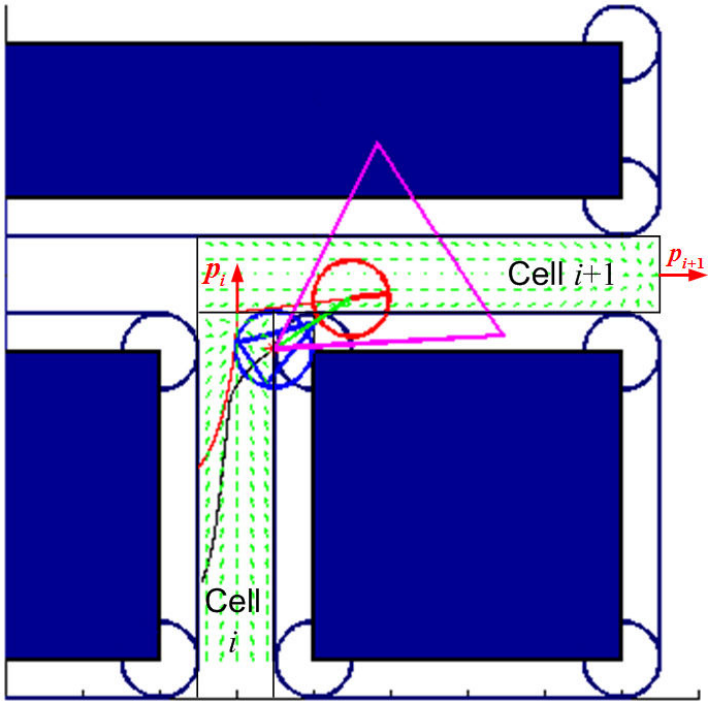

Figure 6.5: The leader L moves through the successive cells i, $i+1$ under (6.23), tracking the vector fields shown in the free space. Nevertheless, it is likely that the resulting trajectory $\boldsymbol{q}_{\mathbf{L}}(t)$ will force the follower F to eventually collide with obstacles. For this reason, L, F should move with minimum turning radii R_{L}, R_{F} around corners.

starts moving along a circle of center C and radius R_{L} when it enters cell $i+1$, it immediately follows that F will move on a circle of the same center C and radius $R_{\mathrm{F}} = \sqrt{{R_{\mathrm{L}}}^2 - {r_d}^2}$.

In order to get an estimate for picking a safe R_{L}, consider Fig. 6.6: Assume that at time instant $t^\star$, L is at the midpoint of the cell i (driven there by (6.23)) and starts moving in cell $i+1$ along a circle of radius R_{L}, while F is at a distance r_d w.r.t. L; given that F kinematically behaves as a trailer, it starts moving along a circle of radius $R_{\mathrm{F}} = \sqrt{{R_{\mathrm{L}}}^2 - {r_d}^2}$. The radius R_{F} is depicted in Fig. 6.6 equal to the critical value $R_{\mathrm{F,crit}}$ for which the trajectories of F remain collision-free. The center of rotation C remains constant, and its position at time $t^\star$ w.r.t. the (time-varying) leader frame $\mathcal{L}$ is

$$x_C(t^\star) = x_{\mathrm{F}}(t^\star) + R_{\mathrm{F}} \sin(\beta(t^\star)),$$
$$y_C(t^\star) = y_{\mathrm{F}}(t^\star) - R_{\mathrm{F}} \cos(\beta(t^\star)).$$

The coordinates of the critical point Z w.r.t. the leader frame $\mathcal{L}$ at time $t^\star$ are

$$x_{\mathrm{Z}}(t^\star) = \frac{r_0\sqrt{2}}{2} - r_0,\ y_{\mathrm{Z}}(t^\star) = -\frac{w_i}{2} + \frac{r_0\sqrt{2}}{2} - r_0. \text{ Thus,}$$
$$R_{\mathrm{F,crit}} = \sqrt{\left(x_C(t^\star) - x_{\mathrm{Z}}(t^\star)\right)^2 + \left(y_C(t^\star) - y_{\mathrm{Z}}(t^\star)\right)^2}.$$

the steering angle and r_d is the wheelbase.

Note also that the smallest critical value $R_{\mathrm{F,crit}}$ corresponds to the worst-case scenario shown in Fig. 6.6, where F is on the boundary of the free space.[6] At this point, one has $x_{\mathrm{F_w}}(t^\star) = -\sqrt{{r_d}^2 - \frac{{w_i}^2}{4}}$, $y_{\mathrm{F_w}}(t^\star) = -\frac{w_i}{2}$, $\cos(\beta_{\mathrm{w}}(t^\star)) = \frac{\sqrt{{r_d}^2 - \frac{{w_i}^2}{4}}}{r_d}$, $\sin(\beta_{\mathrm{w}}(t^\star)) = \frac{w_i}{2r_d}$. Then, after some algebra one can verify out of $R_{\mathrm{F_w,crit}} = R_{\mathrm{F_w}}$ that the worst-case safe $R_{\mathrm{F_w}}$ is

$$R_{\mathrm{F_w}} = \frac{\left(\frac{r_0}{2}\sqrt{2} - r_0 + \sqrt{{r_d}^2 - \frac{{w_i}^2}{4}}\right)^2 + \left(\frac{r_0}{2}\sqrt{2} - r_0\right)^2}{\frac{w_i}{r_d}\sqrt{{r_d}^2 - \frac{{w_i}^2}{4}} + \frac{w_i r_0}{r_d}\left(\frac{\sqrt{2}}{2} - 1\right) - \frac{2r_0}{r_d}\sqrt{{r_d}^2 - \frac{{w_i}^2}{4}}\left(\frac{\sqrt{2}}{2} - 1\right)}, \tag{6.24}$$

where the denominator is positive for $\frac{w_i}{r_d}\sqrt{{r_d}^2 - \frac{{w_i}^2}{4}} + \frac{2r_0}{r_d}\sqrt{{r_d}^2 - \frac{{w_i}^2}{4}}\left(1 - \frac{\sqrt{2}}{2}\right) > \frac{w_i r_0}{r_d}\left(1 - \frac{\sqrt{2}}{2}\right)$.

As one would expect from physical intuition, the critical turning radius for F depends on the robots' dimension r_0, the distance r_d between them and the width w_i of the cell i. Thus, if L moves with turning radius $R_{\mathrm{L}} \geq \sqrt{{r_d}^2 + {R_{\mathrm{F_w}}}^2}$, it follows that the trajectories of F are collision-free. Moreover, one can easily verify out of Fig. 6.6 that the motion of L within cell $i+1$ is collision-free as long as $R_{\mathrm{L}} \leq w_{i+1} + R_{\mathrm{F_w}}\frac{w_i}{2r_d} + \sqrt{{r_d}^2 - \frac{{w_i}^2}{4}}$. In summary, a safe R_{L} for L should satisfy

$$\sqrt{r_d^2 + {R_{\mathrm{F_w}}}^2} \leq R_{\mathrm{L}} \leq w_{i+1} + R_{\mathrm{F_w}}\frac{w_i}{2r_d} + \sqrt{r_d^2 - \frac{w_i^2}{4}}, \tag{6.25}$$

where $R_{\mathrm{F_w}}$ is given by (6.24), and ensures that the trajectories $\boldsymbol{q_{\mathrm{L}}}(t)$, $\boldsymbol{q_{\mathrm{F}}}(t)$ are collision-free. Note that this is a conservative condition, in the sense that $R_{\mathrm{F_w}}$ is computed for the worst-case scenario, since we assumed that L has no information on the position of F at time $t^\star$. Nevertheless, given r_d, r_0 and the cell decomposition, it is easy to a priori check whether a safe R_{L} exists for each one of the transitions between cells that are realized as turning around corners.

Given that a safe R_{L} exists, the control input (6.23) for L is modified as follows: On the exit face of cell i, L orients with the tangent λ_1 to the radius CL, given as $\lambda_1 = -\frac{x_C(t^\star)}{y_C(t^\star)} = -\frac{x_{\mathrm{F_w}}(t^\star) + R_{\mathrm{F_w}}\sin(\beta_{\mathrm{w}}(t^\star))}{y_{\mathrm{F_w}}(t^\star) - R_{\mathrm{F_w}}\cos(\beta_{\mathrm{w}}(t^\star))}$, and moves into cell $i+1$ with

$$w_{\mathrm{L}\,c} = \mathrm{sign}(w_{\mathrm{L}})\frac{u_{\mathrm{L}}}{R_{\mathrm{L}}},$$

where w_{L} is the angular velocity that is dictated by the vector field in cell $i+1$. The angular velocity $w_{\mathrm{L}\,c}$ should be kept until L reaches the point E shown in Fig. 6.6, so that F is guaranteed to enter safely in the cell $i+1$. The coordinates of E w.r.t. the initial frame at time $t^\star$ are $x_{\mathrm{E}} = x_C + R_{\mathrm{L}}\cos\theta_{\mathrm{L}}$, $y_{\mathrm{E}} = y_C - R_{\mathrm{L}}\sin\theta_{\mathrm{L}}$, where θ_{L} is the current orientation of L w.r.t. a global frame, which is online available. After L has reached E, then both robots are in cell $i+1$, with F pointing into the interior of the free space. Thus, L keeps moving under (6.23), tracking the vector field in cell $i+1$, on its way to the exit face of this cell; as discussed above, under these conditions the motion of the robots within the cell $i+1$ is collision-free.

Remark 5 *Clearly, the worst-cases calculations for picking safe R_{L}, R_{F} may produce excessive curvature than actually required. This could be avoided if* L *had access to the position of* F *at*

[6] This holds for the leader taking a right turn. Similarly one can treat the case for a left turn.

time $t^\star$ that L *is on the exit face of cell i. Then,* L *could online calculate the actual $R_{\mathrm{F}_{crit}}$, taking into account the actual $x_{\mathrm{F}}(t^\star)$, $y_{\mathrm{F}}(t^\star)$, and would end up with picking a safe R_{L} that would be less conservative than the one derived for the worst-case scenario.*

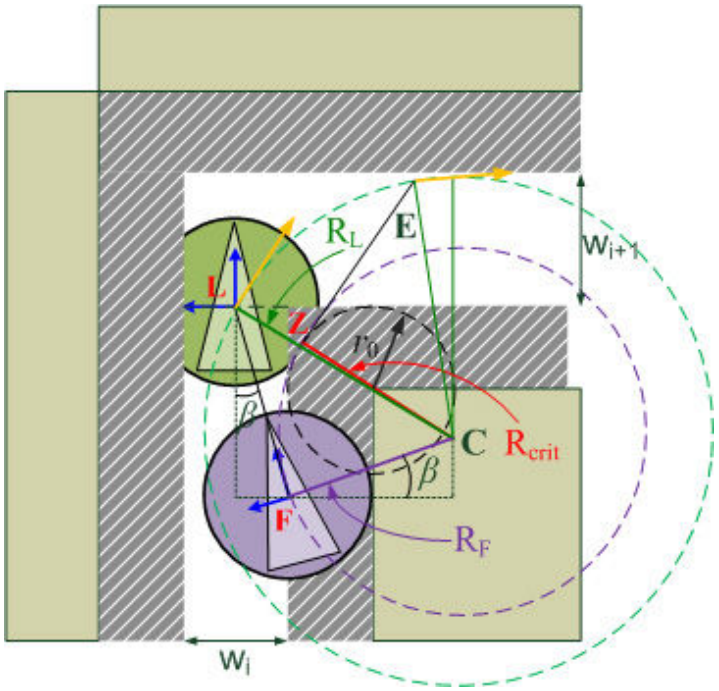

Figure 6.6: After exiting cell i, the leader should move in cell $i+1$ along a circle of radius R_{L} that satisfies (6.25).

6.5.2 Simulation Results

The efficacy of the proposed motion planning and control scheme has been evaluated through computer simulations. A decomposition of the free space in rectangular cells is known to L. The robots start in the same cell i, so that L is visible to F. Initial conditions such that the robots are in different cells should be avoided, in the sense that they may violate the curvature around corners that the robots have to follow.

In the case shown in Fig. 6.7 the robots initiate on the boundary of the obstacle, so that the second visibility constraint is active for F and so that they do not face out of the free space. The follower F is localized w.r.t. to L, but is neither aware of its high-level motion plan, nor of its velocity at each time t; only the bound $u_{\mathrm{L\,m}}$ is available.

The leader L moves with constant linear velocity $u_{\mathrm{L}} \leq u_{\mathrm{L\,m}}$, and tracks the vector field in cell i under (6.23), on its way to the midpoint of the exit face of i. Note that on the boundary of the obstacles, the vector field forces L to move into the interior of the free space.

At the same time, F moves under the control law (6.19), where the control gains are selected such that the visibility constraint $h_2(\boldsymbol{q}(0)) = 0$ is not violated at $t = 0$, and converges into a

neighborhood around the desired configuration $\boldsymbol{q_d}$ (the red mark) w.r.t. L. The motion of F in cell i is also collision-free, for the reasons explained in section 6.5.1.

When L reaches the exit face of cell i, it is forced to follow a bounded curvature within cell $i+1$ to move around the corner, under the angular velocity $w_{\mathrm{L}\,\mathrm{c}} = \mathrm{sign}(w_{\mathrm{L}})\frac{u_{\mathrm{L}}}{R_{\mathrm{L}}}$, where w_{L} is the angular velocity specified by the vector field in cell $i+1$, and R_{L} is the safe turning radius calculated as above. At the same time, F behaves like a trailer and starts moving along a circle of radius R_{F}, which is guaranteed to be collision-free. As soon as L reaches the "exit point" E, shown in Fig. 6.6, it continues moving under the angular velocity w_{L} dictated by the vector field $i+1$, until it reaches the exit face of cell $i+1$, and so on. The resulting trajectories are collision-free, as shown in Fig. 6.7, while the value of the constraints $h_k(x, y, \beta)$, $k = 1, 2$ is always non-positive (Fig. 6.8), which implies that visibility is always maintained.

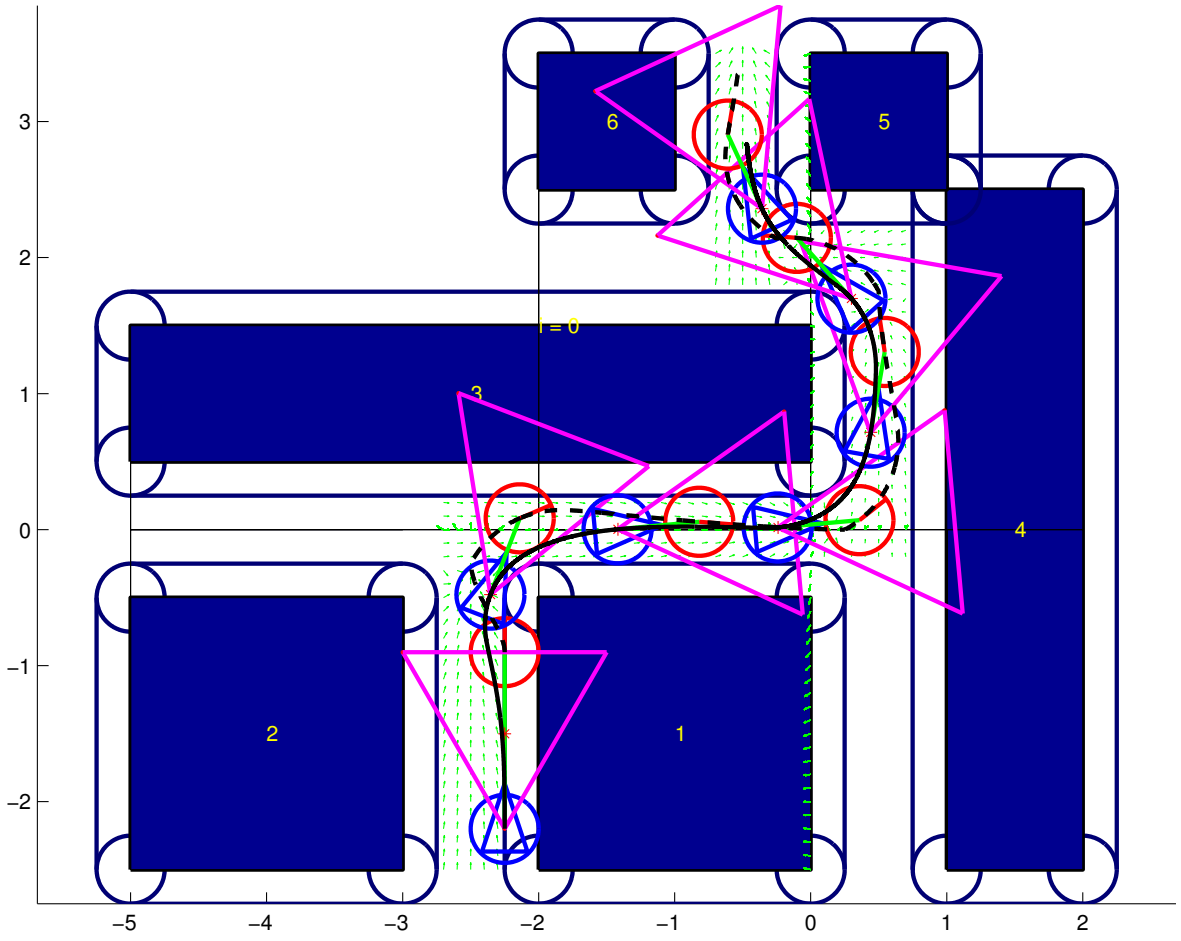

Figure 6.7: The system initiates on a configuration $\boldsymbol{q} \in \mathcal{C}$ on the boundary of the obstacles, where the second visibility constraint is active for F.

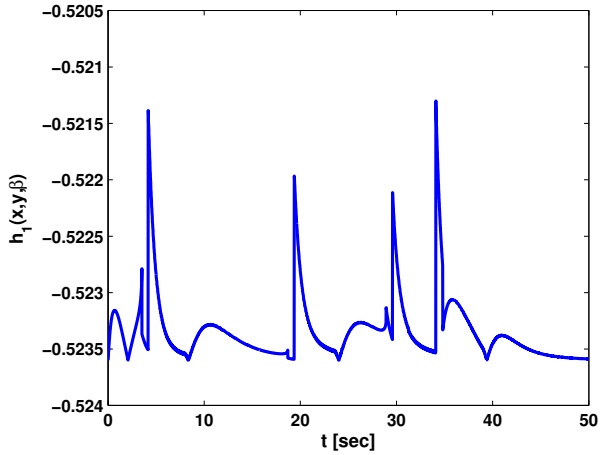

(a) $h_1(x, y, \beta) \leq 0$, $\forall t$.

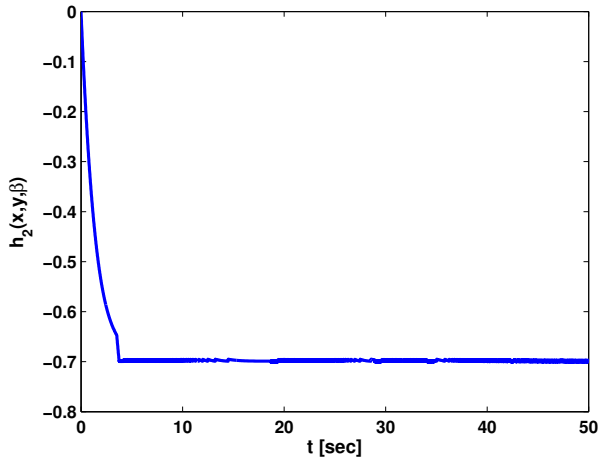

(b) $h_2(x, y, \beta) \leq 0$, $\forall t$.

Figure 6.8: Visibility is always maintained, since the value of the visibility constraints is always negative.

6.6 Discussion

This paper presented a feedback control solution for an L − F formation with visibility constraints in an environment with obstacles. Visibility constraints arise due to the limited sensing of F, and are realized as nonlinear inequality state constraints that constitute a closed visibility set K. The visibility set K contains all system configurations where L is visible to F. The task is to control F w.r.t. L, so that system trajectories starting in K always remain in K. Inspired by ideas from viability theory, the necessary conditions for maintaining visibility were given, as well as a control scheme that forces F to converge and remain into a set of desired configurations w.r.t. L without violating visibility. We additionally proposed a way of controlling L in a known obstacle environment, so that both obstacle avoidance and visibility maintenance are ensured. The proposed control schemes are decentralized, in the sense that there is no direct communication between the robots, nor global state feedback is available to them. Computer simulations demonstrate the efficacy of our algorithms.

Finally, it is worth to mention that the proposed control design ideas are not restricted to the scenarios presented in this paper. In the case of more complex, polygonal obstacle environments, it immediately follows that the collision-free motion control for L can as well be based on the idea presented here: given a cell decomposition of convex polygonal cells, L can be controlled to move from cell i to cell $i+1$ by tracking a dipolar vector field in cell i, defined so that its integral curves converge to the midpoint of the exit face of cell i, while pointing into the interior of the cell i on the remaining faces; if the vector field does not by construction point towards the free space, it can easily be modified to do so by properly blending it with a viable vector field on the boundary. For ensuring the collision-free motion of F as it moves from cell i to cell $i+1$, one can similarly employ the tractor-trailer paradigm, and pick a safe turning radius R_{L} for L by computing the worst-case safe turning radius $R_{\mathrm{F_w}}$ for F, which corresponds to F being on the boundary of cell i at the time that L exits i. Clearly, $R_{\mathrm{F_w}}$ depends on the geometry of cell i, and its analytical expression is in general different from the one given by (6.24), which holds for a rectangular cell i; nevertheless, its "a priori" computation for any transition i to $i+1$ is feasible, given that the decomposition is known.

The tractor-trailer paradigm can be also used to extend the formation control in the case of $\mathrm{N}>2$ robots that move in a chain formation, in the sense that if the tractor (L) moves along a circle of center C and radius R_{L}, then the $\mathrm{N}-1$ trailers (the followers F_j, $j=1,\ldots,\mathrm{N}-1$) move along circles of center C and radii R_{F_j}; thus, one can compute a (conservative) condition on a safe R_{L} so that the (worst-case) turning radius R_{F_j} for the j-th follower, $j=1\ldots,\mathrm{N}-1$, is collision-free. Finally, the assumption on the sensor footprint being an isosceles triangle is not restrictive, since the conditions on maintaining visibility apply to any closed convex footprint.

6.7 Proof of Theorem 1

Proof Take a continuously differentiable function V in terms of the position errors $x_1=x-x_d$, $y_1=y-y_d$ and the orientation error $\theta_{\mathrm{F}}-\varphi$, as

$$V=\frac{1}{2}\left({x_1}^2+{y_1}^2+(\theta_{\mathrm{F}}-\varphi)^2\right),$$

and take its time derivative along the system trajectories

$$\dot{V}=(x_1\cos\theta_{\mathrm{F}}+y_1\sin\theta_{\mathrm{F}})\,u_{\mathrm{F}}+(\theta_{\mathrm{F}}-\varphi)(w_{\mathrm{F}}-\dot{\varphi}),$$

where $\dot{x}_d=0$, $\dot{y}_d=0$. Under the control law (6.12), one gets

$$\dot{V}=-k_1|x_1\cos\theta_{\mathrm{F}}+y_1\sin\theta_{\mathrm{F}}|\|\boldsymbol{r_1}\|-k_2(\theta_{\mathrm{F}}-\varphi)^2\leq 0.$$

According to LaSalle's invariance principle, and given that V is positive definite, the system trajectories converge into the largest invariant set $\mathcal{I}$ contained in the set $\Omega=\{\boldsymbol{q}\in\mathcal{C}\mid\dot{V}=0\}$. The set Ω is given as $\Omega=\Omega_1\vee\Omega_2$, where $\Omega_1=\{\{x_1\cos\theta_{\mathrm{F}}+y_1\sin\theta_{\mathrm{F}}=0\}\wedge\{\theta_{\mathrm{F}}=\varphi\}\}$ and $\Omega_2=\{\{x_1=y_1=0\}\wedge\{\theta_{\mathrm{F}}=\varphi\}\}$. The set Ω_1 is not invariant under the control inputs (6.12), since for $\boldsymbol{q}\in\Omega_1$ one has $u_{\mathrm{F}}\neq 0$, i.e. the state trajectories depart Ω_1, whereas the set $\Omega_2=\{\{x_1=y_1=0\}\wedge\{\theta_{\mathrm{F}}=\varphi|_{x_1=y_1=0}=\theta_d\}\}$ is invariant, since for $\boldsymbol{q}\in\Omega_2$ one has $u_{\mathrm{F}}=w_{\mathrm{F}}=0$. Therefore, the largest invariant set is the singleton $\{\boldsymbol{q_d}\}$; thus, the system trajectories globally asymptotically converge to the equilibrium $\boldsymbol{q_d}=\begin{bmatrix}x_d & y_d & \theta_d\end{bmatrix}^\top$.

Chapter 7

A Viability Formulation based on Optimal Control

Abstract

In this chapter we present a viability formulation for the control of an underactuated underwater vehicle under the influence of a known, constant current and state constraints, based on optimal control. The overall control problem is described by three problems in terms of viability theory. We present a solution to the first problem which addresses the safety of the system, i.e. guarantees that there exists a control law such that the vehicle always remains into the safe set of state constraints. In order to overcome the computational limitations due to the high dimension of the system we develop a two-stage approach, based on forward reachability and game theory. The control law is thus the safety controller when the system viability is at stake, i.e. close to the boundary of the safe set. The viability kernel and the control law are numerically computed.

The chapter is organized as follows; Section 7.1 presents a framework for the stabilization problem based on viability theory. Section 7.2 presents the mathematical modeling of the system and state constraints. Section 7.3 gives the viability analysis and Section 7.4 the computational results. The conclusions are summarized in Section 7.5.

7.1 Problem Formulation into Viability Theory

Viability theory [Aub91] describes the evolution of systems under the consideration that for different reasons, not all system evolutions are feasible. The system must obey state constraints, called viability constraints and system solutions should be viable in the sense that they must satisfy, at each instant, these constraints. Viability theorems characterize the connections between the system dynamics and the constraints, for guaranteeing the existence of at least one viable solution starting from any initial state. They also provide the regulation processes (feedbacks) that maintain viability, or even improve the state according to some preference relation; for example, viability theory provides tools for regulating system evolutions that are viable in a set of state constraints, until they reach a target [Aub03].

The problem of stabilizing an underactuated underwater vehicle in a goal set under state constraints and current disturbances is described by the following viability problems, see also Fig. 7.1. Consider a control system described by

$$\dot{x}(t) \in F\left(x(t)\right) \text{ with } F\big(x(t)\big) = \big\{ f\big(x(t), u\big) | u \in U \big\}, \tag{7.1}$$

where $x(\cdot) \subseteq \mathbb{R}^n$ is the state vector, $u \in U \subseteq \mathbb{R}^m$ is the control vector, $U \subseteq \mathbb{R}^m$ is compact, $f : \mathbb{R}^n \times \mathbb{R}^m \to \mathbb{R}^n$ is the bounded, uniformly continuous single-valued map of system dynamics and $F\big(x(t)\big)$ is the set of available velocities.

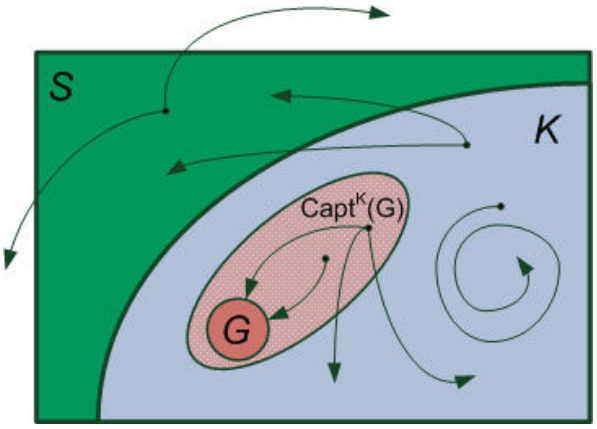

Figure 7.1: Viability set K and the Capture Basin of goal set G in K

1. Given a set S of viability constraints, describing that the target must always be in the camera field of view, determine a set of initial states $K \subseteq S$ such that for every initial state $x_0 \in K$ there exists at least one solution to (7.1) starting at x_0 which remains for ever in S, keeping the target in the camera field of view. We say that K is a viability domain of the system. We would like to determine the maximal viability domain contained in S, known as the viability kernel of S, $Viab_F(S)$.

2. Given the viability kernel K of (7.1) and a goal set $G \subseteq K$, describing that the target is near to the center of the camera field of view, determine the set of initial states $x \in K$ such that there exists at least one solution to (7.1) starting at x that reaches the goal set G in finite time, without leaving S. This set is called the capture basin of the goal G in K, $Capt_F^K(G)$.

3. Finally, determine a control law such that the solutions to (7.1) starting at $x_s \in G$ remain for ever in G, i.e. once the system reaches G, it is then stabilized in it. In that case, G is a viability domain of (7.1).

In this chapter, we consider the first of the three parts, known as the safety problem.

7.2 Mathematical Modeling

We consider the 3-d.o.f. motion on the horizontal plane of an underwater vehicle with two back thrusters but no side thruster; this is a common configuration for marine vehicles. Roll and pitch angles remain always very close to zero, $\phi \approx 0$ and $\theta \approx 0$ respectively, because of the vehicle's mass configuration. The position and orientation vector of the vehicle w.r.t. a global coordinate frame G is defined as

$$\boldsymbol{\eta} = \begin{bmatrix} x & y & \psi \end{bmatrix}^\top$$

and the linear and angular velocity vector is defined in the body-fixed coordinate frame B as

$$\boldsymbol{\nu} = \begin{bmatrix} u & v & r \end{bmatrix}^\top .$$

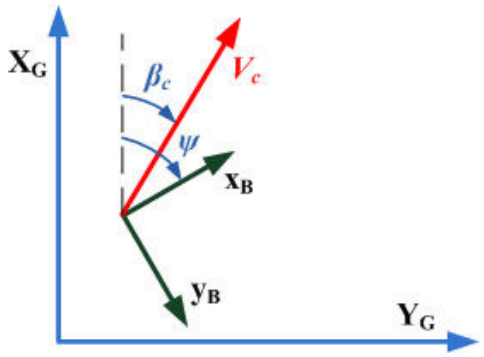

Figure 7.2: Current velocity and direction

Following [Fos02] the 3-d.o.f. kinematic equations are:

$$\dot{\boldsymbol{\eta}} = \boldsymbol{J}(\psi)\boldsymbol{\nu} \Leftrightarrow \begin{bmatrix} \dot{x} \\ \dot{y} \\ \dot{\psi} \end{bmatrix} = \begin{bmatrix} \cos\psi & -\sin\psi & 0 \\ \sin\psi & \cos\psi & 0 \\ 0 & 0 & 1 \end{bmatrix} \begin{bmatrix} u \\ v \\ r \end{bmatrix},$$

and the 3-d.o.f. dynamic equations of motion are:

$$\boldsymbol{M}\dot{\boldsymbol{\nu}} + \boldsymbol{C}(\boldsymbol{\nu})\boldsymbol{\nu} + \boldsymbol{D}(\boldsymbol{\nu})\boldsymbol{\nu} = \boldsymbol{\tau} + \boldsymbol{\tau_E},$$

where $\boldsymbol{M} = \boldsymbol{M}^\top > \mathbf{0} \in \mathbb{R}^{3\times3}$ is the inertia matrix including added mass, $\boldsymbol{C}(\boldsymbol{\nu}) = -\boldsymbol{C}^\top(\boldsymbol{\nu}) \in \mathbb{R}^{3\times3}$ is the matrix of Coriolis terms including added mass, $\boldsymbol{D}(\boldsymbol{\nu}) > \mathbf{0} \in \mathbb{R}^{3\times3}$ is the damping matrix, $\boldsymbol{\tau} \in \mathbb{R}^3$ is the vector of control inputs and $\boldsymbol{\tau_E} \in \mathbb{R}^3$ is the vector of environmental disturbances due to waves, currents and cable effects.

The vehicle is assumed to move under the influence of a known, non-rotational, constant current, with velocity V_c and direction β_c w.r.t. the global frame G, see Fig. 7.2. The effect of current-induced forces and moments is modeled in terms of the body-fixed relative velocity $\boldsymbol{\nu_r} = \boldsymbol{\nu} - \boldsymbol{\nu_c}$ [Fos02], where $\boldsymbol{\nu_c} = \boldsymbol{J^{-1}}(\psi)\boldsymbol{V_C^G}$ and $\boldsymbol{V_C^G} = \begin{bmatrix} V_c\cos\beta_c & V_c\sin\beta_c & 0 \end{bmatrix}^\top$.

The kinematics are then written w.r.t. $\boldsymbol{\nu_r} = \begin{bmatrix} u_r & v_r & r \end{bmatrix}^\top$ as:

$$\dot{\boldsymbol{\eta}} = \boldsymbol{J}(\psi)\boldsymbol{\nu_r} + \boldsymbol{V_C^G} \Rightarrow \begin{bmatrix} \dot{x} \\ \dot{y} \\ \dot{\psi} \end{bmatrix} = \begin{bmatrix} \cos\psi & -\sin\psi & 0 \\ \sin\psi & \cos\psi & 0 \\ 0 & 0 & 1 \end{bmatrix} \begin{bmatrix} u_r \\ v_r \\ r \end{bmatrix} + \begin{bmatrix} V_c\cos\beta_c \\ V_c\sin\beta_c \\ 0 \end{bmatrix},$$

whereas the dynamics are [Fos02]

$$\boldsymbol{M}\dot{\boldsymbol{\nu}} + \boldsymbol{C_{RB}}(\boldsymbol{\nu})\boldsymbol{\nu} + \boldsymbol{C_A}(\boldsymbol{\nu_r})\boldsymbol{\nu_r} + \boldsymbol{D}\big(|\boldsymbol{\nu_r}|\big)\boldsymbol{\nu_r} = \boldsymbol{\tau},$$

where $\boldsymbol{M} = \begin{bmatrix} m-X_{\dot{u}} & 0 & 0 \\ 0 & m-Y_{\dot{v}} & 0 \\ 0 & 0 & I_z-N_{\dot{r}} \end{bmatrix}$, $\boldsymbol{C_{RB}}(\boldsymbol{\nu}) = \begin{bmatrix} 0 & 0 & -mv \\ 0 & 0 & mu \\ mv & -mu & 0 \end{bmatrix}$, $\boldsymbol{C_A}(\boldsymbol{\nu_r}) = \begin{bmatrix} 0 & 0 & Y_{\dot{v}}v_r \\ 0 & 0 & -X_{\dot{u}}u_r \\ -Y_{\dot{v}}v_r & X_{\dot{u}}u_r & 0 \end{bmatrix}$, $\boldsymbol{D_L} = \begin{bmatrix} -X_u & 0 & 0 \\ 0 & -Y_v & -Y_r \\ 0 & -N_v & -N_r \end{bmatrix}$, $\boldsymbol{D_{NL}}\big(|\boldsymbol{\nu_r}|\big) = \begin{bmatrix} -X_{u|u|}|u_r| & 0 & 0 \\ 0 & -Y_{v|v|}|v_r| & 0 \\ 0 & 0 & -N_{r|r|}|r| \end{bmatrix}$, $\boldsymbol{\tau} = \begin{bmatrix} \tau_1 \\ 0 \\ \tau_2 \end{bmatrix}$, m is the mass and I_z is the moment of inertia with respect to z axis of the vehicle, $X_{\dot{u}}$,$Y_{\dot{v}}$,$N_{\dot{r}}$ are the added

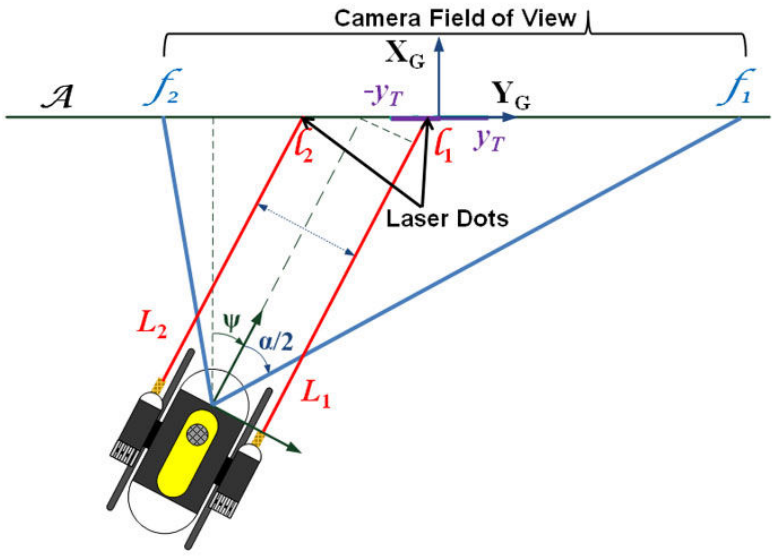

Figure 7.3: Modeling of the State Constraints imposed by the Sensor System

mass terms, X_u,Y_v,Y_r,N_v,N_r are linear drag terms, $X_{u|u|}$,$Y_{v|v|}$,$N_{r|r|}$ are nonlinear drag terms, τ_1 and τ_2 are control inputs in surge and yaw d.o.f..

Under the substitution $\boldsymbol{\nu} = \boldsymbol{\nu_r} + \boldsymbol{\nu_c}$, the kinematic and dynamic equations are rewritten as:

$$\begin{bmatrix} \dot{x} \\ \dot{y} \\ \dot{\psi} \\ \dot{u}_r \\ \dot{v}_r \\ \dot{r} \end{bmatrix} = \begin{bmatrix} u_r \cos\psi - v_r \sin\psi + V_c \cos\beta_c \\ u_r \sin\psi + v_r \cos\psi + V_c \sin\beta_c \\ r \\ \frac{1}{m_{11}} \left(m_{22} v_r r + X_u u_r + X_{u|u|} \left| u_r \right| u_r + X_{\dot{u}} V_c \sin\left(\beta_c - \psi\right) r \right) \\ \frac{1}{m_{22}} \left(-m_{11} u_r r + Y_v v_r + Y_r r + Y_{v|v|} \left| v_r \right| v_r - Y_{\dot{v}} V_c \cos\left(\beta_c - \psi\right) r \right) \\ \frac{1}{m_{33}} \left(\left(m_{11} - m_{22} \right) u_r v_r + N_v v_r + N_r r + N_{r|r|} \left| r \right| r \right) \end{bmatrix} + \begin{bmatrix} 0 \\ 0 \\ 0 \\ \frac{1}{m_{11}} \\ 0 \\ 0 \end{bmatrix} \tau_1 + \begin{bmatrix} 0 \\ 0 \\ 0 \\ 0 \\ 0 \\ \frac{1}{m_{33}} \end{bmatrix} \tau_2$$

$$\Rightarrow \dot{\boldsymbol{x}} = \boldsymbol{f}(\boldsymbol{x}, V_c, \beta_c) + \sum_{i=1,2} \boldsymbol{g}_i \tau_i, \tag{7.2}$$

where $\boldsymbol{x} = \begin{bmatrix} \boldsymbol{\eta}^\top & \boldsymbol{\nu_r}^\top \end{bmatrix}^\top$ is the state vector, $\boldsymbol{f}(\boldsymbol{x}, V_c, \beta_c)$ is the drift vector field, $\boldsymbol{g}_1, \boldsymbol{g}_2$ are the control vector fields, $m_{11} = m - X_{\dot{u}}$, $m_{22} = m - Y_{\dot{v}}$, $m_{33} = I_z - N_{\dot{r}}$.

Moreover, the thrust allocation implies that $\tau_1 = F_P + F_{ST}$ and $\tau_2 = D\left(F_P - F_{ST}\right)$, where $F_P \in [-F_p, F_p]$, $F_{ST} \in [-F_{st}, F_{st}]$ are the port and starboard thrust forces and $2D$ is the distance between the two thrusters. Thus, $\boldsymbol{u} = \begin{bmatrix} F_P & F_{ST} \end{bmatrix}^\top \in U \subset \mathbb{R}^2$ is the vector of control inputs for (7.2), where $U = [-F_p, F_p] \times [-F_{st}, F_{st}]$.

7.2.1 Modeling of Viability Constraints

We consider the set of state constraints that result from a vision-based sensor system, which employs the onboard camera and two laser pointers mounted on the vehicle [KPK06]. The sensor system provides the vehicle's pose vector $\boldsymbol{\eta}$ w.r.t. the global frame G on the center of a target, which is assumed to lay on a vertical surface A, see Fig. 7.3. The target and the

two laser dots projected on the surface are tracked using computer vision algorithms and this information is used to estimate the pose vector $\boldsymbol{\eta}$.

We define the safe set of the system as the set $\boldsymbol{S}$ such that

1. The target and the laser dots must always be in the camera field of view, i.e. $[-y_T, y_T] \subseteq [f_2, f_1]$ and $[l_2, l_1] \subseteq [f_2, f_1]$.
2. The ranges L_1, L_2 must be less than a critical range L.
3. The distance between the laser dots on the image plane must be greater than a minimum distance ε, so that they do not overlap and are effectively detected.
4. The width of the target on the image plane must be greater than a critical value δ, so that the target is sufficiently visible.

These specifications impose k nonlinear inequality constraints $c_j(x, y, \psi) \leq 0,\ j = 1, ..., k$ determining the safe set $\boldsymbol{S}$. The vector $\boldsymbol{\eta}$ must always remain in $\boldsymbol{S}$ for the sensor system to be effective. The analytical expression of $c_j(x, y, \psi) \leq 0,\ j = 1, ..., k$ is omitted here in the interest of space.

7.3 Viability Analysis

We are interested in determining the viability kernel of $\boldsymbol{S}$, $Viab(\boldsymbol{S})$ under (7.2) and a control law which guarantees that the system trajectories starting in the kernel will remain for ever in it. We adopt the approach presented in [Lyg04] which relates viability with minimum-cost optimal control, coding the viability kernel as the level set of the value function of an appropriate optimal control problem.

7.3.1 An Optimal Control Problem related to Viability

Consider the control system (7.1) and let $\mathcal{U}_{[0,T]}$ denote the set of Lebesgue measurable functions $u(\cdot) : [0, T] \to U$, with $T > 0$ an arbitrary time horizon. Given a set of state constraints S, the control input $u(\cdot) \in \mathcal{U}_{[0,T]}$ should be selected so that the viability constraints are met at each time instant $t \in [0, T]$.

Let us define a cost function $\ell(\cdot) : \mathbb{R}^n \to \mathbb{R}$ of the state x, over the time horizon $[0, T]$, such that $\ell(x) > 0$ for $x \in S$ and $\ell(x) \leq 0$ for $x \notin S$. Then, the objective for the control input $u(\cdot)$ is to maximize the minimum value attained by the cost function $\ell(\cdot)$ along the state trajectory $x(t)$ over the horizon $[0, T]$. The value function of this optimal control problem (SUPMIN problem) is defined as

$$V(x, t) = \sup_{u(\cdot) \in \mathcal{U}_{[0,T]}} \min_{t \in [0,T]} \ell(x(t)).$$

One can show [Lyg04] that the set $\{x \in \mathbb{R}^n \big| V(x, t) > 0\}$ is precisely the set of states for which there exists a control input $u(\cdot) \in \mathcal{U}_{[0,T]}$ such that $x(t) \in S$ for all $t \in [0, T]$, i.e. the viability kernel $Viab(S)$.

Moreover, using dynamic programming, it can be also shown [Lyg04] that $V(x,t)$ is the unique, bounded and uniformly continuous viscosity solution to

$$\frac{\partial V}{\partial t}(x,t) + \min\left\{0, \sup_{u\in U} \frac{\partial V}{\partial x}(x,t) f(x,u)\right\} = 0,$$

with $V(x,T) = \ell(x)$ over $(x,t) \in \mathbb{R}^n \times [0,T]$, where the Hamiltonian function is defined as $\mathcal{H}_1 = \sup_{u\in U} p^\top f(x,u)$.

Thus, in our case we encode the viability constraints as the cost function $\boldsymbol{\ell}(\cdot) : \mathbb{R}^3 \to \mathbb{R}$ such that $\boldsymbol{\ell}(\boldsymbol{\eta}) > 0$ for $\boldsymbol{\eta} \in \boldsymbol{S}$ and $\boldsymbol{\ell}(\boldsymbol{\eta}) \leq 0$ for $\boldsymbol{\eta} \notin \boldsymbol{S}$. An illustration of $\boldsymbol{\ell}(\boldsymbol{\eta})$ for orientation angle $\psi = 0$ is given in Fig. 7.4. The region in black color is where $\boldsymbol{\ell}(x,y) > 0$, i.e. the safe state space on the $x-y$ plane for $\psi = 0$.

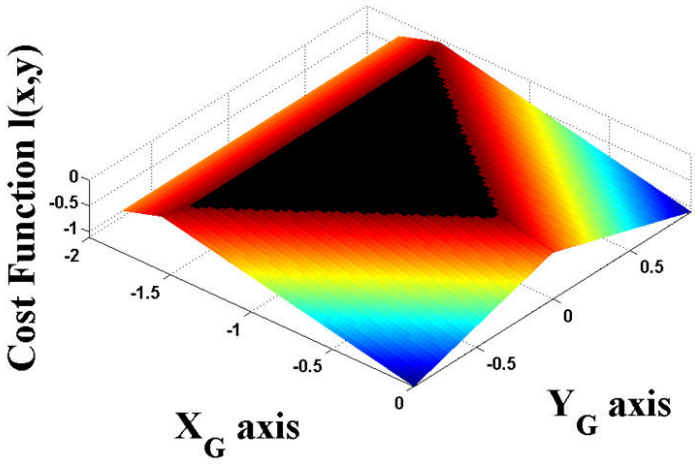

Figure 7.4: Cost Function $\boldsymbol{\ell}(x,y)$

Substituting (7.2) into the Hamiltonian yields:

$$\begin{aligned}
\mathcal{H}_1 = \sup_{\boldsymbol{u}\in U} \big(& p_1 \left(u_r \cos\psi - v_r \sin\psi + V_c \cos\beta_c\right) + p_2 \left(u_r \sin\psi + v_r \cos\psi + V_c \sin\beta_c\right) + p_3 r + \\
& + p_4 \left(\frac{1}{m_{11}} \left(m_{22} v_r r + X_u u_r + X_{u|u|} |u_r| u_r + X_{\dot{u}} V_c \sin(\beta_c - \psi) r \right) \right) + \\
& + p_5 \left(\frac{1}{m_{22}} \left(-m_{11} u_r r + Y_v v_r + Y_r r + Y_{v|v|} |v_r| v_r - Y_{\dot{v}} V_c \cos(\beta_c - \psi) r \right) \right) + \\
& + p_6 \left(\frac{1}{m_{33}} \left((m_{11} - m_{22}) u_r v_r + N_v v_r + N_r r + N_{r|r|} |r| r \right) \right) + \\
& + \left(p_4 \frac{1}{m_{11}} + p_6 \frac{D}{m_{33}} \right) \hat{u}_1 + \left(p_4 \frac{1}{m_{11}} - p_6 \frac{D}{m_{33}} \right) \hat{u}_2 \big)
\end{aligned}$$

where $p_i = \frac{\partial \boldsymbol{V}}{\partial \boldsymbol{x}_i}$, $i = 1, ..., 6$, $u_1 = F_P$ and $u_2 = F_{ST}$. From this, we can conclude that the optimal controls which ensure that the viability constraints are met whenever possible are:

$$\hat{u}_1 = \begin{cases} F_p & \text{if } \frac{p_4}{m_{11}} + \frac{p_6 D}{m_{33}} \geq 0 \\ -F_p & \text{if } \frac{p_4}{m_{11}} + \frac{p_6 D}{m_{33}} < 0 \end{cases}, \quad \hat{u}_2 = \begin{cases} F_{st} & \text{if } \frac{p_4}{m_{11}} - \frac{p_6 D}{m_{33}} \geq 0 \\ -F_{st} & \text{if } \frac{p_4}{m_{11}} - \frac{p_6 D}{m_{33}} < 0 \end{cases} \tag{7.3}$$

whereas the viability kernel $Viab(\boldsymbol{S})$ is given as the set of states for which $\boldsymbol{V}(\boldsymbol{\eta}, t) > 0$.

However, the existing computational tools for time-dependent Hamilton-Jacobi PDEs are effective for low-dimensional problems (1-4 dimensions).

7.3.2 Reachability Analysis

In order to overcome the computational limitations due to the high dimension of the system, we split (7.2) into:

$$\begin{bmatrix} \dot{x} \\ \dot{y} \\ \dot{\psi} \end{bmatrix} = \begin{bmatrix} V_c \cos\beta_c \\ V_c \sin\beta_c \\ 0 \end{bmatrix} + \begin{bmatrix} \cos\psi \\ \sin\psi \\ 0 \end{bmatrix} u_r + \begin{bmatrix} 0 \\ 0 \\ 1 \end{bmatrix} r + \begin{bmatrix} -\sin\psi \\ \cos\psi \\ 0 \end{bmatrix} v_r \tag{7.4}$$

$$\begin{bmatrix} \dot{\psi} \\ \dot{u}_r \\ \dot{v}_r \\ \dot{r} \end{bmatrix} = \begin{bmatrix} r \\ \frac{1}{m_{11}} \left(m_{22} v_r r + X_u u_r + X_{u|u|} |u_r| u_r + X_{\dot{u}} V_c \sin(\beta_c - \psi) r \right) \\ \frac{1}{m_{22}} \left(-m_{11} u_r r + Y_v v_r + Y_r r + Y_{v|v|} |v_r| v_r - Y_{\dot{v}} V_c \cos(\beta_c - \psi) r \right) \\ \frac{1}{m_{33}} \left((m_{11} - m_{22}) u_r v_r + N_v v_r + N_r r + N_{r|r|} |r| r \right) \end{bmatrix} + \begin{bmatrix} 0 \\ \frac{1}{m_{11}} \\ 0 \\ \frac{D}{m_{33}} \end{bmatrix} F_P + \begin{bmatrix} 0 \\ \frac{1}{m_{11}} \\ 0 \\ \frac{-D}{m_{33}} \end{bmatrix} F_{ST} \tag{7.5}$$

At this point, the consideration of (7.4) and (7.5) inspires us

1. to investigate the forward reachability of subsystem (7.5) over the time horizon $[0, T]$, i.e. to compute the set $\mathcal{F}$ of states $\boldsymbol{x_2} = [\psi, u_r, v_r, r]^\top$ which the system trajectories can reach starting from an initial set $\mathcal{N}$. In this way, we acquire an estimation for the bounds of u_r, v_r, r that can be reached from an initial set during the system evolution, so that
2. further on, to investigate the viability of subsystem (7.4), considering the relative velocities u_r, r as the control inputs along the two actuated d.o.f. and the relative velocity v_r as a disturbance along the unactuated d.o.f..

The concept of reachability is mostly used for the safety analysis of continuous and hybrid systems. Given an initial set of states $\mathcal{N}$, the forward reachable set $\mathcal{F}$ is the set of states that can be reached at time $t \in [0, T]$ by the system trajectories starting from $\mathcal{N}$, whereas the backward reachable set $\mathcal{B}$ is the set of states from which start the system trajectories that can reach the set $\mathcal{N}$ at time $t \in [-T, 0]$, $T > 0$ is an arbitrary time horizon.

We consider the relation between reachability and minimum-cost optimal control [Lyg04]. Given the control system (7.1) and a set of states $\mathcal{N}$, the reachable set is

$$Reach(t, \mathcal{N}) = \left\{ x \in \mathbb{R}^n \middle| \exists u(\cdot) \in \mathcal{U}_{[0,T]} \ \exists t \in [0, T] \ x(t) \in \mathcal{N} \right\}.$$

This definition coincides which the one for the backward reachable set $\mathcal{B}$, taking into account that $t \in [-T, 0]$. Furthermore, one can show the connection between the reachability problem and the invariance problem. The invariant set of (7.1) is defined as

$$Inv(t, \mathcal{N}) = \left\{ x \in \mathbb{R}^n \middle| \forall u(\cdot) \in \mathcal{U}_{[0,T]} \ \forall t \in [0, T] \ x(t) \in \mathcal{N} \right\},$$

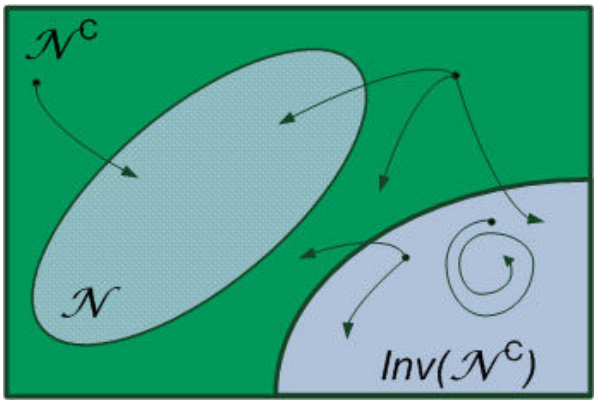

Figure 7.5: Reach(t,$\mathcal{N}$)=(Inv(t,$\mathcal{N}^c$))^c

i.e. as the set of initial states from which *all* the system trajectories remain for ever in $\mathcal{N}$. It is easily verified that

$$Reach(t,\mathcal{N}) = (Inv(t,\mathcal{N}^c))^c,$$

where $\mathcal{N}^c$ is the complement of $\mathcal{N}$; see Fig. 7.5. The invariance problem is formulated as an optimal control problem (INFMIN problem) [Lyg04]. The control objective is to minimize the minimum value of the cost function $\ell(\cdot)$ defined such that $\ell(x) \geq 0$ for $x \in \mathcal{N}$ and $\boldsymbol{\ell}(x) < 0$ for $x \notin \mathcal{N}$, over the time horizon $[0, T]$. The value function

$$V_2(x,t) = \inf_{u(\cdot)\in\mathcal{U}_{[0,T]}} \min_{t\in[0,T]} \ell(x(t))$$

is proven to be the unique, bounded and uniformly continuous viscosity solution to

$$\frac{\partial V_2}{\partial t}(x,t) + \min\left\{0, \inf_{u\in U} \frac{\partial V_2}{\partial x}(x,t) f(x,u)\right\} = 0,$$

with $V_2(x,T) = \ell(x)$ over $(x,t) \in \mathbb{R}^n \times [0,T]$, where the Hamiltonian function is defined as $\mathcal{H}_2 = \inf_{u\in U} p^\top f(x,u)$.

The invariant set of (7.1) is $Inv(t,\mathcal{N}) = \left\{x \in \mathbb{R}^n \middle| V_2(x,t) \geq 0\right\}$. Consequently, if the cost function of the INFMIN problem is defined as $\ell(x) \geq 0$ for $x \in \mathcal{N}^c$ and $\ell(x) < 0$ for $x \notin \mathcal{N}^c$, the solution of the above PDE yields the invariant set $Inv(t,\mathcal{N}^c) = \left\{x \in \mathbb{R}^n \middle| V_2(x,t) \geq 0\right\}$. Then, the (backward) reachable set is $Reach(t,\mathcal{N}) = \left\{x \in \mathbb{R}^n \middle| V_2(x,t) < 0\right\}$.

Therefore, by considering the INFMIN problem for (7.5) we determine the backward reachable set for an initial set of states $\boldsymbol{x_2} \in \mathcal{N}$. Finally, we consider the connection between forward and backward reachability [Mit07a], which states that the forward reachable set of a control system H is the same with the backward reachable set of the system $\overleftarrow{H}$ with inverse dynamics. Thus, by substituting (7.5) with inverse dynamics in the Hamiltonian, $\mathcal{H}_2 = \inf_{\boldsymbol{u}\in U}\left(-p^\top \boldsymbol{f_2}(\boldsymbol{x_2},\boldsymbol{u})\right)$, where $p_i = \frac{\partial V_2}{\partial \boldsymbol{x_{2i}}}$, $i = 1,...,4$ and $\boldsymbol{f_2}$ the drift vector field of (7.5), we can conclude that the optimal control inputs for the forward reachability computation are:

$$\hat{u}_1 = \begin{cases} F_p & \text{if } \frac{p_2}{m_{11}} + \frac{p_4 D}{m_{33}} \geq 0 \\ -F_p & \text{if } \frac{p_2}{m_{11}} + \frac{p_4 D}{m_{33}} < 0 \end{cases}, \; \hat{u}_2 = \begin{cases} F_{st} & \text{if } \frac{p_2}{m_{11}} - \frac{p_4 D}{m_{33}} \geq 0 \\ -F_{st} & \text{if } \frac{p_2}{m_{11}} - \frac{p_4 D}{m_{33}} < 0 \end{cases}$$

The computational results are given in Section 7.4.

7.3.3 Viability Analysis using a Differential Game Formulation

Given the estimation for the bounds of u_r, v_r, r as $u_r = [u_{rm}, u_{rM}]$, $v_r = [v_{rm}, v_{rM}]$, $r = [r_m, r_M]$ we investigate the viability of the subsystem (7.4) in the safe set $\boldsymbol{S}$, where $\boldsymbol{x_1} = \begin{bmatrix} x & y & \psi \end{bmatrix}^\top \in \mathbb{R}^3$ is the state vector, $\boldsymbol{u_1} = \begin{bmatrix} u_r & r \end{bmatrix}^\top \in U_1 \subset \mathbb{R}^2$ are considered as the bounded control inputs, $v_r \in V_r \subset \mathbb{R}$ is considered as a bounded disturbance in the unactuated d.o.f., $\mathcal{U}_{1[0,T]}$ is the set of Lebesgue measurable functions $\boldsymbol{u_1}(\cdot) : [0, T] \to U_1$ and $\mathcal{V}_{r[0,T]}$ is the set of Lebesgue measurable functions $v_r(\cdot) : [0, T] \to V_r$.

We follow the formulation of a differential game with two players [KL05]. The control input $\boldsymbol{u_1}(\cdot)$ is the first player who tries to keep the vehicle into the safe set $\boldsymbol{S}$, whereas the disturbance $v_r(\cdot)$ is the second player who tries to drive the vehicle out of $\boldsymbol{S}$. Furthermore, it is important to define what information the players know about each other's decisions. A state feedback strategy, i.e. allowing both players to choose their actions based on the current state, is the most appropriate for the problem considered here. However, state feedback is not easily formulated into Hamilton-Jacobi PDEs [MBT05]. Besides, it is preferable to underapproximate the viability kernel rather than overapproximate it. Therefore we give the advantage to the disturbance $v_r(\cdot)$, which tries to make the viable set larger, by allowing the control input $\boldsymbol{u_1}(\cdot)$ to use only non-anticipative strategies, as presented in [KL05].

Consequently, computing the viability kernel for (7.4) is equivalent with computing the set of initial states for which the control input $\boldsymbol{u_1}(\cdot)$ wins the game. This set is called the discriminating kernel of $\boldsymbol{S}$,

$$Disc(t, \boldsymbol{S}) = \{\boldsymbol{x_1} \in \mathbb{R}^3 \big| \exists \text{ nonant/ve } \gamma(\cdot)\ \forall v_r \in \mathcal{V}_{r[t,T]}\ \forall t_1 \in [t, T]\ \boldsymbol{x_1}(t_1) \in \boldsymbol{S}\}.$$

One can show [KL05] that

$$Disc(t, \boldsymbol{S}) = \big\{\boldsymbol{x_1} \in \mathbb{R}^3 \big| \boldsymbol{V_1}(\boldsymbol{x_1}, t) > 0\big\}$$

where $\boldsymbol{V_1}(\boldsymbol{x_1}, t)$ is the value function

$$\boldsymbol{V_1}(\boldsymbol{x_1}, t) = \sup_{\text{nonant/ve } \boldsymbol{u_1}(\cdot)} \inf_{v_r(\cdot) \in \mathcal{V}_{r[t,T]}} \min_{t_1 \in [t,T]} \boldsymbol{\ell}\big(\boldsymbol{x_1}(t_1)\big)$$

of a SUPMIN problem with cost function $\boldsymbol{\ell}(\cdot) : \mathbb{R}^3 \to \mathbb{R}$ defined in Section IV-A. Moreover, $\boldsymbol{V_1}(\boldsymbol{x_1}, t)$ is shown to be the unique, bounded and uniformly continuous viscosity solution to

$$\frac{\partial \boldsymbol{V_1}}{\partial t}(\boldsymbol{x_1}, t) + \min\big\{0, \sup_{\boldsymbol{u_1} \in U_1} \inf_{v_r \in V_r} \frac{\partial \boldsymbol{V_1}}{\partial \boldsymbol{x_1}}(\boldsymbol{x_1}, t)\, \boldsymbol{f_1}(\boldsymbol{x_1}, \boldsymbol{u_1}, v_r)\big\} = 0$$

over $t \in [0, T]$ with $\boldsymbol{V_1}(\boldsymbol{x_1}, T) = \boldsymbol{\ell}(\boldsymbol{x_1})$. Thus, the solution of this PDE yields the discriminating kernel of (7.4) and an optimal control law which guarantees that the trajectories of (7.4) starting in $Disc(t, \boldsymbol{S})$ will remain for ever in $\boldsymbol{S}$, despite the effect of the current disturbance. In order to derive the optimal control law we consider the Hamiltonian:

$$\mathcal{H}_3 = \sup_{\boldsymbol{u_1} \in U_1} \inf_{v_r \in V_r} \left(p_1 V_c \cos\beta_c + p_2 V_c \sin\beta_c + p_3 \hat{r} + (p_1 \cos\psi + p_2 \sin\psi)\, \hat{u_r} + (-p_1 \sin\psi + p_2 \cos\psi)\, \hat{v_r}\right) \tag{7.6}$$

where $p_i = \frac{\partial \boldsymbol{V_1}}{\partial \boldsymbol{x_{1_i}}}$, $i = 1...3$. The optimal control inputs are:

$$\hat{u}_r = \begin{cases} u_{rM} & \text{if } (p_1 \cos\psi + p_2 \sin\psi) \geq 0 \\ u_{rm} & \text{if } (p_1 \cos\psi + p_2 \sin\psi) < 0 \end{cases} \quad \hat{r} = \begin{cases} r_M & \text{if } p_3 \geq 0 \\ r_m & \text{if } p_3 < 0 \end{cases} \tag{7.7}$$

whereas the disturbance input is selected such that it has the worst possible impact on the system, as $\hat{v}_r = v_{rm}$ if $(-p_1 \sin\psi + p_2 \cos\psi) \geq 0$ and $\hat{v}_r = v_{rM}$ if $(-p_1 \sin\psi + p_2 \cos\psi) < 0$. Thus we have a robust estimation of the discriminating kernel $Disc(\boldsymbol{S})$, since at each time instance t we consider the effect of the worst-case disturbance v_r, i.e. of the worst-case linear velocity in the unactuated sway d.o.f.. The computational results are given in Section 7.4.

So far we have assumed that the current has known, constant direction β_c. In order to determine viability in a more robust manner, we would like to characterize the discriminating kernel of (7.4) which is irrelevant to the current direction β_c. Thus, we consider the angle β_c as an additional disturbance input, which is trying to minimize the Hamiltonian $\mathcal{H}_3$, i.e. minimize the term $h_3(\beta_c) = p_1 V_c \cos\beta_c + p_2 V_c \sin\beta_c$. The minimum value of $h_3(\beta_c)$ is attained for $\beta_c = \arctan 2(p_2, p_1) + \pi$ if $p_2 < 0$, and for $\beta_c = \arctan 2(p_2, p_1) - \pi$ if $p_2 \geq 0$. Thus, for the computation of $Disc(t, \boldsymbol{S})$ we consider the worst-case current direction $\beta_c(p_1, p_2)$ at each iteration. The computational results are given in Section 7.4.

7.4 Computational Results

The forward reachability computation for the system (7.5) was performed on a $26 \times 26 \times 26 \times 26$ grid of the state space using the Level Set Methods Toolbox [Mit07b]. The initial set $\mathcal{N}$ was defined as a cube centered at the origin. The velocity and direction of the current were selected as $V_c = 0.5$ m/sec and $\beta_c = \pi/2$. The dynamic parameters in (7.5) were chosen to resemble the vehicle properties. The computations were performed for different values of the time horizon T, see Fig. 7.6. We found out that for each time horizon and for all values of angle ψ, the

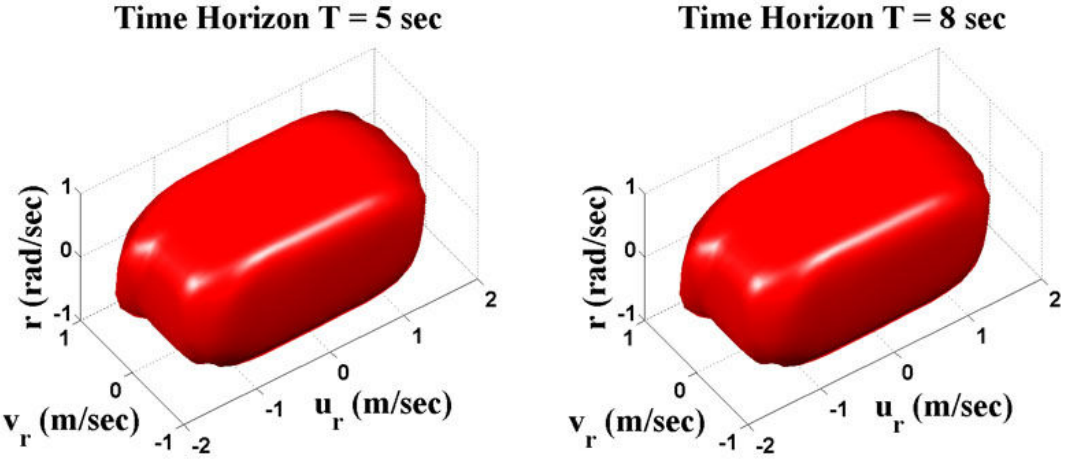

Figure 7.6: Forward Reachable Sets for T=5 and T=8 sec and $\beta_c = \pi/2$

resulting reachable sets of u_r, v_r, r were practically the same. This is justified since the ψ-dependent terms are negligible compared to the other dynamic terms. Furthermore, after a

time horizon the state vector saturates and the reachable set does not expand any more, since the damping forces counterbalance thrust. Since the reachable sets for $T = 5$ sec and $T = 8$ sec are practically the same, it is safe to choose the bounds of u_r, v_r, r. To further justify this, we performed computations for various angles β_c, which verified that the reachable sets do not differ at $T = 5$ sec.

The viability computation for system (7.4) was performed on a $51 \times 51 \times 51$ grid of the state space with $V_c = 0.5$ m/sec and $\beta_c = \pi/2$ rad. The safe set $\boldsymbol{S}$ is given in Fig. 7.7 on the left side. As it was expected, $\boldsymbol{S}$ is shrinking as t increases until a time horizon $T \approx 2.5$ sec. The discriminating kernel $Disc(\boldsymbol{S})$ at time $t = 3$ sec is given in Fig. 7.7, on the right. Their

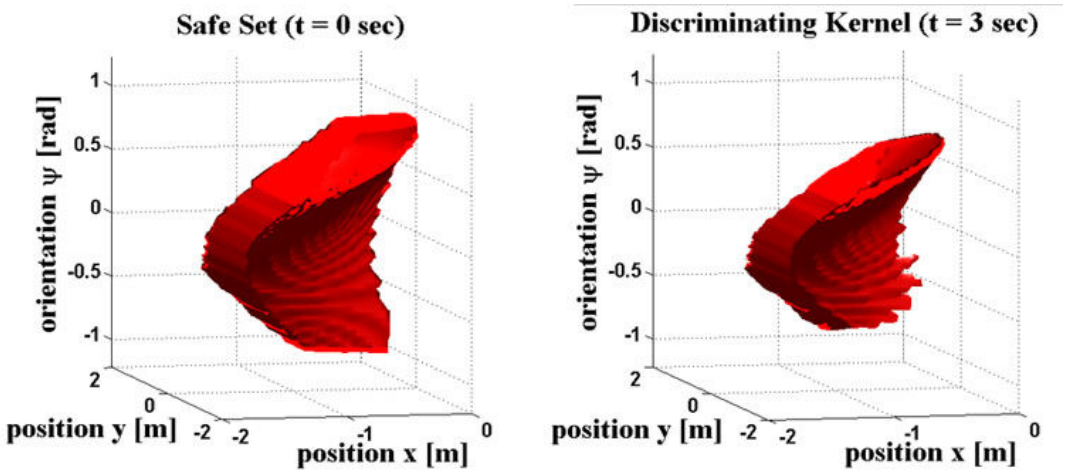

Figure 7.7: Safe Set $\boldsymbol{S}$ and Discriminating Kernel $Disc(\boldsymbol{S})$ at t=3 sec

projections on the $x - y$ plane are given in Fig. 7.8. The shape of $Disc(\boldsymbol{S})$ is consistent with physical intuition, i.e. $Disc(\boldsymbol{S})$ depends on the current direction β_c. The lack of symmetry means that there is no control input (7.7) that can prevent the current to drive the states on the right side out of the $Disc(\boldsymbol{S})$. Moreover, the $Disc(\boldsymbol{S})$ for current direction $\beta_c \in [-\pi, \pi]$

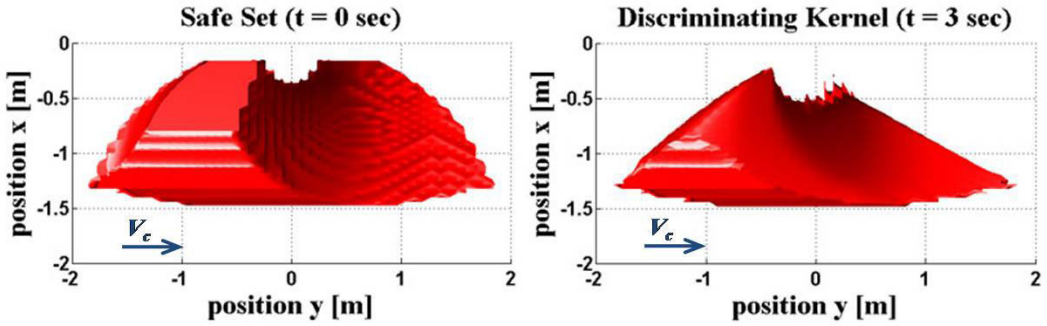

Figure 7.8: Projection of $\boldsymbol{S}$ and $Disc(\boldsymbol{S})$ on the $x - y$ plane for $\beta_c = \pi/2$

and velocity $V_c = 0.5$ m/sec is depicted in Fig. 7.9. This is the set of initial states for which the control law (7.7) ensures that the viability constraints are met for all possible current

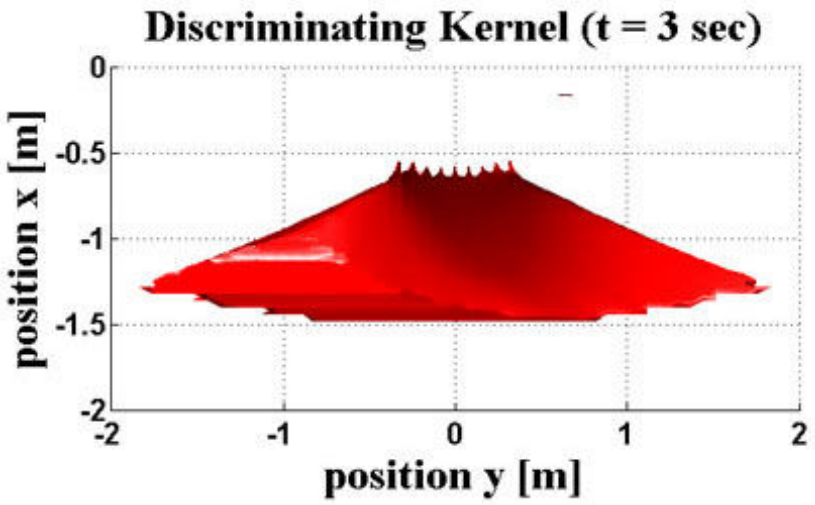

Figure 7.9: Discriminating Kernel $Disc(\boldsymbol{S})$ at t=3 sec for $\beta_c \in [-\pi, \pi]$.

directions. As one would expect, it is smaller than the one computed for fixed angle β_c. The vector field of system (7.4) under (7.7) for $\beta_c = \pi/2$ and $\psi = 0$ is given in Fig. (7.10). It verifies that the system is forced into the $Disc(\boldsymbol{S})$ when the state is close to its boundary, see the velocity vectors on the bound parallel to y axis. Moreover, the velocity vectors close to the other two sides of $Disc(\boldsymbol{S})$, along with the corresponding control input r, see Fig. 7.11, imply that the state remains into $Disc(\boldsymbol{S})$ with $\psi \neq 0$, since $Disc(\boldsymbol{S})$ either expands to the left with $\dot{\psi} > 0$ (red boundary, $\psi > 0$) or to the right with $\dot{\psi} < 0$ (green boundary, $\psi < 0$).

7.5 Conclusions

In this chapter, we presented a viability formulation based on optimal control, for the problem of controlling an underactuated underwater vehicle w.r.t. a target, in the presence of a known, constant current disturbance and under state constraints. Considering a safe set of state constraints resulting from the task specifications and sensor limitations, we investigated whether there exists a control law such that the vehicle remains for ever in this set, despite the influence of the current. This analysis, based on an approach connecting viability and optimal control, yields the viability kernel and an optimal control law that maintains viability. To overcome the computational limitations due to the high dimension of the system, we presented a two-stage analysis, based on forward reachability and game theory. The computation of the viability kernel is necessary so to further proceed to the design of control laws that steer the vehicle into a goal set. The derivation of the safety controller is important, since this control law can be used when viability is at stake, i.e. close to the boundary of the safe set.

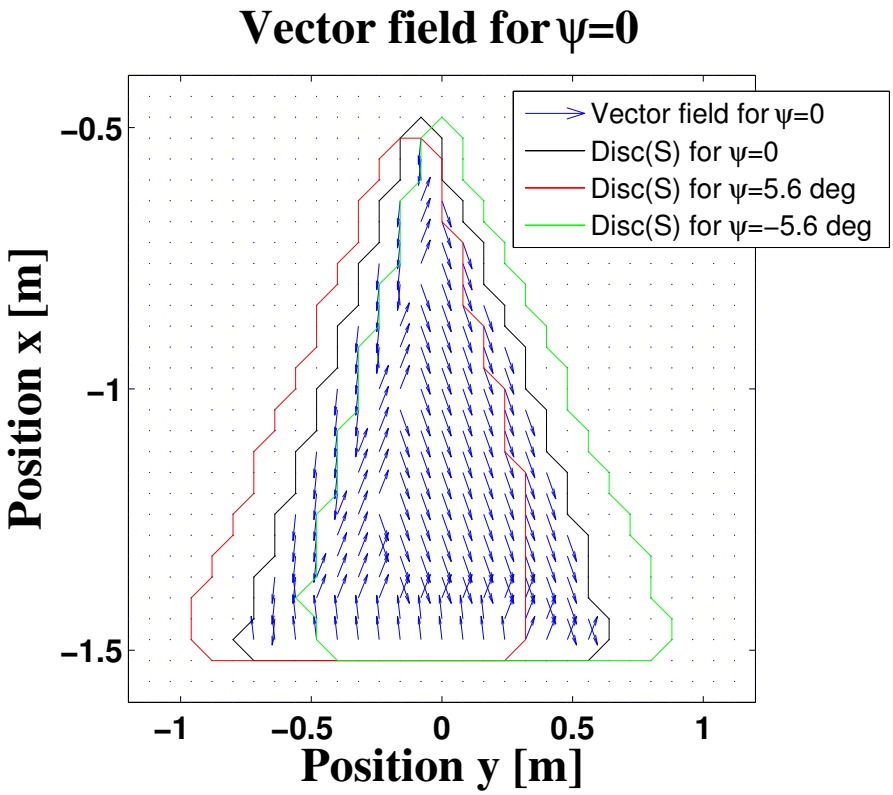

Figure 7.10: Vector field of closed-loop system for $\psi = 0$.

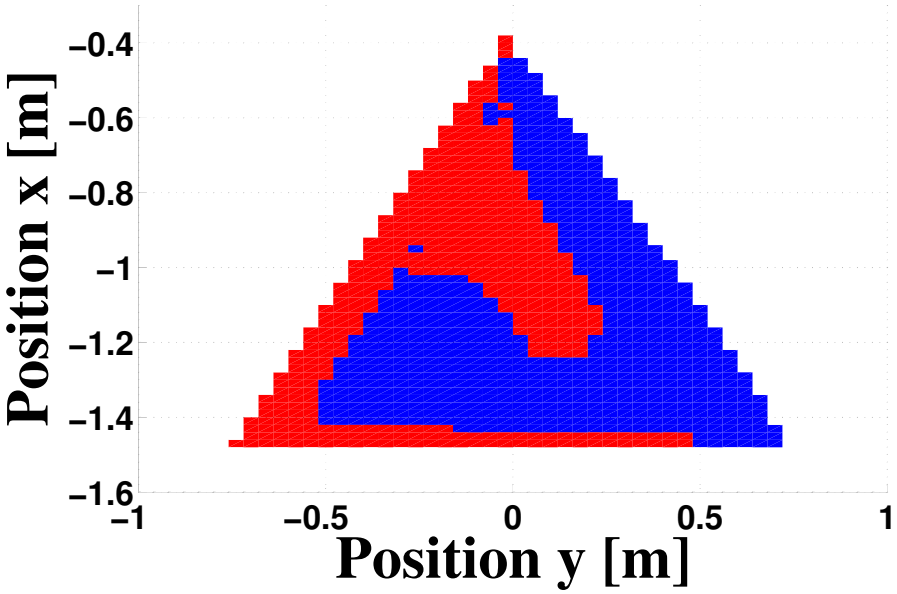

Figure 7.11: Control input $r \geq 0$ in Red Area and $r < 0$ in Blue Area.

Chapter 8

Appendix

Definition 1 *A continuous function $\alpha : [0, a) \to [0, \infty)$ is said to belong to class $\mathcal{K}$ if it is strictly increasing and $\alpha(0) = 0$. It is said to belong to class $\mathcal{K}_\infty$ if $a = \infty$ and $\alpha(r) \to \infty$ as $r \to \infty$.*

Definition 1 *A continuous function $\beta : [0, a) \times [0, \infty) \to [0, \infty)$ is said to belong to class $\mathcal{KL}$ if, for each fixed s, the mapping $\beta(r, s)$ belongs to class $\mathcal{K}$ with respect to r and, for each fixed r, the mapping $\beta(r, s)$ is decreasing with respect to s and $\beta(r, s) \to 0$ as $s \to \infty$.*

Definition 1 *The solutions of $\dot{\boldsymbol{q}} = \boldsymbol{f}(t, \boldsymbol{q})$ are said to be uniformly ultimately bounded with ultimate bound b if there exist positive constants b and c, independent of $t_0 \geq 0$, and for every $\alpha \in (0, c)$ there is $T = T(\alpha, b) \geq 0$, independent of t_0, such that*

$$\|\boldsymbol{q}(t_0)\| < \alpha \Rightarrow \|\boldsymbol{q}(t)\| \leq b, \ \forall t \geq t_0 + T. \tag{1}$$

Moreover, they are said to be globally uniformly ultimately bounded if (1) holds for arbitrarily large α.

Definition 1 *The system (5.1) is input-to-state stable (ISS) if there exist a class $\mathcal{KL}$ function β and a class $\mathcal{K}$ function γ such that for any initial state $\boldsymbol{q}(0) \in \mathbb{R}^n$ and any control input $\boldsymbol{u} \in \mathcal{L}_\infty^m$, the solution $\boldsymbol{q}(t) = \boldsymbol{q}(t, \boldsymbol{q}(0), \boldsymbol{u})$ exists $\forall t \geq 0$ and furthermore it holds that $\|\boldsymbol{q}(t)\| \leq \beta\left(\|\boldsymbol{q}(0)\|, t\right) + \gamma\left(\|\boldsymbol{u}\|_{\mathcal{L}\infty}\right), \ \forall t \geq 0$.*

Definition 1 *A smooth, proper and positive definite function $V : \mathbb{R}^n \to \mathbb{R}$ is an ISS Lyapunov function for (5.1) if there exist two class $\mathcal{K}_\infty$ functions ν and ξ such that*

$$\nabla V(\boldsymbol{q}) \cdot \boldsymbol{f}(\boldsymbol{q}, \boldsymbol{u}) \leq \nu(\|\boldsymbol{u}(t)\|) - \xi(\|\boldsymbol{q}(t)\|), \ \forall \boldsymbol{q}, \boldsymbol{u}.$$

Definition 1 *Consider the system $\dot{\boldsymbol{q}} = \boldsymbol{f}(\boldsymbol{q})$ where $\boldsymbol{f}$ is a continuous vector field, and let $r > 0$. A function $V : B_r \to \mathbb{R}$ is called a generalized weak Lyapunov Function (LF) in the small if it fulfills the following properties: (i) $V(\boldsymbol{0}) = 0$, (ii) for each solution $\boldsymbol{q}(\cdot)$ of the system defined on some interval $\mathcal{I}$ and lying in B_r, the composite map $t \mapsto V(\boldsymbol{q}(t))$ is non-increasing on $\mathcal{I}$, (iii) for some $\eta < r$ and for each $\sigma \in (0, \eta)$ there exists $\lambda > 0$ such that $V(\boldsymbol{q}) > \lambda$ when $\sigma \leq \|\boldsymbol{q}\| \leq \eta$, (iv) $V(\boldsymbol{q})$ is continuous at $\boldsymbol{q} = \boldsymbol{0}$.*

Theorem 5 *Let $\mathcal{D} \subset \mathbb{R}^n$ be a domain containing the origin and $\boldsymbol{f} : [0, \infty) \times \mathcal{D} \to \mathbb{R}^n$ be piecewise continuous in t and locally Lipschitz in $\boldsymbol{q}$. Let $V : [0, \infty) \times \mathcal{D} \to \mathbb{R}$ be a continuously differentiable function such that*

$$W_1(\boldsymbol{q}) \leq V(t, \boldsymbol{q}) \leq W_2(\boldsymbol{q}), \tag{2a}$$

$$\frac{\partial V}{\partial t} + \frac{\partial V}{\partial \boldsymbol{q}} \boldsymbol{f}(t, \boldsymbol{q}) \leq -W_3(\boldsymbol{q}), \ \forall \|\boldsymbol{q}\| \geq \mu > 0, \tag{2b}$$

$\forall t \geq 0$, $\forall \boldsymbol{q} \in \mathcal{D}$ *where* $W_1(\boldsymbol{q})$, $W_2(\boldsymbol{q})$ *and* $W_3(\boldsymbol{q})$ *are continuous positive definite functions on* $\mathcal{D}$. *Take* $r > 0$ *such that* $\mathcal{B}_r \subset \mathcal{D}$ *and suppose that* μ *is small enough such that*

$$\max_{\|\boldsymbol{q}\| \leq \mu} W_2(\boldsymbol{q}) < \min_{\|\boldsymbol{q}\| = r} W_1(\boldsymbol{q}).$$

Let $\eta = \max_{\|\boldsymbol{q}\| \leq \mu} W_2(\boldsymbol{q})$ *and take* ρ *such that*

$$\eta < \rho < \min_{\|\boldsymbol{q}\| = r} W_1(\boldsymbol{q}).$$

Then, there exist a finite time t_1 *(dependent on* $\boldsymbol{q}(t_0)$ *and* μ*) and a class* $\mathcal{KL}$ *function* $\beta(\cdot, \cdot)$ *such that* $\forall \boldsymbol{q}(t_0) \in \{\boldsymbol{q} \in \mathcal{B}_r \mid W_2(\boldsymbol{q}) \leq \rho\}$, *the solutions of* $\dot{\boldsymbol{q}} = \boldsymbol{f}(t, \boldsymbol{q})$ *satisfy*

$$\|\boldsymbol{q}(t)\| \leq \beta(\|\boldsymbol{q}(t_0)\|, t - t_0), \ \forall t_0 \leq t \leq t_1, \tag{3a}$$

$$\boldsymbol{q}(t) \in \{\boldsymbol{q} \in \mathcal{B}_r \mid W_1(\boldsymbol{q}) \leq \eta\}, \ \forall t \geq t_1. \tag{3b}$$

Moreover, if $\mathcal{D} = \mathbb{R}^n$ *and* $W_1(\boldsymbol{q})$ *is radially unbounded, then* (3) *hold for any initial state* $\boldsymbol{q}(t_0)$ *and any* μ.

Bibliography

[AF90] Jean-Pierre Aubin and Helene Frankowska. *Set-valued Analysis*. Birkhäuser, 1990.

[AHP07a] A. P. Aguiar, J. P. Hespanha, and A. M. Pascoal. Switched seesaw control for the stabilization of underactuated vehicles. *IFAC Automatica*, 43(12):1997–2008, December 2007.

[AHP07b] Antonio Pedro Aguiar, Joao P. Hespanha, and Antonio M. Pascoal. Switched seesaw control for the stabilization of underactuated vehicles. *Automatica*, 43:1997–2008, 2007.

[AP01] A. P. Aguiar and A. M. Pascoal. Regulation of a nonholonomic autonomous underwater vehicle with parametric modeling uncertainty using Lyapunov functions. In *Proc. of the 40th IEEE Conf. on Decision and Control*, pages 4178–4183, Orlando, FL, USA, December 2001.

[AP02a] A. P. Aguiar and A. M. Pascoal. Dynamic positioning of underactuated auv in the presence of a constant unknown ocean current disturbance. In *Proc. of the 15th IFAC World Congress*, Barcelona, Spain, 2002.

[AP02b] A. P. Aguiar and A. M. Pascoal. Global stabilization of an underactuated autonomous underwater vehicle via logic-based switching. In *Proc. of the 41st IEEE Conf. on Decision and Control*, pages 3267–3272, Las Vegas, NE, USA, December 2002.

[AP07] Antonio Pedro Aguiar and Antonio M. Pascoal. Dynamic positioning and waypoint tracking of underactuated AUVs in the presence of ocean currents. *International Journal of Control*, 80(7):1092–1108, July 2007.

[Ast96] A. Astolfi. Discontinuous control of nonholonomic systems. *Systems and Control Letters*, 27(1):37–45, January 1996.

[Ast97] Alessandro Astolfi. Discontinuous control of the Brockett integrator. In *Proc. of the 36th IEEE Conference on Decision and Control*, pages 4334–4339, San Diego, CA, USA, December 1997.

[Aub91] Jean-Pierre Aubin. *Viability Theory*. Birkhäuser, 1991.

[Aub01] Jean-Pierre Aubin. Viability kernels and capture basins of sets under differential inclusions. *SIAM Journal on Control and Optimization*, 40(3):853–881, 2001.

[Aub03] Jean-Pierre Aubin. *A Concise Introduction to Viability Theory, Optimal Control and Robotics*. Ecole Normale Supérieure de Cachan. DEA MVA. http://lastre.asso.fr/aubin/CACH000.pdf, 2003.

[BC99] Andrea Bacciotti and Francesca Ceragioli. Stability and stabilization of discontinuous systems and nonsmooth lyapunov functions. *ESAIM: Control, Optimisation and Calculus of Variations*, 4:361–376, January 1999.

[BCM09] Francesco Bullo, Jorge Cortés, and Sonia Martínez. *Distributed Control of Robotic Networks*. Applied Mathematics Series. Princeton University Press, 2009. Electronically available at http://coordinationbook.info.

[BD96] Anthony Bloch and Sergey Dragunov. Stabilization and tracking in the nonholonomic integrator via sliding modes. *Systems and Control Letters*, 29(1):91–99, 1996.

[BDK98] Anthony Bloch, Sergey Dragunov, and Michael Kinyon. Nonholonomic stabilization and isospectral flows. In *Proc. of the 37th IEEE Conference on Decision and Control*, pages 3581–3586, Tampa, FL, USA, December 1998.

[BL05] Francesco Bullo and Andrew D. Lewis. *Geometric Control of Mechanical Systems*. Springer, 2005.

[Bla99] Franco Blanchini. Set invariance in control. *Automatica*, 35(11):1747–1767, November 1999.

[Blo03] Anthony M. Bloch. *Nonholonomic Mechanics and Control*. Springer, 2003.

[BM08] Franco Blanchini and Stefano Miani. *Set-Theoretic Methods in Control*. Birkhauser, 2008.

[BMCH07] Sourabh Bhattacharya, Rafael Murrieta-Cid, and Seth Hutchinson. Optimal paths for landmark-based navigation by differential-drive vehicles with field-of-view constraints. *IEEE Transactions on Robotics*, 23(1):47–59, February 2007.

[BMSS94] L. Bushnell, B. Mirtich, A. Sahai, and M. Secor. Off-tracking bounds for a car pulling trailers with kingpin hitching. In *Proc. of the 33th IEEE Conference on Decision and Control*, pages 2944–2949, Lake Buena Vista, FL, USA, December 1994.

[Boo86] William M. Boothby. *An Introduction to Differentiable Manifolds and Riemannian Geometry - Second Edition*. Academic Press, INC., 1986.

[BR95] M. K. Bennani and P. Rouchon. Robust stabilization of flat and chained systems. In *Proc. of the 3rd European Control Conference*, pages 1781–1786, Rome, Italy, September 1995.

[Bra98] Michael S. Branicky. Multiple Lyapunov functions and other analysis tools for switched and hybrid systems. *IEEE Transactions on Automatic Control*, 43(4):475–482, April 1998.

[BRM92] Anthony M. Bloch, Mahmut Reyhanoglu, and N. Harris McClamroch. Control and stabilization of nonholonomic dynamic systems. *IEEE Transactions on Automatic Control*, 37(11):1746–1757, November 1992.

[Bro83] R. W. Brockett. Asymptotic stability and feedback stabilization. In R.W. Brockett, R.S. Millman, and H.J. Sussmann, editors, *Differential Geometric Control Theory*, pages 181–191. Birkhauser, Boston, 1983.

[CAP05] Daniele Casagrande, Alessandro Astolfi, and Thomas Parisini. Control of nonholonomic systems: A simple stabilizing time-switching strategy. In *16th IFAC World Congress*, Prague, Czech Republic, July 2005.

[CAP08] Daniele Casagrande, Alessandro Astolfi, and Thomas Parisini. Stabilization of a class of non-holonomic systems by means of switching control laws. In *Proc. of the 47th IEEE Conference on Decision and Control*, pages 310–315, Cancun, Mexico, December 2008.

[CBG98] R. Colbaugh, E. Barany, and K. Glass. Adaptive stabilization of uncertain nonholonomic mechanical systems. *Robotica*, 16:181–192, 1998.

[CLH+05] Howie Choset, Kevin Lynch, Seth Hutchinson, George Kantor, Wolfram Burgard, Lydia Kavraki, and Sebastian Thrun. *Principles of Robot Motion. Theory, Algorithms and Implementation*. MIT Press, 2005.

[CLO99] M. L. Corradini, T. Leo, and G. Orlando. Robust stabilization of a mobile robot violating the nonholonomic constraint via quasi-sliding modes. In *Proc. of the American Control Conference*, pages 3935–3939, San Diego, California, June 1999.

[CSVS03] Noah Cowan, Omid Shakernia, Rene Vidal, and Shankar Sastry. Vision-based follow-the-leader. In *Proc. of the 2003 IEEE/RSJ Intl. Conference on Intelligent Robots and Systems*, pages 1796–1801, Las Vegas, Nevada, October 2003.

[CYZ02] J. Cheng, J. Yi, and D. Zhao. Stabilization of an underactuated surface vessel via discontinuous control. In *Proc. of the 2007 American Control Conf.*, pages 206–211, NY City, NY, USA, July 2002.

[DDZB01] Warren E. Dixon, Darren M. Dawson, Erkan Zergeroglu, and Aman Behal. Robustness to kinematic disturbances. In *Nonlinear Control of Wheeled Mobile Robots*, volume 262 of *Lecture Notes in Control and Information Sciences*, pages 113–130. Springer Berlin / Heidelberg, 2001.

[DFB10] Joseph W. Durham, Antonio Franchi, and Francesco Bullo. Distributed pursuit-evasion with limited-visibility sensors via frontier-based exploration. In *Proc. of the 2010 IEEE International Conference on Robotics and Automation*, pages 3562–3568, Anchorage, Alaska, May 2010.

[DFK+02] Aveek K. Das, Rafael Fierro, Vijay Kumar, James P. Ostrowski, John Spletzer, and Camillo J. Taylor. A vision-based formation control framework. *IEEE Transactions on Robotics and Automation*, 18(5):813–825, October 2002.

[DG05] W. Dong and Yi Guo. Global time-varying stabilization of underactuated surface vessel. *IEEE Trans. on Automatic Control*, 50(6):859–864, June 2005.

[DJPN02] K. D. Do, Z. P. Jiang, J. Pan, and H. Nijmeijer. Global output feedback universal controller for the stabilization and tracking of underactuated ODIN-an underwater vehicle. In *Proc. of the 41st IEEE Conf. on Decision and Control*, pages 504–509, Las Vegas, NE, USA, December 2002.

[DJPN04] K. D. Do, Z. P. Jiang, J. Pan, and H. Nijmeijer. A global output-feedback controller for stabilization and tracking of underactuated ODIN: A spherical underwater vehicle. *IFAC Automatica*, 40:117–124, 2004.

[dW01] David A. de Wolf. *Essentials of Electromagnetics for Engineering*. Cambridge University Press, 2001.

[DXH00] Wenjie Dong, Yangsheng Xu, and Wei Huo. On stabilization of uncertain dynamic nonholonomic systems. *International Journal of Control*, 73(4):349–359, 2000.

[FBP03] Thierry Floquet, Jean-Pierre Barbot, and Wilfrid Perruquetti. Higher-order sliding mode stabilization for a class of nonholonomic perturbed systems. *Automatica*, 39:1077–1083, 2003.

[FLMP00] I. Fantoni, R. Lozano, F. Mazenc, and K. Y. Pettersen. Stabilization of a nonlinear underactuated hovercraft. *Int. Journal of Robust and Nonlinear Control*, 10:645–654, 2000.

[Fos02] Thor I. Fossen. *Marine Control Systems: Guidance, Navigation and Control of Ships, Rigs and Underwater Vehicles*. Marine Cybernetics, 2002.

[GE97] John-Morten Godhavn and Olav Egeland. A Lyapunov approach to exponential stabilization of nonholonomic systems in power form. *IEEE Transactions on Automatic Control*, 42(7):1028–1032, July 1997.

[GH08] M. Greytak and F. Hover. Underactuated point stabilization using predictive models with application to marine vehicles. In *Proc. of the 2008 IEEE/RSJ Int. Conf. on Intelligent Robots and Systems*, pages 3756–3761, Nice, France, September 2008.

[Gin95] Jerry H. Ginsberg. *Advanced Engineering Dynamics - 2nd Edition*. Cambridge University Press, 1995.

[Gin07] Jerry H. Ginsberg. *Engineering Dynamics*. Cambridge University Press, 2007.

[GMBD06] J. Ghommam, F. Mnif, A. Benali, and N. Derbel. Asymptotic backstepping stabilization of an underactuated surface vessel. *IEEE Trans. on Control Systems Technology*, 14(6):1150–1157, November 2006.

[Gri99] David J. Griffiths. *Introduction to Electrodynamics. Third Edition*. Prentice Hall, Upper Saddle River, New Jersey, 1999.

[Guo05] Yi Guo. Nonlinear H_∞ control of uncertain nonholonomic systems in chained forms. *International Journal of Intelligent Control and Systems*, 10(4):304–309, December 2005.

[GWL03] S.S. Ge, Zhuping Wang, and T.H. Lee. Adaptive stabilization of uncertain nonholonomic systems by state and output feedback. *Automatica*, 39:1451–1460, 2003.

[GWLZ01] S. S. Ge, J. Wang, T. H. Lee, and G. Y. Zhou. Adaptive robust stabilization of dynamic nonholonomic chained systems. *Journal of Robotic Systems*, 18(3):119–133, 2001.

[Hen94] Michael Henle. *A Combinatorial Introduction to Topology*. Dover Publications, 1994.

[HLM99a] Joao P. Hespanha, Daniel Liberzon, and A. Stephen Morse. Logic-based switching control of a nonholonomic system with parametric modeling uncertainty. *Systems and Control Letters*, 38(3):167–177, October 1999.

[HLM99b] Joao P. Hespanha, Daniel Liberzon, and A. Stephen Morse. Towards the supervisory control of uncertain nonholonomic systems. In *Proc. of the American Control Conference*, pages 3520–3524, San Diego, California, June 1999.

[HLM02] Joao P. Hespanha, Daniel Liberzon, and A. Stephen Morse. Supervision of integral-input-to-state stabilizing controllers. *Automatica*, 38:1327–1335, 2002.

[HLM03] Joao P. Hespanha, Daniel Liberzon, and A. Stephen Morse. Overcoming the limitations of adaptive control by means of logic-based switching. *Systems and Control Letters*, 49(1):49–65, April 2003.

[HM99] Joao P. Hespanha and A. Stephen Morse. Stabilization of non-holonomic integrators via logic-based switching. *Automatica*, 35(3):385–393, 1999.

[HW07] W.P.M.H. Heemels and S. Weiland. On interconnections of discontinuous dynamical systems: an input-to-state stability approach. In *Proc. of the 46th Conference on Decision and Control*, pages 109–114, New Orleans, LA, USA, December 2007.

[Isi95] Alberto Isidori. *Nonlinear Control Systems. Third Edition*. Springer, 1995.

[Jia99] Zhong-Ping Jiang. A unified Lyapunov framework for stabilization and tracking of nonholonomic systems. In *Proc. of the 38th IEEE Conference on Decision and Control*, pages 2088–2093, Phoenix, Arizona, USA, December 1999.

[Jia00] Zhong-Ping Jiang. Robust exponential regulation of nonholonomic systems with uncertainties. *Automatica*, 36:189–209, 2000.

[KBH02] T. Kim, T. Basar, and In-Joong Ha. Asymptotic stabilization of an underactuated surface vessel via logic-based control. In *Proc. of the 2002 American Control Conf.*, pages 4678–4683, Anchorage, AL, USA, May 2002.

[Kha02] Hassan K. Khalil. *Nonlinear Systems. Third Edition*. Prentice-Hall Inc., 2002.

[KL05] I. Kitsios and J. Lygeros. Final glide-back envelope computation for reusable launch vehicle using reachability. In *Proc. of the 44th IEEE Conf. on Decision and Control and the European Control Conf. 2005*, pages 4059–4064, Seville, Spain, December 2005.

[KM95] Ilya Kolmanovsky and N. Harris McClamroch. Stabilization of nonholonomic chaplygin systems with linear base space dynamics. In *Proc. of the 34th IEEE Conference on Decision and Control*, pages 27–32, New Orleans, LA, USA, December 1995.

[KM96] Ilya Kolmanovsky and N. Harris McClamroch. Hybrid feedback laws for a class of cascade nonlinear control systems. *IEEE Transactions on Automatic Control*, 41(9):1271–1282, September 1996.

[KPK06] G. C. Karras, D. Panagou, and K. J. Kyriakopoulos. Target-referenced localization of an underwater vehicle using a Laser-based Vision System. In *Proc. of the 2006 MTS/IEEE OCEANS*, Boston, MA, USA, September 2006.

[KR05] George Kantor and Alfred A. Rizzi. Feedback control of underactuated systems via sequential composition: Visually guided control of a unicycle. In P. Dario and R. Chatila, editors, *Robotics Research*, pages 281–290. Springer Berlin Heidelberg, 2005.

[KRM96] Ilya Kolmanovsky, Mahmut Reyhanoglu, and N. Harris McClamroch. Switched mode feedback control laws for nonholonomic systems in extended power form. *Systems and Control Letters*, 27(1):29–36, January 1996.

[LA05] Dina Shona Laila and Alessandro Astolfi. Input-to-state stability for discrete-time time-varying systems with applications to robust stabilization of systems in power form. *Automatica*, 41:1891–1903, 2005.

[LAN03] David A. Lizarraga, Nnaedozie P. I. Aneke, and Henk Nijmeijer. Robust point stabilization of underactuated mechanical systems via the extended chained form. *SIAM Journal on Control and Optimization*, 42(6):2172–2199, 2003.

[LaV06] Steven M. LaValle. *Planning Algorithms*. Cambridge University Press, 2006.

[Lee02] John M. Lee. *Introduction to Smooth Manifolds*. Springer, 2002.

[Leo95] Naomi E. Leonard. Periodic forcing, dynamics and control of underactuated spacecraft and underwater vehicles. In *Proc. of the 34th IEEE Conf. on Decision and Control*, pages 3980–3985, New Orleans, LA, USA, December 1995.

[Lib03] Daniel Liberzon. *Switching in Systems and Control*. Birkhauser Boston, 2003.

[LK07] Gabriel A. D. Lopes and Daniel E. Koditschek. Visual servoing for nonholonomically constrained three degree of freedom kinematic systems. *International Journal of Robotics Research*, 26(7):715–736, July 2007.

[LL09] S. R. Lindemann and S. M. LaValle. Simple and efficient algorithms for computing smooth, collision-free feedback laws over given cell decompositions. *International Journal of Robotics Research*, 28(5):600–621, 2009.

[LO96] Pasquale Lucibello and Giuseppe Oriolo. Stabilization via iterative state steering with application to chained-form systems. In *Proc. of the 35th IEEE Conference on Decision and Control*, pages 2614–2619, Kobe, Japan, December 1996.

[LO01] Pasquale Lucibello and Giuseppe Oriolo. Robust stabilization via iterative state steering with an application to chained-form systems. *Automatica*, 37:71–79, 2001.

[LOS98] A. De Luca, G. Oriolo, and C. Samson. Feedback control of a nonholonomic car-like robot. In Jean Paul Laumond, editor, *Robot Motion Planning and Control (Lecture Notes in Control and Information Sciences)*, volume 229, pages 171–253. Springer-Verlag, 1998.

[LS93] G. A. Lafferriere and E. D. Sontag. Remarks on control lyapunov functions for discontinuous stabilizing feedback. In *Proceedings of the IEEE Conference on Decision and Control*, pages 306–308, San Antonio, TX, 1993.

[LSW02] Daniel Liberzon, Eduardo D. Sontag, and Yuan Wang. Universal construction of feedback laws achieving ISS and integral-ISS disturbance attenuation. *Systems and Control Letters*, 46:111–127, 2002.

[LT98] Jihao Luo and Panagiotis Tsiotras. Exponentially convergent control laws for nonholonomic systems in power form. *Systems and Control Letters*, 35:87–95, 1998.

[Lyg04] John Lygeros. On reachability and minimum cost optimal control. *IFAC Automatica*, 40(6):917–927, June 2004.

[MA03] Nicolas Marchand and Mazen Alamir. Discontinuous exponential stabilization of chained form systems. *Automatica*, 39:343–348, 2003.

[MBP11] Fabio Morbidi, Francesco Bullo, and Domenico Prattichizzo. Visibility maintenance via controlled invariance for leader-follower vehicle formations. *Automatica*, 47(5):1060–1067, May 2011.

[MBT05] I. M. Mitchell, A. M. Bayen, and C. J. Tomlin. A time-dependent Hamilton-Jacobi formulation of reachable sets for continuous dynamic games. *IEEE Trans. on Automatic Control*, 50(7):947–957, July 2005.

[Mit07a] I. M. Mitchell. Comparing Forward and Backward Reachability as Tools for Safety Analysis. In *Hybrid Systems: Computation and Control*, pages 428–443. Springer Verlag, 2007.

[Mit07b] I. M. Mitchell. *A Toolbox of Level Set Methods*, version 1.1. http://www.cs.ubc.ca/ mitchell/ToolboxLS/index.html, 2007.

[MM97] R. T. M'Closkey and R. M. Murray. Exponential stabilization of driftless nonlinear control systems using homogeneous feedback. *IEEE Transactions on Automatic Control*, 42(5):614–628, 1997.

[MMP+09] Gian Luca Mariottini, Fabio Morbidi, Domenico Prattichizzo, Nicholas Vander Valk, George Pappas, and Kostas Daniilidis. Vision-based localization for leader-follower formation control. *IEEE Transactions on Robotics*, 25(6):1431–1438, December 2009.

[Mor98] A. S. Morse. Control using logic-based switching. In *Trends in Control: A European Perspective*, pages 69–113. Springer-Verlag, 1998.

[MS93] Richard M. Murray and S. Shankar Sastry. Nonholonomic motion planning: Steering using sinusoids. *IEEE Transactions on Automatic Control*, 38(5):700–716, May 1993.

[MS96] P. Morin and C. Samson. Time-varying exponential stabilization of chained form systems based on a backstepping technique. In *Proc. of the 35th IEEE Conference on Decision and Control*, pages 1449–1454, Kobe, Japan, December 1996.

[MS00] Pascal Morin and Claude Samson. Control of nonlinear chained systems: From the Routh-Hurwitz stability criterion to time-varying exponential stabilizers. *IEEE Transactions on Automatic Control*, 45(1):141–146, January 2000.

[MS03] Pascal Morin and Claude Samson. Practical stabilization of driftless systems on Lie groups: The transverse function approach. *IEEE Transactions on Automatic Control*, 48(9):1496–1508, September 2003.

[MS09] Pascal Morin and Claude Samson. Control of nonholonomic mobile robots based on the transverse function approach. *IEEE Transactions on Robotics*, 25(5):1058–1073, October 2009.

[MTX02] B. L. Ma, S. K. Tso, and W. L. Xu. Adaptive/robust time-varying stabilization of second-order non-holonomic chained form with input uncertainties. *International Journal of Robust and Nonlinear Control*, 12:1299–1316, 2002.

[OBNtdW95] Wilco Oelen, Hany Berghuisa, Henk Nijmeijer, and Carlos Canudas de Wit. Hybrid stabilizing control on a real mobile robot. *IEEE Robotics and Automation Magazine*, 2(2):16–23, June 1995.

[ON91] Giuseppe Oriolo and Yoshihiko Nakamura. Control of mechanical systems with second-order nonholonomic constraints: Underactuated manipulators. In *Proc. of the 30th IEEE Conference on Decision and Control*, pages 2398–2403, Brighton, England, December 1991.

[OV05] Giuseppe Oriolo and Marilena Vendittelli. A framework for the stabilization of general nonholonomic systems with an application to the plate-ball mechanism. *IEEE Transactions on Robotics*, 21(2):162–175, April 2005.

[PA03] Christophe Prieur and Alessandro Astolfi. Robust stabilization of chained systems via hybrid control. *IEEE Transactions on Automatic Control*, 48(10):1768–1772, October 2003.

[PDS08] A. Pereira, J. Das, and G. S. Sukhatme. An experimental study of station keeping on an underactuated ASV. In *Proc. of the 2008 IEEE/RSJ Int. Conf. on Intelligent Robots and Systems*, pages 3164–3171, Nice, France, September 2008.

[PE99] K. Y. Pettersen and O. Egeland. Time-varying exponential stabilization of the position and attitude of an underactuated Autonomous Underwater Vehicle. *IEEE Trans. on Automatic Control*, 44(1):112–115, January 1999.

[PF00] K. Y. Pettersen and T. I. Fossen. Underactuated dynamic positioning of a ship - Experimental results. *IEEE Trans. on Control Systems Technology*, 8(5):856–863, September 2000.

[PK11] Dimitra Panagou and Kostas J. Kyriakopoulos. Control of underactuated systems with viability constraints. In *Proc. of the 50th IEEE Conference on Decision and Control and European Control Conference*, pages 5497–5502, Orlando, Florida, December 2011.

[PMS+09] Dimitra Panagou, Kostas Margellos, Sean Summers, John Lygeros, and Kostas J. Kyriakopoulos. A viability approach for the stabilization of an underactuated underwater vehicle in the presence of current disturbances. In *Proc. of the 48th IEEE Conference on Decision and Control*, pages 8612–8617, Shanghai, P.R. China, December 2009.

[PN00] K. Y. Pettersen and H. Nijmeijer. Semi-global practical stabilization and disturbance adaptation for an underactuated ship. In *Proc. of the 39th IEEE Conf. on Decision and Control*, pages 2144–2149, Sydney, Australia, December 2000.

[PN01] K. Y. Pettersen and H. Nijmeijer. Semi-global practical stabilization and disturbance adaptation for an underactuated ship. *Modeling, Identification and Control*, 22(2):89–101, April 2001.

[Pom92] Jean-Baptiste Pomet. Explicit design of time-varying stabilizing control laws for a class of controllable systems without drift. *Systems and Control Letters*, 18:147–158, 1992.

[PTK10] Dimitra Panagou, Herbert G. Tanner, and Kostas J. Kyriakopoulos. Dipole-like fields for stabilization of systems with Pfaffian constraints. In *Proc. of the 2010 IEEE International Conference on Robotics and Automation*, pages 4499–4504, Anchorage, Alaska, May 2010.

[PTK11] Dimitra Panagou, Herbert G. Tanner, and Kostas J. Kyriakopoulos. Control of nonholonomic systems using reference vector fields. In *Proc. of the 50th IEEE Conference on Decision and Control and European Control Conference*, pages 2831–2836, Orlando, Florida, December 2011.

[Rey96] M. Reyhanoglu. Control and stabilization of an underactuated surface vessel. In *Proc. of the 35th IEEE Conf. on Decision and Control*, pages 2371–2376, Kobe, Japan, December 1996.

[RSP07] J. E. Refsnes, A. J. Sorensen, and K. Y. Pettersen. Output feedback control of slender body underwater vehicles with current estimation. *International Journal of Control*, 80(7):1136–1150, July 2007.

[Sam95] Claude Samson. Control of chained systems: Application to path following and time-varying point-stabilization of mobile robots. *IEEE Transactions on Automatic Control*, 40(1):64–77, January 1995.

[SE95] O. J. Sørdalen and O. Egeland. Exponential stabilization of nonholonomic chained systems. *IEEE Transactions on Automatic Control*, 40(1):35–48, January 1995.

[SFPB10] Paolo Salaris, Daniele Fontanelli, Lucia Pallotino, and Antonio Bicchi. Shortest paths for a robot with nonholonomic and field-of view constraints. *IEEE Transactions on Robotics*, 26(2):269–280, April 2010.

[SGHL00] Z. Sun, S.S. Ge, W. Huo, and T. H. Lee. Stabilization of nonholonomic chained systems via nonregular feedback linearization. In *Proc. of the 39th IEEE Conference on Decision and Control*, pages 1906–1911, Sydney, Australia, December 2000.

[SGHL01] Zhendong Sun, S.S. Ge, Wei Huo, and T.H. Lee. Stabilization of nonholonomic chained systems via nonregular feedback linearization. *Systems and Control Letters*, 44(4):279–289, November 2001.

[Tan04] Herbert G. Tanner. ISS properties of nonholonomic vehicles. *Systems and Control Letters*, 53(3-4):229–235, November 2004.

[tdWK95] Carlos Canudas de Wit and H. Khennouf. Quasi-continuous stabilizing controllers for nonholonomic systems: Design and robustness considerations. In *Proc. of the 3rd European Control Conference*, pages 2630–2635, Rome, Italy, September 1995.

[tdWS92] C. Canudas de Wit and O. J. Sørdalen. Exponential stabilization of mobile robots with nonholonomic constraints. *IEEE Transactions on Automatic Control*, 37(11):1791–1797, November 1992.

[TK00] Herbert G. Tanner and Kostas J. Kyriakopoulos. Nonholonomic motion planning for mobile manipulators. In *Proc. of the 2000 IEEE International Conference on Robotics and Automation*, pages 1233–1238, San Francisco, CA, April 2000.

[TL02] Yu-Ping Tian and Shihua Li. Exponential stabilization of nonholonomic dynamic systems by smooth time-varying control. *Automatica*, 38:1138–1143, 2002.

[TMW95] Andrew R. Teel, Richard M. Murray, and Gregory C. Walsh. Non-holonomic control systems: from steering to stabilization with sinusoids. *International Journal of Control*, 62(4):849–870, 1995.

[TSH00] Xavier Tricoche, Gerik Scheuermann, and Hans Hagen. A topology simplification method for 2d vector fields. In *Proc. of Visualization 2000*, pages 359–366, Salt Lake City, UT, USA, October 2000.

[TTR97a] A. Tayebi, M. Tadjine, and A. Rachid. Discontinuous control design for the stabilization of nonholonomic systems in chained form using the backstepping approach. In *Proc. of the 36th IEEE Conference on Decision and Control*, pages 3089–3090, San Diego, CA, USA, December 1997.

[TTR97b] A. Tayebi, M. Tadjine, and A. Rachid. Invariant manifold approach for the stabilization of nonholonomic systems in chained form: Application to a car-like mobile robot. In *Proc. of the 36th IEEE Conference on Decision and Control*, pages 4038–4043, San Diego, CA, USA, December 1997.

[VA03] E. Valtolina and A. Astolfi. Local robust regulation of chained systems. *Systems and Control Letters*, 49:231–238, 2003.

[WC06] Wei Wang and Christopher M. Clark. Modeling and simulation of the videoray pro iii underwater vehicle. In *Proc. of OCEANS 2006 - Asia Pacific*, pages 1–7, Singapore, May 2006.

[WHX99] Sheng Yuan Wang, Wei Huo, and Wei Liang Xu. Order-reduced stabilization design of nonholonomic chained systems based on new canonical forms. In *Proc. of the 38th IEEE Conference on Decision and Control*, pages 3464–3469, Phoenix, Arizona, USA, December 1999.

[WSE95a] K. Y. Wichlund, O. J. Sordalen, and O. Egeland. Control of vehicles with second-order constraints: Underwater vehicles. In *Proc. of the 3rd European Conf. on Control*, pages 3086–3091, Rome, Italy, September 1995.

[WSE95b] K. Y. Wichlund, O. J. Sørdalen, and O. Egeland. Control of vehicles with second-order nonholonomic constraints: Underactuated vehicles. In *Proc. of the 3rd European Control Conference*, pages 3086–3091, Rome, Italy, September 1995.

[WZ08] Yuqiang Wu and Xiuyun Zheng. Robust stabilization of uncertain nonholonomic systems with strong nonlinear drifts. *Journal of Control Theory and Applications*, 6(4):427–430, November 2008.

[XM01] W. L. Xu and B. L. Ma. Stabilization of second-order nonholonomic systems in canonical chained form. *Robotics and Autonomous Systems*, 34:223–233, 2001.

[YMH98] Hui Ye, Anthony N. Michel, and Ling Hou. Stability theory for hybrid dynamical systems. *IEEE Transactions on Automatic Control*, 43(4):461–474, April 1998.

[ZDCH07] Xiaocai Zhu, Guohua Dong, Zixing Cai, and Dewen Hu. Robust simultaneous tracking and stabilization of wheeled mobile robots not satisfying nonholonomic constraint. *Journal of Central South University of Technology*, 14(4):537–545, August 2007.

[ZH08] Jun Zhao and David J. Hill. On stability, L_2-gain and H_∞ control for switched systems. *Automatica*, 44:1220–1232, 2008.